Development of Flame Surface Density Closure for Turbulent Premixed Flames Based on *A Priori* Analysis of Direct Numerical Simulation Data

Mohit Katragadda

School of Mechanical and Systems Engineering

Newcastle University

A thesis submitted for the degree of

Doctor of Philosophy

May 2013

To my loving family

Declaration

- I declare that this thesis is my own work and that I have correctly acknowledged the work of others. This submission is in accordance with University and School guidance on good academic conduct.
- I certify that no part of the material offered has been previously submitted by me for a degree or other qualification in this or any other University.
- I confirm that the word length is within the prescribed range as advised by my school and faculty.
- I confirm that this thesis does not contain collaborative work.

Mohit Katragadda
May 2013

Acknowledgements

I would like to express my gratitude to Prof. Nilanjan Chakraborty for his invaluable expertise, advice and support over the course of this work. I am grateful to Prof. Stewart Cant and Dr. Sean P. Malkeson for their technical advice and guidance, and Dr. Ian Potts and Prof. Kenneth J. Badcock for their encouragement. The comments and suggestions, in the preparation of the final form of this thesis, from Dr. David Swailes and Dr. Nedunchezhian Swaminathan are greatly appreciated. I would like to offer my thanks to Dr. Andy Calder, Mr. Ian Pitcher and Mr. David Wall for their help and support.

I am grateful to the Engineering and Physical Sciences Research Council (EPSRC) for the financial support through the course of this PhD. Additionally, I am grateful to the Combustion Institute for the travel grants, which have allowed me to attend and present many parts of this work.

I am forever indebted to my parents; Kesava and Lata, Rohit and Rachel for their endless patience, encouragement and support.

Abstract

In turbulent premixed flames the modelling of mean or filtered reaction rate translates to the closure of flame surface to volume ratio, which is commonly referred to as the Flame Surface Density (FSD). The FSD based reaction rate closure is well established in the context of Reynolds Averaged Navier-Stokes (RANS) simulations for unity Lewis numbers. However, models for FSD in context of Large Eddy Simulations (LES) are relatively rare. In this study three-dimensional Direct Numerical Simulations (DNS) of freely propagating statistically planar premixed flames encompassing a range of different turbulent Reynolds numbers and global Lewis numbers was used. The variation of turbulent Reynolds number has been brought about by modifying the Karlovitz and the Damköhler numbers independently of each other. The DNS data has been explicitly Reynolds averaged and LES filtered for *a priori* assessment of existing FSD models and for the purpose of proposing new models where necessary.

The closure of FSD can be achieved either by an algebraic expression involving resolved scale quantities or by solving for a modelled transport equation. Both modelling methodologies have been analysed in the current analysis. The performances of existing power-law based algebraic models of FSD have been analysed for a range of different values of global Lewis numbers and turbulent Reynolds numbers. The effects of global Lewis number and turbulent Reynolds number on fractal dimension and inner cutoff scale have been analysed in detail, based on explicitly filtered DNS data. The behaviour of fractal dimension and inner cutoff scale in response to the global Lewis numbers and turbulent Reynolds numbers have been incorporated to propose a

new power-law based algebraic model for the generalised FSD in the context of LES. This new algebraic model was validated using *a priori* analysis, where it has been found to provide accurate estimations for the generalised FSD over a range of global Lewis numbers and turbulent Reynolds numbers, and for a wide range of filter widths. Additionally, it was found that the newly proposed algebraic model performs either comparably to existing models or outperforms them. The statistical behaviours of the unclosed terms of the generalised FSD transport equation have been analysed in detail for a range of different LES filter widths. It has been established that the modelling methodologies which implicitly account for curvature dependence of flame propagation, and are valid for both the corrugated flamelets and thin reaction zones regimes of premixed turbulent combustion, work satisfactorily for turbulent flux term of the generalised FSD transport equation and for the surface weighted displacement speed, for the range of parameters considered here.

The modelling of the unclosed curvature, propagation and strain rate terms in the generalised FSD transport equation have been analysed in the context of RANS and LES simulations based on *a priori* analysis of DNS data, so that the newly proposed RANS and LES models remain valid for both the corrugated flamelets and thin reaction zones regimes of turbulent premixed combustion. Based on these RANS models, new models were proposed for the strain rate term and curvature terms in the context of LES. The performances of the newly proposed models have been assessed with respect to DNS data and they have been found to work satisfactorily for a range of different values of Lewis number, turbulent Reynolds number and LES filter widths.

Contents

List of Journal Publications

[1] N. Chakraborty, G. Hartung, M. Katragadda, and C. F. Kaminski, "Comparison of 2D and 3D density-weighted displacement speed statistics and implications for laser based measurements of flame displacement speed using direct numerical simulation data", *Combustion and Flame*, vol. 158, no. 7, pp. 1372–1390, 2011.

[2] N. Chakraborty, M. Katragadda, and R. S. Cant, "Statistics and Modelling of Turbulent Kinetic Energy Transport in Different Regimes of Premixed Combustion", *Flow, Turbulence and Combustion*, vol. 87, pp. 205–235, 2 2011.

[3] N. Chakraborty, M. Katragadda, and R. S. Cant, "Effects of Lewis number on turbulent kinetic energy transport in premixed flames", *Physics of Fluids*, vol. 23, no. 7, p. 075109, 2011.

[4] M. Katragadda, S. P. Malkeson, and N. Chakraborty, "Modelling of the tangential strain rate term of the Flame Surface Density transport equation in the context of Reynolds Averaged Navier-Stokes simulation", *Proceedings of the Combustion Institute*, vol. 33, no. 1, pp. 1429–1437, 2011.

[5] M. Katragadda and N. Chakraborty, "Modelling of the Curvature Term of the Flame Surface Density Transport Equation for Large Eddy Simulations", *Journal of Combustion*, vol. 2012, Article ID 915482, p. 12, 2012.

[6] M. Katragadda and N. Chakraborty, "A Priori Direct Numerical Simulation Modelling of the Curvature Term of the Flame Surface Density Transport Equation for Nonunity Lewis Number Flames in the Context of Large Eddy Simulations", *International Journal of Chemical Engineering*, vol. 2012, Article ID 103727, p. 12, 2012.

[7] M. Katragadda, N. Chakraborty, and R. S. Cant, "Effects of Turbulent Reynolds Number on the Performance of Algebraic Flame Surface Density Models for Large Eddy Simulation in the Thin Reaction Zones Regime: A Direct Numerical Simulation Analysis", *Journal of Combustion*, vol. 2012, Article ID 353257, p. 13, 2012.

[8] M. Katragadda, N. Chakraborty, and R. S. Cant, "A Priori Assessment of Algebraic Flame Surface Density Models in the Context of Large Eddy Simulation for Nonunity Lewis Number Flames in the Thin Reaction Zones Regime", *Journal of Combustion*, vol. 2012, Article ID 794671, p. 17, 2012.

List of Conference Publications

[1] M. Katragadda and N. Chakraborty, "*A-priori* DNS assessment of algebraic LES Flame Surface Density models for non-unity Lewis number flames in the thin reaction zones regime", 33^{rd} *International Combustion Symposium*, Tsinghua University, Beijing, China, Aug. 2010.

[2] M. Katragadda, S. P. Malkeson, and N. Chakraborty, "Modelling of the curvature term of the Flame Surface Density transport equation for Reynolds Averaged Navier Stokes simulations", 33^{rd} *International Combustion Symposium*, Tsinghua University, Beijing, China, Aug. 2010.

[3] M. Katragadda, S. P. Malkeson, and N. Chakraborty, "Modelling of curvature term of the Flame Surface Density transport equation in the context of Reynolds Averaged Navier Stokes simulations", *7th Mediterranean Combustion Symposium*, Sept. 2011.

[4] M. Katragadda and N. Chakraborty, "Effects of Lewis number on Flame Surface Density transport in the context of Large Eddy Simulation", *5th European Combustion Meeting*, Cardiff University, Cardiff, UK, 28 June - 1 July 2011.

[5] M. Katragadda and N. Chakraborty, "Effects of Lewis number on the curvature term of the Flame Surface Density transport equation for LES", *7th International Symposium on Turbulence, Heat and Mass Transfer*, University of Palermo, Palermo, Sicily, Italy, 24 - 27 September 2012.

[6] M. Katragadda, S. P. Malkeson, and N. Chakraborty, "Statistical behaviour of the curvature term of the FSD transport equation in the context of RANS", *7th International Symposium on Turbulence, Heat and Mass*

Transfer, University of Palermo, Palermo, Sicily, Italy, 24 - 27 September 2012.

[7] M. Katragadda and N. Chakraborty, "Modelling of the curvature term of the Flame Surface Density Transport Equation in the context of Reynolds Averaged Navier Stokes Simulation", 34^{th} *International Combustion Symposium*, Warsaw University of Technology, Warsaw, Poland, 29 July - 3 August 2012.

[8] M. Katragadda and N. Chakraborty, "Modelling of the curvature term of the Flame Surface Density Transport Equation in the context of Reynolds Averaged Navier Stokes Simulation", 34^{th} *International Combustion Symposium*, Warsaw University of Technology, Warsaw, Poland, 29 July - 3 August 2012.

[9] M. Katragadda and N. Chakraborty, "*A priori* DNS modelling of the strain rate term of the Flame Surface Density Transport Equation in the Context of LES", 6^{th} *European Combustion Meeting*, (Accepted), Lund University, Lund, Sweden, June 2013.

[10] M. Katragadda, Y. Gao, and N. Chakraborty, "Modelling of the strain rate contribution to the FSD transport for non-unity Lewis number flames in LES", *24th ICDERS*, (Accepted), National Central University, Taipei, Taiwan, July 2013.

List of Figures

List of Tables

Nomenclature

Latin Symbols

A_1	RANS Curvature term due to reaction and normal diffusion component of S_d
A_2	RANS Curvature term due to tangential diffusion component of S_d
A_L	Laminar flame area
A_m	Frequency factor
A_T	Turbulent flame area
A_{1r}	Resolved RANS Curvature term due to reaction and normal diffusion component of S_d
A_{1ur}	Unresolved RANS Curvature term due to reaction and normal diffusion component of S_d
A_{2r}	Resolved RANS Curvature term due to tangential diffusion component of S_d
A_{2ur}	Unresolved RANS Curvature term due to tangential diffusion component of S_d
A_{ij}	Element of matrix A
a	Acoustic speed in the unburned gas
a^*	Model parameters for A_{1ur}

a_Σ	Model parameters for C_{sg1}
a_c	Local speed of sound
a_j	Constants for central difference scheme
a_m	Strain rate induced by mean flow
a_T	Tangential strain rate
a_t	Strain rate induced by turbulent fluctuation
B^*	Pre-exponent factor
C	Counrant number
C_H	Model parameter
C_i'	A non-homogeneous term
C_p	Specific heat capacity at constant pressure
C_t	Unresolved curvature term
C_V	Mixture heat capacity at constant volume
C_v	Specific heat capacity at constant volume
C_{mean}	Resolved component of curvature term
C_{sg1}	LES subgrid curvature term due to reaction and normal diffusion components of displacement speed
C_{sg2}	LES subgrid curvature term due to tangential diffusion components
C_{sg}	Subgrid curvature term
c	Reaction progress variable
c^*	Arbitary value of reaction progress variable

c°	Model parameters for C_{sg1}
c_{red}	Reduced binarised reaction progress variable
D	Mass diffusivity
Da	Damköhler number
Da_{Δ}	Subgrid Damköhler number
E	Stagnation internal energy
$E(\kappa)$	Turbulent energy spectrum
E_m	Activation energy
$\vec{e_i}$	Unit basis vector
F_i	A representative flux vector
G	LES filter
H	Heat of reaction per unit mass of reactants consumed
h_{α}	Enthalpy of formation of species α
h	Grid spacing
h^0_{α}	Enthalpy of formation of species α
I_0	Correction factor
K	Relaxation parameter
K_{Σ}	Model constant for BML model
Ka	Karlovitz number
Ka_{Δ}	Subgrid Karlovitz number
$\tilde{k}$	Sugbrid turbulent kinetic energy
$\underline{k}$	Mean turbulent kinetic energy

k_1, k_2, k_3, k_4	Model parameters for C_{sg1}
L	DNS Domain size
L_i	Wave amplitude variation
Le	Lewis number
l	Integral length scale
Ma	Mach number
M_i	Resolved flame normal vector
M_{k1}	Scalar flux
m	Model parameters for C_{sg1}
N	Number of grid point in DNS domain
N_i	Flame normal vector
N_s	Number of species
n	Flame normal direction
n°	Order of central difference scheme
n_m	Temperature exponent
P	Pressure
P_{ij}	Element of matrix P
P_{mean}	Resolved component of propagation term
Pr	Prandtl number
Q	Number of grid points within a laminar flame thickness
Q_{ij}	Element of matrix Q
q_k	Heat flux vector

q_1	Heat flux
R_0	Universal gas constant
Re	Reynolds number
Re_Δ	Subgrid Reynolds number
Re_L	Local Reynolds number
Re_t	Turbulent Reynolds number
r_1, r_2, r_3, r_4	Model parameters for C_{sg2}
$(S_m)_M$	Modelled mean LES strain rate
S_c	Flame consumption speed
S_d	Flame displacement speed
S_L	Laminar flame speed
S_n	Normal diffusion component of displacement speed
S_R	Resolved RANS strain rate term
S_r	Reaction rate component of displacement speed
S_T	Turbulent flame speed
S_t	Tangential diffusion component of displacement speed
S_{hr}	Heat release contribution of strain rate
S_{ij}	Eigenvector matrix for Λ_{ij}
S_{RN}	Combined reaction and normal components of displacement speed
S_{sg}	Subgrid strain rate term
S_{UR}	Unresolved RANS strain rate term

Sc	Schmidt number
Sc_Σ	Subgrid schmidt number
T_N	Flame normal strain rate
$\hat{T}$	Instantaneous dimensional temperature
T	Non-dimensional temperature
T^R	Recommended temperature
T_1	Subgrid convection term
T_2	Tangential strain rate term
T_3	Curvature term
T_4	Propagation term
T_D	Dilatation rate term
T_0	Unburned gas temperature
T_{ad}	Adiabatic flame temperature
$\hat{u}$	Velocity field in Fourier space
$\vec{u}$	Velocity vector
u'	rms velocity fluctuation
u^R	Recommended velocity
u'_Δ	Subgrid turbulent kinetic energy
u_i	Velocity vector in the i^{th} direction
V	Volume
$V_{\alpha k}$	Diffusion velocity of species α
$v''_{\alpha,m}$	Product stoichiometric coefficient

$v'_{\alpha,m}$	Reactant stoichiometric coefficient
v^R	Recommended velocity
W_α	Molar mass of species α
$\dot{w}$	Reaction rate
$\dot{w}_\alpha$	Reaction rate of species α
w^R	Recommended velocity
x_1	Mean flame propagation
Y_α	Mass fraction of species α

Greek Symbols

α	Heat release parameter
α_0	Model constant
α_T	Thermal diffusivity
β	Zeldovich number
β_0	Model constant
β_4	Model parameters for C_{sg1}
β_5	Model parameters for C_{sg2}
β_{A1UR}	Model parameters for A_{1ur}
β_{A2UR}	Model parameter for A_{2ur}
β_{CFM}	CFM curvature model parameter
χ	Scalar dissipation rate
Δt	Time step
Δx	Grid size

Δ	Filter width
δA	Elemental flame surface area
δV	Elemental volume
δ	Diffusive flame thickness, $\delta \approx \nu/S_L$
δ_L	Laminar flame thickness
δ_l	Representative Laminar flame thickness, $\delta_l = \alpha_T/S_L$
δ_z	Zel'dovich flame thickness, $\delta_z = \lambda/\rho C_p S_L$
δ_{th}	Thermal flame thickness
ϵ	Dissipation of turbulent kinetic energy
η	Kolmogorov length scale
η_0	Outer cutoff scale
η_i	Inner cutoff scale
Γ	Efficiency function
Γ_k	ITFNS Efficiency function
γ	Ratio of specific heats
κ_m	Mean curvature
κ	Wave number
$\vec{\kappa}$	Linear wave number vector
λ	Thermal conductivity
λ_i	Characteristic velocity
μ	Dynamic viscosity
μ_t	LES eddy viscosity

ν	Kinematic viscosity
ν_t	LES kinematic eddy viscosity
$\tilde{\phi}_i$	Conservative variable vector
ρ	Density
Σ'	Fine grained FSD
Σ_c	Turbulent Schmidt number of FSD
Σ_{gen}	Generalised FSD
Σ_{sg}	Subgrid scale FSD
σ_i	Relaxation parameter
σ_r	Model constant for relaxation parameter
τ	Heat release parameter
τ_η	Kolmogorov time scale
τ_f	Chemical time scale
τ_t	Large scale turbulent time scale
τ_{12}, τ_{13}	Tangential viscous stresses
τ_η	Kolmogorov time scale
τ_c	Chemical time scale
τ_{f0}	Integral eddy turn over time
τ_{sim}	Minimum simulation run time
Ξ	Wrinkling factor
Ξ_{eff}	Effective wrinkling factor

Accents

$\underline{(\dots)}$	Reynolds averaging operation
$\overline{(\dots)}$	LES filtering operation
$\widetilde{(\dots)}$	Favre filtering operation
$\underset{\sim}{(\dots)}$	Favre averaging operation
$\overline{(\dots)}_s$	Surface weighted LES filtering
$\underline{(\dots)}_s$	Surface weighted Reynolds averaging
Q'	Subgrid/RANS fluctuation of Q
Q''	Favre Subgrid/RANS fluctuation of Q
$\widehat{\overline{(\dots)}}$	Dynamic/test level filtering
$\langle \dots \rangle$	Volume averaging operation

Acronyms

BML	Bray Moss Libby
CFD	Computational Fluid Dynamics
CFM	Coherent flamelet model
CPB	Cant Pope Bray
DNS	Direct numerical simulation
EBU	Eddy Breakup Up
FSD	Flame surface density
ITFNS	Intermittent turbulent net flame stretch
LES	Large eddy simulation
RANS	Reynolds averaged Navier-Stokes

rms	Root mean square
SDF	Surface density function

Chapter 1

Introduction

1.1 Background

Combustion has played an important role in the development of human civilisation well before antiquity. Without combustion our ancestors would have been unable to find warmth, safety or cook food. The benefits of combustion have allowed the spread of humanity to hostile environments. Through human ingenuity it was possible to derive plentiful cheap energy from fossil fuels, and through controlled combustion it was possible to shape the world. As the human population grew rapidly over the last century, with it the energy demand grew as well, and as much as 90% of all usable energy is derived through combustion. This places an ever increasing toll on the natural equilibrium found in the atmosphere, leading to global warming. Other harmful phenomenons can also be associated with combustion, such as smog and acid rain. The most straightforward answer to restoring the equilibrium in the atmosphere would be to stop using combustion, which would lead to untold human suffering, and some even believe that it is past the point of reversal. Instead governments have chosen to pass legislation to control the emissions from combustion processes and to meet growing energy demands with renewable energies, with plans of phasing out combustion with nuclear fission and fusion. Renewable sources often offer relatively low energy densities and relying on present day storage methods for this unpredictable source is troublesome. Thus it is expected that combustion will be in use for the

foreseeable future, while changes to infrastructure take place to accommodate renewable sources of energy production. However the necessity of energy efficient and environmentally friendly combustion technology poses a major challenge to the combustion science community. One of the ways to decrease harmful NOx emissions is to use lean premixed combustion.

Many combustors, such as industrial gas turbine engines, can be designed to operate in a premixed mode of combustion that is to say that the reactants are fully mixed prior to combustion, and in most likely case the flow within these combustors will be turbulent. NOx production is dependent on the temperature and resident time. Lean premixed combustion can be used to reduce the flame temperature and thus allowing for reduction in NOx production. This advantage has stirred interest in developing lean premixed prevapourised technology for gas turbines. Moreover premixed combustion can be manipulated to offer increased efficiency and decreased CO emission.

There are however drawbacks to using lean premixed prevapourised technology as it can lead to engine damage through dynamic oscillation in the case of combustion instabilities. These conditions can be taken care of in the design stage. However the cost of designing new engines can reach spectacular heights when using trial and error. Additionally, experimental measurements of combustors remains limited and extremely costly. It is possible to supplement experimental prototyping with Computational Fluid Dynamics (CFD), where it can provide analysis of the processes involved in the instability mechanism. Development of engines in a virtual world can thus result in decrease of costs involved in development, and also increase the safety during the design stages. In the CFD of combustion, additional requirements are called for due to complexity of reacting flows and the subsequent interaction of heat release with the turbulent flow field. Moreover existing methodologies for the analysis of nonreacting turbulent flows may not be suitable for turbulent reacting flow simulations, without modification.

Direct Numerical Simulation (DNS) is a CFD technique where all the length and time scales involved in a turbulent flow are resolved. This method is generally used for research purposes only as the cost it incurs remains far too high for industrial applications. Other CFD techniques such as Large Eddy Simulation (LES) and Reynolds averaged Navier Stokes (RANS) simulation resolve the flow

field only partially, and both techniques often fail to resolve the flame structure completely. In LES and RANS the governing equations are filtered/averaged which results in unclosed quantities such as the filtered/averaged reaction rate. These unclosed terms must be modelled based on fundamental physical arguments in order to obtain accurate simulation predictions. In premixed combustion, Flame Surface Density (FSD) is one of the popular approaches for reaction rate closure. FSD represents the flame surface area per unit volume, and the reaction rate closure can be achieved if the reactant consumption rate of the flame is known. The objective of the current work is to use a DNS database, with a wide range of parameters, to assess FSD modelling strategies for the filtered/averaged reaction rate term. In this analysis, the predictions of the models will be compared to the unclosed terms obtained from suitably processed DNS data, and based on the performance of existing models either suitable models will be identified, or modification to the existing models will be suggested, or new models will be developed based on fundamental physical arguments. In the following section, the underlying philosophies of the different simulation techniques are discussed along with their strengths and limitations.

1.2 Simulation Techniques

Many simulation techniques currently exist for the non-reacting flows such as Direct Numerical Simulation (DNS), Large Eddy Simulation (LES) and Reynolds averaged Navier Stokes (RANS) simulation, many of which have been developed from an aerodynamical or a meteorological point of view [79, 93, 138]. These techniques have been adopted for the analysis of turbulent reacting flows in the past two decades. DNS has played a crucial role in greatly improving the fundamental physical understanding of combustion physics, and RANS simulations have been adopted in industry as a staple method to aid in combustor design. As powerful computational power becomes increasingly accessible, simulation techniques such as LES are becoming more common in an industrial setting. In Fig. 1.1 the resolution of the turbulent energy spectrum, $(E(\kappa))$ according to DNS, LES and RANS are shown, where η, Δ and Δx are the Kolmogorov length scale, filter size and the grid spacing, respectively. It becomes clear that the computational grid

of the DNS resolves the major portion of the turbulent energy spectrum and only a small region associated with the viscous dissipation takes place at a subgrid level. However in LES and RANS the energy spectrum is only partially resolved. In the following sections an introduction is given to the simulation techniques associated with DNS, LES and RANS.

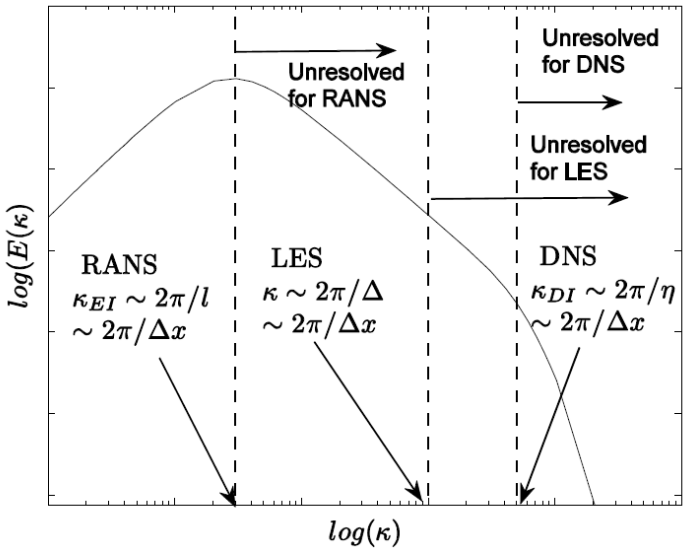

Figure 1.1: A schematic of turbulent energy spectrum ($E(\kappa)$) with wave number (κ) showing the capabilities of different simulation techniques (courtesy of Nilanjan Chakraborty).

1.2.1 Direct Numerical Simulation

DNS is a simulation technique where the smallest length and time scales of the turbulence (Kolmogorov length scale η, Kolmogorov time scale τ_η) are resolved, thus ensuring that the physics involved in a turbulent flow is captured, as such it is the most accurate method of simulating turbulent flows. In combustion DNS, additionally, the flame must be resolved, which tends to be much smaller than the Kolmogorov length scale under most conditions. The interaction between thermo-chemistry and fluid dynamics are accounted for by the equations of conservation of mass, momentum, energy and species together with thermodynamic equations of state. A comprehensive review on the topic of DNS can

be found in Ref [10, 14]. In reality transport properties such as viscosity, mass diffusivity and thermal conductivity change with temperature, and this results in the complex nature of momentum, heat and mass transfer. Additionally, to run three-dimensional DNS cases which include detailed chemistry for a parametric analysis is extremely costly with current hardware. For this reason in the current work a three dimensional compressible DNS with single step chemistry was used. Furthermore the temperature dependence of transport properties were neglected for the sake of simplicity, as this assumption does not change the qualitative nature of the physics [97, 117]. Moreover turbulent reacting flow DNS is often carried out in simple canonical configuration and in simple geometries (e.g. Bunsen burner, planar flame and v-flame), while in reality a combustor tends to have highly complex geometry.

In addition to the above simplifications, the computational cost for DNS increases sharply with turbulent Reynolds number (i.e. $Re_t{}^{11/4}$) for non-reacting flows, which limits the applicability of DNS for moderate Reynolds numbers. In Fig. 1.2 the range of DNS applicability is shown according to Poinsot and Veynante [119], where it makes it clear that the typical operating conditions in spark ignition piston engines and some operating conditions of gas turbine combustors can be accessed using DNS at present time. The scope of DNS will increase with time as increasingly powerful computational hardware becomes available. The specification of appropriate boundary conditions poses one of the major problems in DNS simulations. The lack of theoretical background causes difficulties in identifying boundary conditions appropriately. It is possible to derive the exact boundary conditions to ensure well-posedness for Euler equations, but for the Navier-Stokes equations it is a much more involved task [119]. Therefore only simple boundary conditions are usually specified such as periodic or impenetrable walls. The variable density of combustible flow leads to acoustic activity which must also be dealt with, and this requires an appropriate specification of non-reflecting inlet and outlet boundary conditions. The specification of these boundary conditions is relatively simple for geometries such as a cubic domain, but for complex geometries it can be extremely difficult. As computational power grows exponentially it will be possible to apply DNS for an ever increasing set of engineering problems.

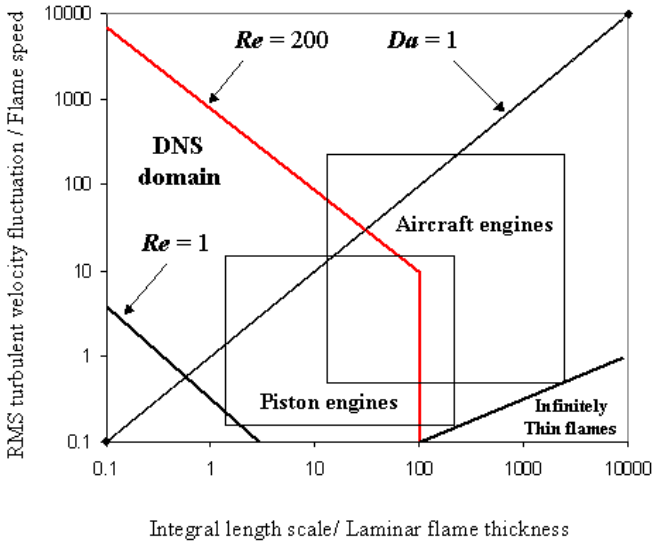

Figure 1.2: DNS domain is shown with a thick red line in relation to engineering applications in reciprocating engines and aircraft engines on a combustion diagram by Poinsot and Veynante [119].

DNS still remains an indispensable part of the analysis of turbulent combustion even with the limitations mentioned earlier. DNS has the ability to correctly predict physical processes which can be verified in experiments, moreover it is possible to obtain statistics related to important quantities such as the flame displacement speed and scalar gradient which are difficult to measure using experimental techniques. The main importance for DNS comes from its usefulness in developing models for LES and RANS. DNS of statistically planar freely propagating turbulent premixed flame can be considered a study of a small element of a flame within a gas turbine combustor. In a similar manner the growth of a flame kernel in a turbulent environment can be considered a generic problem involving the flame propagation in a spark ignition [78]. Thus these simple cases can be used to propose models in the context of LES and RANS.

1.2.2 Large Eddy Simulation

LES resolves the large scales of flow as it can be seen from Fig. 1.1, and the unresolved scales must be modelled. In LES solution to a spatially filtered system of

equations determines the large-scale structures of flow. This allows for this simulation technique to predict for unsteady flows. This is justified as the small scale physical processes are expected to be independent of mean flow perturbations. The unclosed terms of the LES governing equations represent the interaction of the small scales with the large flow structures, and are modelled using subgrid models. As the time dependent nature of turbulent flow is taken care of in LES, unsteady flows such as combustor instabilities can in principle be addressed accurately using this technique. The computational cost for LES remains moderately high but at the same time complex geometries can be addressed, and due to this reason it has been gaining popularity for developing new generation of energy efficient and environmentally friendly combustors. In terms of the flow resolution, it remains an intermediate between DNS and RANS, thus it has less modelling uncertainties in comparison to RANS. However the subgrid scale stresses are unclosed, and are commonly modelled using the Smagorinsky-Lilly model [138], while many studies also use the dynamic Smagorinsky-Lilly model [59, 96]. While these models have been proposed for non-reacting flows, relatively limited effort have been made to assess their applicability in reacting flow simulation. Additionally for a reacting flow the filtered reaction rate is unclosed and must be modelled. In this regard, DNS data can be processed in the context of LES to offer fundamental understanding of existing model performances and allow for the development of new models wherever necessary.

1.2.3 Reynolds Averaged Navier-Stokes Simulation

As mentioned earlier RANS is the most commonly used simulation technique for industrial problems. In this technique an appropriately spatially/temporally averaged flow field is obtained as a solution, since the grid size is greater than the integral length scale l. As such modelling is required for all turbulent scales. This means that all the governing equations must be averaged resulting in unclosed terms, these are the Reynolds stress terms, mean reaction rate and terms representing turbulent transport of heat and species. Closure to these terms is either achieved through algebraic models or additional modelled transport equations are solved. In order to solve for unsteady cases, time average must be redefined as

ensemble average in order to allow for time dependence of mean quantities, where the short time scale modelling must be examined in order to avoid invalidating existing RANS models. The Reynolds stresses are usually taken care of using different versions of $k - \epsilon$ model, however it has the well known limitations in dealing with buoyancy, strain, variable density, mean pressure gradient induced effects and swirling flows. Reynolds stress closure could possibly solve some of the listed problems partially, but at the expense of high cost and without actually addressing the central issue of unsteadiness. Many of the $k - \epsilon$ models are aimed for non reacting flow and as such their applicability to reacting flows is questionable. Recently, studies have examined this problem by using DNS to model for the unclosed terms of the turbulent kinetic energy transport equation [42, 43]. In another study Chakraborty et al. [46] looked into the existing models of dissipation rate transport equation, where the existing modelling methodology for the standard $k - \epsilon$ closure were found unsuitable for turbulent premixed combustion. However it is possible to deal with unsteady flows using unsteady RANS, where the transient solution is acquired at a fraction of the cost of LES. While unsteady RANS has advantage of lowered cost, compared to LES, it is yet unclear how applicable such a technique is to a combustion problem if a flow is not dominated by vortex shedding. This is due to the fact that large scale instabilities remain unresolved in unsteady RANS and thus the implications of modelling uncertainties of the unclosed terms are likely to be more severe than LES simulations.

1.2.4 Modelling of the Reaction Rate Term

The filtered/mean reaction rate term shows strong nonlinear behaviour and cannot be modelled effectively as a function of mean quantities, such as the mean mass fraction, density and temperature. At which point if one were to expand the filtered/mean reaction rate defined based on the Arrhenius law using Taylor series for the temperature fluctuations, it would lead to unclosed correlation of temperature and mean mass fraction. These quantities are unclosed and must be modelled either using an algebraic expression or a transport equation. Additional difficulties via truncation errors occur by only including a few leading

order terms of the Taylor series expansion of filtered/mean reaction rate term, due to its strong nonlinear nature [119]. Furthermore this approach is only valid for cases where the chemical time scales are non negligible compared to the flow time scales, for example supersonic reacting flows or chemical reactions in an atmospheric boundary layer where the temperature remains roughly constant [119]. Thus reaction rate closure is dealt with by using physical analysis, i.e. comparing the chemical and turbulent time scales [119].

In turbulent premixed combustion there are three main branches to modelling the filtered/mean reaction rate term, which are 1) geometric analysis 2) turbulent mixing and 3) one-point statistics [119]. In the geometric analysis the flame front is treated as an evolving geometric surface which is typically linked to the instantaneous iso-surface of a mass or mixture fraction. Additionally in the geometric analysis a flamelet assumption is used, i.e. a flame locally resembles that of a laminar flame. The closure for the filtered/mean reaction rate is given by the product of the available flame area per unit volume (flame surface density) with the mean reaction rate per unit of flame area [119]. In the turbulent mixing models the reaction rate is assumed to be turbulent mixing rates, where the assumption of long turbulent time scales with chemical time scales is assumed [119]. Turbulent mixing rates must be modelled, which is carried out using the scalar dissipation rate. The last method which is the one-point statistics relies on combination of the instantaneous reaction rates given from the Arrhenius law with the joint probability density function [119]. Poinsot and Veynante [119] demonstrate that all three approaches are closely related and all approaches are equally viable. Finally, the FSD (geometrical analysis), scalar dissipation rate (turbulent mixing) and probability density function (one-point statistics) are unclosed, and can be estimated using an algebraic expression or by solving an additional transport equation. In chapter 3 a review of the FSD, wrinkling factor, artificially thickened flame and G equation based approaches are examined.

In this thesis the geometrical analysis will be examined, while concentrating on the FSD closure. In §.3.3 it is demonstrated that the G equation methodology does not provide a suitable link between the flame surface and the temperature field, and in the case of the artificially thickened flame approach a resolved flame is available on a LES grid but its characteristics are modified due to the modification

of thermal diffusivity. The main motivation behind a study into the FSD based closure is that the approach is well established in the context of RANS while still in its infancy in the context of LES. Thus in this thesis the examination of FSD model performances in the context of RANS simulation is firstly sought after and new modelling approaches are identified where existing models are deficient, these models are then extended to LES.

1.3 Aim of the Present Work

The objectives of the current work can be stated as follows:

- To use a DNS database with a wide range of parameters, and to assess the performances of existing algebraic generalised FSD models for reaction rate closure in the context of LES, and to propose a new model for improved performance.
- Assessment of existing models for the curvature and strain rate terms of the generalised FSD transport equation for a range of different Lewis numbers and turbulent Reynolds numbers, for both RANS and LES.
- To propose suitable models for the curvature and strain rate terms of the FSD transport equation based on a detailed *a priori* analysis, so that the models could account for different values of Lewis number and turbulent Reynolds number.
- To analyse the behaviours of turbulent transport term of the generalised FSD transport equation and assess the existing model performances in the context of LES for flames with different values of Lewis number and turbulent Reynolds number.
- To assess the existing models for the density weighted surface filtered displacement speed $\overline{(\rho S_d)}_s$ in the context of LES for flames with different values of Lewis number and turbulent Reynolds number.

1.4 Outline of the Thesis

The rest of this thesis will be organised as follows, chapter 2 will give a brief summary of the mathematical background to the current work and highlight the assumptions. chapter 3 introduces the various modelling approaches related to the reaction rate closure. This will be followed by the chapter 4 where a summary of numerical schemes along with a discussion of the DNS database and finally post-processing techniques associated with filtering and Reynolds averaging process are presented. In chapter 5 existing algebraic models for the generalised FSD in context of LES are assessed, and a newly proposed model is described along with comparison of its performance. The behaviour of the unclosed terms of the generalised FSD transport equation are examined in chapter 6, along with the existing modelling for the subgrid convection term and the surface filtered density weighted displacement speed. This is followed by the model assessment and modelling of the curvature term of the generalised FSD transport equation in chapter 7, in context of both LES and RANS. Similarly in chapter 8 the models of the strain rate term of FSD transport equation are assessed in context of LES and RANS and a new modelling approach is presented. Finally, the main findings of this work are summarised and conclusions are drawn in chapter 9 along with recommendations of future analysis.

Chapter 2

Mathematical Background

In this chapter an overview of the governing equations for the analysis of turbulent reacting flows are presented, along with the assumptions that are made in the current analysis. This is followed by a description of the problem setup. Additionally the derivation of the FSD transport equation is provided.

2.1 Setup of the DNS Domain

A DNS code SENGA [77] was used to generate the DNS database used in the current work. The DNS domain in all of cases was taken to be cuboid. The faces of the computational domain would require proper boundary conditions, these are shown in Fig. 2.1, where a schematic diagram is shown labeling the boundary condition for the various faces. The boundaries in the direction of the mean flame propagation (x_1) were taken to be partially non-reflecting. Further description on the boundary conditions can be found in §.A.3.

The spatial discretisation was carried out using a 10^{th} order central differencing scheme [77]. The order of the spatial discretisation scheme decreases in accuracy gradually in the x_1 direction to a 2^{nd} order one sided scheme at the non-periodic boundaries. This drop in accuracy towards the boundaries of x_1 direction is expected to have little effect on the simulation itself, as the flame which is the focus of the current analysis remains at a substantial distance from the boundaries. A statistically planar unstrained laminar premixed flame is used

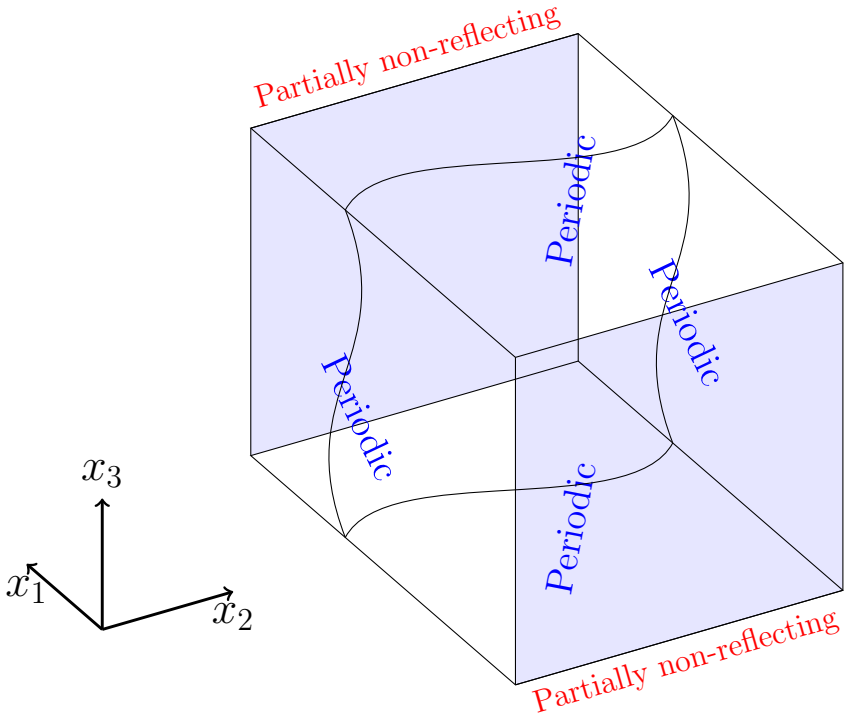

Figure 2.1: A schematic of the DNS domain with each face labeled by its respective boundary conditions.

to initialise the combustion process and the ignition process itself is ignored. The planar laminar flame is then subjected to an initially homogeneous isotropic turbulence flow field, which decays as time progresses. As the planar laminar flame interacts with the turbulence, it stretches and wrinkles leading to a three dimensional structure, which is representative of an actual flame (see Fig. 1.2 for flames that can be studied through DNS).

2.2 Governing Equations

The three dimensional motion of reactive gases is governed by mass, continuity, momentum, energy and species conservation equations. These governing equations in three dimensional form may be stated in Cartesian tensor notation as follows:

$$\frac{\partial \rho}{\partial t} + \frac{\partial}{\partial x_k} \rho u_k = 0 \tag{2.1}$$

$$\frac{\partial \rho u_i}{\partial t} + \frac{\partial}{\partial x_k}\rho u_k u_i = -\frac{\partial P}{\partial x_i} + \frac{\partial}{\partial x_k}\tau_{ki} \tag{2.2}$$

$$\frac{\partial \rho E}{\partial t} + \frac{\partial}{\partial x_k}\rho u_k E = -\frac{\partial}{\partial x_k}u_k P + \frac{\partial}{\partial x_k}\tau_{ki}u_i - \frac{\partial}{\partial x_k}q_k \tag{2.3}$$

$$\frac{\partial \rho Y_\alpha}{\partial t} + \frac{\partial}{\partial x_k}\rho u_k Y_\alpha = \dot{w}_\alpha - \frac{\partial}{\partial x_k}\rho V_{\alpha k} Y_\alpha \text{ where } \alpha = 1, \ldots, N \tag{2.4}$$

where ρ is the density, u_i is the i^{th} component of velocity vector, P is the pressure, E is the stagnation internal energy and Y_α is the mass fraction of species α in the reacting mixture that contains N species in total. The viscous stress tensor takes the following form:

$$\tau_{ij} = \mu\left(\frac{\partial u_i}{\partial x_j} + \frac{\partial u_j}{\partial x_i}\right) - \frac{2}{3}\delta_{ij}\frac{\partial u_k}{\partial x_k} \tag{2.5}$$

where μ is the viscosity, and the heat flux vector q_k is given by:

$$q_k = -\lambda\frac{\partial \hat{T}}{\partial x_k} + \rho\sum_{\alpha=1}^{N} h_\alpha V_{\alpha k} Y_\alpha \tag{2.6}$$

where λ is the thermal conductivity, $\hat{T}$ is the temperature, h_α is the enthalpy of formation of species α and $V_{\alpha k}$ is the diffusion velocity of the species α relative to the mixture. The chemical reaction rate of species α is given by:

$$\dot{w}_\alpha = W_\alpha \sum_{m=1}^{M}\left[(v''_{\alpha,m} - v'_{\alpha,m})A_m \hat{T}^{n_m}\exp\left(\frac{-E_m}{R^0\hat{T}}\right)\prod_{\beta=1}^{N}\left(\frac{\rho Y_\beta}{W_\beta}\right)^{v'_{\beta,m}}\right] \tag{2.7}$$

For a reaction mechanism involving N species and M steps, where W_α is the molar mass of species α and R^0 is the universal gas constant. For step m, $v''_{\alpha,m}$,$v'_{\alpha,m}$ are respectively the product and reactant stoichiometric coefficients, while A_m, n_m, E_m are respectively, the frequency factor, temperature exponent and activation energy. The compatibility condition of the species mass fraction is given as:

$$\sum_{\alpha=1}^{N} Y_\alpha = 1 \tag{2.8}$$

The thermal equation of state is given as follows:

$$P = \rho R^0 \hat{T} \sum_{\alpha=1}^{N} \frac{Y_\alpha}{W_\alpha} \tag{2.9}$$

and the calorific equation of state is:

$$E = C_V \hat{T} + \frac{1}{2} u_k u_k + \sum_{\alpha=1}^{N} h_\alpha^0 Y_\alpha^0 \tag{2.10}$$

where C_V is the mixture heat capacity at constant volume and h_α^0 is the enthalpy of formation of species α. The assumptions made for the current analysis are as follows:

- A single irreversible reaction is assumed, where the reactants go straight to products (i.e. Reactants→Products).
- A reaction progress variable is defined based on the mass fraction of the product species.
$$c = \frac{Y_p - Y_{p0}}{Y_{p\infty} - Y_{p0}} \tag{2.11}$$
- The reaction progress variable which is defined above raises monotonically from 0 to 1 from unburned reactants to fully burnt products.
- A simplified Arrhenius rate law governs the reaction rate for the one-step reaction given as:
$$\dot{w} = B * \rho(1 - c)\exp\left[\frac{-E}{R^0 \hat{T}}\right] \tag{2.12}$$
where $B*$ is the pre-exponential factor and E is the activation energy.
- The diffusion velocities are accounted for by the Fick's Law of diffusion which can be stated as follow:
$$\rho V_{ck} c = -\rho D \frac{\partial c}{\partial x_k} \tag{2.13}$$
The single diffusion coefficient D is a known function of local thermo-chemical state. The simplified chemical treatment leads to the replacement of N-1 conservation equation for the species mass fraction equations by a single conservation

equation for the reaction progress variable.

$$\frac{\partial(\rho c)}{\partial t} + \frac{\partial(\rho u_k c)}{\partial x_k} = \dot{w} + \frac{\partial}{\partial x_k}\left[\rho D \frac{\partial c}{\partial x_k}\right] \tag{2.14}$$

Eq. 2.14 can be written in the kinematic form on a $c = c^*$ isosurface [56] as:

$$\left.\frac{\partial c}{\partial t}\right|_{c=c^*} + u_j|_{c=c^*} \left.\frac{\partial c}{\partial x_j}\right|_{c=c^*} = S_d |\nabla c|_{c=c^*} \tag{2.15}$$

where S_d is the the displacement speed of an isosurface $c = c^*$ given by:

$$S_d = \frac{\dot{w}|_{c=c^*} + \frac{\partial}{\partial x_k}\left[\rho D \frac{\partial c}{\partial x_k}\right]_{c=c^*}}{\rho_{c=c^*} \sqrt{\left|\frac{\partial c}{\partial x_k}\frac{\partial c}{\partial x_k}\right|}\Big|_{c=c^*}} \tag{2.16}$$

- The simplified form for the equations of state are:

$$P = \rho R \hat{T} \tag{2.17}$$

$$E = C_V \hat{T} + \frac{1}{2} u_k u_k + H(1 - c) \tag{2.18}$$

where H is the specific heat of reaction per unit mass of reactants consumed. The heat flux vector can be simplified as:

$$q_k = -\lambda \frac{\partial \hat{T}}{\partial x_k} + \rho D H \frac{\partial c}{\partial x_k} \tag{2.19}$$

- All the equations are non-dimensionalised using a set of reference values based on the principle variables, these are u_0, l_0, $t_0 = l_0/u_0$, ρ_0, T_0. The reference velocity u_0 and the length scale l_0 are taken to be the unstrained laminar flame speed S_L and a function of thermal flame thickness δ_{th} (defined later), respectively. The remainder of the reference variables are the unburned gas density ρ_0 and unburned gas temperature T_0.

- Additionally reference values (i.e. values in the unburned reactants) must be

chosen for the transport coefficients μ_0, λ_0, $\rho_0 D_0$ and C_{V0}. The specific heats C_p and C_V, thermal conductivity λ and ρD are assumed to be constant and not a function of temperature. Furthermore in the mass transfer formulation the Soret and Dufour effects are neglected.

- The reference pressure P_0 is chosen to be representative of dynamic rather than thermo-chemical effects and the relation $P_0 = \rho_0 u_0^2$ is employed. The temperature was normalised as follows:

$$T = \frac{\hat{T} - T_0}{T_{ad} - T_0} \tag{2.20}$$

where $\hat{T}$ denotes the instantaneous dimensional value, T_0 is the unburnt gas temperature and T_{ad} is the adiabatic flame temperature, given as $T_{ad} = T_0 + H/C_{P0}$. The non-dimensional temperature T ranges from 0 to 1 for adiabatic heating in the absence of differential diffusion for low Mach number flows. The internal energy is non-dimensionalised with respect to $C_{P0}T_0$. Under the conditions of low Mach number, adiabatic combustion with unity Lewis number (i.e. $Le = \lambda/\rho C_{P0} D = 1.0$) the non-dimensional temperature equals the reaction progress variable.

Based on the above assumptions it is then possible to rewrite the governing equations in non-dimensional forms, which are given below:

$$\frac{\partial \rho}{\partial t} + \frac{\partial}{\partial x_k}\rho u_k = 0 \tag{2.21}$$

$$\frac{\partial \rho u_i}{\partial t} + \frac{\partial}{\partial x_k}\rho u_k u_i = -\frac{\partial P}{\partial x_i} + \frac{1}{Re}\frac{\partial}{\partial x_k}\tau_{ki} \tag{2.22}$$

$$\begin{aligned}\frac{\partial \rho E}{\partial t} + \frac{\partial}{\partial x_k}\rho u_k E = &-(\gamma-1)\mathrm{Ma}^2\frac{\partial}{\partial x_k}u_k P + \frac{(\gamma-1)\mathrm{Ma}^2}{Re}\frac{\partial}{\partial x_k}\tau_{ki}u_i \\ &+ \frac{\tau}{RePr}\frac{\partial}{\partial x_k}\left[\lambda\frac{\partial T}{\partial x_k}\right] - \frac{\tau}{ReSc}\frac{\partial}{\partial x_k}\left[\rho D\frac{\partial c}{\partial x_k}\right]\end{aligned} \tag{2.23}$$

$$\frac{\partial}{\partial t}\rho c + \frac{\partial}{\partial x_k}\rho u_k c = \dot{w} + \frac{1}{ReSc}\frac{\partial}{\partial x_k}\left[\rho D\frac{\partial c}{\partial x_k}\right] \tag{2.24}$$

The non-dimensional parameter that were used in the above equations are defined as follows:

$$Re = \frac{\rho_0 u_0 l_0}{\mu_0},\ Pr = \frac{\mu_0 C_{P0}}{\lambda_0},\ Sc = \frac{\mu_0}{\rho_0 D_0},\ \mathrm{Ma} = \frac{u_0}{a_0} \tag{2.25}$$

These non-dimensional quantities are the Reynolds number Re, Prandtl number Pr, Schmidt number Sc and the Mach number Ma, where $a_0 = \sqrt{\gamma R T_0}$ is the sonic speed under reference conditions. The ratio of specific heats γ, the heat release parameter τ and α, the Zeldovich number β, and the pre-exponential factor B^* take the following form:

$$\begin{aligned} \gamma &= \frac{C_{P0}}{C_{V0}},\ \tau = \frac{\alpha}{1-\alpha} = \frac{T_{ad} - T_0}{T_0} \\ \beta &= \frac{E(T_{ad} - T_0)}{R T_{ad}^2},\ B^* = \frac{B l_0}{\rho_0 u_0} \exp\left[-\frac{\beta}{\alpha}\right] \end{aligned} \tag{2.26}$$

where the reaction rate term $\dot{w}$ is given as:

$$\dot{w} = B^* \rho (1-c) \exp\left[-\frac{\beta(1-T)}{1-\alpha(1-T)}\right] \tag{2.27}$$

The above equation under the conditions of unity Lewis number, low Mach number and adiabatic conditions, the temperature T can be replaced by reaction progress variable c. The non-dimensional equations of state are given as:

$$P = \frac{1}{\gamma \mathrm{Ma}^2} \rho (1 + \tau T) \tag{2.28}$$

$$E = \frac{1}{\gamma}(1 + \tau T) + \frac{1}{2}(\gamma - 1)\mathrm{Ma}^2 u_k u_k + \tau(1 + c) \tag{2.29}$$

2.3 Surface Density Function

In order to understand the origin of flame surface density, the related quantity of surface density function (SDF) σ must be defined, which is given as:

$$\sigma = |\nabla c| \tag{2.30}$$

The transport equation of the SDF on a given $c = c^*$ isosurface takes the following form:

$$\frac{\partial}{\partial t}|\nabla c| + \frac{\partial}{\partial x_k}u_k|\nabla c| + \frac{\partial}{\partial x_k}N_k S_d|\nabla c| = (\delta_{ij} - N_i N_j)\frac{\partial u_i}{\partial x_j}|\nabla c| + S_d\frac{\partial N_i}{\partial x_i}|\nabla c| \tag{2.31}$$

where N_i is the i^{th} component of the local flame normal vector at the $c = c^*$ isosurface, which is defined as:

$$N_i = -\frac{1}{|\nabla c|}\left.\frac{\partial c}{\partial x_i}\right|_{c=c^*} \tag{2.32}$$

From the above equation it is evident that the local flame normal vector N_i will point towards the reactants.

The fine grained FSD is defined as $\Sigma' = |\nabla c|\delta(c - c^*)$ [18, 121, 151], and the transport equation for the fine grained FSD can be obtained using Eq. 2.31 [18, 121] as:

$$\frac{\partial \Sigma'}{\partial t} + \frac{\partial}{\partial x_k}\Sigma' u_k + \frac{\partial}{\partial x_k}N_k S_d \Sigma' = (\delta_{ij} - N_i N_j)\frac{\partial u_i}{\partial x_j}\Sigma' + S_d\frac{\partial N_i}{\partial x_i}\Sigma' \tag{2.33}$$

Flame surface density is an averaged/filtered quantity and can be defined using the fine grained FSD as follows:

$$\begin{aligned} \Sigma &= \underline{(\Sigma')}\text{: For RANS} \\ \Sigma &= \overline{(\Sigma')}\text{: For LES} \end{aligned} \tag{2.34}$$

where an underline $\underline{(\dots)}$ represent the Reynolds averaging operation and the over bar $\overline{(\dots)}$ represents an LES filtering operation. Boger et al. [8] introduced the concept of a generalised FSD (Σ_{gen}) in such a manner that it no longer depends on the choice of an arbitrary $c = c^*$ isosurface. The generalised FSD is defined in

the following manner [8]:

$$\begin{aligned} \Sigma_{gen} &= \underline{|\nabla c|}\text{: For RANS} \\ \Sigma_{gen} &= \overline{|\nabla c|}\text{: For LES} \end{aligned} \tag{2.35}$$

According to the property of LES filtering $\lim_{\Delta\to 0}\overline{Q} = Q$, where Q is a general quantity and Δ is the LES filter width. Based on this argument it is possible to show that:

$$\lim_{\Delta\to 0}\Sigma_{gen} = \lim_{\Delta\to 0}\overline{|\nabla c|} = |\nabla c| \tag{2.36}$$

Thus the quantities for the SDF and generalised FSD become identical in the limit of zero filter width ($\Delta \to 0$).

2.4 Reaction Rate Closure

In this section reaction rate or the source term in the reaction progress variable transport equation closure based on FSD is discussed. The filtering and averaging of the Instantaneous equation for the transport of reaction progress variable results in unclosed quantities. The LES Favre filtered and Reynolds averaged transport equation of reaction progress variable are given as follows:

$$\overline{\rho}\frac{\partial\tilde{c}}{\partial t} + \bar{\rho}\tilde{u}_j\frac{\partial\tilde{c}}{\partial x_j} = \overline{\frac{\partial}{\partial x_j}\left(\rho D\frac{\partial c}{\partial x_j}\right)} + \overline{\dot{w}} - \frac{\partial}{\partial x_j}\left[\bar{\rho}\left(\widetilde{u_j c} - \tilde{u}_j\tilde{c}\right)\right] \tag{2.37}$$

$$\underline{\rho}\frac{\partial\underset{\sim}{c}}{\partial t} + \underline{\rho}\underset{\sim}{u}_j\frac{\partial\underset{\sim}{c}}{\partial x_j} = \underline{\frac{\partial}{\partial x_j}\left(\rho D\frac{\partial c}{\partial x_j}\right)} + \underline{\dot{w}} - \frac{\partial}{\partial x_j}\underline{\left[\rho(u_j'' c'')\right]} \tag{2.38}$$

where an undertilde $\underset{\sim}{(\ldots)}$ represents a Favre averaged variable. The terms on the right hand side of Eqs. 2.37 and 2.38 are unclosed and must be modelled. The first term of the right hand side is referred to as the filtered/mean molecular diffusion term, second is the filtered/mean reaction rate term and the last term denotes the subgrid convection term/Reynolds transport of reaction variable. The expression $(\widetilde{u_j c} - \tilde{u}_j\tilde{c})$ which appears in the last term of Eq. 2.37 is most commonly referred to as the subgrid scalar flux in the j^{th} direction. Similarly, the expression $\left(\underline{\rho u_j'' c''}\right)/\underline{\rho}$ is referred to as the Reynolds scalar flux in the j^{th}

direction. The subgrid scalar flux and the Reynolds scalar flux are known to be gradient type and counter gradient in flows with heat release, depending on the relative magnitude of turbulence intensity and heat release parameter [66, 149, 150, 155]. The modelling of the combined filtered/mean reaction rate and molecular diffusion term, can be carried out using the density weighted surface averaged displacement speed $\overline{(\rho S_d)}_s$ and FSD, in the following manner:

$$\overline{\dot{w}} + \overline{\frac{\partial}{\partial x_i}\left(\rho D \frac{\partial c}{\partial x_i}\right)} = \overline{(\rho S_d)}_s \Sigma_{sg} \tag{2.39}$$

In the limiting case of a statistically planar quasi-laminar flame the density weighted surface averaged displacement speed $\overline{(\rho S_d)}_s$ can be expressed in the following manner [8, 66, 68], which is only relevant for corrugated flamelets regime where flame curvature effects are relatively weak:

$$\overline{(\rho S_d)}_s = \rho_0 S_L \tag{2.40}$$

In a similar manner to the filtered reaction rate closure shown in Eq. 2.39 can be applied to the mean reaction rate in Reynolds averaged approach:

$$\underline{\left[\dot{w} + \frac{\partial}{\partial x_i}\left(\rho D \frac{\partial c}{\partial x_i}\right)\right]} = \underline{(\rho S_d)}_s \Sigma \tag{2.41}$$

Although, in the case of RANS the mean molecular diffusion term can be assumed to be negligible (i.e. $\underline{(\nabla.(\rho D \nabla c))} \approx 0$) [40] which allows for the following simplification of Eq. 2.41:

$$\underline{(\dot{w})} = \underline{(\rho S_d)}_s \Sigma = I_0 \rho_0 S_L \Sigma \tag{2.42}$$

where I_0 is a correction factor which takes care of the modification of laminar flame due to the effects of strain and curvature.

The physical meaning behind the expression $\rho_0 S_L$ is representative of the reactant consumption per unit area. Laminar flame speed is defined in the following manner:

$$S_L = \frac{1}{\rho_0} \int_{-\infty}^{+\infty} \dot{w} dx \tag{2.43}$$

In this context it is worth mentioning a quantity known as the consumption speed S_c, which is commonly used in combustion literature:

$$S_c = -\frac{1}{\rho_0}\int_{-\infty}^{+\infty} \dot{w}\vec{N}.d\vec{x} \tag{2.44}$$

From the definitions of displacement speed S_d (Eq. 2.16), laminar flame speed S_L (Eq. 2.43) and consumption speed S_c (Eq. 2.44) it is clear that they represent different physical ideas. The displacement speed measures the flame front speed relative to the flow. The consumption speed represents the speed at which reactants are consumed. It is clear that the displacement speed is a local quantity, unlike the consumption speed and laminar flame speeds which are global quantities. The relationship between S_d, S_L and S_c is also not straightforward for general conditions of flame propagation. Although there are special cases where the relationship can be comparable, for example in the limiting case of a planar laminar flame, the volume integrated consumption speed S_c is equal to the laminar flame speed S_L.

2.4.1 Limitations

The closure of the filtered/mean reaction rate using FSD has limitations. This is due to the FSD approach implicitly assuming an existing flame. The FSD approach becomes invalid when there are significant discontinuities of the flame surface such as pocket formation and flame quenching. The FSD based closure implicitly requires flamelet assumption and thus this approach cannot be used for conditions where the large scale turbulent time scale remains much smaller than the chemical time scale (alternatively, flame thickness remains much larger than the reaction zone thickness (i.e. $Da \ll 1$, $Ka \gg 1$).

2.5 FSD Transport equation

2.5.1 Fine grained FSD Transport Eqaution

In this section of the chapter the derivation of the fine grained FSD is carried out, according to Pope [121]. Let the points $X[x, y, t]$ represent the flame surface, defined by the $c = c^*$ isosurface, where $x, y \in U$ are local coordinates parametrising the flame surface and U denotes the flame surface. It is then possible to define the fine grained surface to volume ratio $\Sigma'(c; \vec{x})$ as:

$$\Sigma'(c^*, \vec{x}, t) \equiv \iint_U \delta(\vec{x} - X[x, y, t]) A(x, y, t) dxdy \tag{2.45}$$

where

$$A(x, y, t) = \left| \frac{\partial X}{\partial x} \times \frac{\partial X}{\partial y} \right| \tag{2.46}$$

$A(x, y, t)dxdy$ represents a differential element of area, and when integrating Σ' over a volume results in the instantaneous flame surface area for the given volume. Differentiating Eq. 2.45 with respect to time results in the following expression:

$$\frac{\partial \Sigma'}{\partial t} = \iint_U \frac{\partial}{\partial t}(\delta(\vec{x} - X[x, y, t])) A(x, y, t) dxdy \tag{2.47}$$

It may be shown that since $\vec{x}$ is an independent variable and $\dot{X}_t$ is not a function of $\vec{x}$,

$$\frac{\partial}{\partial t}\delta(\vec{x} - X[x, y, t]) = -\frac{\partial X_i}{\partial t}\frac{\partial}{\partial x_i}\delta(\vec{x} - X[x, y, t]) = -\frac{\partial}{\partial x_i}(\dot{X}_i \delta(\vec{x} - X[x, y, t])) \tag{2.48}$$

Since $A(x, y, t)dxdy$ is the local differential element of area, $\dot{S} = \dot{A}/A$ represents the local surface stretch rate. Using the definition for $\dot{S}$ it is possible to show

that:

$$\frac{\partial \Sigma'}{\partial t} + \frac{\partial}{\partial x_i} \iint_U \dot{X}_i[x,y,t]\delta(\vec{x} - X[x,y,t])dxdy = \iint_U \dot{S}(x,y,t)\delta(\vec{x} - X[x,y,t])A(x,y,t)dxdy \tag{2.49}$$

If a quantity $R(x,y,t)$ is defined on the flame surface then it is possible to define $R^*(\vec{x},t)$ in the following manner:

$$R^*(\vec{x},t) = \iint_U R(x,y,t)\delta(\vec{x} - X[x,y,t])A(x,y,t)dxdy \tag{2.50}$$

If one then integrates the above equation over a volume V it leads to the following equation:

$$\begin{aligned} \iiint_V R^*(\vec{x},t)d\vec{x} &= \iint_U \left[\iiint_V \delta(\vec{x} - X[x,y,t]d\vec{x}) \right] R(x,y,t)A(x,y,t)dxdy \\ &= \iint_{U_V} R(x,y,t)A(x,y,t)dxdy \end{aligned} \tag{2.51}$$

In the above equation U_V denotes the subset of the parameter space corresponding to the element of the surface within the volume V. The last expression is the surface integral of R(x,y,t), and hence the quantity:

$$\frac{\iiint_V R^*(\vec{x},t)d\vec{x}}{\iiint_V \Sigma' d\vec{x}} \tag{2.52}$$

which is the surface average of $R(x,y,t)$. This however only stands for any volume V, and thus also in the limit of volume tending towards zero, so $R^*(\vec{x},t)/\Sigma'(\vec{x},t)$ must be the local value of R, conditional of the flame surface being at the point $\vec{x}$ and time t. This quantity will be denoted as $R_{\vec{x}=X}$, and it becomes undefined if the flame is not present at $\vec{x}$ and t.

It is then possible to write the following expression for the fine grained FSD:

$$\frac{\partial \Sigma'}{\partial t} + \frac{\partial}{\partial x_i}\left(\Sigma' \dot{X}_i\right)_{\vec{x}=\vec{X}} = \Sigma'\left(\dot{S}\right)_{\vec{x}=\vec{X}} \tag{2.53}$$

The surface velocity can be decomposed as shown:

$$\vec{\dot{X}} = \vec{u} + S_d \vec{N} \tag{2.54}$$

where $\vec{u}$ is the flow velocity, $\vec{N} = -\nabla c/|\nabla c|$ is the flame surface normal pointing into the reactants and S_d is the flame displacement speed.

The flame stretch $\dot{S}$ can be split into the contribution from fluid straining and flame curvature and propagation in the following manner:

$$\dot{S} = a_T + S_d \frac{\partial N_i}{\partial x_i} \tag{2.55}$$

where the surface stretch due to tangential strain rate a_T by fluid motion can be expressed as:

$$a_T = \left(\delta_{ij} - N_i N_j\right) \left.\frac{\partial u_i}{\partial x_j}\right|_{c=c^*} \tag{2.56}$$

The surface stretch rate due to flame curvature can be written as:

$$S_d \frac{\partial N_i}{\partial x_i} = 2 S_d \kappa_m \tag{2.57}$$

where κ_m is the mean curvature of the flame surface given by:

$$\kappa_m = \frac{1}{2} \left.\frac{\partial N_i}{\partial x_i}\right|_{c=c^*} \tag{2.58}$$

According to the above expression a positive term corresponds to the flame surface that is convex towards the reactants and vice versa.

Candel and Poinsot [18] have taken an alternative approach to derive the FSD transport equation. In this approach the fine grained FSD was defined as:

$$\Sigma' = \frac{\delta A}{\delta V} \tag{2.59}$$

In the above equation δA and δV are elemental flame surface area and volume of the concerned element, respectively. Candel and Poinsot [18] derived a transport equation of the flame surface area to volume ratio ($\delta A/\delta V$) based on transport theorems of area and volume. This transport equation for $\delta A/\delta V$ is identical to the fine grained FSD transport equation given by Eq. 2.53.

2.5.2 SDF and FSD transport equations

In this section the interrelationships between the SDF and FSD transport equations will be discussed. The fine grained FSD Σ' is defined as [151]:

$$\Sigma' = |\nabla c|\delta(c - c^*) \tag{2.60}$$

In the above equation, c^* is an arbitrary value if c is chosen *a priori* as a location representative of the flame. This chosen $c = c^*$ isosurface will then be considered the flame surface. c^* is neither a function of time nor space. Using these assumptions it is possible to write the following expression for the fine grained FSD:

$$\frac{\partial \Sigma'}{\partial t} = \delta(c - c^*)\frac{\partial |\nabla c|}{\partial t} + |\nabla c|\frac{\partial \delta(c - c^*)}{\partial c}\frac{\partial c}{\partial t} \tag{2.61}$$

Applying the property of Dirac delta function to the above expression it is possible to come up with the following expression:

$$\frac{\partial \Sigma'}{\partial t} = \delta(c - c^*)\frac{\partial |\nabla c|}{\partial t} - |\nabla c|\frac{\partial \delta(c - c^*)}{\partial c^*}\frac{\partial c}{\partial t} \tag{2.62}$$

In the above equation both $\partial c/\partial t$ and $|\nabla c|$ are independent of c^* the above expression can be simplified as follows:

$$\frac{\partial \Sigma'}{\partial t} = \delta(c - c^*)\frac{\partial |\nabla c|}{\partial t} - \frac{\partial}{\partial c^*}\left[|\nabla c|\frac{\partial c}{\partial t}\delta(c - c^*)\right] \tag{2.63}$$

Following the above procedure it is then possible to write:

$$\frac{\partial \Sigma'}{\partial x_j} = \delta(c - c^*)\frac{\partial |\nabla c|}{\partial x_j} - \frac{\partial}{\partial c^*}\left[|\nabla c|\frac{\partial c}{\partial x_j}\delta(c - c^*)\right] \tag{2.64}$$

The fluid velocities are independent of the choice of c^* this leads to the following expression:

$$\frac{\partial(u_j\Sigma')}{\partial x_j} = \frac{\partial(u_j|\nabla c|)}{\partial x_j}\delta(c-c^*) - \frac{\partial}{\partial c^*}\left[|\nabla c|u_j\frac{\partial c}{\partial x_j}\delta(c-c^*)\right] \tag{2.65}$$

By using the above derivations it is possible to express the left hand side of the FSD transport equation:

$$\begin{aligned}\frac{\partial\Sigma'}{\partial t} + \frac{\partial(u_j\Sigma')}{\partial x_j} = &\left[\frac{\partial|\nabla c|}{\partial t} + \frac{\partial(u_j|\nabla c|)}{\partial x_j}\right]\delta(c-c^*) \\ &- \frac{\partial}{\partial c^*}\left[|\nabla c|\left\{\frac{\partial c}{\partial t} + u_j\frac{\partial c}{\partial x_j}\right\}\delta(c-c^*)\right]\end{aligned} \tag{2.66}$$

If one were to compare the above equation with the SDF transport equation it becomes clear that identical terms appear in both equations. In order to do this, it is required to show the derivation of the SDF transport equation, this can be done by starting with the reaction progress variable transport equation and then rearranging it as follows:

$$\rho\frac{\partial c}{\partial t} + \rho u_j\frac{\partial c}{\partial x_j} = \dot{w} + \frac{\partial}{\partial x_j}\left[\rho D\frac{\partial c}{\partial x_j}\right] \tag{2.67}$$

The above equation is equivalent to:

$$\frac{\partial c}{\partial t} + u_j\frac{\partial c}{\partial x_j} = S|\nabla c| \tag{2.68}$$

where S takes the following form:

$$S = \frac{\dot{w} + \nabla.(\rho D\nabla c)}{\rho|\nabla c|} \tag{2.69}$$

If Eq. 2.68 were then to be differentiated on both sides with respect to x_k and followed by a multiplication by $\partial c/\partial x_k$, which is then divided on both sides by $|\nabla c|$ will result in the derivation of the SDF transport equation, as shown [22]:

$$\frac{\partial\sigma}{\partial t} + \frac{\partial(u_k\sigma)}{\partial x_k} = (\delta_{ij} - m_i m_j)\frac{\partial u_i}{\partial x_j}\sigma + S\frac{\partial m_i}{\partial x_i}\sigma - \frac{\partial(Sm_i\sigma)}{\partial x_i} \tag{2.70}$$

where $\vec{m} = -\nabla c/|\nabla c|$. By using Eq. 2.68 and Eq. 2.70 it is possible to rewrite Eq.2.66 as [22]:

$$\begin{aligned}\frac{\partial \Sigma'}{\partial t} + \frac{\partial (u_i \Sigma')}{\partial x_j} = &\left[(\delta_{ij} - m_i m_j)\frac{\partial u_i}{\partial x_j}\sigma + S\nabla.\vec{m}\sigma - \nabla.(S\vec{m}\sigma)\right]\delta(c-c^*) \\ &- \frac{\partial}{\partial c^*}[S\sigma^2\delta(c-c^*)]\end{aligned} \tag{2.71}$$

At this point it is important to use the identity:

$$-\frac{\partial (S m_i \Sigma')}{\partial x_i} = -\frac{\partial (S m_i \sigma)}{\partial x_i}\delta(c-c^*) - S m_i \sigma \frac{\partial [\delta(c-c^*)]}{\partial c}\frac{\partial c}{\partial x_i} \tag{2.72}$$

which can be rewritten by using the relationships $\vec{m} = -\nabla c/|\nabla c|$ and $\sigma^2 = \nabla c.\nabla c$ as:

$$-\frac{\partial (S m_i \Sigma')}{\partial x_i} = -\frac{\partial (S m_i \sigma)}{\partial x_i}\delta(c-c^*) - S\sigma^2 \frac{\partial [\delta(c-c^*)]}{\partial c} \tag{2.73}$$

It is then possible to use Eqs. 2.72 and 2.73 to write the following expression for the fine grained FSD transport using the relationship $\Sigma' = |\nabla c|\delta(c-c^*)$ [22]:

$$\frac{\partial \Sigma'}{\partial t} + \frac{\partial (u_k \Sigma')}{\partial x_k} = (\delta_{ij} - m_i m_j)\frac{\partial u_i}{\partial x_j}\Sigma' + S\frac{\partial m_i}{\partial x_i}\Sigma' - \frac{\partial (S m_i \Sigma')}{\partial x_i} \tag{2.74}$$

The value of Σ' is identical to zero when $c \neq c^*$ due to the property of delta function $\delta(c-c^*)$ [22]. The transport equation for Σ' is only applicable for a given $c = c^*$ isosurface, and on this isosurface $\vec{m}$ reduces to the flame normal vector $\vec{N}$ as [22]:

$$\vec{N} = -\left.\frac{\nabla c}{|\nabla c|}\right|_{c=c^*} = \vec{m}_{c=c^*} \tag{2.75}$$

and S becomes the local flame displacement speed:

$$S_d = \left.\frac{\dot{w} + \nabla.(\rho D \nabla c)}{\rho |\nabla c|}\right|_{c=c^*} = S_{c=c^*} \tag{2.76}$$

Using Eqs. 2.74, 2.75 and 2.76, it is possible to derive the following equation for the fine grained FSD [22]:

$$\frac{\partial \Sigma'}{\partial t} + \frac{\partial (u_k \Sigma')}{\partial x_k} = (\delta_{ij} - N_i N_j)\frac{\partial u_i}{\partial x_j}\Sigma' + S_d \frac{\partial N_i}{\partial x_i}\Sigma' = \frac{\partial (S_d N_i \Sigma')}{\partial x_i} \tag{2.77}$$

Strain rate term	$(\delta_{ij} - N_i N_j)\frac{\partial u_i}{\partial x_j}\lvert\nabla c\rvert = a_T\sigma$
Curvature term	$S_d\nabla.\vec{N}\sigma = 2\kappa_m S_d\sigma$
Propagation term	$-\nabla.(S_d\vec{N}\sigma) = -\frac{\partial(S_d N_i\sigma)}{\partial x_i}$
Curvature and Propagation term	$S_d\nabla.\vec{N}\sigma - \nabla.(S_d\vec{N}\sigma) = S_d\frac{\partial N_i}{\partial x_i}\sigma - \frac{\partial(S_d N_k\sigma)}{\partial x_k}$

Table 2.1: Important terms of the SDF transport equation and the associated terminology.

This is exactly the same as the transport equation for the fine grained FSD derived by Pope [121] and Candel and Poinsot [18]. For a given $c = c^*$ isosurface the SDF transport equation on a c isosurface can be expressed as:

$$\frac{\partial\sigma}{\partial t} + \frac{\partial(u_k\sigma)}{\partial x_k} = (\delta_{ij} - N_i N_j)\frac{\partial u_i}{\partial x_j}\sigma + S_d\frac{\partial N_i}{\partial x_i}\sigma = \frac{\partial(S_d N_i\sigma)}{\partial x_i} \tag{2.78}$$

The above two equations are similar. The terms of the SDF transport equation (Eq. 2.78) and their associated naming convention is shown in Table. 2.1.

Although the fine grained FSD $\Sigma' = |\nabla c|\delta(c - c^*)$ is only relevant on a $c = c^*$ isosurface, when it is either LES filtered or Reynolds averaged it becomes a field quantity [8]. LES filtering the FSD can be written as:

$$\Sigma_{sg} = \int_{-\infty}^{\infty} |\nabla c|\delta(c - c^*)G(\vec{x} - \vec{x}')d\vec{x}' \tag{2.79}$$

$$\Sigma_{gen} = \int_0^1 \Sigma_{sg}dc^* = \overline{|\nabla c|} \tag{2.80}$$

where $G(\vec{x}-\vec{x}')$ is the LES filtering function. Based on the expression in Eqs. 2.79 and 2.80 one can conclude that both Σ_{sg} and Σ_{gen} are field quantities. Similar analysis can be carried out for RANS which would also give rise to field quantities.

In the strict flamelet limit the reaction progress variable consists of only the reactants and products. Under this limit the reaction progress variable can be described using the Heaviside function [8, 148, 152, 153]. Using the Heaviside function it is possible to define a reduced binarised reaction progress variable c_{red}

as follows:

$$c_{red} = H(c - c^*) \tag{2.81}$$

It is then possible to write the following expression for the gradient of the reduced reaction progress variable c_{red}:

$$\nabla c_{red} = \nabla c \delta(c - c^*) \tag{2.82}$$

The above expression can be used to define the Reynolds averaged FSD Σ and LES filtered FSD Σ_{sg} as follows:

$$\Sigma = \underline{(|\nabla c_{red}|)} \text{ and } \Sigma_{sg} = \overline{(|\nabla c_{red}|)} \tag{2.83}$$

From the above expressions it is clear that both the Reynolds averaged FSD Σ and LES filtered FSD Σ_{sg} are continuous properties of three-dimensional space. For a thin flame surface the reaction progress variable field can be thought of as a binarised scalar field given by the reduced reaction progress variable c_{red}. If one were to assume that the $c = c_{red}$, which is the case for thin flames, then it is possible to write:

$$\Sigma = \underline{(|\nabla c_{red}|)} = \underline{(|\nabla c|)} \text{ and } \Sigma_{sg} = \overline{(|\nabla c_{red}|)} \approx \overline{(|\nabla c|)} = \Sigma_{gen} \tag{2.84}$$

Reynolds averaged FSD Σ is equal to the generalised FSD Σ_{gen} in the limiting case of very large filter width (i.e. $\lim_{\Delta \to \infty} \overline{|\nabla c|} = \underline{(|\nabla c|)}$), and at this limiting condition Σ transport equation can also be interpreted as the generalised FSD transport equation. Conversely, it is possible to describe the generalised FSD Σ_{gen} as being equal to SDF for the limiting condition of zero LES filter width (i.e. $\lim_{\Delta \to 0} \overline{|\nabla c|} = |\nabla c|$), and the transport equation for the generalised FSD Σ_{gen} reduces to the SDF transport equation.

2.6 Unclosed FSD Transport Equation

2.6.1 FSD Transport Eqaution for LES

By LES filtering of Eq. 2.53 it is possible to derive the unclosed transport equation for Σ_{sg}:

$$\frac{\partial \Sigma_{sg}}{\partial t} + \frac{\partial}{\partial x_i}\overline{\left\{\Sigma' \dot{X}_i\right\}}_{\vec{x}=\vec{X}} = \overline{\left\{\Sigma' \dot{S}\right\}}_{\vec{x}=\vec{X}} \tag{2.85}$$

Examining the term $\overline{\left\{\Sigma' \dot{X}_i\right\}}_{\vec{x}=\vec{X}}$ it is possible to write:

$$\begin{aligned}\overline{\left\{\Sigma' \dot{X}_i\right\}}_{\vec{x}=\vec{X}} &= \iiint_{V_{sg}} G(\vec{x}' - \vec{x}) \iint_x \dot{X}_i(x,y,t)\delta(\vec{x}' - \vec{X}(x,y,t))A(x,y,t)dxdyd\vec{x}' \\ &= \iint_{U_{sg}} G(\vec{X}[x,y,t] - \vec{x})\dot{X}_i[x,y,t]A(x,y,t)dxdy\end{aligned} \tag{2.86}$$

where U_{sg} is the subset of parameter space corresponding to the element of the flame surface within the subgrid volume. $\overline{\left\{\Sigma' \dot{X}_i\right\}}_{\vec{x}=\vec{X}}$ is a term that is a filter weighted surface integral of $\dot{X}_i$. In physical terms, this corresponds to an LES flame surface integral of $\dot{X}_i$. On division by FSD $\overline{\{\Sigma'\Xi\}}\vec{x} = \vec{x}$ becomes an average of the quantity $\dot{X}_i$ over the flame surface, weighted by the LES filter. It is possible to use the definition of a surface weighted average to rewrite Eq. 2.85 as follows:

$$\frac{\partial \Sigma_{sg}}{\partial t} + \frac{\partial}{\partial x_i}\left[\overline{(\dot{X})}_s \Sigma_{sg}\right] = \overline{(\dot{S})}_s \Sigma_{sg} \tag{2.87}$$

where $\overline{(\dots)}_s$ denotes the surface (area) weighted filtering, which is defined for an arbitrary variable Q as follows:

$$\overline{(Q)}_s = \frac{\overline{Q\Sigma'}}{\Sigma'} \tag{2.88}$$

Strain rate term	$\overline{\left((\delta_{ij} - N_i N_j)\frac{\partial u_i}{\partial x_j}\right)}_s \Sigma_{sg} = \overline{(a_T)}_s \Sigma_{sg}$
Curvature term	$\overline{\left(S_d \frac{\partial N_i}{\partial x_i}\right)}_s \Sigma_{sg} = 2\overline{(S_d \kappa_m)}_s \Sigma_{sg}$
Propagation term	$-\frac{\partial}{\partial x_i}[\overline{(S_d N_i)}_s \Sigma_{sg}]$
Curvature and Propagation term	$\overline{\left(S_d \frac{\partial N_i}{\partial x_i}\right)}_s \Sigma_{sg} - \frac{\partial}{\partial x_i}[\overline{(S_d N_i)}_s \Sigma_{sg}]$
Subgrid convection term	$\frac{\partial}{\partial x_i}[\overline{(u_i)}_s - \tilde{u}_i]\Sigma_{sg}$
Subgrid flux of FSD in i^{th} direction	$[\overline{(u_i)}_s - \tilde{u}_i]\Sigma_{sg}$
FSD transport term in i^{th} direction	$[\overline{(u_i)}_s - \tilde{u}_i]$

Table 2.2: Terms of importance for the LES filtered transport equation of the FSD.

Based on the definitions for $\dot{X}_i$ and $\dot{S}$ the following form may be derived for the unclosed transport equation:

$$\frac{\partial \Sigma_{sg}}{\partial t} + \frac{\partial(\tilde{u}_j \Sigma_{sg})}{\partial x_j} + \frac{\partial}{\partial x_i}[\overline{(u_i)}_s - \tilde{u}_i]\Sigma_{sg} = \overline{\left((\delta_{ij} - N_i N_j)\frac{\partial u_i}{\partial x_j}\right)}_s \Sigma_{sg} - \frac{\partial}{\partial x_i}[\overline{(S_d N_i)}_s \Sigma_{sg}] + \overline{\left(S_d \frac{\partial N_i}{\partial x_i}\right)}_s \Sigma_{sg} \tag{2.89}$$

where $\tilde{u}_i$ is the Favre filtered velocity in the i^{th} direction, which is defined as:

$$\tilde{u}_i = \frac{\overline{\rho u_i}}{\overline{\rho}} \tag{2.90}$$

The important terms of Eq. 2.89 have been given in Table. 2.2 along with the naming convention that is commonly used.

The generalised FSD transport equation can be derived by simply filtering

the instantaneous transport equation for the SDF given in Eq. 2.78 as:

$$\frac{\partial \Sigma_{gen}}{\partial t} + \frac{\partial (\tilde{u}_j \Sigma_{gen})}{\partial x_j} + \frac{\partial}{\partial x_i}[\overline{(u_i)}_s - \tilde{u}_i]\Sigma_{gen} = \overline{\left((\delta_{ij} - N_i N_j)\frac{\partial u_i}{\partial x_j}\right)}_s \Sigma_{gen} - \frac{\partial}{\partial x_i}[\overline{(S_d N_i)}_s \Sigma_{gen}] + \overline{\left(S_d \frac{\partial N_i}{\partial x_i}\right)}_s \Sigma_{gen} \tag{2.91}$$

In the above equation the surface weighted filtered value can be defined for an arbitrary variable Q, according to [8], in the following manner:

$$\overline{(Q)}_s = \frac{\overline{Q|\nabla c|}}{\overline{|\nabla c|}} \tag{2.92}$$

2.6.2 FSD Transport Equation for RANS

The FSD is defined for RANS as:

$$\Sigma = \underline{[|\nabla c|\delta(c - c^*)]} \tag{2.93}$$

The above equation can be written as:

$$\Sigma = \underline{|\nabla c|\delta(c - c^*)} = \int_0^\infty \int_0^1 |\nabla c|\delta(c - c^*)P(c, |\nabla c|)dcd(|\nabla c|) \tag{2.94}$$

where $P(c, |\nabla c|)$ is a joint pdf of c and $|\nabla c|$ which can be written in terms of marginal pdfs as:

$$P(c, |\nabla c|) = P(|\nabla c|| \, c = c^\circ)P(c^\circ) \tag{2.95}$$

where $P(|\nabla c|| \, c = c^\circ)$ is the conditional pdf of $|\nabla c|$ at $c = c^\circ$. Using the Eqs. 2.94 and 2.95 it possible to write:

$$\Sigma = \underline{|\nabla c|| \, c = c^*}P(c^*) \;\; \because \;\; \underline{|\nabla c|| \, c = c^\circ} = \int_0^\infty |\nabla c|P(|\nabla c|| \, c = c^\circ)d(|\nabla c|) \tag{2.96}$$

The surface average in the RANS context can be defined as:

$$\underline{(Q)}_s = \frac{\overline{Q\Sigma'}}{\overline{\Sigma'}} = \frac{\overline{Q\,|\nabla c||_{c=c^*}}}{\underline{|\nabla c||_{c=c^*}}} \tag{2.97}$$

Using the definition in Eq. 2.96 and 2.97, while Reynolds averaging the fine grained FSD transport equation in Eq. 2.77 it is possible to derive the FSD transport equation for RANS:

$$\begin{aligned}\frac{\partial \Sigma}{\partial t} + \frac{\partial (\underset{\sim}{u}_j \Sigma)}{\partial x_j} + \frac{\partial}{\partial x_i}[\underline{(u_i)}_s - \underset{\sim}{u}_i]\Sigma \\ = \underline{\left[(\delta_{ij} - N_i N_j)\frac{\partial u_i}{\partial x_j}\right]}_s \Sigma - \frac{\partial}{\partial x_i}[\underline{(S_d N_i)}_s \Sigma] + \underline{\left(S_d \frac{\partial N_i}{\partial x_i}\right)}_s \Sigma\end{aligned} \tag{2.98}$$

The transport equation for FSD in RANS and LES are quite similar. In the above equation $\underset{\sim}{u}_i$ is the Favre averaged velocity in the i^{th} direction given by:

$$\underset{\sim}{u}_i = \frac{\overline{\rho u_i}}{\underline{\rho}} \tag{2.99}$$

The terms given in Table. 2.2 are equally applicable where only change that is required is notation for LES filtering with Reynolds averaging.

2.7 Kinematic Form of the Reaction Progress Variable

The reaction progress variable transport equation given by Eq. 2.15 can be rewritten in the following manner [56]:

$$\left.\frac{\partial c}{\partial t}\right|_{c=c^*} + u_j \left.\frac{\partial c}{\partial x_j}\right|_{c=c^*} = S_d |\nabla c|_{c=c^*} \tag{2.100}$$

Eq. 2.100 is the kinematic form of the reaction progress variable equation and can only be valid for a given $c = c^*$ isosurface. The above equation is actually

equivalent to the level set equation (G equation) [107]:

$$\frac{\partial G}{\partial t} + u_j \frac{\partial G}{\partial x_j} = S_d |\nabla G| \tag{2.101}$$

2.7.1 Analysis of the Kinematic Form

The molecular diffusion term in Eq. 2.15 can be split in the following manner:

$$\nabla.(\rho D \nabla c)|_{c=c^*} = \vec{N}.\nabla(\rho D \vec{N}.\nabla c)|_{c=c^*} - \rho D |\nabla c| \nabla.\vec{N}|_{c=c^*} \tag{2.102}$$

where the first and second terms on the right hand side correspond to normal and tangential diffusion respectively. Using the same approach the displacement speed S_d can be decomposed as:

$$S_d = S_r + S_n + S_t \tag{2.103}$$

where S_r is the reaction rate component of displacement speed S_d, and is defined as:

$$S_r = \left. \frac{\dot{w}}{\rho |\nabla c|} \right|_{c=c*} \tag{2.104}$$

whereas S_n is the normal diffusion component of displacement speed S_d defined for $c = c^*$ isosurfaces as:

$$S_n = \left. \frac{\vec{N}.\nabla(\rho D \vec{N}.\nabla c)}{\rho |\nabla c|} \right|_{c=c*} \tag{2.105}$$

and S_t is the tangential diffusion component of displacement speed S_d, expressed as:

$$S_t = -2 D \kappa_m \tag{2.106}$$

In premixed turbulent combustion modelling it is common to combine the reaction and normal diffusion components of displacement speed S_d, which can be written as:

$$S_{RN} = S_r + S_n \tag{2.107}$$

By using the decomposition shown in Eq. 2.103, it is possible to rewrite Eq. 2.100 and 2.101 in the following manner:

$$\left.\frac{\partial c}{\partial t}\right|_{c=c^*} + u_j \left.\frac{\partial c}{\partial x_j}\right|_{c=c^*} = S_{RN}|\nabla c|_{c=c^*} - 2D\kappa_m|\nabla c|_{c=c^*} \tag{2.108}$$

$$\frac{\partial G}{\partial t} + u_j\frac{\partial G}{\partial x_j} = S_{RN}|\nabla G| - 2D\kappa_m|\nabla G| \tag{2.109}$$

The above equations can then be normalised with respect to Kolmogorov time, length and velocity scales:

$$t^+ = \frac{t}{t_\eta},\ u_i^+ = \frac{u_i}{v_\eta},\ x_i^+ = \frac{x_i}{\eta},\ \kappa_m^+ = \eta\kappa_m,\ \nabla^+ = \eta\nabla \tag{2.110}$$

Thus the normalised form of the kinematic reaction progress variable and G equation can be written as:

$$\left.\frac{\partial c}{\partial t^+}\right|_{c=c^*} + u_j^+ \left.\frac{\partial c}{\partial x_j^+}\right|_{c=c^*} = \frac{S_{RN}}{v_\eta}|\nabla c|_{c=c^*} - \frac{2D\kappa_m}{\nu}|\nabla c|_{c=c^*} \tag{2.111}$$

$$\frac{\partial G}{\partial t^+} + u_j^+\frac{\partial G}{\partial x_j^+} = \frac{S_{RN}}{v_\eta}|\nabla G| - \frac{2D\kappa_m}{\nu}|\nabla G| \tag{2.112}$$

Peters [107] argued that the derivatives, normalised velocities u_i^+ and non dimensional curvature κ_m^+ are of the order unity, as Kolmogorov eddies perturb the flow field as well as the c and G fields. For hydrocarbon flames the Schmidt number (ν/D) is close to unity. Based on two dimensional [108] and three dimensional [24, 25] DNS studies it was shown that S_{RN} is of the same order of magnitude as $S_L(1+\tau c^*)$ on a $c = c^*$ isosurface.

To analyse Eqs. 2.111 and 2.112 it is further useful to define the Karlovitz number [107]:

$$Ka = \frac{\tau_f}{\tau_\eta} \sim \frac{\delta_z^2}{\eta^2} \sim \frac{v_\eta^2}{S_L^2} \tag{2.113}$$

where δ_l is the flame length scale representative of laminar flame thickness given by α_T/S_L and τ_f is flame time scale given by α_T/S_L^2 and α_T is the thermal diffusivity. Examining the first term on the right hand side of Eqs. 2.111 and

2.112 using the definition of Karlovitz number in Eq. 2.113 it is possible to conclude that it is proportional to $Ka^{-1/2}$, which indicates that when $Ka > 1$ this term becomes small. Thus under the condition of $Ka > 1$ the second term on the right hand side of Eqs. 2.111 and 2.112 becomes dominant, that is to say that the contribution due to the tangential component of displacement speed may locally supersede the combined contribution of reaction and normal diffusion components. As a result of this strong curvature effect, a locally negative displacement speed may result at highly positive curvature locations. In the case of $Ka > 1$ using Eq. 2.113 it is possible to conclude that the flame thickness must be greater than Kolmogorov length scale. As a result of this, turbulent eddies can penetrate into the flame structure which results in unsteady fluctuations ahead of the reaction zone. A flame can become extinguished if the Kolmogorov length scale becomes smaller than the reaction zone thickness δ_r. Based on this an alternative definition may be proposed for the Karlovitz number Ka_δ such that:

$$Ka_\delta = \frac{\delta_r^2}{\eta^2} \tag{2.114}$$

It is worth noting that δ_r remains typically one order magnitude smaller than δ_z (i.e. $\delta_r \sim \delta_z/10$) and thus Ka_δ can be estimated as $Ka_\delta \sim Ka/100$. This Karlovitz number Ka_δ must be smaller than unity ($Ka_\delta < 1$) to prevent flame extinction. A flame regime was defined by Peters [107] based on the bounding conditions ($100(Ka_\delta = 100) > Ka > 1$) as the thin reaction zones regime.

In a similar fashion it is possible to examine the condition of $Ka < 1$, which would lead to $v_\eta < S_{RN}$. As a result the laminar propagation becomes the leading order term, while the curvature effects become higher order terms. Under the Klimov-Williams criterion the laminar flame exists in a turbulent flow when the flame stretch is less than a critical value. Under some assumptions this is equivalent to a case where $Ka < 1$. Peters [107] termed this regime of combustion as the corrugated flamelets regime. Based on the above arguments Peters [107] proposed a regime diagram for premixed combustion, which will be discussed in detail in Chapter 3.

2.8 Summary

In this chapter the governing equations and the underlying assumptions of the DNS were mentioned. These assumptions were that the reaction mechanism was determined by a single step irreversible Arrhenius rate law, whereby allowing for the species field to be represented using a reaction progress variable, which is based on the product mass fraction. Additionally the diffusion velocities was accounted for by using Fick's law. The governing equations were non-dimensionalised using reference values in the unburned gases. The reaction progress variable transport equation was then introduced. This was followed by an in depth discussion into the derivation of the transport equation for the FSD, in context of LES and RANS. Furthermore an introduction was made to the unclosed terms of the FSD transport equations and naming convention for the various quantities encountered in this thesis. In the following chapter the chemical and turbulent time scales which govern the flow are introduced, along with a commonly used regime diagram for premixed combustion. This was then followed by the modelling strategy that was used in previous works for the FSD closure.

Chapter 3

Literature Survey

In this chapter an introduction to the flamelets approach is provided, followed by a review of the turbulent premixed combustion modelling using FSD, wrinkling factor, artificially thickened flame and G equation methodologies, which are a part of the geometrical anaylsis as mentioned in §.1.2.4. The FSD based approach is well established in the context of RANS. However *a priori* analysis of FSD models in the context of LES is lacking, which will be addressed in this thesis. The existing modelling strategies for the FSD in context of RANS and LES are mentioned in this chapter. In the following section the length and time scales that define the turbulent premixed combustion are stated.

3.1 Flamelet Approach for Turbulent Premixed Combustion

3.1.1 Combustion Regimes

A flame is commonly decomposed into three different zones, these are the preheat zone, reaction zone and the oxidation zone. Chemical time scales in turbulent premixed flames are often shorter than the large-scale turbulent time scales [11]. This implies that the chemical reaction is confined to a thin propagating surface. Thus in premixed combustion the reacting mixture is composed of packets of unburned reactants and completely burned products which is separated by a

thin reacting interface referred to as flamelets. This forms the basic assumption of the flamelet concept, which reduces the modelling of the turbulent combustion analysis to a two fluid problem. In other words the analysis reduces to a description of the flow variables in the fresh and burnt gases, burning rate and the flame surface. Additional simplifications can be made by assuming the local flame structure resembles that of a strained and curved laminar flame, which leads to the assumption that the reactant consumption rate in turbulent flames can be approximated by the corresponding strained laminar flame values. Thus the flamelet assumption decouples turbulence and chemistry. The chemical effects lead to the variations in local flame speed which can be calculated separately [20]. While the effect of turbulence result in the wrinkling and straining of the flamelets. These assumptions have attracted much controversy towards the limitations of the flamelet assumption. It is instructive to refer to a regime diagram in order to appreciate the strengths and limitations of the flamelet assumption. The various regimes of turbulent combustion are traditionally expressed using a phase diagram as a function of non-dimensional parameters. The regime diagram proposed by Peters [107] is shown in Fig. 3.1. The non-dimensional numbers used in Fig. 3.1 are the turbulent Reynolds number Re_t, turbulent Damköhler number Da and the Karlovitz numbers Ka and Ka_δ. The Karlovitz numbers Ka and Ka_δ were defined in Eq. 2.113 and Eq. 2.114, respectively. The turbulent Reynolds number Re_t can be defined as:

$$Re_t = \frac{u'l}{\nu} \tag{3.1}$$

where u' is the turbulent velocity fluctuation and l is the characteristic integral length scale. It is possible to define the Damköhler number in the following manner in terms of the ratio of large-scale turbulent time scale τ_t and chemical time scale τ_f:

$$Da = \frac{\tau_t}{\tau_f} \tag{3.2}$$

where

$$\tau_t = \frac{l}{u'} \text{ and } \tau_f = \frac{\nu}{S_L^2} \tag{3.3}$$

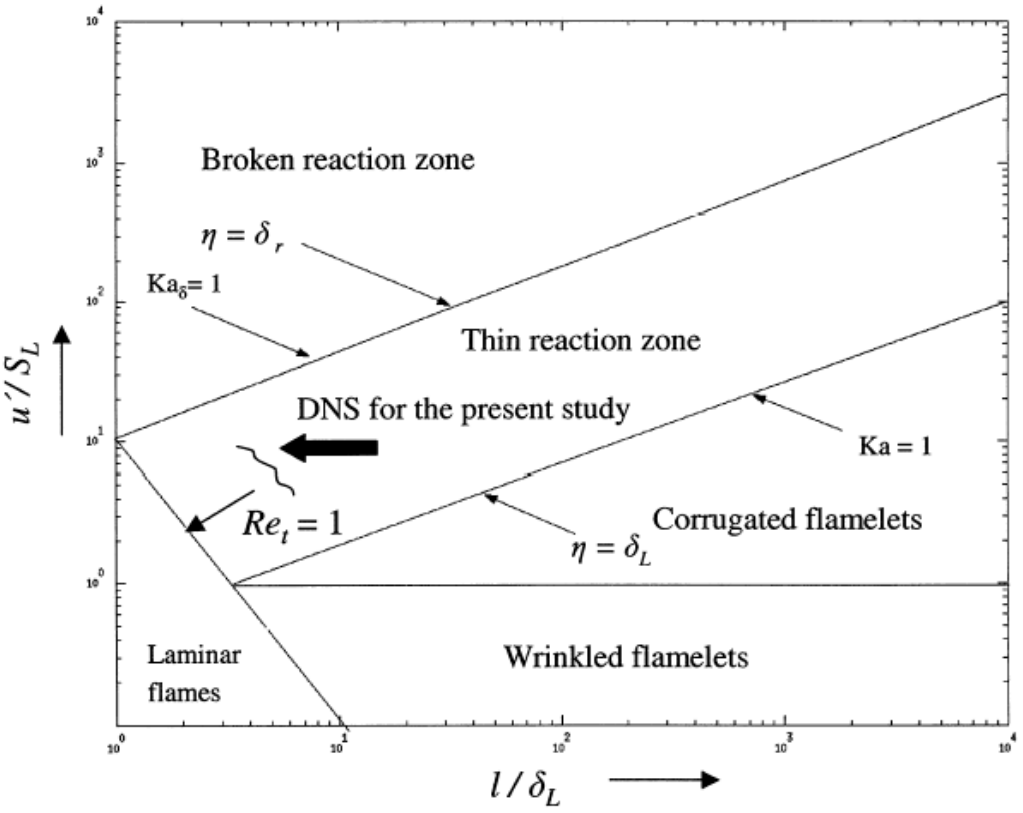

Figure 3.1: A regime diagram for Turbulent premixed combustion [107].

The non-dimensional numbers Re_t, Da and Ka are related to each other as follows:

$$Re_t \sim Da^2 Ka^2 \tag{3.4}$$

The combustion regime that is given by the conditions of $Re_t > 1$ and $Ka \leq 1$ is termed as the corrugated flamelets regime. Based on the conditions for the corrugated flamelets regime it is possible to deduce that in this regime the laminar flame thickness δ_L remains smaller than the Kolmogorov length scale η, and thus the inner structure of the flame remains unperturbed by the turbulent velocity fluctuations. The regime of combustion given by $1 < Ka < Ka_\delta$ and $Re_t > 1$ is known as the thin reaction zones regime. Based on the definitions for Re_t, Ka and Ka_δ it becomes clear that the energetic turbulent eddies can penetrate the flame structure, which results in unsteady fluctuations in the preheat zone leading

to a thickening of the flame, while the reaction zone remains undisturbed by turbulent motion. If the conditions $Re_t > 1$ and $Ka_\delta > 1$ occur then the resulting combustion regime is known as the broken zones regime. In the broken zones regime the flame shows significant amount of quenching and starts to resemble passive scalar mixing.

Much of the flamelet based modelling is strictly valid for $Ka < 1$ and $Re_t > 1$, and the boundary given by $Ka = 1$ is known as the Klimov-William criterion. Flame vortex interaction analysis by Poinsot et al. [115, 116] have found that the Klimov-Williams criterion (i.e. $Ka = 1$) underestimates the flamelet regime by an order of magnitude greater. Kolmogorov eddies are believed to penetrate the flame front but they are not energetic enough to give rise to significant flame stretch. Poinsot et al. [115, 116] have suggested that the flamelet assumption could be extended to accommodate the flames whose internal structures are altered due to small scale turbulence, but quenching of the flame significantly is yet to take place.

3.1.2 Flamelet Approaches

A well established flamelet model is the Bray Moss Libby (BML) model [13]. In BML the reaction progress variable c is represented using a presumed probability density function, which consists of two weighted delta functions at $c = 0$ and $c = 1$. This represents the case of a thin reacting surface that is embedded in a turbulent flow. Second order closure is used for moment equations, using a double delta pdf to provide closure for a range of mean quantities in terms of conditional moments at $c = 0$ and $c = 1$. An example of this approach is given for the turbulent scalar flux of reaction progress variable:

$$\widetilde{u''c''} = \tilde{c}(1 - \tilde{c}) \left[\overline{(u_i)}_P - \overline{(u_i)}_R \right] \tag{3.5}$$

where the quantities $\overline{(u_i)}_P$ and $\overline{(u_i)}_R$ represent conditional Reynolds averaged velocity components in the products and reactants respectively.

In BML, the Reynolds averaged reaction rate is modelled by using the local

surface area to volume ratio given by the FSD Σ [13]:

$$\overline{\dot{w}} = \rho_0 S_L I_0 \Sigma \tag{3.6}$$

where the factor I_0 accounts for the effects of flame stretch [107].

Another method for the thermo-chemical closure, in the flamelet regime, is to use a level set approach which makes use of the so called G equation. In this approach, a Reynolds averaged transport equation for the G field and its variance are solved. A detailed description of this approach is presented by Peters [107], and a brief overview is given in §.3.3.2. Alternatively thermo-chemical closure in the flamelet regime can be accomplished using a presumed pdf of reaction progress variable. The flamelet pdf is used in conjunction with a strained laminar flame calculation. Laminar flame calculations can be used to tabulate the reaction rate as a function of progress variable and flame stretch, and this may be combined with a presumed joint pdf for the progress variable and flame stretch, and this may be combined with a presumed joint pdf for the progress variable and flame stretch to estimate the mean reaction rate. Pope [120] suggests that simplifications can be made to the pdf approach by assuming flamelets, which can be used to simplify the pdf transport equation by allowing the reaction and diffusion terms to be combined and treated as a function of reaction progress variable based on a laminar flame structure. Vervisch et al. [151] provided a link between pdf and FSD approaches.

3.2 Flame Surface Density Approach

In this section a discussion of FSD closure both in RANS and LES is provided. FSD is typically modelled in LES and RANS using an algebraic closure or by solving a modelled transport equation. One of the simplest ways of utilising the algebraic closure approach is to apply the BML model, which is derived from the intermittency between the fresh reactants and the fully burnt gases. The BML model for the FSD Σ can be expressed as[13]:

$$\Sigma = \frac{g\bar{c}(1-\bar{c})}{\bar{\sigma}_y \bar{L}_y} \tag{3.7}$$

where $\bar{\sigma}_y$ is a flamelet orientation factor, $\bar{L}_y$ is the integral length scale of the spatial random flamelet crossing process, and g is a model parameter. The integral length scale $\bar{L}_y$ is modelled by Cant and Bray [20] as the local turbulent length scale. An alternative algebraic closure for Σ relies on fractal concepts proposed by Gouldin et al. [61], where FSD Σ is estimated from the inner and outer cutoff scales of the flame front and fractal dimension.

The approach of solving a modelled transport equation for Σ was first applied to non-premixed turbulent combustion by Marble and Broadwell [101], since then there have been a large number of studies into this approach. Marble and Broadwell [101] proposed their coherent flamelet model (CFM) based on the physical processes that create and destroy flame surface area. Later studies have led to an exact transport equation for the FSD based on theoretical considerations for a propagating surface [18, 121]. In this exact formulation the FSD is convected by the bulk flow, propagated by flame propagation, and produced or destroyed by the combined action of propagation and curvature. In this approach the main modelling concerns arise from effects of fluid strain rate and due to the effects of curvature and propagation. Many strategies have evolved to implementing a transport equation approach. It is common in these approaches to employ a model for the fluid strain rate effects which scales with large scale turbulent strain rate. The effects of propagation and curvature are generally modelled as a destruction term.

There have been many extensions and variants of the original CFM [101] approach. An exact transport equation approach was devised by Cant et al. [21], where the strain rate term is scaled with the Kolmogorov strain rate. A variable density implementation is described by Maistret et al. [98]. Candel et al. [19] proposed an extension to include partially premixed combustion and results are presented for a stabilised ducted flame and reactive shear layer. Boudier et al. [9] coupled a laminar ignition model with the CFM approach to simulate spark ignition engine combustion. Cheng and Diringer [51] discussed the one-dimensional CFM model with reference to interesting characteristics of the model, including turbulent flame speed, turbulent flame thickness and ignition characteristics. Duclos et al. [54] reviewed a variety of FSD models in the context of turbulent flame speed predictions. Wu and Bray [162] used a combination of the CFM and

CPB (Cant Pope Bray) [21] models to a counterflow geometry, where satisfactory agreement with experimental data was found. Lee et al. [94] have also investigated the same geometry with special attention to the extinction effects induced by the large flame stretch. Choi and Huh [52] applied a variety of models to a spark ignition problem. Prasad and Gore [126] compared a range of FSD models for turbulent jet flames. Prasad et al. [127] have extended some FSD models to cope with non-isenthalpic flames, and have compared predictions from these with the experimental data for a reacting jet.

Mantel and Borghi [100] use a different perspective by deriving transport equation for the FSD by using a modelled equation for scalar dissipation rate χ, which is defined as:

$$\chi = D|\nabla c|^2 \tag{3.8}$$

Pope and Cheng [124] describe stochastic methods for the determination of the FSD Σ. Weller et al. [158] suggests a spectral method for modelling the FSD. Many DNS based studies currently exist for the evaluation of FSD based on the transport equation ([17, 72, 92, 114, 118, 147, 148, 164]). Finally, Veynante et al. [152] and Veynante et al. [153] have analysed the FSD transport equation from an experimental perspective in the context of RANS simulation.

3.2.1 Algebraic Models

A simple approach to estimating the FSD Σ in LES and RANS is to use an algebraic model. These algebraic models are developed based on physical arguments and DNS or experimental data. Additionally in LES it is possible to define some model constants using the dynamic approach [59, 60]. In the Eddy Break Up (EBU) modelling for RANS uses an expression for $\overline{\dot{w}}$ that is equivalent to Σ of the form [16]:

$$\Sigma = \frac{\underset{\sim}{\epsilon}}{\underset{\sim}{k}} \frac{1}{S_L} \underline{c}(1 - \underline{c}) \tag{3.9}$$

In the above expression the reaction rate is inversely proportional to the turbulent mixing time scale. The BML [12] model for Σ takes a similar form to the EBU approach. Boger et al. [8] proposed an algebraic model for FSD in the context of

LES which is reminiscent of EBU and BML models.

$$\Sigma_{sg} \approx K_{\Sigma} \frac{\bar{c}(1-\bar{c})}{\Delta} \tag{3.10}$$

where K_{Σ} is a model constant, which shows dependence on a wide range of parameters. A more refined model would approximate K_{Σ} as a function of subgrid kinetic energy. Boger et al. [8] defined the value for model constant K_{Σ} to take the value of $4\sqrt{6/\pi}$. It was also found by Boger et al. [8] that the value of K_{Σ} depends on the filter size Δ and on the turbulence level. The dependence on Δ is undesirable for a model constant as a wide range of filter sizes are used depending on the problem at hand. This filter width dependence of the model constant K_{Σ} should decrease as the filter width is comparably large compared to the flame thickness. As the filter width Δ approaches the turbulent length scale, the above expression resembles the BML model [13]. The DNS data analysis by Boger et al. [8] shows leveling of K_{Σ} with increasing Δ.

For thin flames, the subgrid FSD $\Sigma_{sg} \approx \Sigma_{gen} = \overline{|\nabla c|}$, as the scalar gradients are near zero everywhere except near the reaction surface. In that case the resolved part of FSD can be written as:

$$\Sigma_{res} = |\nabla \bar{c}| \tag{3.11}$$

The flame becomes fully resolved when $\Sigma_{sg} \rightarrow \Sigma_{res}$ which indicates no subgrid variations of FSD under fully resolved condition. The condition $\Sigma_{sg} \rightarrow |\nabla \bar{c}|$ can only occur when either $\Delta \rightarrow 0$ or when a flame is a planar surface. Charlette et al. [48] provides the following model for the subgrid scale FSD, which is similar to BML and EBU expressions, but also includes a term that accounts for the resolved part of FSD:

$$\Sigma_{sg} = |\nabla \bar{c}| + a\Gamma_k \left(\frac{\Delta}{\delta_z}, \frac{\sqrt{2\tilde{k}/3}}{S_L} \right) \frac{\sqrt{\tilde{k}}}{S_L} \frac{\bar{c}(1-\bar{c})}{\Delta} \tag{3.12}$$

where Γ_k is the efficiency function of the intermittent turbulent Net Flame Stretch (ITFNS) model of Meneveau and Poinsot [102], $\tilde{k}$ represents subgrid scale turbulent kinetic energy given as $\tilde{k} = 1/2(\widetilde{u_i u_i} - \tilde{u_i}\tilde{u_i})$ and a is a model constant. In

a highly turbulent flow simulation in LES, Σ_{sg} is much greater than the resolved FSD, and the expression for subgrid component reverts to one similar to the successful RANS derived BML model for LES (using the estimate $L_y = S_L l/u'$ [15]).

The model for the subgrid FSD Σ_{sg} given in Eq. 3.12 which was derived by balancing the subgrid production and dissipation terms of a modelled transport equation for FSD. The transport equation only included subgrid production and dissipation terms. These terms dominate in a highly turbulent situation, but in LES it is possible to exploit the resolved propagation and curvature terms to achieve a more accurate transport modelling of FSD. Finally the model does not take into account dilatation effects, and in most cases $\bar{c}$ is generally unavailable, as the Favre averaged value of progress variable $\tilde{c}$ is typically solved for in a compressible LES simulation.

Another algebraic model suggested by Angelberger et al. [2] but not implemented in the context of FSD, is:

$$\Sigma_{sg} = \left(1 + a\Gamma\left\{\frac{\Delta}{\delta_z}, \frac{u'_\Delta}{S_L}\right\}\frac{u'_\Delta}{S_L}\right)|\nabla\bar{c}| \tag{3.13}$$

where u'_Δ is the subgrid velocity fluctuation ($u'_\Delta = \sqrt{2\tilde{k}/3}$). The efficiency function Γ is similar to the ITFNS efficiency function Γ_k. The model features a resolved component and an increase in flame wrinkling due to subgrid scale velocity fluctuations.

Piana et al. [110] proposed a model based on G-equation using the concept of a flame-wrinkling factor. The flame wrinkling model of Weller et al. [159] can also be regarded as a class of algebraic models. These models simplify to the exact fully resolved expression as flow becomes completely resolved (i.e. $u'_\Delta/S_L \to 0$).

Algebraic models can be employed with sufficient accuracy when it is possible to assume that there is a local balance between production and destruction of FSD. However, in unsteady conditions there may be a complex dynamic response of the flame to the stretch, which is not correctly represented by an algebraic model. It may be argued that a dynamic determination of the model constants would overcome this and other difficulties. Although, it is not clear whether the

scale similarity argument can be applied to a flame situation due to the jump of progress variable across the flame. Moreover it is not clear whether dynamic approaches could potentially offer any advantages.

A modelled transport equation can exploit knowledge of physical mechanisms of flame curvature and propagation to achieve a more realistic estimation of FSD. This applies particularly well to a situation where the flame is partially resolved and the resolved physics can also be exploited in the modelling of the FSD transport equation.

3.2.2 Transport Equation Closure for FSD

In this section a brief summary is made of the various, existing, modelling methodologies based on the transport equation closure of FSD. The derivation of the FSD transport equation was made in the previous chapter, the exact transport equation for the FSD is given by:

$$\frac{\partial \Sigma'}{\partial t} + \frac{\partial (u_k \Sigma')}{\partial x_k} + \frac{\partial (N_k S_d \Sigma')}{\partial x_k} = (\delta_{ij} - N_i N_j) \frac{\partial u_i}{\partial x_j} \Sigma' + S_d \frac{\partial N_i}{\partial x_i} \Sigma' \tag{3.14}$$

The FSD balance equation is unclosed and requires modelling for the turbulent flux of FSD, the displacement speed S_d, and strain rate and curvature effects. Using the Favre decomposition ($u_i = \tilde{u}_i + u_i''$), the FSD strain rate term may be split into mean flow and turbulent fluctuation contributions:

$$\underline{\left((\delta_{ij} - N_i N_j) \frac{\partial u_i}{\partial x_j} \right)}_s = \underbrace{\left(\delta_{ij} - \underline{(N_i N_j)}_s \right) \frac{\partial \tilde{u}_i}{\partial x_j}}_{a_m} + \underbrace{\underline{\left((\delta_{ij} - N_i N_j) \frac{\partial u_i''}{\partial x_j} \right)}}_{a_t} \tag{3.15}$$

where a_m, a_t correspond to the strain rate acting on the flame surface, induced by mean flow and turbulent fluctuation respectively. If the instantaneous FSD transport equation shown in Eq. 3.14 is Favre averaged, it will result in the following transport equation:

$$\frac{\partial \Sigma}{\partial t} + \frac{\partial \Sigma (\tilde{u}_i)}{\partial x_i} = -\frac{\partial}{\partial x_i} \left(\underline{(u_i'')}_s \Sigma \right) + (a_m + a_t) \Sigma + \underline{\left(S_d \frac{\partial N_i}{\partial x_i} \right)}_s \Sigma - \underline{\left(\frac{\partial (S_d N_i \Sigma)}{\partial x_i} \right)} \tag{3.16}$$

Various closures may be found for the above equation. The general form of the closed equation can be written as [21, 40]:

$$\frac{\partial \Sigma}{\partial t} + \frac{\partial}{\partial x_i}(\underline{u}_i \Sigma) = \frac{\partial}{\partial x_i}\left(\frac{\mu_t}{\sigma_c}\frac{\partial \Sigma}{\partial x_i}\right) + (a_m + a_t)\Sigma - DI \tag{3.17}$$

where DI is a destruction term. In the above form the turbulent flux of FSD is expressed using a classical gradient transport assumption, where μ_t is the eddy viscosity and σ_c is the turbulent Schmidt number for FSD. The DI term has to be included as the surface strain rate contribution a_m, a_t are generally positive. Without a destruction term, the flame surface area will increase indefinitely, which is a property of a non-reacting material surface but in the present case flame surface is lost when flames interact. At present it is not clear how this destruction terms originates, whether heat release induced effects, curvature effects or additional effects such as flame front interactions have a major role.

A simple phenomenological closure may be derived as follows. First, the flame stretch generated by the turbulent flow may be estimated using $\underset{\sim}{\epsilon}/\underset{\sim}{k}$, using the integral time scale as the flame time. The flame surface consumption term is assumed to be proportional to the mean reaction term and inversely proportional to available reactants per unit area measured by $\underline{c}(1-\underline{c})/\Sigma$. Then the transport equation for the FSD takes following form:

$$\frac{\partial \Sigma}{\partial t} + \frac{\partial}{\partial x_i}(\underline{u}_i \Sigma) = \frac{\partial}{\partial x_i}\left(\frac{\mu_t}{\sigma_c}\frac{\partial \Sigma}{\partial x_i}\right) + \alpha_0 \frac{\underset{\sim}{\epsilon}}{\underset{\sim}{k}}\Sigma - \beta_0 S_L \frac{\Sigma^2}{\underline{c}(1-\underline{c})} \tag{3.18}$$

where α_0, β_0 are model constants and the mean reaction rate is given by Eq. 3.6. If equilibrium is assumed between production and destruction of FSD then the mean reaction rate can be described as:

$$\overline{\dot{w}} = \rho_0 \frac{\alpha_0}{\beta_0}\frac{\underset{\sim}{\epsilon}}{\underset{\sim}{k}}(1-\underline{c})\underline{c} \tag{3.19}$$

The above expression shows that the EBU model (i.e. Eq. 3.19) can be obtained by simplifying the modelled FSD transport equation.

The filtered transport equation for the FSD is given as [22, 66, 67, 68]:

$$\frac{\partial \Sigma_{sg}}{\partial t} + \frac{\partial}{\partial x_i}(\tilde{u}_i \Sigma_{sg}) = \frac{\partial}{\partial x_i}\left[\left(\overline{(u_i)}_s - \tilde{u}_i\right)\Sigma_{sg}\right] - \frac{\partial}{\partial x_i}\left[\overline{(S_d N_i)}_s \Sigma_{sg}\right] + \overline{\left(S_d \frac{\partial N_i}{\partial x_i}\right)}_s \Sigma_{sg} \tag{3.20}$$

The main modelling difference between LES and RANS for the FSD is that in LES it is possible to use the resolved propagation and strain rate effects. It is expected that the performance of a LES model should be independent of the filter width. This leads to two important considerations for modelling for FSD: 1) the FSD transport equation must revert to the exact instantaneous transport equation for the FSD as the velocity and the scalar fields become resolved 2) the model should reflect accepted RANS models for a situation in which filter width is comparable to the integral length scale. For the first point a flow is said to be fully resolved when the subgrid fluxes of the momentum and $\tilde{k}$ vanish. This can only occur in the condition of a planar flame or as the filter width tends to zero.

In Eq. 3.20 the last two terms represent the combined effects of propagation and curvature. The surface averaged normal components are given by:

$$\overline{(N_i)}_s = \frac{\overline{N_i \Sigma'}}{\Sigma_{sg}} \tag{3.21}$$

It is possible to use the above expression along with the definition for Σ' to obtain an alternative definition for the surface integrated normal, $\overline{(\vec{N})}_s \Sigma_{sg}$:

$$\overline{(\vec{N})}_s \Sigma_{sg} = -\overline{\frac{\nabla c}{|\nabla c|}|\nabla c|\delta(c - c^*)} = -\overline{\delta(c - c^*)\nabla c} = -\overline{\nabla H(c - c^*)} \tag{3.22}$$

where $H(c - c^*)$ is the Heaviside function. Under a strict assumption, the c field consists only of reactants and burned products, and hence $H(c - c^*) \approx c$. Thus for thin flame the surface integrated normal takes the form:

$$\overline{(\vec{N})}_s = -\frac{\nabla \bar{c}}{\Sigma_{sg}} \tag{3.23}$$

This expression is exactly the same as the relation derived by Cant et al. [21] for RANS simulation. This expression holds exactly (independent of flame regime)

for the generalised FSD definition given by Boger et al. [8]. The combined curvature and propagation terms of the LES filtered transport equation can be split into resolved scale and subgrid scale contributions as:

$$-\nabla.(\overline{(S_d\vec{N})_s}\Sigma_{sg}) + \overline{(S_d\nabla.\vec{N})}_s\Sigma_{sg} = P_{mean} + C_{mean} + C_{sg} \tag{3.24}$$

where

$$P_{mean} = -\nabla.\left[\overline{(S_d)}_s\overline{(\vec{N})}_s\Sigma_{sg}\right] \tag{3.25a}$$

$$C_{mean} = \overline{(S_d)}_s\nabla.\overline{(\vec{N})}_s\Sigma_{sg} \tag{3.25b}$$

$$C_{sg} = -\nabla.\left[\overline{(S_d\vec{N})}\Sigma_{sg}\right] + \overline{(S_d\nabla.\vec{N})}_s\Sigma_{sg} - P_{mean} - C_{mean} \tag{3.25c}$$

The term P_{mean} represents the resolved component of the propagation term and C_{mean} represents the resolved component of the curvature term. The sum of these may be seen to revert to the fully resolved expression as $\Delta \to 0$. The term C_{sg} represents the difference between the actual net effect of the curvature and propagation terms, and the combined effects of P_{mean} and C_{mean}. The surface averaged displacement speed $\overline{(S_d)}_s$ is dependent on the $c = c^*$ isosurface chosen to define the flame. Hawkes [66], Hawkes and Cant [67, 68] estimated $\overline{(\rho S_d)}_s$ for a statistically planar flame by assuming locally one-dimensional steady flame behaviour. By continuity for a one-dimensional flame, $\rho S_d = \rho_0 S_L$, so

$$\overline{(S_d)}_s \approx S_L\overline{(1+\tau c)} = S_L(1+\tau c^*) \tag{3.26}$$

Hawkes [66], Hawkes and Cant [67, 68] used unstrained laminar flame speed S_L in Eq. 3.26 in order to estimate $\overline{(S_d)}_s$, and local strain rate and curvature effects on S_d were not considered. This assumption implicitly makes the model valid only for the corrugated flamelet regime [107] as the laminar propagation terms are of higher importance than the curvature terms in this regime of premixed combustion. In order to use the model in a different regime (such as the thin reaction zones regime) a dependence on strain and curvature must be incorporated. This was carried out by Chakraborty and Cant [29, 35] where the effects

of curvature effects on $\overline{(S_d)}_s$ were modelled, which allows for the extension of the above models for the thin reaction zones regime.

Some RANS models have included a mean propagation term [7, 21, 126, 162]. Except Cant et al. [21] all have neglected the mean contribution associated with curvature. Veynante et al. [153] have shown that mean propagation contribution is not negligible as expected. In case of LES partial resolution of turbulent fluctuation makes the proper handling of the propagation term more important than in the case of RANS modelling. Hawkes and Cant [67, 68] argue that P_{mean} can be closed exactly under the flamelet assumptions using $\overline{(S_d N_i)}_s = \overline{(S_d)}_s \overline{(N_i)}_s$. It was demonstrated by Chakraborty and Cant [29, 35] that S_d and N_i remain uncorrelated and statistically independent throughout the flame brush based on *a priori* DNS analysis. It was further shown by Chakraborty and Cant [29, 35] that $-\nabla/(\overline{S_d \vec{N}}_s \Sigma_{gen})$ can be accurately modelled by $-\nabla.[\overline{(S_d)}_s \overline{(\vec{N})}_s \Sigma_{gen}]$ throughout the flame brush for a large range of filter widths. However, different possibilities exist for the modelling of resolved curvature term C_{mean}. Hawkes and Cant [67] presented two different forms of C_{mean} given by:

$$C_{mean} = \overline{(S_d)}_s \frac{\partial \overline{(N_i)}_s}{\partial x_i} \Sigma_{sg} \tag{3.27}$$

$$C_{mean} \approx \overline{(S_d)}_s \frac{\partial M_i}{\partial x_i} \Sigma_{sg} \tag{3.28}$$

where M_i is referred to as i^{th} component of the resolved flame normal given by:

$$M_i = -\frac{1}{|\nabla \bar{c}|} \frac{\partial \bar{c}}{\partial x_i} \tag{3.29}$$

The curvature term of the unclosed FSD transport equation can be written in the following manner [29, 35, 66]:

$$S_d \frac{\partial N_i}{\partial x_i} \Sigma' = (\delta_{ij} - N_i N_j) \frac{\partial (S_d N_i)}{\partial x_j} \Sigma' \tag{3.30}$$

Following the above expression an alternative expression for C_{mean} can be pro-

posed:

$$C_{mean} = \left(\delta_{ij} - \overline{(N_i N_j)}_s\right) \frac{\partial \overline{(S_d)}_s \overline{(N_i)}_s}{\partial x_j} \Sigma_{sg} \tag{3.31}$$

This also satisfies the requirement of reversion to the exact expression as $\Delta \to 0$. The expressions for C_{mean} given in Eqs. 3.27, 3.28 and 3.31 were, tested based on *a priori* analysis, by Chakraborty and Cant [29, 35] and Katragadda and Chakraborty [82, 83] where it was shown that expression given in Eq. 3.27 gives the most accurate prediction among the options for C_{mean}.

In RANS simulation, the equivalent of C_{sg} has been traditionally modelled as a destruction term proportional to Σ^2 [54]. Cant et al. [21] have shown from the realisability argument that the subgrid curvature term is on average a destruction term considering that the fluid straining term is a production term on average. In most RANS model [54] the destruction term is written in the following manner:

$$C_t = -\beta_0 S_L \frac{\Sigma^2}{1 - \underline{c}} \tag{3.32}$$

where C_t denotes the RANS equivalent of C_{sg}. Pope and Cheng [124] have found that a model of this form describes the rate of flame destruction for a variety of geometrically simple surfaces. Trouvé and Poinsot [148] have shown for RANS that the combined curvature and propagation terms acts as a production term on fresh gas side and dissipation term on the burnt gas side of the flame brush. In the context of RANS, Veynante et al. [153] suggested the following model for the combined effects of curvature and propagation incorporating this effect:

$$C_t = -\beta_0' S_L (\underline{c} - c_0) \frac{\Sigma^2}{\underline{c}(1 - \underline{c})} \tag{3.33}$$

where β_0' is a model constant and c_0 is the point at which the term changes from production to destruction of FSD. A similar approach was adopted by Han and Huh [65], Chakraborty and Cant [40] for the modelling of the unresolved part of the combined curvature and propagation contribution to the FSD transport. However it is difficult for this approach to apply in the LES context. The value of $\bar{c}$ in LES does not necessarily supply any information about the subgrid curvature structure of the flame at a given point. LES cells centered at different locations,

giving a different value of $\bar{c}$, could include the same element of flame area. This is different from the RANS simulation where a low value of $\bar{c}$ means the point usually corresponds to the fresh gas side of the instantaneous flame front, thus the curvature distribution tends to favour FSD production. Since partial resolution of scalar fluctuation is available in LES study the model proposed by Hawkes and Cant [67, 68] is capable of taking into account the production effect in fresh gas side through P_{mean} and C_{mean}. Cant et al. [21] have proposed a RANS model which if extended to LES cause the subgrid term C_{sg} to vanish when the flow is fully resolved. It can be shown from a realisability argument that net destruction goes to zero as $\alpha_R \rightarrow 0$ where $\alpha_R = 1 - |\underline{(\vec{N})}_s|^2$. Satisfying the above condition for LES, Hawkes and Cant [67, 68] modified a version of CFM [19] for the purpose of modelling the subgrid curvature term C_{sg} as:

$$C_{sg} = \frac{-\alpha_N \beta_1 S_L \Sigma_{gen}^2}{(1-\bar{c})} \tag{3.34}$$

where $\alpha_N = 1 - \overline{(N_k)}_s \overline{(N_k)}_s$ is an orientation factor and α_N is identically zero when the flow is fully resolved. Charlette et al. [48] also suggested a model for C_{sg} as:

$$C_{sg} = -\beta_2 S_L \frac{(\Sigma - |\nabla \bar{c}|)\Sigma_{gen}}{\bar{c}(1-\bar{c})} \tag{3.35}$$

This model is similar to CFM approaches [54] but modified in such a manner that it vanishes, as FSD gets fully resolved. Hawkes and Cant [67] also discussed a possibility of modifying the model proposed by Cant et al. [21] for the purpose of LES as:

$$C_{sg} = \frac{-C_H S_L \Sigma_{gen}^2}{(1-\bar{c})} \tag{3.36}$$

where C_H is given as:

$$C_H = \alpha\beta_3 \left[1 - \frac{1}{3}\left\{1 - \exp\left(\frac{-A(1-\bar{c})\sqrt{\tilde{k}}}{\Sigma_{gen} S_L \Delta}\right)\right\}\right] \tag{3.37}$$

where $A = 10$ is a model parameter.

The term $\overline{(a_T)}_s \Sigma_{sg}$ represents the straining effect of the surrounding fluid on the flame surface. In homogeneous isotropic turbulence it has been found that the

average effect of strain rate on the flame is the production of FSD [148]. This is in spite of the fact that in isotropic turbulence the strain rate tensor is randomly oriented and thus strain rate experienced by a fixed surface will have a mean of zero. Since flame elements are not fixed surfaces, they tend to align preferentially with persistent local velocity gradients, resulting in a net non-zero contribution. The term $\overline{(a_T)}_s$ may be split as:

$$S_{mean} = (\delta_{ij} - \overline{(N_i N_j)}_s)\frac{\partial \tilde{u}_i}{\partial x_j} \tag{3.38a}$$

$$S_{sg} = \overline{(a_T)}_s - S_{mean} - S_{hr} \tag{3.38b}$$

where a suitable model is required for the expression $\overline{(N_i N_j)}_s$ which acts as an orientation factor for the flame strain rate with respect to the mean flow gradients, and S_{hr} is the term responsible for the expansion effects associated with heat release. Hawkes [66] extended the RANS model for $\underline{(N_i N_j)}_s$ proposed by Cant et al. [21] in order to model $\overline{(N_i N_j)}_s$ in LES AS:

$$\overline{(N_i N_j)}_s = \overline{(N_i)}_s \overline{(N_j)}_s + \frac{1}{3}\delta_{ij}\left(1 - \overline{(N_k)}_s \overline{(N_k)}_s\right) \tag{3.39}$$

Cant et al. [21] assumed the fluctuations on N_i are isotropic in order to propose a model for $\underline{(N_i N_j)}_s$. This model assumes that any contribution to the resolved scale quantity $\overline{(N_i N_j)}_s$ arising from the subgrid scale fluctuations are isotropic in nature. The second term in Eq. 3.39 acts to distribute the subgrid contribution equally along the three principal directions for $\overline{(N_i N_{j=i})}_s$. Veynante et al. [152], based on an experimental study of two-dimensional V-flames, showed that the fluctuations in the normal are not isotropic and suggested an alternative RANS model for $\underline{(N_i N_j)}_s$ in two dimensions taking the anisotropy into account. This model is give as:

$$\underline{(N_i N_{j=i})} = \underline{(N_i)}_s \underline{(N_{j=i})}_s + \frac{\sum_{m \neq i} \underline{(N_m)}_s \underline{(N_m)}_s}{\underline{(N_k)}_s \underline{(N_k)}_s}\left[1 - \underline{(N_k)}_s \underline{(N_k)}_s\right] \tag{3.40a}$$

$$\underline{(N_i N_{j \neq i})} = \frac{\left(2\underline{(N_k)}_s \underline{(N_k)}_s - 1\right)}{\underline{(N_k)}_s \underline{(N_k)}_s} \underline{(N_i)}_s \underline{(N_{j \neq i})}_s \tag{3.40b}$$

where $i, j = 1, 2$. It is important to note that the model given by Eq. 3.40a and 3.40b is applicable only for two dimensions and three-dimensional extension of the model for LES purpose is not straightforward.

Mantel and Borghi [100] proposed an alternative RANS model for $\underline{(N_i N_j)}_s$ in two dimensions:

$$\underline{(N_i N_j)}_s = \frac{\widetilde{u_i'' u_j''}}{2\underline{k}};\ i, j = 1, 2 \tag{3.41}$$

where $\widetilde{u_i'' u_j''}$ denotes the Favre averaged Reynolds stress. Veynante et al. [153] extended the original Mantel and Borghi [100] model for three-dimensional flows in the RANS context as:

$$\underline{(N_i N_{j=i})}_s = \frac{\sum_{k\neq 1} \widetilde{u_k'' u_k''}}{4\underline{k}},\ \underline{(N_i N_{j\neq i})}_s = \frac{\widetilde{u_i'' u_j''}}{2\underline{k}};\ i, j = 1, 3 \tag{3.42}$$

The above model can be used for LES purposes replacing the Favre averaged quantities by Favre filtered quantities and the turbulent kinetic energy by subgrid turbulent kinetic energy. Chakraborty and Cant [27] proposed the following model for $\overline{(N_i N_j)}$ by combining the two earlier models given in Eqs. 3.42 and 3.41:

$$\begin{aligned}
\overline{(N_i N_{j=i})}_s &= \overline{(N_i)}_s \overline{(N_{j=i})}_s + \frac{\sum_{m\neq i} \overline{(N_m)}_s \overline{(N_m)}_s}{2\overline{(N_k)}_s \overline{(N_k)}_s}[1 - \overline{(N_k)}_s \overline{(N_k)}_s] \\
\overline{(N_i N_{j\neq i})}_s &= \overline{(N_i)}_s \overline{(N_{j\neq i})}_s
\end{aligned} \tag{3.43}$$

In the above model in the condition of resolved flow the strain rate will equal the tangential strain rate a_T. The unresolved strain rate term is usually modelled as proportional to the inverse of turbulent time scale. The simplest approach is to scale the term with the LES subgrid scale strain rate $\sqrt{\tilde{k}}/\Delta$. However it may be argued that the Kolmogorov scales are principally responsible for flame surface stretching due to large velocity gradients. Cant et al. [21] found using DNS of a premixed flame with low values of u'/S_L that the mean of the tangential strain rate could be approximated as:

$$\underline{(a_T)}_s \approx \frac{0.28}{\tau_\eta} \tag{3.44}$$

This scaling for the strain rate has also been observed in DNS of propagating material surfaces in isotropic turbulence [164]. Thin flames with small propagation speed are a good approximation of material surfaces. Yeung et al. [164] showed that the distance between a propagating surface and initially co-incident material surface remains small if the displacement speed S_d is small compared with the Kolmogorov velocity scale for incompressible flow. Using Kolmogorov scaling the subgrid strain term can be expressed in the following form:

$$S_{sg} = C_A \sqrt{\frac{C_\epsilon \tilde{k}^{3/2}}{\nu \Delta}} \tag{3.45}$$

where $\tilde{\epsilon} = C_\epsilon(\tilde{k}^{3/2}/\Delta)$ represents the subgrid scale dissipation rate of turbulent kinetic energy. A Kolmogorov scaling may well apply in the limit of a very thin flame, but it has been shown by Meneveau and Poinsot [102] in their flame-vortex interaction analysis that Kolmogorov scaling overestimates the strain of the flame surface. Curvature effects may also reduce the stretch through the local thermo-diffusive effects. Duclos et al. [54], Prasad and Gore [126], Prasad et al. [127] support this result. The other reason behind the non-approval of Kolmogorov scaling is that it predicts the flame thickness in LES which tends to infinity as $\tilde{k} \to 0$ [66]. Hawkes [66] pointed out that a scaling based on subgrid scale strain rate does not suffer from this problem.

The models based on turbulent time scales do not account for any chemical effects in the representation of flame stretch. Differently sized vortices have different effects on the flame structure. The ITFNS method proposed by Meneveau and Poinsot [102] attempts to model these effects. These methods multiply the flame strain rate by an efficiency function Γ_k developed by Meneveau and Poinsot [102] from two dimensional simulation of discrete vortices. For LES a modified version can be used which takes the following form:

$$S_{sg} = \Phi \Gamma_k \frac{\sqrt{k}}{\Delta} \tag{3.46}$$

where Φ is a model constant. This model is based on a two-dimensional study where the turbulence structure is fundamentally different from the three-dimensional

flow structures. A study by Angelberger et al. [2] has shown an alternative to the ITFNS model where a different form of efficiency function is suggested and the provision for application in the context of LES is kept. The performance of the model given by Eq. 3.46 was assessed by Chakraborty [22] and Chakraborty and Cant [35] based on *a priori* DNS analysis. It was shown that Eq. 3.46 does not adequately capture the behaviour of S_{sg} and the model parameters remain a function of filter width. The model given in Eq. 3.46 performs better for Angelberger et al. [2] efficiency function than by the efficiency function give by Meneveau and Poinsot [102].

The term $\overline{(u_i'')}_s\Sigma_{sg} = \left[\overline{(u_i)}_s - \tilde{u_i}\right]\Sigma_{sg}$ may be interpreted as a subgrid flux of FSD. This term is strongly related to the subgrid scalar flux $\widetilde{uc} - \tilde{u}\tilde{c}$. Cant et al. [21] have derived a theoretical relation between the RANS equivalents of these two for the case of an infinitely thin flame where it can be assumed that the fluctuation of the surface normal is uncorrelated with fluctuations in velocity. An expression can be derived relating the two based on an assumption of a linear variation of velocity across the flame front, which was substantiated later by the *a priori* DNS analysis of [155]. The form of this expression shows that if the FSD is closely related to the turbulent scalar flux, and a counter-gradient (gradient) transport of $\tilde{c}$ leads to a counter-gradient (gradient) transport of Σ_{gen}. A counter-gradient transport has been observed for scalar fluxes in the context of LES in a number of experimental [109], and numerical [8, 149, 150] studies. Therefore non-gradient transport must be expected in the FSD flux. It is expected where the turbulence level is low and expansion effects are significant. In the work by Hawkes [66] non-gradient transport effects were included in the proposed LES model. The non-gradient transport is related to the slip velocity between the products and reactants, $\overline{(u_i)}_P - \overline{(u_i)}_R$. Reactant conditional filtered values for the reactants can be defined in the following manner in the context of LES [29, 32, 66, 67, 68]:

$$\overline{(u_i)}_R = \frac{\iiint G(\vec{x}-\vec{x}',\Delta)H(-c(\vec{x}'))u_i(\vec{x}')d\vec{x}'}{\iiint G(\vec{x}-\vec{x}',\Delta)H(-c(\vec{x}'))d\vec{x}'} \tag{3.47}$$

Assuming a linear variation of velocity across the flame, the surface fluid velocity $(u_i)_s = (u_i)_R + K((u_i)_P - (u_i)_R)$ where K depends on the isosurface used to define

the flame, and $(u_i)_P$, $(u_i)_R$ are velocity components on reactant and product side respectively. Making a strong flamelet assumption it can be shown that:

$$\tilde{u}_i = \overline{(u_i)}_R + \tilde{c}\left[\overline{(u_i)}_P - \overline{(u_i)}_R\right] \tag{3.48}$$

Therefore:

$$\begin{aligned}\overline{(u_i'')}_s = \overline{(u_i)}_s - \tilde{u}_i = &\left\{\overline{(u_i)}_{Rs} - \overline{(u_i)}_R + K\left[\left(\overline{(u_i)}_{Ps} - \overline{(u_i)}_P\right) - \left(\overline{(u_i)}_{Rs} - \overline{(u_i)}_R\right)\right]\right\} \\ &+ (K - \tilde{c})\left[\overline{(u_i)}_P - \overline{(u_i)}_R\right]\end{aligned} \tag{3.49}$$

The term in the braces may be seen to represent a component of transport that is connected with turbulent fluctuations in velocity. This term is represented by conventional gradient transport as follow:

$$\begin{aligned}&\left\{\overline{(u_i)}_{Rs} - \overline{(u_i)}_R + K\left[\left(\overline{(u_i)}_{Ps} - \overline{(u_i)}_P\right) - \left(\overline{(u_i)}_{Rs} - \overline{(u_i)}_R\right)\right]\right\} \\ &= -\frac{1}{\Sigma_{gen}}\frac{\mu_t}{Sc_\Sigma}\frac{\partial}{\partial x_i}\left(\frac{\Sigma_{gen}}{\bar{\rho}}\right)\end{aligned} \tag{3.50}$$

where μ_t is the LES eddy viscosity and Sc_Σ is the subgrid Schmidt number for FSD. The second term of Eq. 3.49 represents a transport term that is primarily dependent on the effects of heat release. This is referred to as the non-gradient transport term. This term also contains the turbulent fluctuations contribution. To establish the form for the non-gradient transport component of the transport term it is instructive to consider two simple cases. Firstly consider the case of steady planar laminar propagation for which $\Delta >> \delta_z$. It may be seen that in absence of turbulence and pressure gradient effects for a planar flame, $\vec{u}_P - \vec{u}_R = \tau S_L\left(\nabla\bar{c}/|\nabla\bar{c}|\right)$, where τ is the heat release parameter. Secondly consider a steady one dimensional turbulent propagation problem where the filter size is much larger than the turbulent flame brush thickness, in the present, $\vec{u}_P - \vec{u}_R = \tau S_T\left(\nabla\bar{c}/|\nabla\bar{c}|\right)$ where S_T is the turbulent flame speed and can be defined as: $S_T \approx S_L\int_{-\infty}^{\infty}\Sigma_{sg}dx$. In more general situations of one-dimensional character, it is expected that the slip velocity usually lies between these two limits. However for curved flame surfaces it is possible that the magnitude of the slip velocity reduces below the

laminar flame speed. This is a result of the normals being no longer aligned in the same direction, which reduces the expansion effect on the mean velocities. As the flame becomes more wrinkled at the subgrid level, two competing effects play an important role. On one hand the flame propagates faster, resulting in a greater slip velocity, and on the other hand the normals become less aligned, leading to a reduced slip velocity. The reduction in slip velocity due to the variation in orientation of the flame normals at the subgrid level is modelled assuming the flame is locally one-dimensional in nature. In this case the unfiltered slip velocities across the flame element is given by:

$$(\vec{u}_P)_s - (\vec{u}_R)_s \approx -\tau S_L \vec{N} \tag{3.51}$$

If these elements can be assumed to act additively to give a resultant LES filtered slip velocity, Hawkes [66] proposed a model for LES filtered slip velocity as:

$$\overline{(u_i)}_P - \overline{(u_i)}_R \approx -\tau S_L \overline{(N_i)}_s \tag{3.52}$$

It may be seen that since $\Sigma_{sg} \geq |\nabla \bar{c}|$, the above model will result in a reduced slip velocity for wrinkled flames, which Hawkes and Cant [67, 68] applied for their LES modelling. Chakraborty [22] and Chakraborty and Cant [35] accounted for localised curvature effects on slip velocity by modifying the expression given in Eq. 3.51 to give rise to the following expression:

$$\overline{(u_i)}_P - \overline{(u_i)}_R = -\tau \frac{\overline{(\rho S_d)}_s}{\rho_0} \overline{(N_i)}_s \tag{3.53}$$

The heat release contribution on the strain rate term S_{hr} is given by following expression [66]:

$$\overline{\left[(\delta_{ij} - N_i N_j) \frac{\partial (u_i'')_s}{\partial x_j} \right]_s} \tag{3.54}$$

The above expression could be compared with the resolved component of the following curvature term [66]:

$$\overline{\left[(\delta_{ij} - N_i N_j) \frac{\partial (S_d N_i)}{\partial x_j} \right]_s} \tag{3.55}$$

Inspecting the form of Eq. 3.54 and Eq. 3.55 reveals that the heat release term acts like a curvature term only with a different propagation velocity. Following this argument Hawkes [66] modelled the effect of heat release on the strain rate as an adjustment to the resolved curvature term as:

$$S_{hr} = -(K - \tilde{c})\tau S_L \frac{\partial \overline{(N_i)}_s}{\partial x_i} \Sigma_{sg} \tag{3.56}$$

In the same way the non-gradient component of subgrid transport was modelled as an adjustment to the mean propagation term [66] in the following manner:

$$\text{Non-gradient transport part of } -\frac{\partial \overline{(u_i'')}_s \Sigma_{sg}}{\partial x_i} = \frac{\partial}{\partial x_i}\left[-(K - \tilde{c})\,\tau S_L \overline{(N_i)}_s \Sigma_{sg}\right] \tag{3.57}$$

This modelling approach for the slip velocity and S_{hr} might not be very accurate as the model given by Eq. 3.52 tends to underestimate the slip velocity. Chakraborty [22] and Chakraborty and Cant [35] modified the models given by Eqs. 3.56 and 3.57 by replacing S_L with $\overline{(\rho S_d)}_s/\rho_0$ where the local effects of S_d is explicitly accounted for. This allowed for the models to be viable in both the corrugated flamelets regime and the thin reaction zones regime. Weller et al. [159] suggested an alternative way of modelling the slip velocity as:

$$\overline{(u_i)}_P - \overline{(u_i)}_R \approx -\tau S_L \Xi M_i \tag{3.58}$$

where M_i is the resolved normal given by:

$$M_i = -\frac{1}{|\nabla \bar{c}|}\frac{\partial \bar{c}}{\partial x_i} \tag{3.59}$$

and Ξ is the wrinkling factor, defined as:

$$\Xi = \frac{\Sigma_{sg}}{|\nabla \bar{c}|} \tag{3.60}$$

$|\nabla \bar{c}|$ represents the resolved FSD, and the wrinkling factor Ξ itself represents a measure of unresolved flame wrinkling, such that when $\Xi = 1$ the flame is completely resolved. The model presented in Eq. 3.58 tends to overestimate the

slip velocity as it ignores product velocity variation within the subgrid volume [149].

3.2.3 Wrinkling Factor

Weller et al. [159] proposed an algebraic model for wrinkling factor:

$$\Xi = 1 + 2(1 - \tilde{b})(\Theta - 1) \tag{3.61}$$

where $\tilde{b} = 1 - \tilde{c}$ is the regression variable and $\Theta = 1 + 0.62\sqrt{u'_\Delta / S_L}$ and $Re_\eta = l_\eta^2/(\tau_\eta \nu)$. Algebraic models of the wrinkling factor can be used to describe FSD and vice versa. An algebraic model for the wrinkling factor should predict a wrinkling factor equal to unity when the flow is fully resolved, since the wrinkling factor is a measure of unresolved flame wrinkling. From the expression in Eq. 3.61 it is clear that Ξ approaches to unity as the flow is fully resolved (i.e. $u'_\Delta \to 0$). Colin et al. [53] proposed an algebraic model for the wrinkling factor which takes the form:

$$\Xi = 1 + \alpha' \Gamma \left(\frac{\Delta}{\delta_z}, \frac{u'_\Delta}{S_L} \right) \frac{u'_\Delta}{S_L} \tag{3.62}$$

where $\Gamma\left[(\Delta/\delta_z), (u'_\Delta/S_L)\right]$ is an efficiency function determined by a counter rotating eddy and flame interaction study as:

$$\Gamma \left(\frac{\Delta}{\delta_z}, \frac{u'_\Delta}{S_L} \right) = 0.75 \exp \left[- \frac{1.2}{(u'_\Delta / S_L)^{0.3}} \right] \left(\frac{\Delta}{\delta_z} \right) \tag{3.63}$$

The factor α' is given as:

$$\alpha' = \beta' \frac{2 \ln(2)}{3 c_{ms} (Re_t^{1/2} - 1)} \tag{3.64}$$

where the subgrid turbulent velocity is given as $Re_t = u'_\Delta l/\nu$, β' is a model constant of order unity and $c_{ms} = 0.28$ according to a surface propagation study by Yeung et al. [164]. Colin et al. [53] used an estimation of the subgrid turbulent velocity scale u'_Δ based on resolved vorticity field in the following manner:

$$u'_\Delta = 2\Delta^3 |\nabla^2 (\nabla \times \overline{\vec{u}})| \tag{3.65}$$

Colin et al. [53] used this model to simulate combustion in a Lateral Injections Combustor (LIC) together with the thickened flame approach and got good agreement with experimental results.

Model proposed by Colin et al. [53] requires three quantities namely u'_Δ/S_L, Δ/δ_z and Re_t. Charlette et al. [49] proposed a model which reduced the required inputs of Colin et al. [53] model to two, namely u'_Δ/S_L and Δ/δ_z. Charlette et al. [49] model takes the following form:

$$\Xi = \left(1 + \min\left[\frac{\Delta}{\delta_z}, \Gamma\frac{u'_\Delta}{S_L}\right]\right)^{\beta'} \tag{3.66}$$

where Γ is the efficiency function which is fitted based on its limiting behaviours in the framework of Von Karman-Pao spectrum. Charlette et al. [49] proposed the efficiency function which takes the following form:

$$\Gamma\left(\frac{u'_\Delta}{S_L}, \frac{\Delta}{\delta_z}, Re_\Delta\right) = \left\{\left[(f_u^{-a} + f_\Delta^{-a})^{-1/a}\right]^{-b} + f_{Re}^{-b}\right\}^{-1/b} \tag{3.67}$$

where

$$f_u = 4\left(\frac{27C_k}{110}\right)^{1/2}\left(\frac{18C_k}{55}\right)\left(\frac{u'_\Delta}{S_L}\right)^{1/2} \tag{3.68a}$$

$$f_\Delta = \left\{\frac{27C_k\pi^{4/3}}{110}\left[\left(\frac{\Delta}{\delta_z}\right)^{4/3} - 1\right]\right\}^{1/2} \tag{3.68b}$$

$$f_{Re} = \left[\frac{9}{55}\exp\left(-\frac{3}{2}C_k\pi^{4/3}Re_\Delta^{-1}\right)\right]^{1/2} Re_\Delta^{1/2} \tag{3.68c}$$

where the exponents a and b are given by:

$$a = 0.6 + 0.2\exp\left(-0.1\frac{u'_\Delta}{S_L}\right) - 0.2\exp\left(-0.01\frac{\Delta}{\delta_z}\right) \tag{3.69a}$$

$$b = 1.4 \tag{3.69b}$$

In the power-law version of the model given by Eq. 3.66 the exponent β' is taken to be 0.5. Charlette et al. [50] proposed a dynamic approach to evaluate the

exponent where β' is given by:

$$\beta' = \log\left[\gamma\frac{\widetilde{\langle W_\Delta \tilde{c}\rangle}}{\langle W_{\gamma\Delta}\hat{\tilde{c}}\rangle}\right] \Big/ \log\left[\frac{1+\min\left(\frac{\gamma\Delta}{\delta_z}, \Gamma_{\gamma\Delta}\frac{\langle u'_{\gamma\Delta}\rangle}{S_L}\right)}{1+\min\left(\frac{\Delta}{\delta_z}, \frac{\langle u'_{\Delta}\rangle}{S_L}\right)}\right] \tag{3.70}$$

where $W_\Delta = \overline{\dot{w}}\Delta/\Xi$ and test filter size is given by $\gamma\Delta$. The filtering operation at filter scale $\gamma\Delta$ is denoted by the overbrace $\widetilde{(\dots)}$ and the angle brackets $\langle\dots\rangle$ indicates LES volume averaging in order to avoid non-physical oscillations in dynamic filtering operation. Charlette et al. [49, 50] showed that both the power-law and dynamic versions of their model predict the turbulent flame behaviour accurately based on *a posteriori* DNS analysis of the wrinkling factor model in the framework of thickened flame approach. It is important to note that the u'_Δ estimation using Eq. 3.65 yields meaningful results only when a particular kind of central differencing approach is used [53]. A model should be independent of the choice of numerics but both [53] and Charlette et al. [49, 50] models are dependent on a particular type of numerical implementation. In spite of these shortcomings both of these models present a new modelling approach based on subgrid scale wrinkling factor.

Wrinkling factor is related to the turbulent flame speed S_T by the following relationship:

$$\Xi = \frac{S_T}{S_L} \tag{3.71}$$

This allows for S_T models to be applicable for the wrinkling factor and thus to the FSD.

As in the case of FSD, a transport equation can be solved for the wrinkling factor Ξ which was derived by Weller [157], it takes the following form:

$$\frac{\partial\Xi}{\partial t} + \overline{(\dot{X}_j)_s}\frac{\partial\Xi}{\partial x_j} = -\overline{\left[N_i N_j \frac{\partial X_i}{\partial x_j}\right]_s}\Xi + M_i M_j \frac{\partial W}{\partial x_j}\Xi + (W_i - \overline{(\dot{X}_j)_s})\frac{\partial|\nabla c|}{\partial x_i}\frac{\Xi}{|\nabla\bar{c}|} \tag{3.72}$$

where $\overline{(\dot{X}_j)_s} = u_i + S_d N_i$ and W_i is the resolved net velocity given by:

$$\frac{\partial\bar{c}}{\partial t} + W_i\frac{\partial\bar{c}}{\partial x_i} = 0 \tag{3.73}$$

Weller et al. [159] modelled Eq. 3.72 using the following expression:

$$\frac{\partial \Xi}{\partial t} + \overline{(\dot{X}_j)}_s \frac{\partial \Xi}{\partial x_j} = G_\Xi \Xi - R_\Xi(\Xi - 1) + (\Sigma_s - \Sigma_t)\Xi \tag{3.74}$$

In the above equation $G_\Sigma = R_\Sigma(\Xi_{eq} - 1)/\Xi_{eq}$ and $R_\Xi = (0.28/\tau_\eta)[\Xi^*_{eq}/(\Xi^*_{eq} - 1)]$ where $\Xi_{eq} = 1 + 2\tilde{c}(\Xi^*_{eq} - 1)$ and $\Xi^*_{eq} = 1 + 0.62\sqrt{(u'_\Delta/S_L)}Re_\eta$. $Re_\eta = i'_\Delta \eta/\tau_\eta \nu$, is the Kolmogorov Reynolds number, where η is considered to be the inner cutoff scale according to the ideas of passive scalar mixing. The surface filtered flame velocity is given by:

$$\Sigma_s = (\delta_{ij} - M_i M_j)\frac{\partial \tilde{u}_i}{\partial x_j}\frac{1}{\Xi} + \frac{\Xi - 1}{2\Xi}(\delta_{ij} - M_i M_j)\frac{\partial (S_L M_i)}{\partial x_i} \tag{3.75}$$

This includes both resolved strain rate mean S_{mean} and resolved curvature term C_{mean} equivalents of the FSD transport equation [67, 68]. In spite of a number of similarities between the FSD based models of Hawkes and Cant [67, 68], and the wrinkling factor based models by Weller et al. [159] and Tabor and Weller [144], there are important differences between the models in the respect of turbulent transport and flame normal modelling. The propagation term is not naturally closed in the formulation by Weller et al. [159] and Tabor and Weller [144]. On the whole Hawkes and Cant [67, 68] model seems to be less complicated and the modelling is less ambiguous in several respects compared to the wrinkling factor model by Weller et al. [159] and Tabor and Weller [144]. The important feature of the model of Weller et al. [159] lies in solving a transport equation for laminar burning velocity, which takes care of the unsteady effects of strain rate and curvature of flame propagation. The model of Weller et al. [159] is applied to LES of a reactive shear layer at a rearward facing step and good agreement was obtained when the time averaged profiles of velocities, their fluctuations, temperature and reaction products were compared with the corresponding experimental data.

3.3 Other Flamelet based Approaches

A brief summary of other alternative approaches which address the reaction rate closure in turbulent premixed combustion are discussed in this section.

3.3.1 Artificially Thickened Flame

In the artificially thickened flame approach, the thickness of the flame is increased such that it becomes resolved on an LES mesh, which has the advantages of allowing for flame-wall interactions and ignition. The flame is solved for by using a single step Arrhenius mechanism. In such a situation the flame speed S_L and the Zel'dovich flame thickness δ_z scale in the following manner:

$$S_L \propto \sqrt{\alpha_T B^*} \text{ and } \delta_z = \frac{\alpha_T}{S_L} \tag{3.76}$$

where B^* is the pre-exponent factor associated with chemical reaction rate and α_T is the thermal diffusivity. If the thermal diffusivity α_T is increased by a factor F and the pre-exponent is decreased by the same factor F, it is possible to maintain the same flame speed, while at the same time increasing the flame thickness. The quantity F is chosen in such a manner that the reaction layer given by $F\delta_L$ is resolved in the LES grid. Under these modification of the thickening factor F the transport equation for the reaction progress variable takes the following form:

$$\frac{\partial(\rho c)}{\partial t} + \frac{\partial(\rho u_j c)}{\partial x_j} = \frac{\partial}{\partial x_j}\left[\rho D F \frac{\partial c}{\partial x_j}\right] + \frac{1}{F}\rho B^*(1-c)\exp\left[\frac{-\beta(1-T)}{1-\alpha(1-T)}\right] \tag{3.77}$$

In this approach the subgrid transport terms and reaction term are modelled simultaneously. Artificially thickened flame model is suited for the case where the flame-turbulence interaction is dominated by the large scales. Addtionally the subgrid flame structure is assumed to correspond to that of a unwrinkled laminar flame propgating at the speed of the laminar flame. This, however, is not true in reality as even small eddies with the right amount of energy are able to cause some degree of subgrid wrinkling, and these eddies will remain unresolved by LES. Moreover the thickening of the flame decreases the response in terms of resolved wrinkling to small-scale resolved strains. Structures much smaller than the flame thickness fail to produce significant flame stretch [116]. A study by Veynante and Poinsot [154] has shown this by comparing a DNS case with an artificially thickened flame. Additionally the sensitivity of laminar flame speed to strain rate and curvature is increased by the artificial modification of B^* and δ_z, since the Markstein length is proportional to the Zeldovich flame thickness δ_z,

which in turn leads to easier quenching of the flame. These shortcomings were acknowledged by Veynante and Poinsot [154], and in order to rectify this Poinsot et al. [116] and Angelberger et al. [2] proposed an efficiency function ξ based on DNS. This efficiency function can also be treated as the ratio of actual flame wrinkling factor the wrinkling factor corresponding to the thickened flame:

$$\xi = \frac{\Xi(\Delta/\delta_L)}{\Xi(\Delta/F\delta_L)} \tag{3.78}$$

Reduction in flame front wrinkling can be compensated by increasing the flame speed by a factor ξ which amounts to a ξ^2 fold increase in pre-exponential factor Colin et al. [53]. Alternatively, the efficiency function ξ can be used to multiply both the reaction rate and diffusivities which would result in increased laminar flame speed, but resulting in an unchanged flame width. With this modification the c transport equation takes the following form:

$$\frac{\partial(\rho c)}{\partial t} + \frac{\partial(\rho u_j c)}{\partial x_j} = \frac{\partial}{\partial x_j}\left[\xi\rho DF\frac{\partial c}{\partial_j}\right] + \frac{\xi}{F}\rho B^*(1-c)\exp\left[\frac{-\beta(1-T)}{1-\alpha(1-T)}\right] \tag{3.79}$$

Angelberger et al. [2] have shown promising results with this approach in simulation of combustion instabilities. New models were proposed by Colin et al. [53] and Charlette et al. [49, 50] for the wrinkling factor in the context of artificially thickened flame approach. The model by Colin et al. [53] shown in Eq. 3.62 leads to the following limits for the efficiency function ξ:

$$1 \leq \xi \leq F^{2/3} \tag{3.80}$$

3.3.2 *G* Equation

The G equation formulation adopts the opposite view to the artificially thickened flame approach. In G equation the flame is treated as an infinitely thin propagating surface which is tracked by a scalar field G which is given by the following equation:

$$\frac{\partial G}{\partial t} + \vec{u}.\nabla G = S_d|\nabla G| \tag{3.81}$$

Here the level surface $G = G_0$ represents the flame sheet and S_d is the local displacement speed. It is a very important method of turbulent premixed flame description [122] provided the statistics of S_d are appropriately accounted for, although it is only applicable for wrinkled flamelets regimes [160]. Naitoh et al. [104] and Naitoh et al. [105] has applied the G equation for a reciprocating internal combustion engine application. In another study Candel et al. [19] extended the method for variable density flows and compared the results with DNS. It is not made clear how filtering process relates to the surface propagation equation. In many studies the effect of filtering is seen to increase the displacement speed of flame surface by subgrid wrinkling. When Eq. 3.81 is filtered it results in the following equation:

$$\frac{\partial \bar{G}}{\partial t} + \tilde{u}_j \frac{\partial \bar{G}}{\partial x_j} = S_T |\nabla \bar{G}| \tag{3.82}$$

It is then possible to estimate the LES turbulent flame speed using renormalised group assumptions as [108]:

$$S_T = S_L \exp\left(\frac{2\tilde{k}}{3S_L^2}\right) \tag{3.83}$$

As of yet it remains unclear whether or not the G equation is intended to be explicitly filtered or what the model for the turbulent flame speed S_T is intended to describe. Filtering the G equation results in the following expression:

$$\frac{\partial \bar{G}}{\partial t} + \tilde{u}_j \frac{\partial \bar{G}}{\partial x_j} + \left(\overline{u_j \frac{\partial G}{\partial x_j}} - \tilde{u}_j \frac{\partial \bar{G}}{\partial x_j}\right) = \overline{S_d |\nabla G|} \tag{3.84}$$

If the above equation is to be solved in a LES simulation the last term on the left hand side must be modelled (commonly referred to as the G-flux). This reflects the fact that subgrid scale velocity fluctuations contribute to transport of G, in addition to affecting the displacement speed S_d. In the above equation it is clear that it lacks a diffusion term and that leads to numerical instabilities. Additionally, there is no lower limit for radius of curvature of the G field, which can result in cusps with zero radius of curvature to form as the flame evolves. These cusps of zero curvature cannot be captured using a computational grid. In a study by Pope et al. [125] where DNS of material surfaces was used to show

that numerical difficulties occur due to the undefined lower limit for the radius of curvature. Cusps in LES are generally not expected as the filter width generally tends to be much larger the flame thickness δ_z. One of way of addressing the cusp problem is to introduce artificial diffusion [110] or through numerical methods which introduce diffusivity.

Another problem faced by the G equation is the inclusion of gas expansion effects across the flame. In G equation studies it is quite common to assume a constant density and the displacement speed S_d is assumed to be equal to the laminar flame speed S_L. The displacement speed S_d is found in the filtered G equation but the effect of heat release and chemical reaction is described by the consumption speed S_c. As discussed earlier these two quantities are not the same, but are interrelated although their magnitude can be quite different if the flame is curved [117]. It is possible to relate the temperature field with G equation using the following relation: $h = C_p\hat{T} + Gh_f$, where h is the enthalpy and h_f is the heat of combustion of the premixed fuel [103]. Therefore the spatial distribution of heat release depends on the G profile thickness. If filtering of G equation is not used then the thickness of the G profile depends entirely on numerical diffusion. In a LES simulation it is common to the see the distribution of the heat release to have a thickness in order of the filtered flame thickness (at least equal to or greater than the filter width Δ). Work by Piana et al. [110] has made progress by using a normalised *ad hoc* shape function such that G can be resolved on the computational mesh. Im et al. [74] propose more consistent work on G equation for the constant density reacting flows such that:

$$\overline{\vec{u}.\nabla G} - \overline{\vec{u}}.\nabla\bar{G} \approx -\frac{\mu_t}{Sc_G}\nabla G \tag{3.85}$$

It is then proposed that the right hand side of the Eq. 3.84 is modelled in the following manner:

$$\overline{S_d|\nabla G|} = S_T|\nabla\bar{G}| \tag{3.86}$$

where the LES turbulent flame speed S_T is given by:

$$\frac{S_T}{S_L} = 1 + A\left(\frac{\sqrt{\tilde{k}}}{S_L}\right)^q \tag{3.87}$$

The parameters Sc_G and A were determined using a dynamic approach. The gradient transport closure for subgrid flux introduces diffusion and this avoids numerical difficulties associated with the formation of cusps in the original G equation. Comparisons with DNS results, even at relatively high level of resolution, (Δ equal to DNS grid size) were unsatisfactory.

Problem due to heat release have been addressed by Piana et al. [110] and Kim et al. [88]. The G equation can be written in conservative form as:

$$\frac{\partial \rho G}{\partial t} + \nabla.(\rho \vec{u} G) = \rho S_d |\nabla G| \tag{3.88}$$

Filtering the above equation results in:

$$\frac{\partial \bar{\rho}\tilde{G}}{\partial t} + \frac{\partial \bar{\rho}\tilde{u}_j\tilde{G}}{\partial x_j} + \left(\frac{\partial \overline{\rho u_j G}}{\partial x_j} - \frac{\partial \bar{\rho}\tilde{u}_j\tilde{G}}{\partial x_j} \right) = \overline{\rho S_d |\nabla G|} \tag{3.89}$$

Kim et al. [88] used the gradient model for the flux term ($\overline{\rho u_i G)} - \bar{\rho}\tilde{u}_i\tilde{G}$) where the eddy diffusivity is evaluated using a dynamic one equation ($\tilde{k}$) model [87] and finally the right hand side of the equation is modelled according to [87]. In a study by Piana et al. [110] the subgrid flux was modelled using a filtered structure function. Peters [107] used an order of magnitude analysis to propose the following form of the G equation by taking into account the curvature dependence on displacement speed so that it can be used for both the corrugated flamelets and the thin reaction zones regime.

$$\rho \frac{\partial G}{\partial t} + \rho u_j \frac{\partial G}{\partial x_j} = \rho S_L |\nabla G| - 2\rho D \kappa_m |\nabla G| \tag{3.90}$$

where $\kappa_m = 1/2\nabla.\vec{N}$ is the local curvature. The above equation can be LES filtered or RANS averaged, and when subjected to gradient transport modelling of $\overline{\rho u_i G} - \bar{\rho}\tilde{u}_i\tilde{G}$, the Reynolds averaged/LES filtered G equation assumes the following form [107, 111]:

$$\bar{\rho}\frac{\partial \tilde{G}}{\partial t} + \bar{\rho}\tilde{u}_j \frac{\partial \tilde{G}}{\partial x_j} = \rho_0 S_T |\nabla \tilde{G}| - \bar{\rho} D_t \tilde{\kappa} |\nabla \tilde{G}| \tag{3.91}$$

where $\tilde{\kappa} = \nabla.\left(-\nabla\tilde{G}/|\nabla\tilde{G}|\right)$. The equation shown in Eq. 3.90 and 3.91 does not depend on numerical diffusion, but the diffusion effect is taken care of by the presence of the curvature term.

The turbulent flame speed S_T is predicted from the expressions provided by different turbulent flame speed S_T models. Yakhot [163] provided the following modelling expression for S_T:

$$\frac{S_T}{S_L} = \exp\left(\frac{2\tilde{k}}{3S_L^2}\right) \tag{3.92}$$

Pocheau [112] presented an alternative model for S_T as:

$$\frac{S_T}{S_L} = \left(1 + A\frac{u_\Delta'^2}{S_L^2}\right)^{1/2} \tag{3.93}$$

where A is model parameter (see Eq. 3.87). Pocheau [112] has implemented this model for a gas turbine geometry and it was possible obtain satisfactory results when compared with experimental findings. It was found by Pocheau [112] that the expression for the flame speed by Pocheau [112] outperforms the Yakhot [163] expression in Eq.3.92. In another study Piana et al. [110] was able to model for S_T using a flame wrinkling description: Pocheau [112] presented an alternative model for S_T as:

$$\frac{S_T}{S_L} = 1 + (\Xi_{max} - 1)\left[1 - \exp\left(-B\frac{\Delta}{L_{out}}\right)\right] \tag{3.94}$$

where B is a model constant, L_{out} is the outer cutoff scale for the flame wrinkling (modelled as a turbulent length scale) and Ξ_{max} is the level of flame wrinkling corresponding to the large Δ limit (modelled identically to S_T/S_L as in Eq. 3.87). In a recent study by Pitsch and Lageneste [111] the following expression was presented for the evaluation of turbulent flame speed for the closure of the LES version of Eq. 3.91:

$$\frac{S_T - S_L}{S_L} = \frac{u'\Delta}{S_L} b_3 \sqrt{\frac{Da_\Delta/Sc_\Delta}{1 + [(b_3^2 Da_\Delta)/(b_1^2 Sc_\Delta)]}} \tag{3.95}$$

where the local Damköhler number is given by $Da_\Delta = Ka_\Delta'^{-2}(u'_\Delta/S_L)^2$ and the local Karlovitz number is given as $Ka'_\Delta = (u'_\Delta/S_L)^{3/2}(\delta_z/\Delta)^{1/2}$ and the model constants takes the following values $b_3 = 1.0$, $b_2 = 2.0$, $Sc_\Delta = 0.5$. This expression was used by Pitsch and Lageneste [111] to achieve good agreement with experimental results for a methane-air Bunsen burner flame.

The approach taken by Im et al. [74], Kim et al. [88], Piana et al. [110] to solve the G equation is closer to the progress variable c approach than than original idea of G equation. The evolution equation of $\tilde{c}$ can be written in terms of flame speed with flame speed defined by combined reaction and molecular diffusion rates of progress variable, as shown by Vervisch et al. [151]. In the G equation approach the turbulent flame speed while turbulent flame speed can be obtained as a part of the solution in the FSD based approach. The G equation approach has the advantage of capturing the spatial distribution of heat release since the flame speed is explicitly included. Other methods calculate for the flame speed using other models which use the internal structure of the flame. In LES only partial resolution of the internal flame structure is possible, this leaves the question of whether it is possible to accurately represent the flame propagation. On the other hand the existence of turbulent flame speed is a controversial issue, and in any case the experimental data is highly scattered and subject to considerable uncertainty [10, 12, 14, 90, 91]. It is also not clear that a single expression can be used to predict the turbulent flame speed which describes turbulence flame interaction. In the G equation approach coupling between the G equation and energy equation is not very straightforward, while in the reaction progress variable c approach no such problem occurs. The G equation is based on a kinematic description of the flow field, which involves the displacement speed S_d. On the other hand the chemical consumption and heat release are governed by the consumption speed. As discussed earlier consumption speed can be different to displacement speed in regions of large flame curvature [117]. This problem can be addressed by adopting a geometrical approach, which estimates the volume of burned gas as well as the heat release from the displacement of the flame front. This technique is commonly known as flame front tracking technique [139, 156]. An alternative of estimating temperature field from G field is discussed by Kim et al. [88]. In this approach the temperature field is constructed from the G field and the energy equation is

not solved. The temperature field $\hat{T}$ is given as follows:

$$\hat{T} = T_0 + \frac{Q}{C_P} H(G - G_0) \tag{3.96}$$

where T_0 is the the initial temperature. This method is commonly know as the temperature reconstruction technique [156]. However this method is not valid when heat loss and compressibility effects are significant. Piana et al. [110] proposed a method known as the forward estimation of temperature method for estimating heat release from the G field, which removes the limitations faced by the temperature reconstruction technique. In this method G equation is time advanced before the Navier Stokes equations and based on the knowledge of the $G = G_0$ isosurface an estimation of presumed temperature field T^* is made by a suitable relationship such as [110]:

$$T^* = \hat{T}_{G=G_0} + \frac{1}{2}\left[\tanh\left(\frac{(G - G_0)\pi}{2\delta}\right) + 1\right](T_b - T_0) \tag{3.97}$$

where $\hat{T}_{G=G_0}$ is the temperature at $G = G_0$ isosurface, T_b is the burned gas temperature and δ is adjustable parameter which takes care of the stiffness of the presumed temperature. The energy release source term in the energy equation is estimated using T^* and already temperature field T as [110]:

$$\dot{w}_T = \rho(1 - c)C_P(T^* - \hat{T}) \tag{3.98}$$

Menon and Jou [103] presented an alternative method of coupling temperature and G field in the following form:

$$h = C_P\hat{T} + h_f G \tag{3.99}$$

This coupling is very similar to the coupling of reaction progress variable field with the temperature field.

3.4 Summary

In this chapter a combustion regime diagram for turbulent premixed combustion as proposed by Peters [107] was introduced, with the help of the turbulent and chemical length scales. Following this a review of the flamelet based reaction rate closures for turbulent premixed combustion were examined. In the case of FSD based closure, a description of existing algebraic models was provided, which was followed by the transport equation approach. The behaviour of the algebraic models in the context of LES within the current DNS database for a range of filter widths can be found in chapter 5. It was discussed that in the transport equation modelling, the subgrid/mean FSD convection term was typically dealt with using the gradient hypothesis, although non-gradient transport can be expected. Additionally the propagation term is considered closed if $\overline{(\rho S_d)}_s$ is modelled accurately. Then the closure for the FSD transport equation relies on the accurate modelling of the curvature and strain rate terms, which forms the basis for chapters 7 and 8, respectively. This discussion was followed by the wrinkling factor modelling, where both algebraic and transport equation closures were reviewed. Finally a discussion of the other flamelet modelling strategies was given in §.3.3 i.e. thickened flame model and G equation model. In the following chapter a discussion of the DNS database is presented with the parameters of interest and their effects on the flame surface. Additionally a description of the numerical techniques used to calculate and post-process the database are presented.

Chapter 4

DNS Database

In the current work several DNS cases were used to carry out *a priori* analysis of existing models (shown in §.3.2) and newly proposed models (chapters 5, 6, 7 and 8). Thus an overview on how the simulations were carried out and a clear description of the DNS cases is provided in this chapter. In the following sections an introduction to the numerics involved in carrying out the DNS is provided, which is followed by the presentation of the DNS database that is used for the current analysis. Finally an overview of the LES filtering and Reynolds averaging techniques is given.

4.1 DNS Procedure

The fairly complex behaviour of momentum, heat and mass transports seen in a turbulent flow are governed by a set of coupled conservation equations of mass, momentum, energy and species. Analytical solutions for these coupled conservation equations do not exist for even the simplest turbulent case. A way to get around this problem is to solve these equations numerically without any recourse to physical approximation regarding turbulent flow physics, and this method is known as DNS. The requirements of length and time scale resolution in DNS becomes more stringent with increasing Reynolds number, and the value of turbulent Reynolds number limits the applicability of DNS as the computational costs become unaffordable even for the fastest and largest supercomputers

for the turbulent Reynolds numbers encountered in practical engineering applications. Another problem that stems from using any numerical simulations is the appropriateness of the choice of boundary conditions. Without proper implementation of the boundary conditions numerical artifacts can easily affect a simulation. Computation time can also be saved through an efficient initialisation process. In the current study, the statistics were extracted from the DNS data after a certain run time and the choice of this time must also be justified. High accuracy must be maintained when evaluating spatial and temporal derivatives. The above topics relevant to the DNS database will be discussed in detail in the following subsections.

4.1.1 Requirements for Spatial and Temporal Resolution

A detailed parametric analysis is carried out to explore the effects of non-dimensional numbers such as Le, Ka and Re_t on FSD using the DNS code called SENGA, which was developed at the University of Cambridge [77]. This code uses a uniform Cartesian grid for the purpose of spatial discretisation. One of the main constraints imposed on DNS is the number of grid point required to resolve the flow, since this directly affects computational cost. In order to fully resolve a flow the smallest length scale of turbulence must be resolved. At the same time the domain size of the simulation should be large enough to encompass the largest scales involved in the flow. These two conditions, i.e. resolution of the smallest and largest scales, has been used to define the domain size L and the grid spacing $\Delta x = L/N$, where N is the number of grid points and $N+1$ grid points are used to discretise the domain.

For a non-reacting isothermal turbulent flow, the smallest length scale involved is the Kolmogorov length scale η thus it is possible to write the following resolution criterion:

$$\frac{L}{\eta} < N \tag{4.1}$$

The Kolmogorov length scale can be scaled as $\eta \sim l/(Re_t)^{(3/4)}$, where l is the integral length scale and Re_t is the turbulent Reynolds number. Eq. 4.1 can then

be written in the following form:

$$N > Re_t^{3/4} \tag{4.2}$$

Eq. 4.2 can be recast in the following manner:

$$Re_t < N^{4/3} \tag{4.3}$$

So for an isothermal non-reacting turbulent flow simulation, the above inequalities determine the number of grid points $(N + 1)$, for a given turbulent Reynolds number. The domain size must be greater than or equal to the largest turbulent scale of the flow i.e. the integral length scale l, this leads to:

$$L = N\Delta x \geqslant l \tag{4.4}$$

In a combustion simulation where the flame thickness can be much smaller than the Kolmogorov length scale, a new criterion must be specified for the grid spacing Δx to resolve the flame. In the current DNS database the simulations were carried out using a single step Arrhenius type chemistry, and in order to resolve the flame, 10 grid points span the thickness of the flame. If the laminar flame thickness is denoted by δ_L and $Q = 10$ is the number cells allotted to resolve the flame then the following criterion can be obtained for domain size:

$$L = \frac{N}{Q}\delta_L \tag{4.5}$$

where laminar flame thickness δ_L was defined using the reaction progress variable in the following manner:

$$\delta_L = 1.0/\max\left|\frac{\partial c}{\partial n}\right|_L \tag{4.6}$$

where n is the flame normal direction and the subscript L refers to the quantities in unstrained laminar planar laminar flames. Through Eq. 4.5 an upper limit can be set for the domain size which should be larger than the integral length scale i.e.

$$\frac{l}{\delta_L} < \frac{L}{\delta_L} < \frac{N}{Q} \tag{4.7}$$

The above expression can be recast in term of Da and Re_t if the diffusive flame thickness $\delta \approx \nu/S_L$ is used instead of δ_L, by using the product of Re_t and Da, Eq. 4.5 can be written as:

$$Re_t Da = \frac{l^2 S_L}{\nu \delta} = \left(\frac{l}{\delta}\right)^2 \tag{4.8}$$

If it is assumed that δ and the Zeldovich flame thickness $\delta_z = D/S_L$ are of the same order, Eq. 4.8 can be rearranged to lead to the following inequality:

$$Re_t Da < \left(\frac{N}{Q}\right)^2 \tag{4.9}$$

From Eq. 4.9 it is possible to conclude that when Re_t is limited by the value given by Eq. 4.3, and Da is bound by Eq. 4.9, thus the parametric range explorable by DNS at present remains quite limited.

Temporal resolution, too, plays an important role in determining the computational cost of a DNS. In a combustion DNS a number of requirements ultimately determine the time step size Δt. The first criterion based on which Δt is based on is the Kolmogorov time scale t_η, which can be written as:

$$\Delta t \leq t_\eta \text{ or } \Delta t < \left(\frac{\nu}{\epsilon}\right)^{1/2} \tag{4.10}$$

where ν is the kinematic viscosity and ϵ is the dissipation of turbulent kinetic energy. One of ways to ensure numerical stability in compressible simulation is to choose the time step Δt using the Courant number criterion C [123], which is defined in the following manner:

$$C = |u_i \pm a|\Delta t/\Delta x \tag{4.11}$$

where a is the acoustic speed in the unburned gas. For the purpose of numerical stability the Courant number criterion needs to be smaller than unity (i.e. $C \leq 1$). However, Pope [123] suggests that the Courant number criterion C should be around 1/20, for the solution to be accurate by allowing a fluid particle

to traverse only a fraction of the grid spacing in a single time step. While in DNS of compressible flows requires that acoustic waves rather than a fluid particle traverses only a fraction of the grid spacing in a single time step to ensure accuracy.

Another important parameter which determines the data extraction time is the simulation run time τ_{sim}. To define the simulation run time τ_{sim}, it is required that two separate time scales are defined; these are the integral eddy turn over time τ_{f0} and the chemical time scale τ_c:

$$\tau_{f0} = \frac{l}{u'} \tag{4.12a}$$

$$\tau_c = \frac{\delta_{th}}{S_L} \tag{4.12b}$$

where the thermal flame thickness δ_{th} is defined in the following manner:

$$\delta_{th} = \frac{(T_{ad} - T_0)}{\max |\nabla \hat{T}|_L} \tag{4.13}$$

The criterion τ_{sim} should be:

$$\tau_{sim} \geq \max(\tau_{f0}, \tau_c) \tag{4.14}$$

The simulation time given by Eq. 4.14 ensures that the simulation results when the statistics are extracted remains reasonably independent of the choice of initial conditions.

4.1.2 Numerical Schemes

A brief overview of the numerical methods that were used in the DNS code SENGA are presented in this section and a more in depth discussion can be found in appendix A. The boundary conditions in the direction of mean flame propagation are taken to be partially non-reflecting and the transverse boundaries are taken to be periodic [113]. The spatial derivatives for the internal grid points are calculated using a tenth order central differencing scheme. However, for non-periodic boundaries the spatial derivaties gradually decreases in accuracy

till it reaches a one sided second order finite difference scheme. The time advancement is carried out using a third order low storage Runge-Kutta scheme [161]. The turbulent fluctuating velocity field is initialised based on an incompressible homogeneous isotropic velocity distribution, which is generated using a pseudo-spectral method [133]. In all cases the simulation is run under decaying turbulence for one chemical time scale. The flame is initialised by a steady unstrained planar laminar flame solution.

4.2 DNS Database

Ten DNS cases have been used in this work to analyse the modelling of turbulent premixed combustion using the generalised FSD, by investigating both the algebraic and transport equation approaches. The simulation parameters for the DNS database have been chosen to analyse the effects of Lewis number and turbulent Reynolds number. Table 4.1 shows the prescribed initial parameters for the DNS database, which are the normalised rms velocity fluctuation u'/S_L, normalised integral length scale l/δ_{th}, turbulent Reynolds number Re_t, Damköhler number Da, Karlovitz number Ka and Lewis number Le. According to Peters [107] all cases in Table 4.1 belong to the thin reaction zones regime. To study the effects of Lewis number cases F-J were used. From Table 4.1 it is clear that for cases F-J the Lewis number ranges from 0.34 to 1.2, whereas all other parameters remain identical to each other. Cases A-E were used to analyse the effects of turbulent Reynolds number Re_t. In the unity Lewis number flames Re_t scales as $Re_t \sim Da^2Ka^2$ [107]. As Da and Ka are often used to characterise the combustion process on regime diagrams, the values of Da and Ka were altered independently of each other in cases A-E to bring about the variation of Re_t from 20 to 100. In Fig. 4.1 the contours of reaction progress variable $c < 0.9$ along with the $c = 0.9$ isosurface is plotted for all DNS cases. From Fig. 4.1 it is clear that the flame wrinkling increases with decreasing Lewis number, and increasing Reynolds number. It is clear from Fig. 4.1 that there are significant differences in the distribution of c. The effects of Lewis number and turbulent Reynolds number will be discussed briefly in the following sections.

Case	u'/S_L	l/δ_{th}	Re_t	Da	Ka	τ	Le
A	5.00	1.67	22.0	0.33	8.67	4.5	1.0
B	6.25	1.44	23.5	0.23	13.00	4.5	1.0
C	7.50	2.50	47.85	0.33	13.00	4.5	1.0
D	9.00	4.31	100.0	0.48	13.00	4.5	1.0
E	11.25	3.75	110.0	0.33	19.50	4.5	1.0
F	7.50	2.45	47.0	0.33	13.17	4.5	0.34
G	7.50	2.45	47.0	0.33	13.17	4.5	0.6
H	7.50	2.45	47.0	0.33	13.17	4.5	0.8
I	7.50	2.45	47.0	0.33	13.17	4.5	1.0
J	7.50	2.45	47.0	0.33	13.17	4.5	1.2

Table 4.1: List of initial parameters for the DNS database.

4.2.1 Lewis Number Effects

Cases F-J have been extensively used for the basic understanding of flame turbulence interaction. Cases H-J were used by Chakraborty and Klein [32] to analyse the effects of Le on the surface density function $|\nabla c|$ transport equation and scalar dissipation rate. Chakraborty and Cant [36] studied the effects of Lewis number on turbulent scalar transport using cases F-J. Using the same DNS cases, Chakraborty and Swaminathan [45] examined the influence of Lewis number on scalar variance transports and in a similar study the Lewis number effects on FSD transport were studied by Chakraborty and Cant [40].

Further these DNS cases were used to propose closure models. Cases F-J were also used by Chakraborty et al. [43] to analyse the statistical behaviour unclosed terms in turbulent kinetic energy transport equation in context of RANS. In a different study by Katragadda et al. [80, 81] cases F-J were used to analyse the effects of Le on the FSD strain rate term and curvature term in the context of RANS.

Thus the DNS cases F-J are well established in the existing literature and ob-

servations on the physical nature of these flames can be found in several previous studies: [36, 37, 40, 43, 45]. The reaction progress variable c isosurfaces can be seen for cases F-J in Fig. 4.1. It becomes evident from Fig. 4.1 that the flame wrinkling increases with decreasing Lewis number Le, which is consistent with several previous studies [1, 4, 26, 28, 36, 37, 39, 72, 95, 132, 135, 137, 148, 165].

The rates of burning, heat release and flame area generation increase with

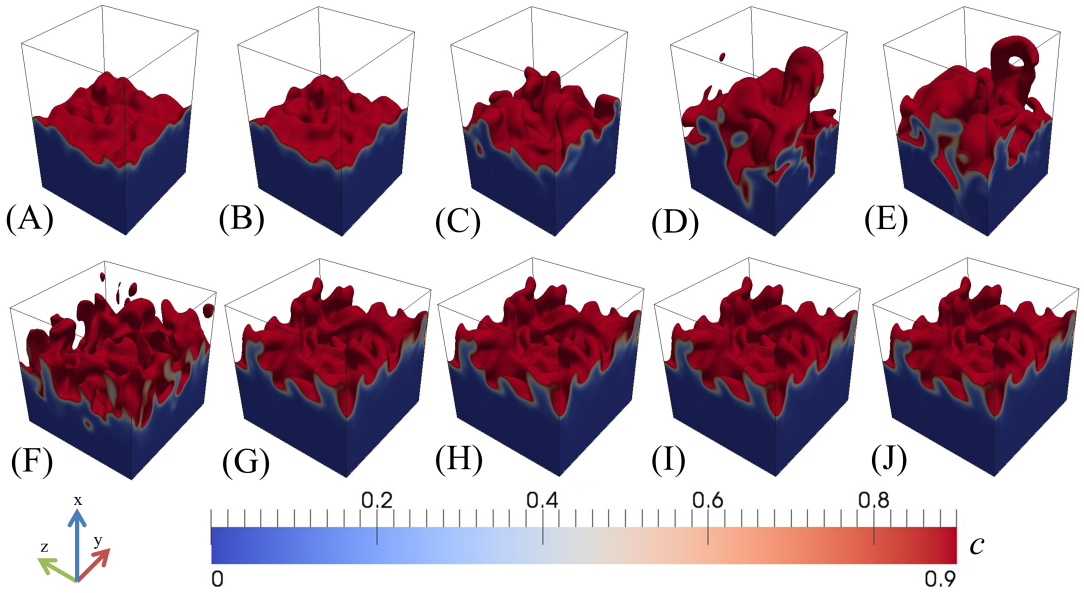

Figure 4.1: Instantaneous view of $c \leq 0.9$ contours and $c = 0.9$ isosurface for all cases at the time when the statistics were extracted (i.e. $\tau_{sim} = \tau_c = 3.34\tau_{f0}$).

decreasing Lewis number. In cases F-H, where the Le is smaller than unity, the reactants diffuse into the reaction zone at a comparably higher rate than the rate at which heat is conducted out of the flame. High burning rates occur for cases with Le smaller than unity, due to the compounded effect of simultaneous presence of both high concentration of reactants and high temperature. Quite the opposite behaviour occurs to the concentration of reactants and high temperature for the cases with Le greater than unity, this results in smaller burning rates compared to the corresponding unity Lewis number flames. In Table 4.2 the values for turbulent flame speed normalised by laminar flame speed S_T/S_L and turbulent flame area normalised by laminar flame area A_T/A_L are provided.

The turbulent flame speed S_T was evaluated using the following expression [36]:

$$S_T = \frac{1}{\rho_0 A_P} \int_V \dot{w} dV \tag{4.15}$$

where A_P is the projected area of the flame in the direction of mean flame propagation. The normalised turbulent flame area A_T/A_L was evaluated by volume integrating surface density function $|\nabla c|$ for turbulent and laminar flames i.e.

$$A_T = \int_V |\nabla c| dV \tag{4.16}$$

Table 4.2 shows that the ratios S_T/S_L and A_T/A_L decrease with increasing Lewis number, which indirectly points to the decreasing burning rates with increasing Lewis number.

Case	Le	S_T/S_L	A_T/A_L
C	0.34	13.70	3.93
D	0.60	4.58	2.66
E	0.80	2.53	2.11
F	1.00	1.83	1.84
G	1.20	1.50	1.76

Table 4.2: Effects of Lewis number on S_T/S_L and A_T/A_L at three eddy turn over time.

It was shown in Ref. [36, 43] that high temperature zones are associated with flame surfaces that are curved convex towards the reactants for cases where Lewis number is smaller than unity. This is clearly visible in Fig. 4.2, where the non-dimensional temperature T field is shown for the central mid-plane according to Chakraborty et al. [43]. When the Lewis number Le is unity the temperature on a given reaction progress variable isosurface remains uniform. It was also shown by Chakraborty et al. [43] that in the DNS case with Lewis number equal to 1.2, the high temperature zones were found where the c isosurfaces have concave curvature. Furthermore it was shown by [43] (see Fig. 4.2) that superadiabatic

temperatures (i.e. $T > 1$) occurs in concave regions for Le > 1.0 and convex regions for Le < 1.0, due to differential rates of diffusion of heat and mass at these locations. It can also be seen from Fig. 4.2 that the temperature inhomogeneity tends to increase with decreasing Lewis number. Moving away from the flame into the burnt gases the temperature becomes uniform reaching the adiabatic temperature under the globally adiabatic condition and this tends to happen faster with increasing Le due to the increased rate of thermal diffusion.

4.2.2 Turbulent Reynolds Number Effects

From Fig. 4.1 it is clear that the flame wrinkling increases with increasing $u'/S_L \sim Re_t^{1/2}/Da^{1/2} \sim Re_t^{1/4}Ka^{1/2}$ (or with increasing Re_t). In order to change the turbulent Reynolds number for cases A-E, the Damköhler number Da and the Karlovitz number Ka were altered independently of each other. The turbulent flame speed S_T normalised by laminar flame speed S_L, and turbulent flame area A_T normalised by laminar flame area are A_L are shown in Table. 4.3. It becomes clear from Table. 4.3 that increasing the turbulent Reynolds number leads to increased flame area generation and thus increasing burning rates. As Re_t increases for a given value of Da the preheat zone ($c < 0.5$) becomes increasingly distorted. This is an effect of increasing Karlovitz number $Ka \sim {Re_t}^{1/2}/Da$, since the scale separation between δ_{th} and η increase with increasing Ka. As the scale separation increases, increasingly energetic eddies are able to penetrate into the preheat zone, and this results in the increased distortions.

Case	Re_t	S_T/S_L	A_T/A_L
G	22.0	1.83	1.15
H	23.5	1.83	1.33
I	47.85	1.83	1.87
J	100.0	1.83	3.63
K	110.0	1.83	3.70

Table 4.3: Effects of turbulent Reynolds number on S_T/S_L and A_T/A_L at one chemical time scale $\tau_c = \delta_{th}/S_L$.

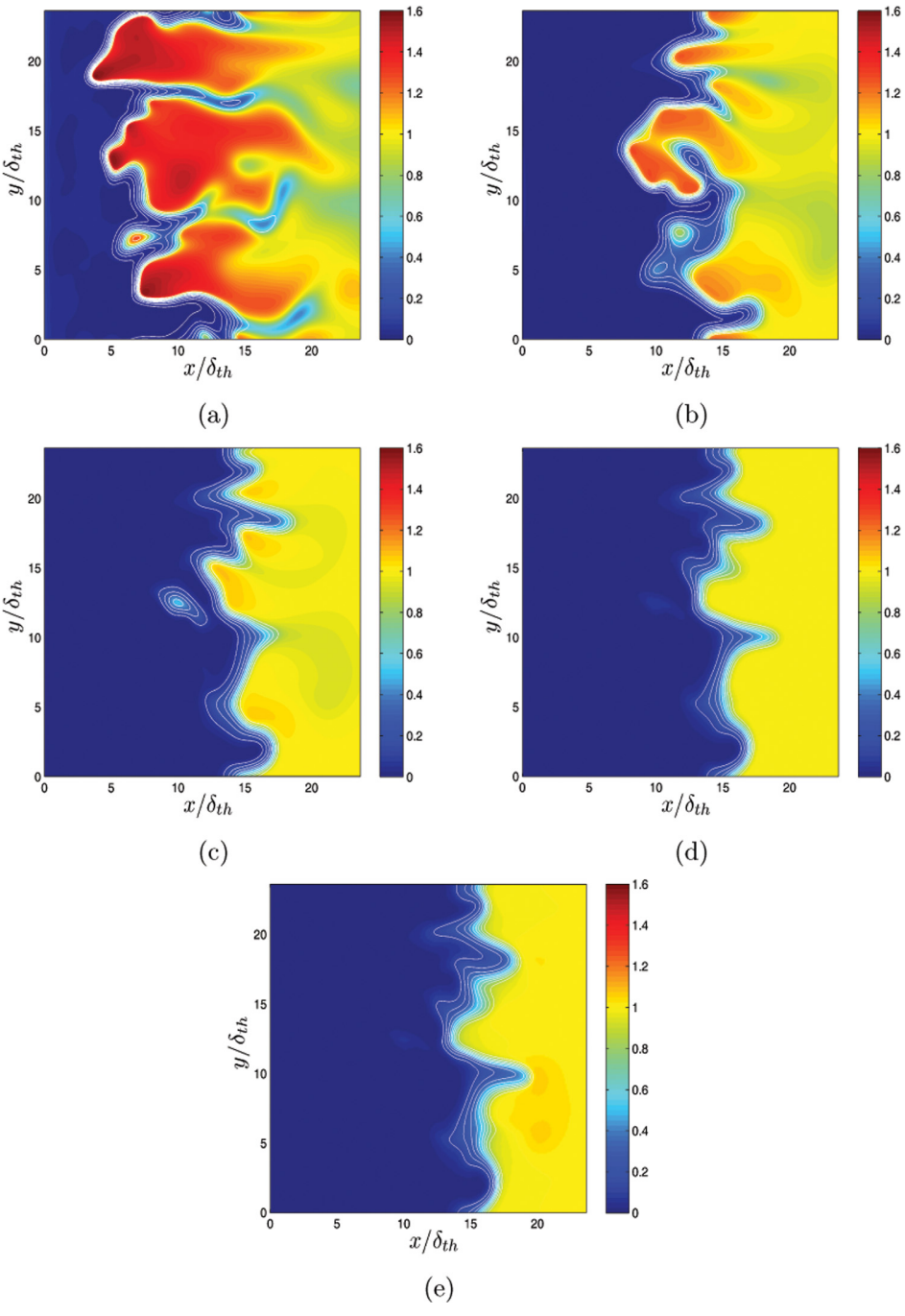

Figure 4.2: Non dimensional temperature T field at the central $x_1 - x_2$ plane of the DNS domain after three eddy turn over time, for cases F(a), G(b), H(c), I(d) and J(e). White line represent the contours of reaction progress variable $c = 0.1$ to 0.9 in steps of 0.1 (from left to right)

4.3 Processing of DNS Data

In the current study DNS data is explicitly filtered and Reynolds averaged to analyse the statistical behaviours of the various unclosed terms related to the FSD based reaction rate closure, in the context of LES and RANS respectively. The actual values of the unclosed terms in the context of LES and RANS can be obtained from the explicitly filtered/Reynolds averaged DNS data. The model predictions are compared with the values of these unclosed terms obtained from explicitly filtered/Reynolds averaged DNS data for the purpose of *a priori* DNS analysis.

4.3.1 Main Filtering Methodologies

Several methods can be employed to filter DNS data, some of the main methodologies are cutoff filter in spectral space, box filter in physical space or Gaussian filter in physical space. In the cutoff filter, variables are filtered in spectral space by removing components that are greater than a certain, predefined, cutoff wave number [119]. In the box filter and Gaussian filter a variable is filtered by using weighted average over a given volume [119]. The filtered variable $\bar{q}$ takes the following form:

$$\bar{q} = \int q(x')G(x - x')dx' \tag{4.17}$$

where G is the LES filter kernel. Filtering in spectral space using a cutoff filter can be performed in the following manner:

$$G(\kappa) = \begin{cases} 1 & \text{if } \kappa \leqslant \kappa_c = \pi/\Delta \\ 0 & \text{otherwise} \end{cases} \tag{4.18}$$

where κ is the spatial wave number and Δ is the filter width. This filter allows length scales greater than the cutoff length scale [119]. The box filter in physical space can be carried out as follows:

$$G(x) = G(x_1, x_2, x_3) = \begin{cases} 1/\Delta^3 & \text{if } |x_i| \leqslant \Delta/2, i = 1, 2, 3 \\ 0 & \text{otherwise} \end{cases} \tag{4.19}$$

It is evident from Eq. 4.19 that an averaging operation is carried out in a cubic box. A Gaussian filter in physical space can be carried out as:

$$G(x) = G(x_1, x_2, x_3) = \left(\frac{6}{\pi\Delta^2}\right)^{3/2} \exp\left[-\frac{6}{\Delta^2}(x_1^2 + x_2^2 + x_3^2)\right] \tag{4.20}$$

In the current study a Gaussian filter is used to filter the DNS data. This filter was chosen as the filtering operation is commutative with the differential operation. The DNS data was filtered for a range of filter widths Δ (i.e. $\Delta = 0.4\delta_{th}$ to $\Delta = 2.4\delta_{th}$ increasing insteps of $0.4\delta_{th}$). This range of filter widths has been chosen as it allows for the study of filters where there is partial resolution of the flame (i.e. $\eta < \Delta < \delta_{th}$) and to cases where there is no resolution of the flame (i.e. $\Delta > \delta_{th}$). The higher end of the range also coincides roughly to the integral length scale, and if the filter width Δ is greater than integral length scale the resulting filtered data will have lost all the information of large scales of flow, therefore this condition was used to set the upper boundary for the filter range.

4.3.2 Reynolds Averaging of DNS Data

All Reynolds and Favre averages were carried out by ensemble averaging the relevant quantities in the $x_2 - x_3$ plane at a given x_1 location. In order to check for the statistical convergence, the averaged quantities were evaluated using a spatially distinct half of the available sample size in the $x_2 - x_3$ plane and were compared to the corresponding quantities obtained using the full sample size available in the same plane, and good qualitative and quantitative agreements were found between the results obtained based on half and full sample sizes [40]. The results corresponding to the full sample size will be presented in chapter 7 and 8 for the sake of conciseness.

4.4 Summary

In this chapter a review of the requirements for the DNS were presented along with the numerical methodology that was used. Additionally more information on the numerical methodology can be found in appendix A. This was followed by

a discussion of the main parameters of interest in the current work, i.e. the Lewis number and the turbulent Reynolds number. Increasing (decreasing) turbulent Reynolds number (Lewis number) was shown to result in increased flame area generation. Moreover explanations to the increased flame area generation are presented in §.4.2.1 and §.4.2.2. Approaches available for LES filtering are then presented, and in this work a Gaussian filter in physical space is used which results in the analysis shown chapters 5, 6, 7 and 8. Similarly the methodology to Reynolds average the DNS data is presented, which was used in chapters 7 and 8 to analyse the curvature and strain rate terms of the generalised FSD transport equation respectively. In the following chapter, analysis of algebraic FSD models using filtered DNS data is presented. Additionally, two algebraic models that currently exist in literature are modified based on the current DNS database.

Chapter 5

Algebraic Modelling of FSD in the context of LES

One of the ways to implement the FSD based reaction rate closure in LES would be to evaluate the generalised FSD using an algebraic model. Thus in this chapter a summary of existing algebraic models for the generalised FSD in the context of LES has been provided. In addition to this the performance of a sub-set of models known as the power-law based algebraic FSD models are assessed using *a priori* DNS analysis. In addition to this a new power-law model is proposed based on the current analysis of DNS data.

5.1 Generalised Algebraic Flame Surface Density Models

Many models are currently available for the generalised FSD. Additionally it is possible to use algebraic models originally proposed for related quantities such as the wrinkling factor Ξ and turbulent flame speed S_T. Models proposed for the wrinkling factor Ξ can be used to predict for the generalised FSD using the following relationship:

$$\Xi = \frac{\Sigma_{gen}}{|\nabla \bar{c}|} \tag{5.1}$$

A model for Ξ was suggested by Angelberger et al. [2] and it can be written in the context of generalised FSD in the following manner:

$$\Sigma_{gen} = [1 + a\Gamma(u'_\Delta/S_L)]|\nabla\bar{c}| \tag{5.2}$$

where $a = 1.0$, $u'_\Delta = \sqrt{2\tilde{k}_\Delta/3}$, $\tilde{k}_\Delta = (\widetilde{u_i u_i} - \tilde{u}_i\tilde{u}_i)/2$ is the subgrid turbulent kinetic energy and the efficiency function Γ takes the same form as in Eq. 5.2:

$$\Gamma = 0.75exp\left[\frac{-1.2}{(u'_\Delta/S_L)^{0.3}}\right]\left(\frac{\Delta}{\delta_z}\right)^{2/3} \tag{5.3}$$

One of the first models to be proposed for the wrinkling factor was done by Weller et al. [159], which can be written to express the generalised FSD in the following manner:

$$\Sigma_{gen} = [1 + 2\tilde{c}(\Theta - 1)]|\nabla\bar{c}| \tag{5.4}$$

where $\Theta = 1 + 0.62\sqrt{(u'_\Delta/S_L)}Re_\eta$ and $Re_\eta = u'_\Delta\eta/\nu$ with τ_η and ρ_0 denote Kolmogorov scale and unburned gas density respectively. Colin et al. [53] proposed a model for the wrinkling factor Ξ which takes the same form as Eq. 5.2 but the model constant a is give as:

$$a = 2\beta\ln(2)/[3c_{ms}(Re_t^{1/2} - 1)] \tag{5.5}$$

where $Re_t = \rho_0 u' l/\mu_0$ (where μ_0 is the unburned viscosity and l is the turbulence integral length scale), $\beta = 1.0$ and $c_{ms} = 0.28$ and Γ is given by Eq. 5.3. By modifying the model proposed by Colin et al. [53], Charlette et al. [49] proposed an alternative model by reducing the input parameters from three to two (i.e. u'_Δ/S_L and Δ/δ_z):

$$\Sigma_{gen} = \left\{1 + min\left[\frac{\Delta}{\delta_z}, \Gamma_\Delta\left(\frac{u'_\Delta}{S_L}\right)\right]\right\}^{\beta_1}|\nabla\bar{c}| \tag{5.6}$$

where the model parameters takes the following form:

$$\Gamma_\Delta = [((f_u^{-a_1} + f_\Delta^{-a_1}))^{b_1}] \tag{5.7a}$$

$$f_u = 4\left(\frac{27C_k}{110}\right)^{1/2}\left(\frac{18C_k}{55}\right)(u'_\Delta/S_L)^2 \tag{5.7b}$$

$$f_\Delta = \left\{\left(\frac{27C_k\pi^{4/3}}{110}\right)\left[\left(\frac{\Delta}{\delta_z}\right)-1\right]\right\}^{1/2} \tag{5.7c}$$

$$f_{Re} = \left[\left(\frac{9}{55}\right)\exp\left(\frac{-1.5C_k\pi^{4/3}}{Re_\Delta^{-1}}\right)\right]^{1/2} Re_\Delta^{1/2} \tag{5.7d}$$

$$a_1 = 0.60 + 0.2\exp\left[-0.1\left(\frac{u'_\Delta}{S_L}\right)\right] - 0.2\exp\left[-0.01\left(\frac{\Delta}{\delta_z}\right)\right] \tag{5.7e}$$

$$b_1 = 1.4;\ \beta_1 = 0.5;\ C_k = 1.5;\ Re_\Delta = u'_\delta(\Delta/\nu) \tag{5.7f}$$

A dynamic algebraic model for Σ_{gen} was proposed by Knikker et al. [89] which uses a power-law approach:

$$\Sigma_{gen} = \left(\frac{\Delta}{\eta_i}\right)^{\beta_k}|\nabla\bar{c}| \tag{5.8}$$

where the inner cut off scale η_i is taken to be $\eta_i = 3\delta_z$ and β_k is estimated based on a dynamics formulation given as: $\beta_k = [\log\widehat{\langle|\nabla\bar{c}|\rangle} - \log\langle\nabla\hat{\bar{c}}\rangle]/\log\gamma$ where $\hat{\bar{c}}$ denotes progress variable at the test filter level $\gamma\Delta$. A model for the wrinkling factor Ξ using the power-law approach was proposed by Fureby [58]. This model can be expressed in terms of the generalised FSD in the following form.

$$\Sigma_{gen} = \left[\Gamma\frac{u'_\Delta}{S_L}\right]^{D-2}|\nabla\bar{c}| \tag{5.9}$$

where Γ is given by Eq. 5.3 and D is the fractal dimension defined using the following parameterisation:

$$D = \frac{2.05}{(u'_\Delta/S_L)+1} + \frac{2.35}{(S_L/u'_\Delta)+1} \tag{5.10}$$

A power-law based model was proposed by Chakraborty and Klein [33] for the generalised FSD which takes the following form:

$$\Sigma_{gen} = |\nabla \bar{c}| \left\{ \exp\left(\frac{-\Theta\Delta}{\eta_i}\right) + \left[1 - f\exp\left(\frac{-\Theta\Delta}{\eta_i}\right)\right]\left(\frac{\Delta}{\eta_i}\right)^{D-2} \right\} \tag{5.11}$$

where Θ and f are model constants and η_i is the inner cut off scale which is parameterised as $\eta_i = [0.345Ka^{-2}\exp(-Ka) + 6.41Ka^{-1/2} \times [1 - \exp(-Ka)]]\delta_z$, where Ka is the Karlovitz number. The inner cut off scale was formulated using a DNS database where a case of corrugated flamelets regime and thin reaction zones regime were used. The term D in the Eq. 5.11 is the fractal dimension, which was shown to be dependent on the regime of combustion by Chakraborty and Klein [33], which resulted in the following expression for D: $D = (1/3)erf(2Ka)$. The model by Chakraborty and Klein [33] was modified in the current study to incorporate the effects of Lewis number and local turbulent Reynolds number, additionally the usage of localised Karlovitz number instead of the global Karlovitz number was explored. This analysis is presented in the following section.

5.2 Power-law Based Modelling

The wrinkling factor Ξ can be expressed in terms of the following power-law, utilising the fractal approach for flamelet modelling [50, 53, 58, 61]:

$$\frac{\Sigma_{gen}}{|\nabla \bar{c}|} = \Xi = \left(\frac{\eta_0}{\eta_i}\right)^{D-2} \tag{5.12}$$

where the terms η_i, η_0 and D represent the inner cut off scale, outer cut off scale and the fractal dimension respectively. A power-law model for the generalised FSD represents a fractal surface between the ranges defined by the inner and outer cut off scales for a given volume. The fractal dimension D itself represents the dimension of the surface occupying the volume, for example if $D = 2$ then the surface is a flat two dimensional surface while $D = 3$ represents a wrinkled surface which occupies the entire volume. In LES of premixed flames the outer cut off scale η_0 is taken to be the filter width Δ [107] and the inner cut off scale

η_i is scaled differently based on the regime of combustion. In the corrugated flamelets regime η_i is taken to scale with the Gibson scale $L_G = S_L^3/\epsilon$, while in the corrugated flamelets regime it is typically scaled with Kolmogorov length scale $\eta = (\nu^3/\epsilon)^{1/4}$ [32, 107]. It was shown by Gülder [63] using experimental data that the inner cut off scale can be taken to scale with the laminar flame thickness δ_L, this was later confirmed by Knikker et al. [89] using experimental data. Previous *a priori* DNS analysis by Chakraborty and Klein [32] demonstrated that η_i indeed scales with L_G and η in the corrugated flamelets and thin reaction zones regimes respectively, additionally in both the regimes the inner cut off scale η_i was shown to scale with the thermal flame thickness δ_{th}. Kerstein [86] showed that the fractal dimension D increases from 2 to 7/3 with increasing normalised turbulent velocity fluctuation u'/S_L. This is an important finding as $D = 7/3$ represents a material surface transport in a turbulent environment. A parameterisation was proposed by North and Santavicca [106] which takes the following form:

$$D = \frac{2.05}{(u'/S_L + 1)} + \frac{2.35}{(S_L/u' + 1)} \tag{5.13}$$

It is evident from the foregoing discussion that a number of algebraic models are available for the FSD and a list of power-law model along with the naming convention used to display the results is shown in Table. 5.1. In the following sections the effects of turbulent Reynolds and Lewis numbers are analysed on the fractal dimension and the inner cut off scale. By using the data a new parameterisation is proposed for D, which was eventually used to extend the model proposed by Chakraborty and Klein [33]. This is followed by a thorough analysis of the performances of existing power-law models using a number of assessment criteria.

5.2.1 Fractal Dimension and Inner Cut off

In order to estimate the fractal dimension Eq. 5.12 is firstly rearranged and then volume averaged before taking log of both sides to yield the following relation, as

proposed by Chakraborty and Klein [33]:

$$\log\left(\frac{\langle\Sigma_{gen}\rangle}{\langle|\nabla\bar{c}|\rangle}\right) = (D-2)\log\Delta - (D-2)\log(\eta_i) \tag{5.14}$$

where the $\langle\ldots\rangle$ denotes the volume averaging process. The quantity $\langle|\nabla\bar{c}|\rangle$ decreases with increasing Δ due to an increase in the propotion of flame wrinkling that occurs at the sub-grid scales with increasing Δ. By contrast, $\langle\Sigma_{gen}\rangle$ indicates the total flame surface area in the computational domain, thus remaining independent of Δ. As a result, $\log\left(\langle\Sigma_{gen}\rangle / \langle|\nabla\bar{c}|\rangle\right)$ increases with increasing Δ, which can substantiated from Fig. 5.1. The variation of $\log\left(\langle\Sigma_{gen}\rangle / \langle|\nabla\bar{c}|\rangle\right)$ with $\log(\Delta/\delta_z)$ is linear when $\Delta \gg \delta_z$ but becomes non-linear for $\Delta \ll \delta_z$. The slope of the best-fit straight-line representing the greatest slope of the variation of $\log\left(\langle\Sigma_{gen}\rangle / \langle|\nabla\bar{c}|\rangle\right)$ with $\log(\Delta/\delta_z)$ gives D while the intersection point of this straight line with the abscissa gives $\log(\eta_i)$. It has been found that η_i/δ_z remains about 2.0 for all cases (i.e.$\eta_i/\delta_z \approx 1.79$), and that $\delta_{th} = 1.79\delta_z$ for the present thermochemistry which is qualitatively consistent with previous experimental [64, 89] and computational [33] findings.

Figs. 5.1 (a-e) suggest that the fractal dimension D is greater for flames with higher Re_t, and that D attains an asymptotic value of 7/3 for flames with the largest Re_t. The extent of flame wrinkling and the flame area generation increases with increasing u'/S_L. This can be substantiated from the values of normalised flame surface area A_T/A_L obtained by volume integrating $|\nabla c|$, which yields $A_T/A_L = 1.15, 1.33, 1.87, 3.63$ and 3.70 for cases A-E, respectively, at the time when statistics were extracted [41]. This behaviour is consistent with Fig. 4.1 which demonstrates the wrinkling of c isosurfaces increases with increasing $u'/S_L \sim Re_t^{1/4}Ka^{1/2} \sim Re_t^{1/2}/Da^{1/2}$. Fig. 5.1 (a-e) suggests that D is expected to increase with increasing $Re_t \sim Da^2Ka^2$ before assuming an asymptotic value when either Da or Ka is held constant. This behaviour is also qualitatively similar to the trend predicted by the parameterisation of North and Santavicca [106]. The parameterisation by Chakraborty and Klein [33], i.e. $D = 2 + 1/3erf(2Ka)$, predicts $D = 7/3$ for all cases considered here because this parameterisation accounts for the dependence of D on Ka only. Based on the variation of D

shown in Fig. 5.1 the following model was proposed for the fractal dimension:

$$D = 2 + \left(\frac{1}{3}\right) erf(3.0Ka) \left[1 - \exp\left\{-0.1\left(\frac{Re_t}{7.5}\right)^{1.6}\right\}\right] \tag{5.15}$$

In the above expression the models constants are chosen such that, for large values of Re_t the model tends to $D = 7/3$, while as the turbulent Reynolds number tends to 0 the fractal dimension equals two (i.e. $D = 2$). Based on Fig. 5.1 (f-j) it is evident that η_i/δ_z remains independent of Le, and for all cases η_i remains on the order of thermal flame thickness δ_{th} (i.e. $\eta_i = 1.79\delta_z \approx 1.0\delta_{th}$). Fig. 5.1 (f-j) shows that the slope of the linear region decreases with increasing Lewis number (i.e., in moving from case F-J), which suggests that fractal dimension D decreases with increasing Le. Fig. 4.1 shows that with decreasing Le results in greater flame area generation due to the thermo-diffusive instabilities [26, 38, 40, 75, 135, 148]. The ratio of A_T/A_L for cases F-J is $A_T/A_L = 3.93, 2.66, 2.11, 1.84,$ and 1.2, respectively, at the time when the statistics were extracted [38, 40]. The experimental findings of North and Santavicca [106] suggest that D increases with increasing $u'/S_L \sim Re_t^{1/4} Ka^{1/2}$, which indicates that D is expected to have a dependence on both Re_t and Ka. Analysis of cases F-J suggests that D is influenced by Le, in addition to Re_t and Ka, and that D can assume values greater than 7/3 for flame with $Le \ll 1.0$, see Fig. 5.1 (f-j). In Eq. 5.15 the model proposed by Chakraborty and Klein [33] for the fractal dimension D was modified to incorporate the effects of turbulent Reynolds number Re_t, and this expression (Eq. 5.15) was then modified to include the effects of Lewis number which can be seen in Fig. 5.1 in the following manner [84]:

$$D = 2 + \left(\frac{1}{3}\right) erf(3.0Ka) \left[1 - \exp\left(-0.1\left\{\frac{Re_t}{7.5}\right\}^{1.6}\right)\right] Le^{-0.45} \tag{5.16}$$

In the above expression a power-law is used (i.e. $Le^{-0.45}$) to include the Lewis number effects, it is however unclear at this point about the variation of fractal dimension for cases with $Le > 1.2$, and for $Le < 0.34$. As such the above model is based on an optimised fit of the DNS data. Using Eq. 5.16 and the DNS values for the inner cut off scale η_i the power-law ($\langle\Sigma_{gen}\rangle / \langle|\nabla\bar{c}|\rangle = (\Delta/\eta_i)^{D-2}$) was

solved, the results from this were plotted on Fig. 5.1, which indicates satisfactory agreement between the power-law prediction and DNS findings. In Eq. 5.16 the quantities Re_t and Ka were evaluated based on the unburned quantities of u'/S_L and l/δ_{th}. However, in an actual LES simulation, D needs to be evaluated based on local velocity and length scale ratio (i.e., u'_Δ/S_L and Δ/δ_z). Here u'_Δ is evaluated based on the sub-grid turbulent kinetic energy as: $u'_\Delta = \sqrt{(2\tilde{k}_\Delta/3)}$ following previous studies [58, 144, 159]. The local Karlovitz number Ka_Δ can be evaluated as $Ka_\Delta = C_{Ka}(\sqrt{\tilde{k}}/S_L)^{3/2}(\delta_z/\Delta)^{1/2}$, where C_{Ka} is a model parameter. Similarly, the local turbulent Reynolds number is given as: $Re_{t\Delta} = C_{Re}(\rho u'_\Delta \Delta/\mu_0)$. The choice of model constants $C_{Ka} = 6.6$ and $C_{Re} = 4.0$ ensures an accurate prediction of D for $\Delta \geq \eta_i$ and yields the value of D obtained based on the global quantities according to Eq. 5.16. By using the modelling strategies proposed by Chakraborty and Klein [33] the following model is proposed for the generalised FSD Σ_{gen} [85] as:

$$\Sigma_{gen} = |\nabla \bar{c}| \left[(1-f) + f \left(\frac{\Delta}{\eta_i} \right)^{D-2} \right] \tag{5.17}$$

where f is a bridging function which increases monotonically from zero for small Δ (i.e., $\Delta/\delta_{th} \to 0$ or $\Delta \ll \delta_{th}$) to unity for large Δ (i.e., $\Delta \gg \delta_{th}$). This ensures that $\Sigma_{gen} = |\nabla c|$ in the limit of small filter sizes and Σ_{gen} follows the power-law for large filter widths. It was found based on the current DNS database that the transition occurs between the filter width $0.8\delta_{th}$ and $1.0\delta_{th}$, and to accomplish this the following bridging function f is proposed:

$$f = \frac{1}{1 + \exp\left[-60(\Delta/\eta_i - 1.0)\right]} \tag{5.18}$$

As the inner cut off scale was found to scale according to δ_z (i.e. $\eta_i = \delta_{th} \approx 2\delta_z$), in the present thermochemistry that, it was decided to use the expression $\eta_i = \delta_{th}$ in the expression given by Eq. 5.17 and D is evaluated using the expression given by Eq. 5.17 using Ka_Δ and $Re_{t\Delta}$. This model will be referred to as FSDNEW in the results section.

As discussed earlier when the flow becomes fully resolved (i.e., $\lim_{\Delta \to 0} u'_\Delta = 0$) the model prediction for the generalised flame surface density Σ_{gen} must tend towards the surface density function $|\nabla c|$. However the model proposed by Fureby

[58] fails to achieve this and in order ensure that this model follows the asymptotic trends given by $\lim_{\Delta\to 0}\Sigma_{gen} = |\nabla c|$ this model is modified here using a bridging function such that at large filter widths $\Delta \gg 1.0\delta_{th}$ the model predicts based on the original proposed by Fureby [58], while for small filter widths $\Delta \ll \delta_{th}$ approaches $|\nabla c|$ The modified Fureby [58] model takes the following form:

$$\Sigma_{gen} = |\nabla \bar{c}| \left[(1-f) + f\left(\Gamma \frac{u'_\Delta}{S_L}\right)^{D-2} \right] \tag{5.19}$$

where f is calculated using the bridging function given in Eq. 5.18, $D = 2.05 /(u'_\Delta/S_L + 1) + 2.35/(S_L/u'_\Delta + 1)$ (i.e. Eq. 5.10) and the efficiency function proposed by Angelberger et al. [2] given by Eq. 5.3.

5.2.2 Assessment Criteria

A list of power-law based models can be seen in Table 5.1, which will be tested. Three criteria have been used to access the performance of these power-law based models using *a priori* analysis of DNS data. The three criteria are as follows [33]:

1. The volume-averaged Σ_{gen} represents the total flame surface area, and therefore should not change with Δ.

2. The model should be able to capture the correct variation of the averaged values of Σ_{gen} conditional on $\bar{c}$ across the flame brush.

3. The correlation coefficient between the modelled and actual values of Σ_{gen} should be as close to unity as possible to accurately capture the local strain rate and curvature effects on Σ_{gen}.

The performances of the models listed in Table. 5.1 will be presented in the following subsections.

5.2.2.1 Criterion I: Volume Averaged generalised FSD Behaviour

The volume-averaged Σ_{gen} represents the total flame surface area, and therefore should not change with Δ, and thus to carry this out the model assessment

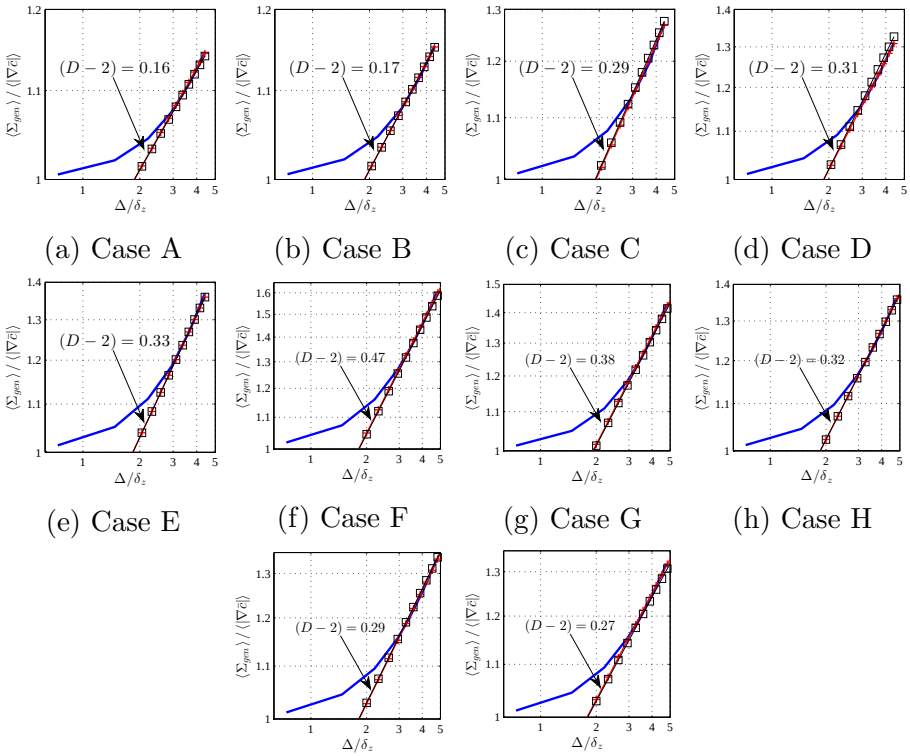

(a) Case A (b) Case B (c) Case C (d) Case D

(e) Case E (f) Case F (g) Case G (h) Case H

(i) Case I (j) Case J

Figure 5.1: Variation of $\langle \Sigma_{gen} \rangle / \langle |\nabla \bar{c}| \rangle$ (——) with Δ/δ_z on a log − log plot for: cases (a-e) A-E, respectively. The prediction of $\langle \Sigma_{gen} \rangle / \langle |\nabla \bar{c}| \rangle = (\Delta/\eta_i)^{D-2}$ (—|—) with η_i obtained from DNS and D according to newly proposed model given by Eq. 5.17 (—□—) is also shown.

according to this criterion the modelling error in the prediction of $\langle \Sigma_{gen} \rangle$ is characterised based on the following expression which is referred to as the percentage error (PE):

$$PE = \frac{\langle \Sigma_{gen} \rangle_{model} - \langle \Sigma_{gen} \rangle}{\langle \Sigma_{gen} \rangle} \times 100 \tag{5.20}$$

where $\langle \Sigma_{gen} \rangle_{model}$ is the volume averaged value of the model prediction for $\langle \Sigma_{gen} \rangle$. Results for the percentage error PE are shown for a range of filter widths in Fig. 5.2 and 5.3 for cases A-E and F-J, respectively.

The FSDW model shows significant overpredictions for all cases tested (see Figs. 5.2 and 5.3). Additionally the level of overprediction for the FSDW model increases with decreasing Lewis number. The model FSDCH shows worsening

Name	Reference	Expression
FSDA	Angelberger et al. [2]	Eq. 5.2
FSDC	Colin et al. [53]	Eq. 5.5
FSDW	Weller et al. [159]	Eq. 5.4
FSDCH	Charlette et al. [49]	Eq. 5.6
FSDK	Knikker et al. [89]	Eq. 5.8
FSDF	Fureby [58]	Eq. 5.9
FSDNEW	Katragadda et al. [84, 85]	Eq. 5.17
MFSDF	Katragadda et al. [84, 85]	Eq. 5.19

Table 5.1: A list of power-law models with the naming convention used to display the results.

of performances with decreasing Lewis number although it remains within the bound of $5-10\%$ for cases with unity Lewis number and small values of low turbulent Reynolds numbers. As the turbulent Reynolds number increases the model prediction FSDCH worsens. The model FSDK shows underprediction for all filter widths and for all cases. It is evident that this model improves with increasing filter width where the power-law functions well. Although the performance of FSDK model does not get significantly affected by Lewis number. In Fig. 5.3 it can be seen that models FSDC and FSDA overpredicts for the volume averaged generalised FSD for all Lewis numbers. Additionally the level of overprediction from models FSDC and FSDA increases with increasing filter width Δ. Similarly FSDC and FSDA models show increasing overprediction of $\langle\Sigma_{gen}\rangle$ with increasing Δ. Moreover it can be seen from Fig. 5.3 that the level of overprediction increases with increasing Δ. The extent of overprediction of $\langle\Sigma_{gen}\rangle$ is greatest for the FSDC model, and the extent of overprediction for the FSDA model remains comparable to FSDC.

The newly proposed model FSDNEW satisfactorily predicts $\langle\Sigma_{gen}\rangle$, when the local Karlovitz number Ka_{Δ} and local turbulent Reynolds number $Re_{t\Delta}$ are used, although the model FSDF performs slightly better in the unity Lewis number

cases. In all cases the model predictions from models FSDF, FSDNEW and MFSDF remain comparable, which is well below 10% PE in all cases.

Note that the parameterisation of D and Γ according to Eq. 5.10 and 5.3 is essential for the satisfactory performance of the FSDF model. Using Eq. 5.16 for D in the FSDF model is found to lead to a deterioration in its performance. Similarly using D as given by Eq. 5.10 for FSDNEW model worsens its performance.

The FSDK model is based on the power-law model for Ξ ($\Xi = (\eta_0/\eta_i)^{D-2}$, see Eq. 5.8) which is strictly valid only for filter sizes Δ, which are sufficiently greater than η_i (i.e.,$\Delta \gg \eta_i$), as can be seen from Figs. 5.2 and 5.3. However, the FSDK model prediction for $\langle \Sigma_{gen} \rangle$ improves as the filter width becomes larger than the inner cut off scale η_i (i.e. $\Delta > \eta_i$). Moreover, Σ_{gen} vanishes when $\Delta \to 0$ according to the FSDK model, whereas Σ_{gen} should approach $|\nabla c|$ when the filter width tends to 0 (i.e. $\Delta \to 0$). This limitation can be avoided by modifying the FSDK model in the same manner as shown in Eq. 5.19 for the FSDF model. The performance of the modified FSDK has not been shown here for the sake of brevity.

The stretch rate $K = (1/\delta A)d(\delta A)/dt = a_T + S_d \nabla.\vec{N}$ represents the fractional rate of change of flame surface area A, where $S_d = Dc/dT/|\nabla c|$ is the displacement speed, $\vec{N} = -\nabla c/|\nabla c|$ is the local flame normal vector and $a_T = (\delta_{ij} - N_i N_j)\partial u_i \partial x_j$ is the tangential strain rate. It is possible to decompose S_d into the reaction, normal diffusion and tangential diffusion components (i.e. S_r, S_n and S_t) as shown in Eqs. 2.103-2.106 [29, 33, 35, 57, 108].

It has been shown in several previous studies [29, 35, 67, 68, 148] that $\overline{(a_T)}_s$ remains positive throughout the flame brush and thus acts to generate flame surface area, whereas the contribution of curvature to stretch $\overline{(S_d \nabla.\vec{N})}_s = \overline{\left[(S_r + S_n)\nabla.\vec{N}\right]}_s - \overline{\left[D_c(\nabla.\vec{N})^2\right]}_s$ is primarily responsible for flame surface area destruction. The equilibrium of flame surface area generation and destruction yields $\overline{K}_s = 0$, which gives rise to [33]:

$$\overline{(a_T)}_s = -\overline{\left[(S_r + S_n)\nabla.\vec{N}\right]}_s + \overline{\left[D_c(\nabla.\vec{N})^2\right]}_s \tag{5.21}$$

The stretch rate induced by $\overline{\left[D_c(\nabla.\vec{N})^2\right]}_s$ becomes the leading order sink term in the thin reaction zones regime [29, 33, 35, 70]. However, most algebraic models (e.g. FSDA, FSDC, FSDCH and FSDW) were proposed in the CF regime based on the equilibrium of the stretch rates induced by $\overline{\left[(S_r+S_n)\nabla.\vec{N}\right]}_s$ and $\overline{(a_T)}_s$ and the flame surface area destruction rate in the thin reaction zones regime which leads to the overprediction of $\langle\Sigma_{gen}\rangle$ for the models FSDA, FSDC, FSDCH and FSDW.

The disagreement between the FSDF model prediction and DNS data originates principally due to the inaccuracy in the estimating Γ and D, while the difference between the FSDK prediction and DNS data arises from inaccurate estimation of η_i (i.e. $\eta_i \approx 3\delta_z$ is considered by Knikker et al. [89] but here $\eta_i = 1.79\delta_z$). Hence a more accurate estimation of Γ, D and η_i will result in better performance of both the FSDF and FSDK models.

5.2.2.2 Criterion II: Conditionally Averaged FSD Behaviour

Criterion II allows for the assessment of model performance with respect to the variations of mean Σ_{gen} conditionally averaged $\bar{c}$. The variation of Σ_{gen} conditionally averaged on $\bar{c}$ is shown for $\Delta = 8\Delta_m = 0.8\delta_{th}$ for cases A-E and E-J in Figs. 5.4 and 5.6, respectively. This filter width has been used to show a case where $\Delta < \eta_i$ which corresponds to case where partial resolution of flame is available. The behaviour of the models at this filter width ($\Delta = 8\Delta_m = 0.8\delta_{th}$) for the current database can be summarised as follows:

1. The FSDW model tends to overpredict the value of Σ_{gen} for flames with higher Re_t (e.g., cases D and E). However, the extent of this overprediction is relatively lower in the low Re_t cases (e.g., cases A and B). In cases E-J the model FSDW consistently overpredicts the conditional mean value of Σ_{gen} for all cases. The FSDW model also predicts a skewed shape, which fails to capture the trend predicted by DNS. This skewness appears towards the burned gas side i.e. $\bar{c} > 0.6$, whereas the peak of Σ_{gen} obtained from DNS is roughly at location given by $\bar{c} \approx 0.6$.

2. The model FSDK tends to underpredict the value of Σ_{gen} for all the cases

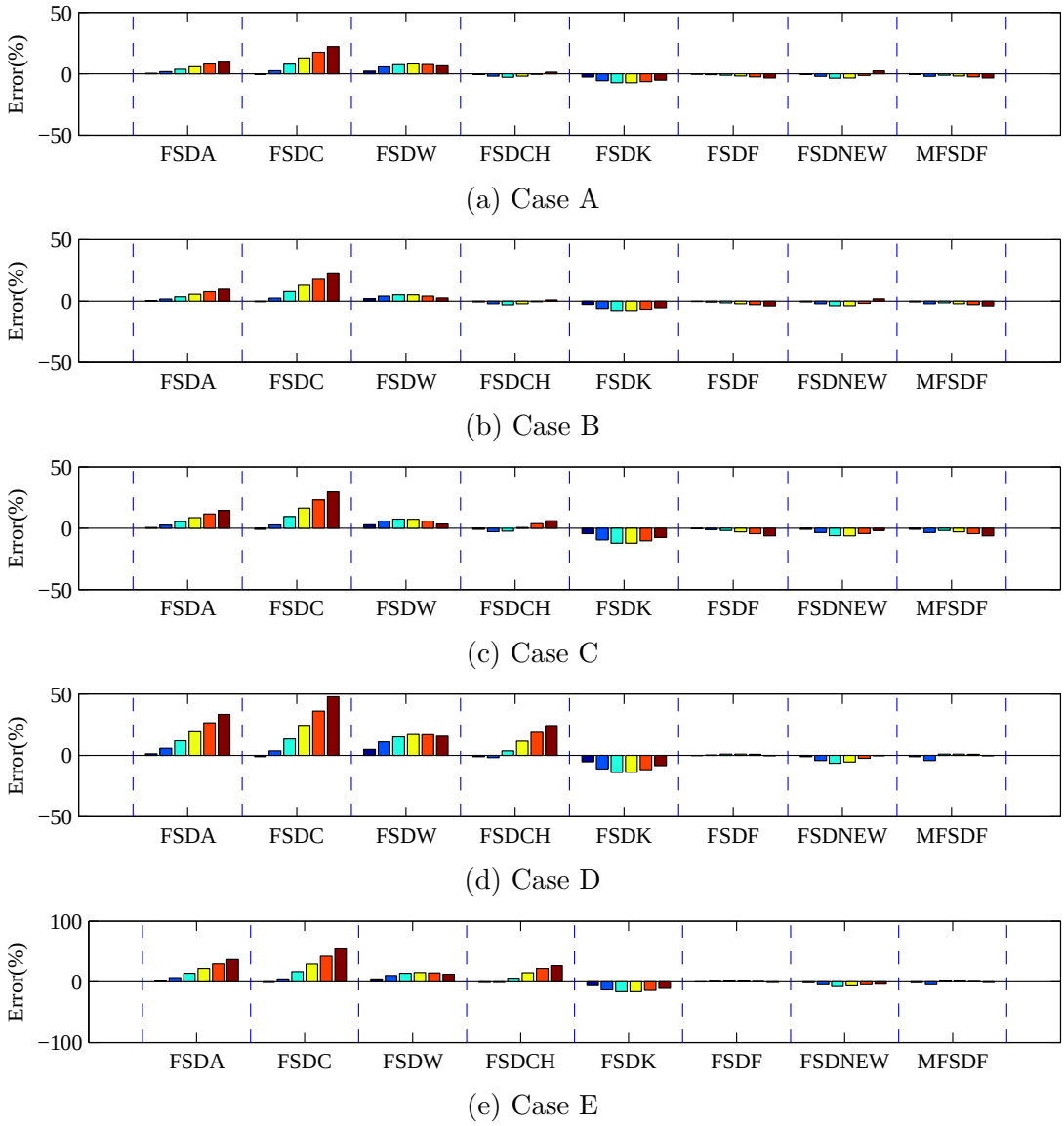

Figure 5.2: Percentage error of the model prediction from $\langle \Sigma_{gen} \rangle$ obtained from DNS for LES filter widths $\Delta = 4\Delta_m = 0.4\delta_{th}$ (■), $\Delta = 8\Delta_m = 0.8\Delta_{th}$ (■), $\Delta = 12\Delta_m = 1.2\delta_{th}$ (■), $\Delta = 16\Delta_m = 1.6\delta_{th}$ (■), $\Delta = 20\Delta_m = 2.0\delta_{th}$ (■), $\Delta = 24\Delta_m = 2.4\delta_{th}$ (■) for: (a-e) corresponding to cases A-E, respectively. The DNS grid size is given by Δ_m

shown in Figs. 5.4 and 5.6.

3. Models FSDA, FSDC, FSDCH, FSDF and FSDNEW all tend to capture the

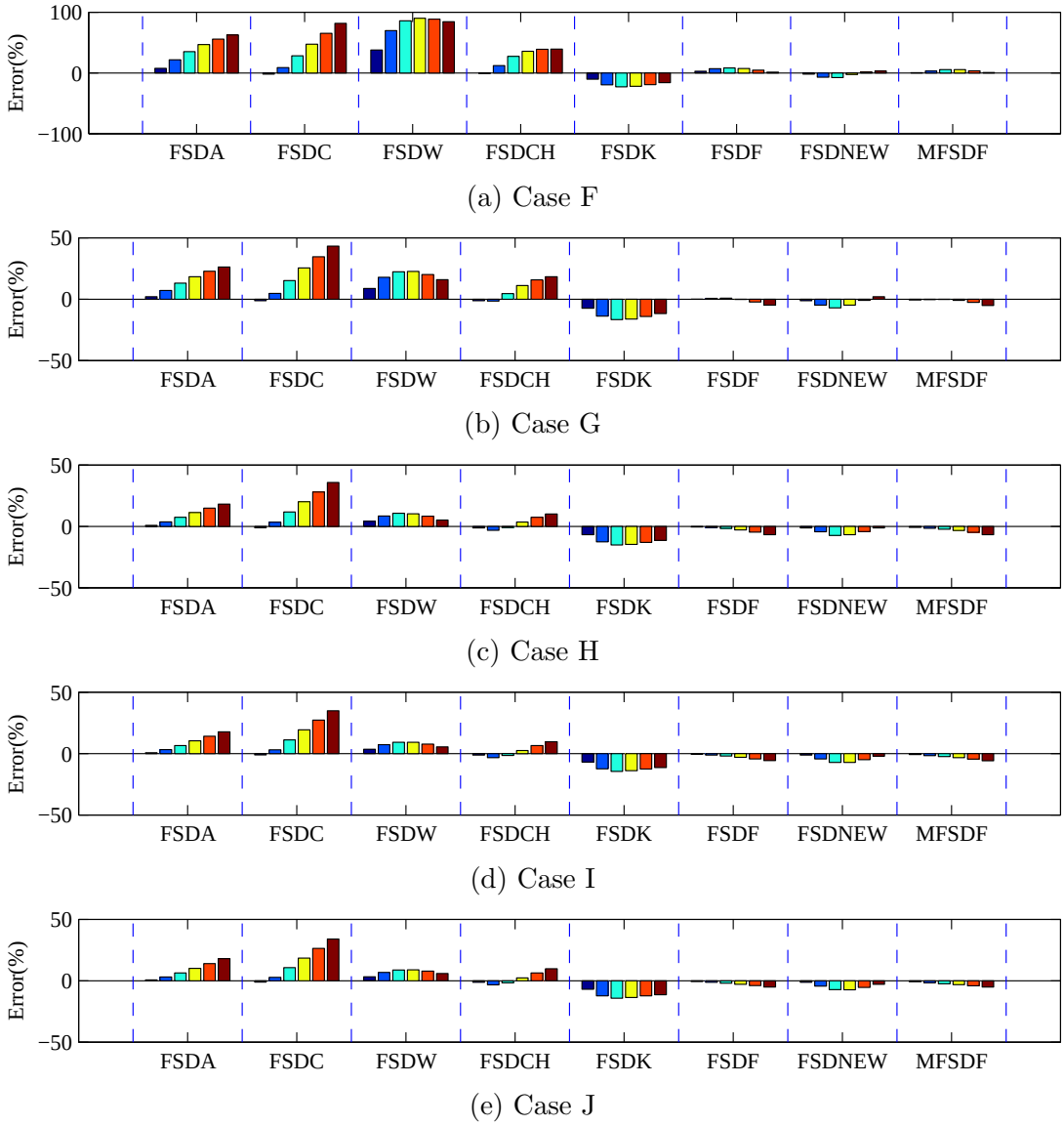

Figure 5.3: Percentage error of the model prediction from $\langle \Sigma_{gen} \rangle$ obtained from DNS for LES filter widths $\Delta = 4\Delta_m = 0.4\delta_{th}$ (■), $\Delta = 8\Delta_m = 0.8\Delta_{th}$ (■), $\Delta = 12\Delta_m = 1.2\delta_{th}$ (■), $\Delta = 16\Delta_m = 1.6\delta_{th}$ (■), $\Delta = 20\Delta_m = 2.0\delta_{th}$ (■), $\Delta = 24\Delta_m = 2.4\delta_{th}$ (■) for: (a-e) corresponding to cases F-J, respectively.

Σ_{gen} variation with $\bar{c}$ obtained from DNS data. The prediction of MFSDF model remains comparable to that of the FSD model for $\Delta = 8\Delta_m = 0.8\delta_{th}$.

In order to examine the models behaviour at a filter width where the flame is unresolved, the filter widht $\Delta = 24\Delta_m = 2.4\delta_{th}$. The model predictions conditionally averaged on $\bar{c}$ are shown for $\Delta = 24\Delta_m = 2.4\delta_{th}$ in Figs. 5.5 and 5.7. The behaviour of the model predictions can be summarised as follows:

1. Models FSDW, FSDA and FSDC all overpredict the value of Σ_{gen}, and the overprediction increases with increasing Re_t. The FSDCH model captures the behaviour of Σ_{gen} for small values of Re_t (e.g. cases A-C), but it overpredicts the value of Σ_{gen} for higher Re_t cases (e.g. cases D-E).

2. In cases F-J the model FSDW predicts a peak at $\bar{c} > 0.6$, whereas the peak value of conditionally averaged Σ_{gen} from DNS occurs at $\bar{c} \approx 0.5$ for all the cases. Additionally the models FSDW, FSDA, FSDC and FSDCH tend to overpredict the conditionally averaged value of Σ_{gen} and the level of overprediction increases with decreasing Lewis number (i.e. cases F-J, Fig. 5.7).

3. The FSDF, FSDK, FSDNEW and MFSDF models predict Σ_{gen} satisfactorily throughout the flame brush. Additionally at this filter width the models FSDF and MFSDF predict almost identical predictions.

Unlike the other models the behaviour of model FSDK improves with increasing Δ, which is consistent with observations made in the context of Figs. 5.2 and 5.3. Moreover the predictions from FSDW remains skewed towards the burned products due to the $\bar{c}$ dependence of Ξ (i.e. $\Xi = 1 + 1.24\tilde{c}\sqrt{(u'_\Delta/S_L)}Re_\eta$). The models FSDW, FSDA and FSDC underestimate the destruction of flame surface area in the thin reaction zones regime by ignoring Σ_{gen} destruction arising due to $\overline{[D_c(\nabla.\vec{N})^2]}_s$ which eventually leads to the overpredictions of Σ_{gen}. The efficiency function Γ in the FSDCH model is parameterised to capture the turbulent flame speed behaviour for both high and low Damköhler combustion [49], and hence this model performs satisfactorily with respect to criterion 1 and 2 for cases with $Le \approx 1.0$ flames considered here. As the efficiency function proposed by Charlette et al. [49] was not parameterised to account for Le effects, the performance of FSDCH worsens with decreasing Le and this model starts to overpredict for $Le \ll 1$ flames.

The use of local Karlovitz number Ka_Δ and turbulent Reynolds number $Re_{t\Delta}$ enables local variation of D, and a satisfactory performance of the FSDNEW model with respect to criteria 1 and 2 indicates that Eq. 5.16 captures the local Reynolds and Karlovitz number dependence of D for the present definitions of these numbers (i.e. $Ka_\Delta = 6.66\left(\sqrt{(\widetilde{k})_\Delta}/S_L\right)^{3/2}(\Delta/\delta_z)^{-1/2}$ and $Re_{t\Delta} = 4.0(\rho_0 u'_\Delta \Delta/\mu_0)$.

5.2.2.3 Criterion III: Correlation Coefficients

The FSD predicted by the models should have the correct resolved strain rate and curvature dependence in the context of LES and thus the correlation coefficient between the FSD obtained from DNS and from the model prediction should remain as close to unity as possible. The variation of the correlation coefficients between the model prediction and generalised FSD Σ_{gen} obtained from DNS in the range of filtered reaction progress variable $0.1 \leq c \leq 0.9$ are shown in Fig. 5.8 and 5.9 for different filter widths. The regions corresponding to $0.1 < \bar{c}$ and $\bar{c} > 0.9$ have been ignored since the correlation coefficients have little physical significance in these regions due to small values of Σ_{gen} obtained from both DNS and model predictions. Figs 5.8 and 5.9 indicate that the correlation coefficients decrease with increasing Δ due to increased unresolved subgrid wrinkling, which makes the local variation of Σ_{gen} different from $|\nabla\bar{c}|$. The extent of the deviation of the correlation coefficients from unity increases with decreasing (increasing) Le (Re_t) for a given value of Δ. Figs. 5.8 and 5.9 indicates that the models FSDA, FSDC, FSDCH, FSDF, MFSDF, FSDK, FSDNEW and FSDW have comparable correlation coefficients, which deviate considerably from unity for large values of Δ. This indicates that algebraic models may not be able to adequately predict the local strain rate and curvature dependencies of Σ_{gen}, especially in the thin reaction zones regime. Hence a transport equation for FSD might need to be solved to account for the local strain rate and curvature effects on Σ_{gen} [29, 35, 67, 68, 73].

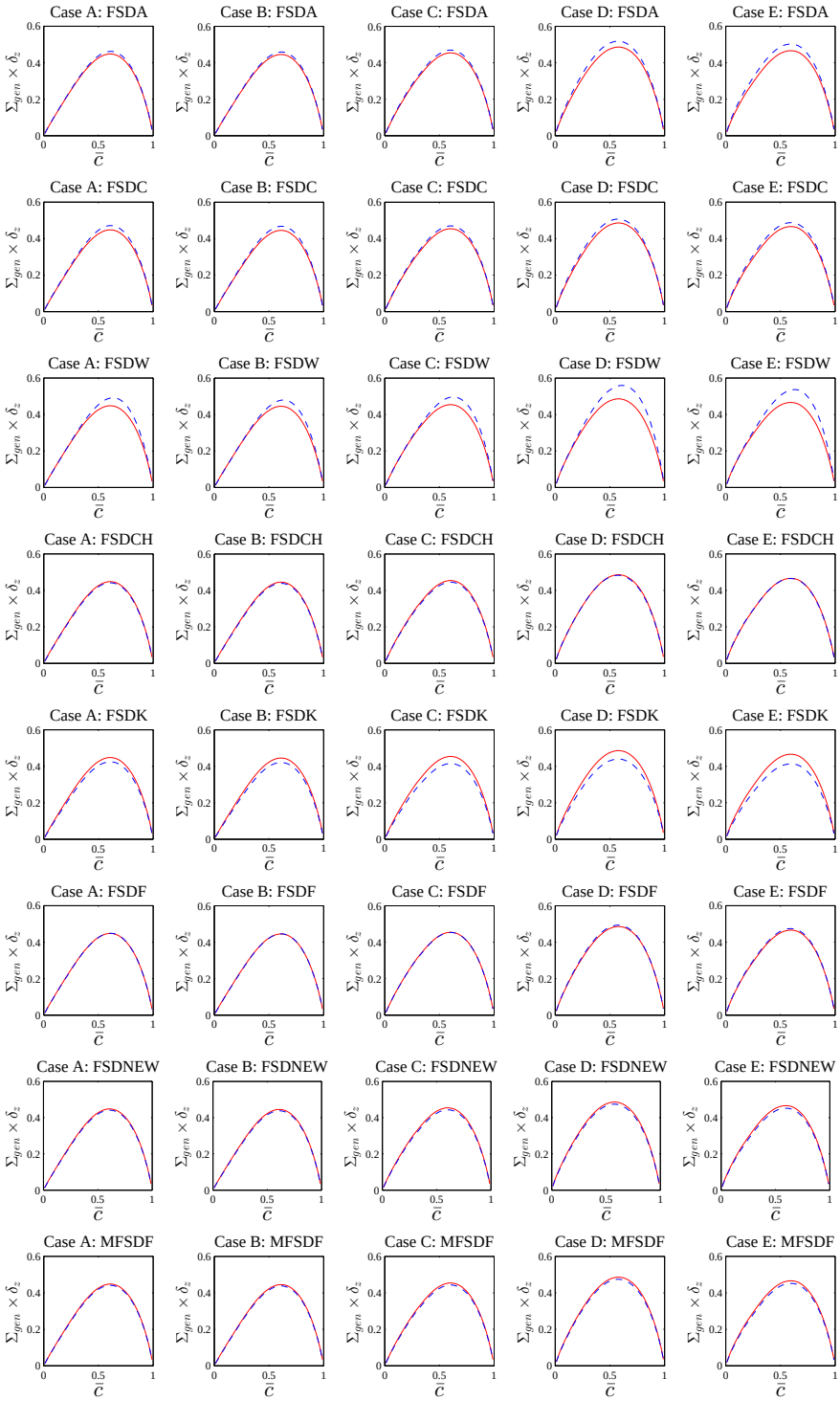

Figure 5.4: Variation of the mean values of $\Sigma_{gen} \times \delta_z$ conditional on $\bar{c}$ across the flame brush for $\Delta = 8\Delta_m = 0.8\delta_{th}$ according to DNS (——) and model (— —) for cases A-E.

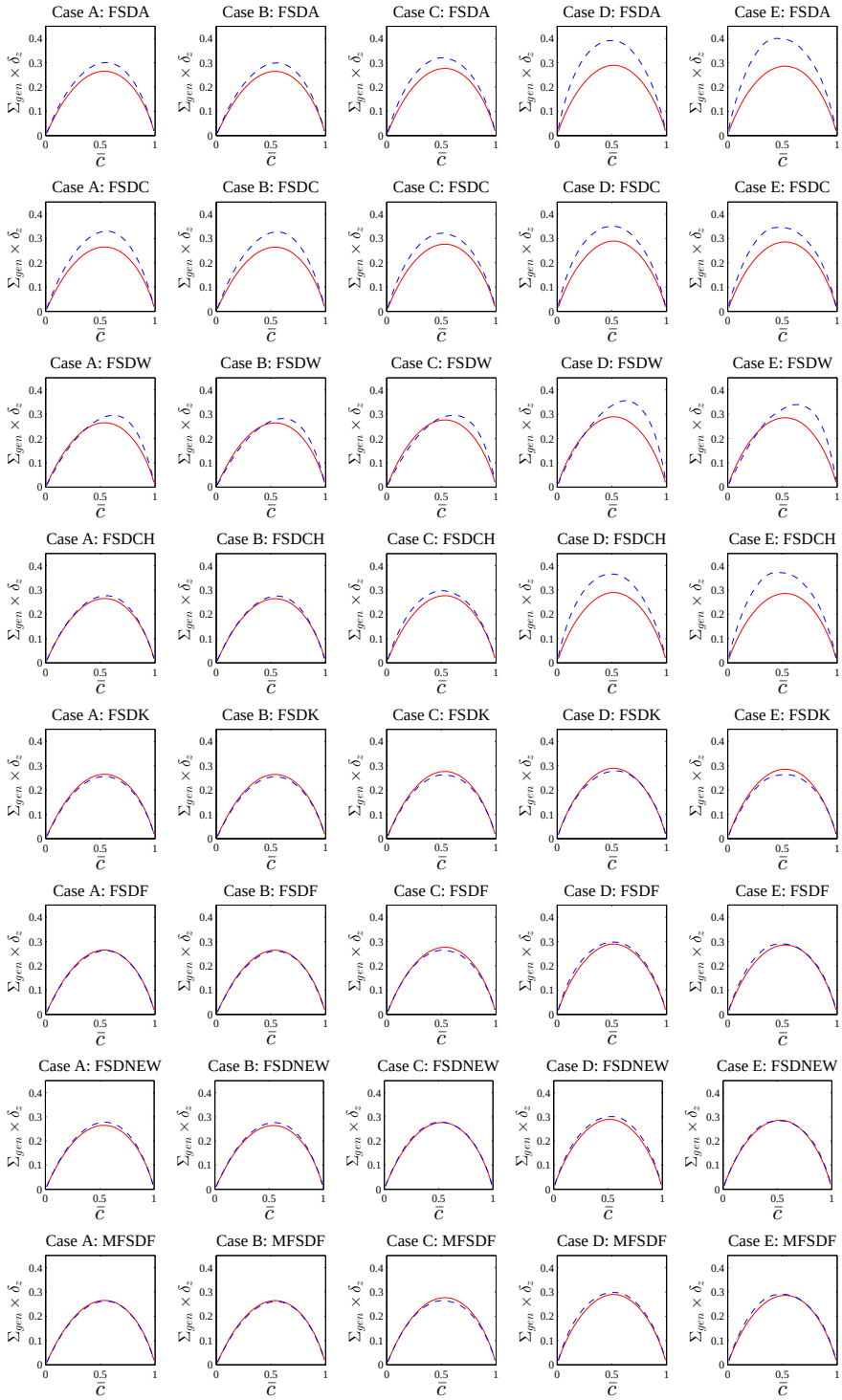

Figure 5.5: Variation of the mean values of $\Sigma_{gen} \times \delta_z$ conditional on $\bar{c}$ across the flame brush for $\Delta = 24\Delta_m = 2.4\delta_{th}$ according to DNS (——) and model (— —) for cases A-E.

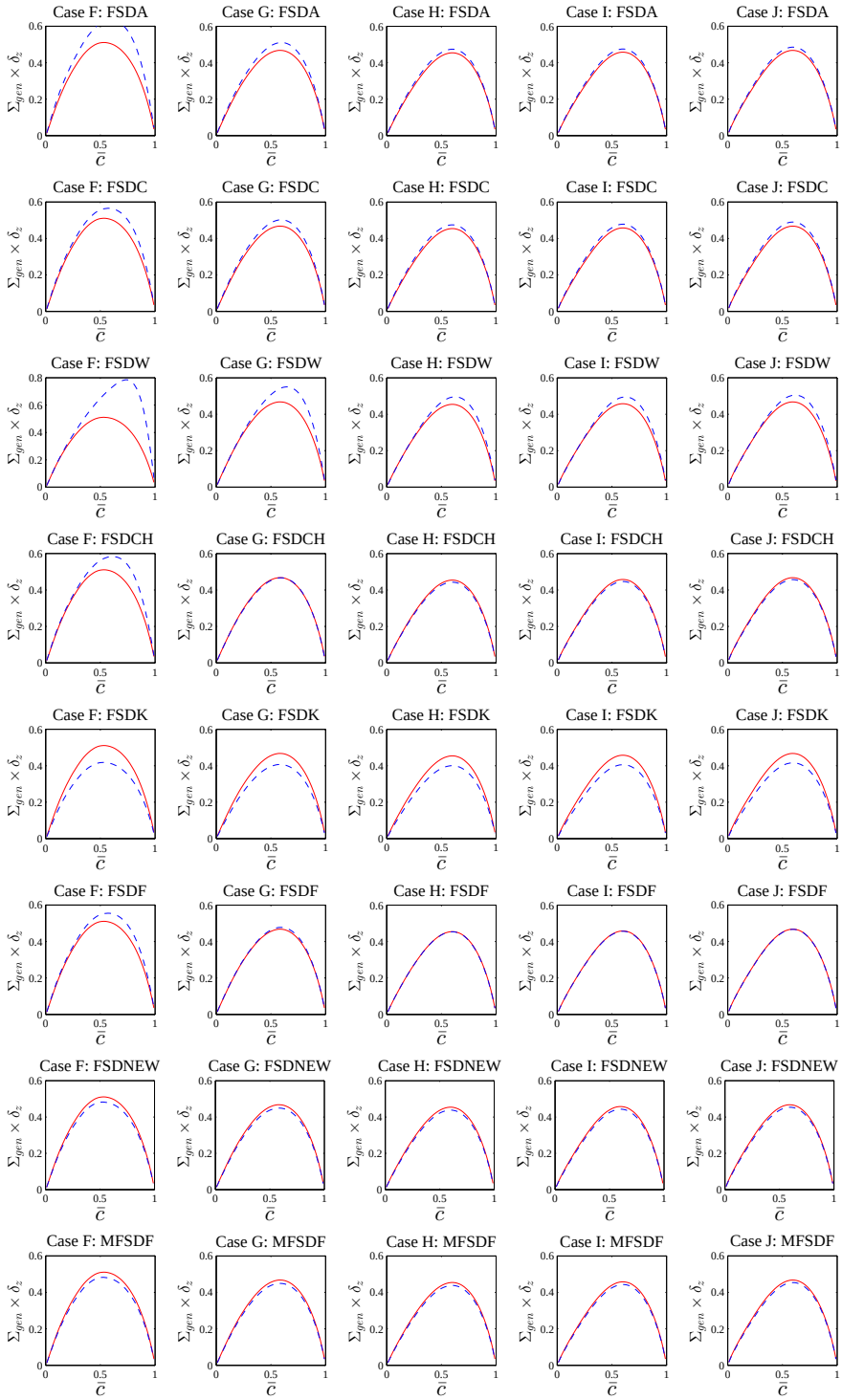

Figure 5.6: Variation of the mean values of $\Sigma_{gen} \times \delta_z$ conditional on $\bar{c}$ across the flame brush for $\Delta = 8\Delta_m = 0.8\delta_{th}$ according to DNS (——) and model (— —) for cases F-J.

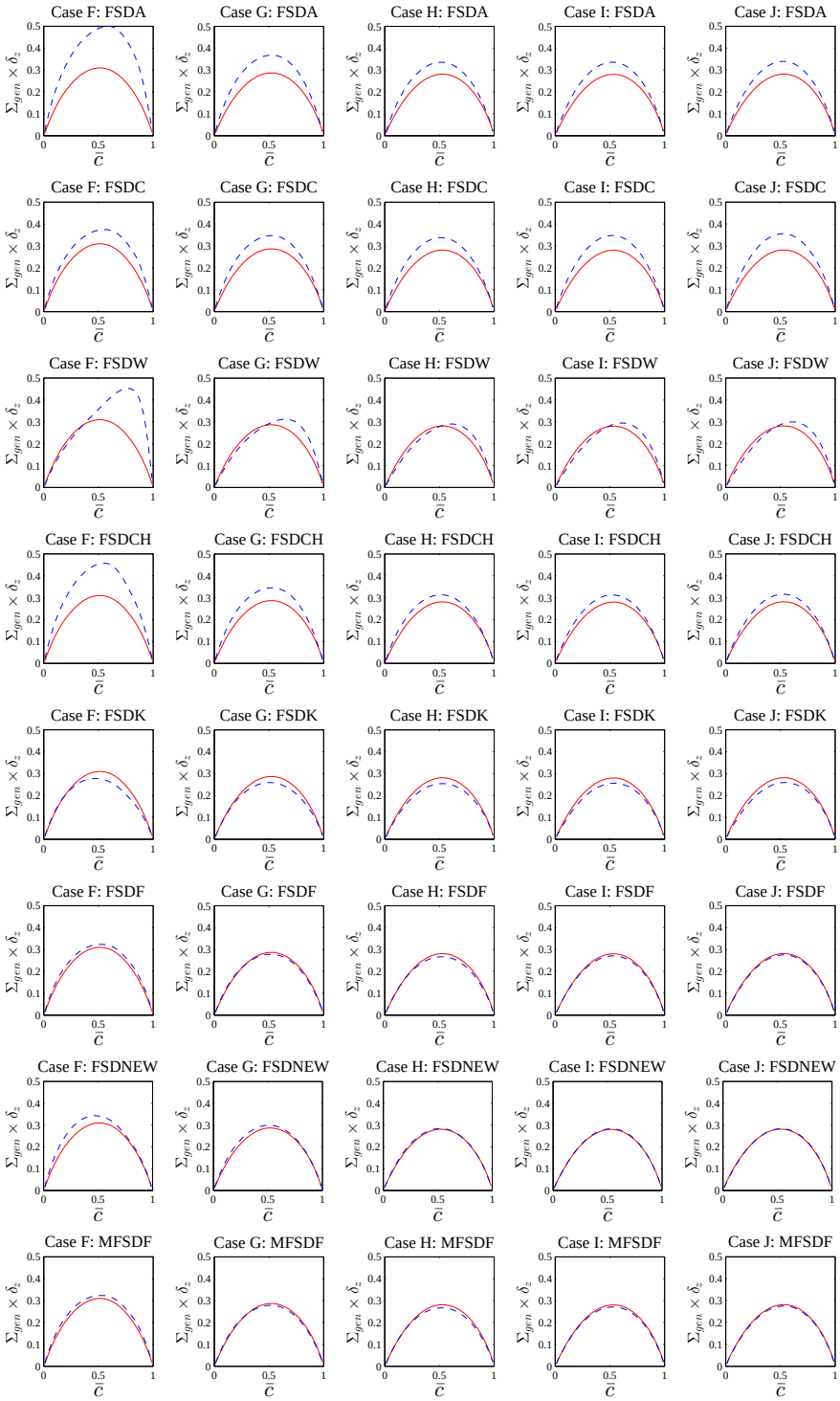

Figure 5.7: Variation of the mean values of $\Sigma_{gen} \times \delta_z$ conditional on $\bar{c}$ across the flame brush for $\Delta = 24\Delta_m = 2.4\delta_{th}$ according to DNS (——) and model (— —) for cases F-J.

5.3 Summary

The performance of several power-law based algebraic models of Σ_{gen} have been assessed in context of LES for a large range of filter width, using *a priori* based DNS database of varying turbulent Reynolds and Lewis numbers. It was found that the fractal dimension increases with decreasing Lewis number and increasing turbulent Reynolds number. However the inner cut off scale was shown to be unaffected by turbulent Reynolds and Lewis numbers and additionally the inner cut off scale was shown to be approximately equal to the thermal flame thickness (i.e. $\eta_i \approx \delta_{th}$) for all the DNS cases. A new parameterisation was proposed for the fractal dimension D which took into account the variation of turbulent Reynolds number, Karlovitz number and Lewis number. This new D parameterisation was used to propose a power-law based model for Σ_{gen}, which was found to perform comparably or better than the existing algebraic models, for the current DNS database.

The algebraic models for turbulent flame speed S_T may also be used to predict for the generalised FSD [63, 111, 112, 166] using the following relationship: $\Sigma_{gen} = \Xi|\nabla\bar{c}| = (S_T/S_L)|\nabla\bar{c}|$. These model were however were not used in the current analysis as the relationship $S_T/S_L = \Xi = A_T/A_L$ can only be applied for cases with $Le = 1.0$ [38, 40, 42], and many of these models have been proposed based on the assumptions which are strictly valid in the context of RANS.

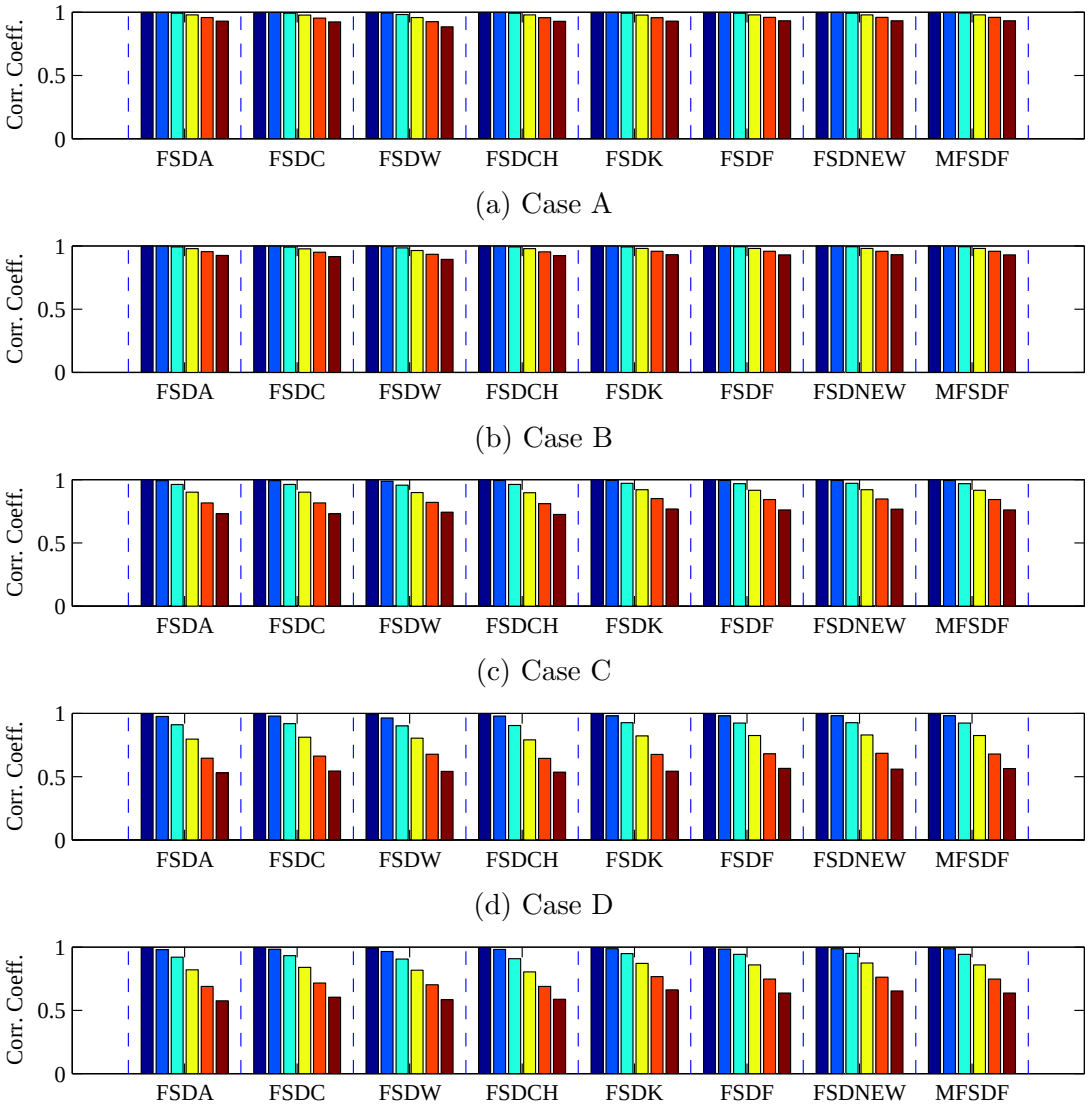

(a) Case A

(b) Case B

(c) Case C

(d) Case D

(e) Case E

Figure 5.8: Correlation coefficients between modelled and actual values of Σ_{gen} in the $\bar{c}$ range of $0.1 \leq \bar{c} \leq 0.9$ for LES filter widths $\Delta = 4\Delta_m = 0.4\delta_{th}$ (■), $\Delta = 8\Delta_m = 0.8\Delta_{th}$ (■), $\Delta = 12\Delta_m = 1.2\delta_{th}$ (■), $\Delta = 16\Delta_m = 1.6\delta_{th}$ (■), $\Delta = 20\Delta_m = 2.0\delta_{th}$ (■), $\Delta = 24\Delta_m = 2.4\delta_{th}$ (■) for: (a-e) corresponding to cases A-E, respectively.

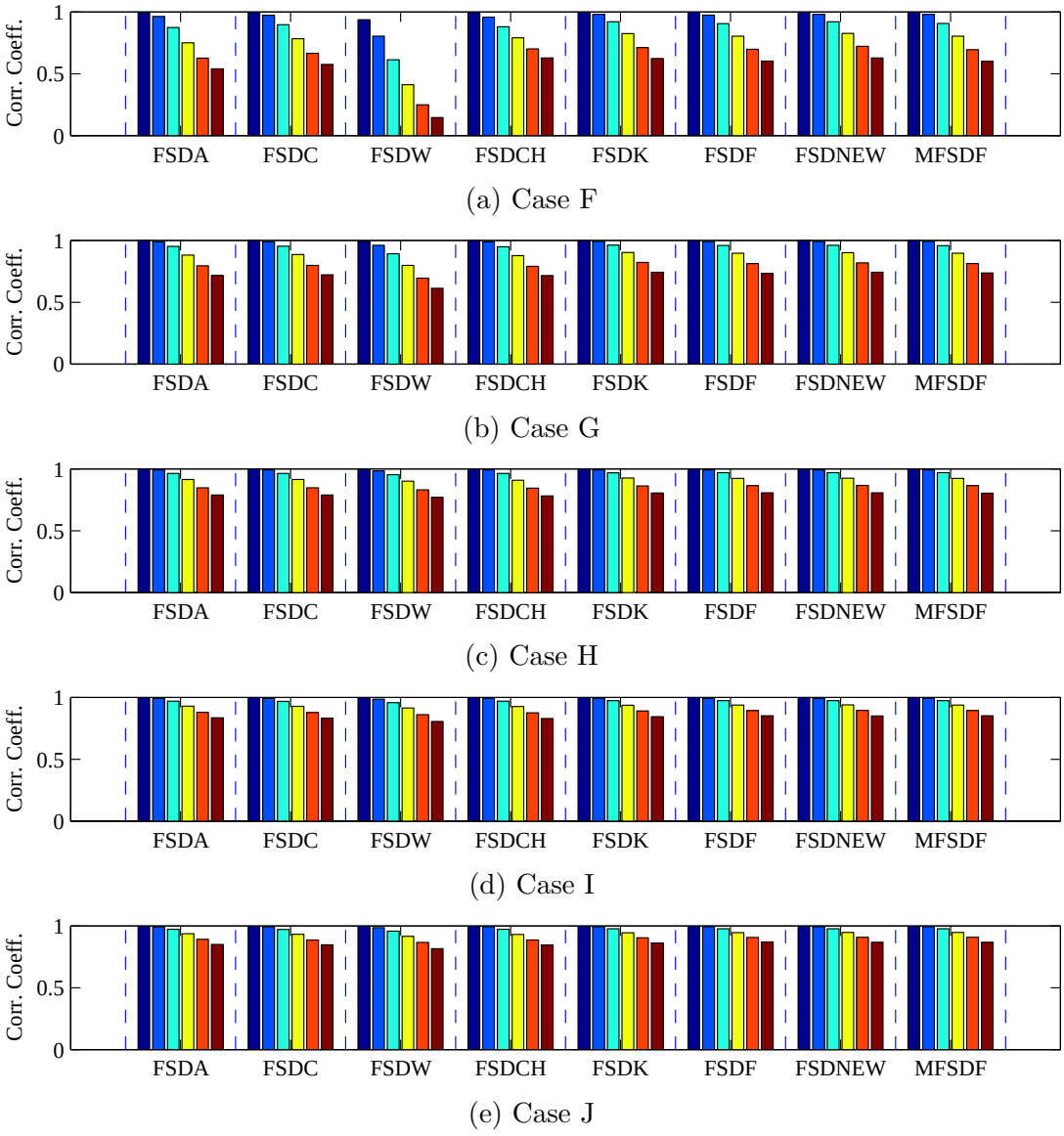

(a) Case F

(b) Case G

(c) Case H

(d) Case I

(e) Case J

Figure 5.9: Correlation coefficients between modelled and actual values of Σ_{gen} in the $\bar{c}$ range of $0.1 \leq \bar{c} \leq 0.9$ for LES filter widths $\Delta = 4\Delta_m = 0.4\delta_{th}$ (■), $\Delta = 8\Delta_m = 0.8\Delta_{th}$ (■), $\Delta = 12\Delta_m = 1.2\delta_{th}$ (■), $\Delta = 16\Delta_m = 1.6\delta_{th}$ (■), $\Delta = 20\Delta_m = 2.0\delta_{th}$ (■), $\Delta = 24\Delta_m = 2.4\delta_{th}$ (■) for: (a-e) corresponding to cases F-J, respectively.

Chapter 6

Statistical Behaviour of the Generalised FSD Transport

The LES generalised FSD Σ_{gen} is an unclosed quantity in the context of LES, and it is closed either by using an algebraic expression or by solving a modelled transport equation alongside other conservation equations. In the previous chapter the *a priori* analysis of algebraic models of the generalised FSD was discussed. The algebraic closure is valid when the generation rate of flame surface area is assumed to be in equilibrium with its destruction rate. Under unsteady conditions it is often advantageous to solve a modelled transport equation of the generalised FSD Σ_{gen}. In this chapter the behaviour of the unclosed terms of the FSD transport equation are examined through scaling and by *a priori* analysis of the DNS database. This analysis then forms the basis for the remaining two chapters of this thesis where the modelling of the curvature and strain rate terms is shown.

6.1 Generalised FSD Transport Equation

The exact transport equation for the generalised FSD Σ_{gen} is given as [29, 35, 48, 66, 67, 68], which is repeated here from Eq. 2.91 in order to present the naming

convention that is used:

$$\frac{\partial \Sigma_{gen}}{\partial t} + \frac{\partial (\tilde{u}_j \Sigma_{gen})}{\partial x_j} = \underbrace{-\frac{\partial \{[\overline{(u_i)}_s - \tilde{u}_i]\Sigma_{gen}\}}{\partial x_i}}_{T_1} + \underbrace{\overline{\left[(\delta_{ij} - N_i N_j)\frac{\partial u_i}{\partial x_j}\right]}_s \Sigma_{gen}}_{T_2} + \underbrace{\overline{\left[S_d \left(\frac{\partial N_i}{\partial x_i}\right)\right]}_s \Sigma_{gen}}_{T_3} \underbrace{- \frac{\partial \overline{(S_d N_i)}_s \Sigma_{gen}}{\partial x_j}}_{T_4} \tag{6.1}$$

The terms on the left hand side of 6.1 denote transient and mean advection effects respectively. The unclosed terms T_1, T_2, T_3 and T_4 are known as subgrid convection term, tangential strain rate term, curvature term and propagation term respectively [29, 39, 66, 68, 73].

In order to model for the various unclosed terms of the generalised FSD transport equation the statistical behaviour of these terms must be examined, but firstly an order of magnitude analysis was used. To carry out the order of magnitude analysis, it is assumed that the Favre filtered velocity in the i^{th} direction is scaled with a reference velocity scale u_{ref} i.e.

$$\tilde{u}_i \sim u_{ref} \tag{6.2}$$

The gradients of filtered quantities are scaled according to Δ^{-1}, the gradients of the sub grid scale quantities are scaled according to δ_L^{-1} (e.g. $\Sigma_{gen} \sim 1/\delta_L$) and time t scales as $t \sim \Delta/u_{ref}$. Based on the above scaling analysis the local turbulent Reynolds number may be scaled as $Re_\Delta \sim (u'_\Delta \Delta)/(S_L \delta_L)$, the local Damköhler number and Karlovitz number are taken to scale as $Da_\Delta \sim (\Delta S_L)/(u'_\Delta \delta_L)$ and the local Karlovitz number can be expressed as $Ka_\Delta \sim (u'_\Delta/S_L)^{3/2}(\Delta/\delta_L)^{-1/2}$. The transient term of the generalised FSD transport equation may then be scaled in the following manner:

$$\begin{aligned} \frac{\partial \Sigma_{gen}}{\partial t} &\sim \frac{1}{\delta_L} \times \frac{u_{ref}}{\delta_L} \times \frac{\delta_L}{\Delta} \times \frac{1}{Re_\Delta^{1/2} Da_\Delta^{1/2}} \\ &\sim \frac{u_{ref}}{S_L} \times \frac{S_L}{\delta_L^2} \frac{\delta_L}{\Delta} \end{aligned} \tag{6.3}$$

Similarly the mean advection term may be scaled in the following manner:

$$\frac{\partial}{\partial x_i}(\tilde{u}_i \Sigma_{gen}) \sim \frac{S_L}{\delta_L^2} \times \frac{1}{Re_\Delta^{1/2} Da_\Delta^{1/2}} \times \frac{u_{ref}}{S_L} \tag{6.4}$$

The subgrid convection term T_1 can be split into terms arising from heat release and due to subgrid turbulent velocity fluctuation. The heat release contribution of the T_1 term maybe scaled as follows:

$$\begin{aligned} T_1 \text{ due to Heat release: } -\frac{\partial}{\partial x_i}\{[\overline{(u_i)}_s - \tilde{u}_i]\Sigma_{gen}\} &\sim \frac{S_L}{\Delta \delta_L} \\ &\sim \frac{S_L}{\delta_L^2}\frac{\delta_L}{\Delta} \\ &\sim \frac{S_L}{\delta_L^2} \times \frac{1}{Re_\Delta^{1/2} Da_\Delta^{1/2}} \end{aligned} \tag{6.5}$$

and the contribution due to turbulent velocity fluctuation can be scaled as:

$$\begin{aligned} T_1 \text{ due to turbulent velocity fluctuation: } -\frac{\partial}{\partial x_i}\{[\overline{(u_i)}_s - \tilde{u}_i]\Sigma_{gen}\} &\sim \frac{u'_\Delta}{\Delta \delta_L} \\ &\sim \frac{u'_\Delta \delta_L}{S_L \Delta} \times \frac{S_L}{\delta_L^2} \\ &\sim \frac{S_L}{\delta_L^2}\frac{1}{Da_\Delta} \end{aligned} \tag{6.6}$$

The tangential strain rate term T_2 can be split as follows:

$$\overline{(a_T)}_s \Sigma_{gen} = S_m + S_{hr} + S_{sg} \tag{6.7}$$

where S_m, S_{hr} and S_{sg} are the mean, heat release and the subgrid contributions of the T_2 term. The mean component of the tangential term S_m can be scaled in

the following manner:

$$S_m = [\delta_{ij} - \overline{(N_i N_j)}_s]\frac{\partial \tilde{u}_i}{\partial x_j}\Sigma_{gen} \sim \frac{u_{ref}}{\Delta\delta_L} \sim \frac{u_{ref}}{S_L} \times \frac{S_L}{\delta_L^2} \times \frac{1}{Re_\Delta^{1/2} Da_\Delta^{1/2}} \tag{6.8}$$

and the heat release contribution of the strain rate term S_{hr} can be scaled as:

$$\begin{aligned} S_{hr} \sim \frac{S_L}{\delta_L \Delta} &\sim \frac{S_L}{\delta_L^2} \times \frac{\delta_L}{\Delta} \\ &\sim \frac{S_L}{\delta_L^2} \times \frac{1}{Da_\Delta^{1/2} Re_\Delta^{1/2}} \end{aligned} \tag{6.9}$$

If the subgrid velocity gradients are scaled using δ_L one obtains the following scaling for S_{sg}:

$$\text{Reactive contribution of } S_{sg}\text{: } T_2 \sim \frac{S_L}{\delta_L^2} \tag{6.10}$$

The non-reacting contribution of S_{sg} can be scaled as:

$$\begin{aligned} S_{sg} \sim \frac{u'_\Delta}{\Delta\delta_L} &\sim \frac{u'_\Delta}{S_L} \times \frac{\delta_L}{\Delta} \times \frac{S_L}{\delta_L^2} \\ &\sim \frac{S_L}{\delta_L^2 Da_\Delta} \end{aligned} \tag{6.11}$$

The curvature term, T_3, $\overline{(S_d \nabla . \vec{N})}_s \Sigma_{gen}$ can be split as follows:

$$\overline{(S_d \nabla . \vec{N})}_s \Sigma_{gen} = C_{mean} + C_{sg} \tag{6.12}$$

where C_{mean} is the resolved curvature term and C_{sg} is the subgrid curvature term. The resolved curvature term C_{mean} can be scaled as:

$$\begin{aligned} C_{mean} &= \overline{(S_d)}_s \frac{\partial \overline{(N_i)}_s}{\partial x_i} \Sigma_{gen} \\ &\sim \frac{S_L}{\Delta} \frac{1}{\delta_L} \\ &\sim \frac{S_L}{\delta_L^2} \frac{1}{Da_\Delta^{1/2} Re_\Delta^{1/2}} \end{aligned} \tag{6.13}$$

The subgrid curvature term C_{sg} can be scaled as:

$$C_{sg} \sim \frac{S_L}{\delta_L^2} \tag{6.14}$$

Finally the propagation term T_4 can be scaled in the following manner:

$$T_4 = -\frac{\partial}{\partial x_i} [\overline{(S_d \nabla . \vec{N})}_s \Sigma_{gen}] \sim \frac{1}{\Delta} \frac{S_L}{\delta_L} \sim \frac{S_L}{\delta_L^2} \frac{1}{Re_\Delta^{1/2} Da_\Delta^{1/2}} \tag{6.15}$$

Therefore from the above analysis the following order of magnitude scaling can be prescribed to the terms of generalised FSD transport equation:

$$\frac{\partial \Sigma_{gen}}{\partial t} \sim O \frac{u_{ref}}{S_L} \times \frac{S_L}{\delta_L^2} \frac{\delta_L}{\Delta} \tag{6.16}$$

$$\begin{aligned} \frac{\partial}{\partial x_i} (\tilde{u}_i \Sigma_{gen}) &\sim O \left(\frac{u_{ref}}{u'_\Delta} \frac{1}{Da_\Delta} \times \frac{S_L}{\delta_L^2} \right) \\ &\sim O \left(\frac{S_L}{\delta_L^2} \times \frac{1}{Re_\Delta^{1/2} Da_\Delta^{1/2}} \times \frac{u_{ref}}{S_L} \right) \end{aligned} \tag{6.17}$$

T_1 contribution due to heat release:

$$\sim O \left(\frac{S_L}{\delta_L^2} \times \frac{1}{Da_\Delta} \right) \tag{6.18}$$

T_1 contribution due to turbulent velocity fluctuation:

$$\sim O\left(\frac{S_L}{\delta_L^2} \times \frac{1}{Da_\Delta}\right) \tag{6.19}$$

$$S_m \sim O\left(\frac{u_{ref}}{S_L} \times \frac{S_L}{\delta_L^2} \times \frac{1}{Re_\Delta^{1/2} Da_\Delta^{1/2}}\right) \tag{6.20}$$

$$S_{hr} \sim O\left(\frac{S_L}{\delta_L^2} \times \frac{1}{Da_\Delta}\right) \tag{6.21}$$

$$\text{Reactive contribution of: } S_{sg} \sim O\left(\frac{S_L}{\delta_L^2}\right) \tag{6.22}$$

$$\text{Nonreating contribution of: } S_{sg} \sim O\left(\frac{S_L}{\delta_L^2} \times \frac{1}{Da_\Delta}\right) \tag{6.23}$$

$$C_{mean} \sim O\left(\frac{S_L}{\delta_L^2} \frac{1}{Re_\Delta^{1/2} Da_\Delta^{1/2}}\right) \tag{6.24}$$

$$C_{sg} \sim O\left(\frac{S_L}{\delta_L^2}\right) \tag{6.25}$$

$$T_4 \sim O\left(\frac{S_L}{\delta_L^2} \frac{1}{Re_\Delta^{1/2} Da_\Delta^{1/2}}\right) \tag{6.26}$$

The above scaling analysis was used, alongside, with *a priori* analysis of the current DNS database. Furthermore this analysis can be used to propose models in the context of LES, which can be seen in chapters 7 and 8. In the following section the behaviour of the unclosed terms of the FSD transport equation are looked into using filtered DNS data.

6.1.1 Statistical Behaviour of the Generalised FSD

The variation of $\Sigma_{gen} \times \delta_{th}$ with $\tilde{c}$ is shown in Fig. 6.1 for cases A-J, where values have been ensemble averaged on $\tilde{c}$ isosurfaces following Boger et al. [8] in order to avoid the data scatter. It can be seen from Fig. 6.1 that the distribution of Σ_{gen} with $\tilde{c}$ remains slightly skewed towards the burned gas side (i.e. $\tilde{c} > 0.5$) for small filter widths (e.g. $\Delta = 0.4\delta_{th}$) for the $Le = 0.8$, 1.0 and 1.2 flames but the profile becomes skewed towards $\tilde{c} < 0.5$ for large values of filter widths (e.g.

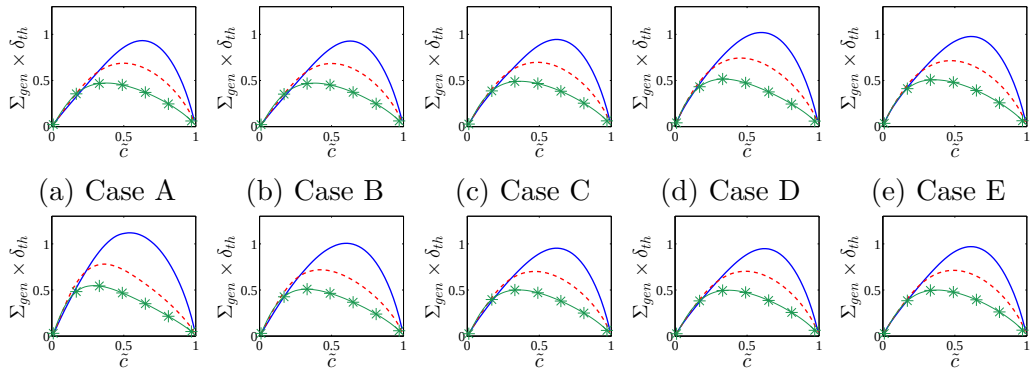

(a) Case A (b) Case B (c) Case C (d) Case D (e) Case E

(f) Case F (g) Case G (h) Case H (i) Case I (j) Case J

Figure 6.1: Variations of $\Sigma_{gen} \times \delta_{th}$ with $\tilde{c}$ at filter widths $\Delta = 0.4\delta_{th}$ (——), $\Delta = 1.2\delta_{th}$ (– – –) and $\Delta = 2.4\delta_{th}$ (—*—) for cases A-J (a-j).

$\Delta < 2.4\delta_{th}$). Similar behaviour has been observed for the $Le = 0.34$ case but the conditionally averaged value of $\Sigma_{gen} \times \delta_{th}$ peaks at $\tilde{c} \approx 0.5$ at small values of filter width (e.g. $\Delta = 0.4\delta_{th}$). At the smallest filter widths $\Sigma_{gen} \times \delta_{th}$ assumes values that is roughly equal to unity. This is due to the fact that $\Sigma_{gen} \approx 1/\delta_{th}$. It can also be seen from Fig. 6.1 that the magnitude of $\Sigma_{gen} \times \delta_{th}$ decreases with increasing filter width Δ due to smearing of local information and weighted averaging process over a larger volume. Moreover, for a given filter width the $\Sigma_{gen} \times \delta_{th}$ assumes greater magnitudes for $Le = 0.34$ flames in comparison to the flames with $Le \approx 1$. Moreover increasing turbulent Reynolds number leads to a slight increase in the peak value of the generalised FSD, Σ_{gen}.

6.1.2 Statistical Behaviour of the Unclosed Terms

The contributions of T_1, T_2, T_3 and T_4 for different filter widths for cases A-E and F-J are shown in Fig. 6.2 and Fig. 6.3 where the values have been ensemble averaged on $\tilde{c}$ isosurfaces. Based on Fig. 6.2 the following statistical observations can be made:

- The Behaviours of T_1, T_2, T_3 and T_4 are consistent with scaling arguments $Re_\Delta \times Da_\Delta \sim (\Delta/\delta_L)^2$ with Δ and thus T_1 is expected to decrease in comparison to T_2 and T_3 for $\Delta \gg \delta_{th}$

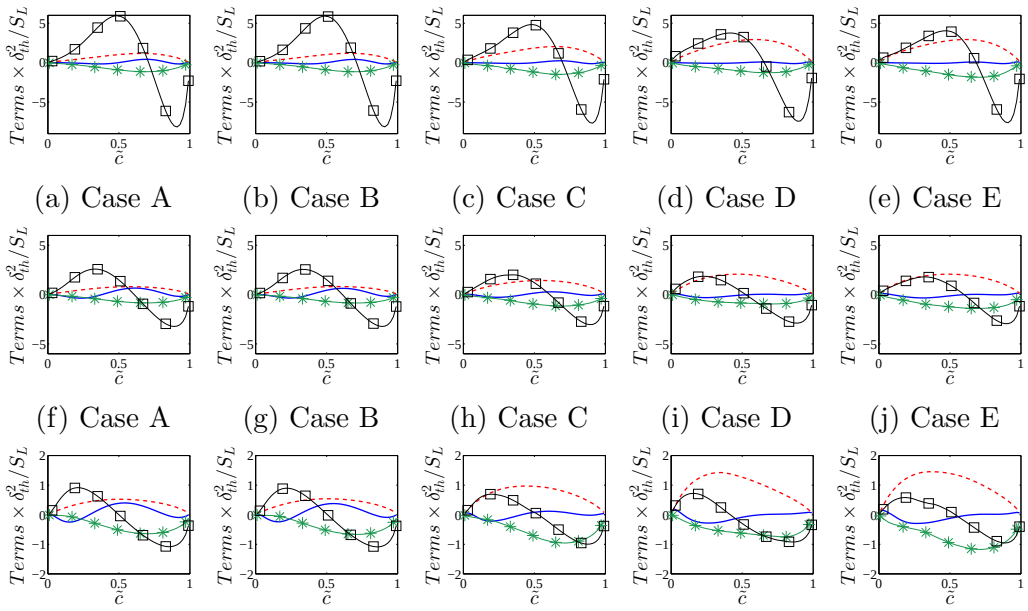

(a) Case A (b) Case B (c) Case C (d) Case D (e) Case E

(f) Case A (g) Case B (h) Case C (i) Case D (j) Case E

(k) Case A (l) Case B (m) Case C (n) Case D (o) Case E

Figure 6.2: Variation of normalised T_1 (——), T_2 (– – –), T_3 (—✳—), T_4 (—□—) with $\tilde{c}$ shown at filter widths $\Delta = 0.4\delta_{th}$ (top row), $\Delta = 1.2\delta_{th}$ (middle row) and $\Delta = 2.4\delta_{th}$ for cases A-E.

- For smallest filter width shown here ($\Delta = 0.4\delta_{th}$) the T_4 term dominates the remainder of the unclosed terms. For the intermediate filter width $\Delta = 1.2\delta_{th}$ the terms T_2, T_3 and T_4 are comparable and the term T_1 remains very small. At the largest filter width shown ($\Delta = 2.4\delta_{th}$) the magnitude of T_2, T_3 and T_4 remain comparable. Additionally the magnitudes of the conditional mean value of the propagation term T_4 strengthens with decreasing turbulent Reynolds number Re_t.

- The tangential strain rate term T_2 has been found to be a source of Σ_{gen} in all the cases for all filter widths, However the magnitude of its contribution increases with increasing turbulent Re_t. At the smallest filter width shown ($\Delta = 0.4\delta_{th}$) the magnitude of T_2 is found to be comparable with T_3 and T_4 for the high values of Re_t, while for the smaller values of Re_t the magnitude of T_2 remains only comparable to T_3. As the filter width increases the T_2 term becomes a leading order source term, especially in the case of the high Re_t flames.

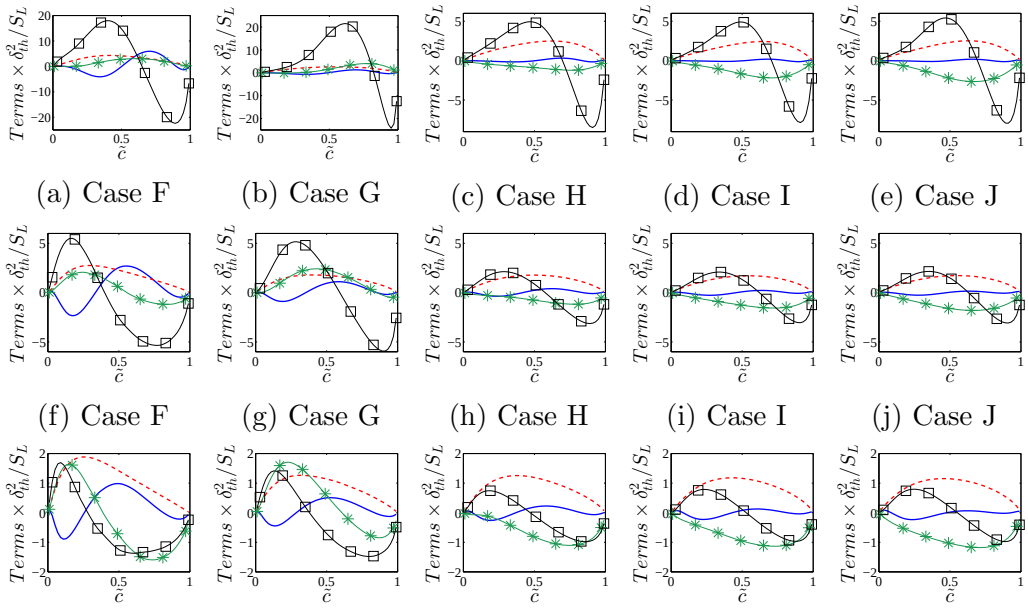

Figure 6.3: Variation of normalised T_1 (——), T_2 (– – –), T_3 (—✳—), T_4 (—□—) with $\tilde{c}$ shown at filter widths $\Delta = 0.4\delta_{th}$ (top row), $\Delta = 1.2\delta_{th}$ (middle row) and $\Delta = 2.4\delta_{th}$ for cases F-J.

- The curvature term T_3 has been found to be a sink term in cases A-E, for all filter widths. The T_3 term is relatively small compared to the T_4 term at $\Delta \ll \delta_{th}$, but as the filter width increases T_3 becomes a leading order sink term. Additionally it was found that increasing the Re_t results in a greater magnitude of the term T_3.

- The subgrid convection term T_1 can be seen to be have the smallest magnitude among the terms of the Σ_{gen} transport equation, for cases A-E at all filter widths. Although the magnitude of T_1 is small, at filter widths $\Delta \ll \delta_{th}$, it is however comparable to the other terms for the filter width of $\Delta = 1.2\delta_{th}$ and $\Delta = 2.4\delta_{th}$. Additionally the behaviour of T_1 changes from one case to the other, for example the conditional mean value of T_1 assumes negative value towards the reactants whereas the contribution towards the products is positive, for small values of Re_t. However, the contribution of T_1 remains negative throughout the flame brush for large values of Re_t.

The following observations can be made from Fig. 6.3 on the effects of Lewis number of the Σ_{gen} transport equation:

- For all flames the terms T_1, T_2 and T_3 remain small in comparison to the contribution of T_4 at small Δ but the contributions of all the terms remain comparable for large Δ. The contribution of the propagation term T_4 remains positive (negative) towards the unburned (burned) gas side of the flame brush.

- For a given filter width Δ, the relative magnitude of the contribution of T_1 in proportion to the magnitude of the terms T_2, T_3 and T_4 increases with decreasing Le.

- The strain rate term T_2 remains a source term for all the filter widths for all the terms considered here.

- The curvature term T_3 is a sink term for the $Le = 0.8$, 1.0 and 1.2 flames for all filter widths and the contribution of T_3 remains almost in equilibrium with the source contribution of T_2. For $Le = 0.34$ and 0.6 flames the curvature term T_3 remains positive throughout the flame brush for small filter widths (e.g. $\Delta = 4\Delta_m = 0.4\Delta_{th}$) but the contribution of T_3 remains positive (negative) towards the reactants (products) gas side of the flame brush for large filter widths (e.g.$\Delta = 24\Delta_m = 2.4\delta_{th}$).

- It can be seen from Fig. 6.3 that the net positive contribution arising from T_2 and T_3 overcomes the negative contributions of T_3 by a large amount in the $Le = 0.34$ and 0.6 flames. This suggests that the generation of flame surface area is greater than its destruction in these flames. By contrast, the generation and destruction rate of FSD remains approximately in equilibrium in the $Le = 0.8$, 1.0 and 1.2 flames. This higher rate of area generation rate in the small Lewis number flames can be substantiated from the values of turbulent flame surface area normalised by the corresponding laminar value A_T/A_L for these flames (i.e. A_T/A_L =3.93, 2.63, 2.11, 1.84 and 1.76 for the $Le = 0.34$, 0.6, 0.8, 1.0 and 1.2 flames respectively), which are presented in Chapter 4, Table 4.2.

  Higher generation rate of FSD than its destruction rate in the $Le \ll 1$ flame gives rise to higher magnitude of $\Sigma_{gen} \times \delta_{th}$ in the $Le = 0.34$ flame than in the $Le \approx 1.0$ flames, as shown in Fig. 4.1.

In the following sections each of the unclosed terms of the Σ_{gen} transport equation are examined in detail to understand their behaviour in response to the variations of Re_t and Le.

6.1.2.1 Behaviour of the Subgrid Convection Term

The behaviour of the subgrid convection term depends on the statistical behaviour of the subgrid flux of generalised FSD (i.e. $[\overline{(u_i)}_s - \tilde{u}_i]\Sigma_{gen}$). The distributions of $[\overline{(u_i)}_s - \tilde{u}_i]\Sigma_{gen}$ and $(\partial\Sigma_{gen}/\partial x_i)M_i$ conditionally averaged on $\tilde{c}$ isosurfaces are shown in Fig. 6.4 and Fig. 6.5 for cases A-J, where $M_i = -(\partial\bar{c}/\partial x_i)/|\nabla\bar{c}|$ is the i^{th} component of the resolved flame normal vector. Comparing the signs of $[\overline{(u_i)}_s - \tilde{u}_i]\Sigma_{gen}$ and $(\partial\Sigma_{gen}/\partial x_i)M_i$ it is evident that the subgrid flux of FSD shows predominantly gradient type transport (i.e. $[\overline{(u_i)}_s - \tilde{u}_i]\Sigma_{gen} = -(\nu_t/Sc_\Sigma)\partial\Sigma_{gen}/\partial x_i)$ for the $Le = 0.8$, 1.0 and 1.2 (cases C, D, E, H, I and J) flames but a predominantly counter-gradient transport is prevalent in the $Le = 0.34$, 0.6 and cases with low Re_t (cases A and B). The rate of burning increases with decreasing Le and this behaviour is particularly prevalent in the $Le \ll 1$ flames because of thermo-diffusive instabilities. This can be substantiated from the normalised turbulent flame speed S_T/S_L values (i.e. $S_T/S_L = 13.70$, 4.58, 2.53, 1.83 and 1.50 for the $Le = 0.34$, 0.6, 0.8, 1.0 and 1.2 flames) (see Chapter 4, Table 4.2). The S_T/S_L values for the cases A-E in response to the variation of Re_t can be seen in Table 4.3. The enhanced burning rate in the small Lewis number flames gives rise to stronger flame normal acceleration which overcomes the turbulent velocity fluctuation effects to result in a counter-gradient transport of FSD. Similarly in Re_t cases A and B the turbulent velocity fluctuations are not strong enough to overcome the flame normal acceleration and thus resulting in a counter gradient transport. The similar behaviour of the unresolved turbulent flux of FSD in response to Le has been demonstrated earlier in the context of RANS by Chakraborty and Cant [36, 40]. The effects of Re_t on the modelling of turbulent flux of FSD were analysed by Chakraborty and Cant [47] in the context of RANS. The subgrid FSD transport term $\overline{(u_i)}_s - \tilde{u}_i$ can be modelled as [66]:

$$\begin{aligned}\overline{(u_i)}_s - \tilde{u}_i = [\overline{(u_i)}_{Rs} - \overline{(u_i)}_R + K\{(\overline{(u_i)}_{Ps} - \overline{(u_i)}_P) - (\overline{(u_i)}_{Rs} - \overline{(u_i)}_R)\} \\ + (K - \tilde{c})[\overline{(u_i)}_P - \overline{(u_i)}_R]\end{aligned} \quad (6.27)$$

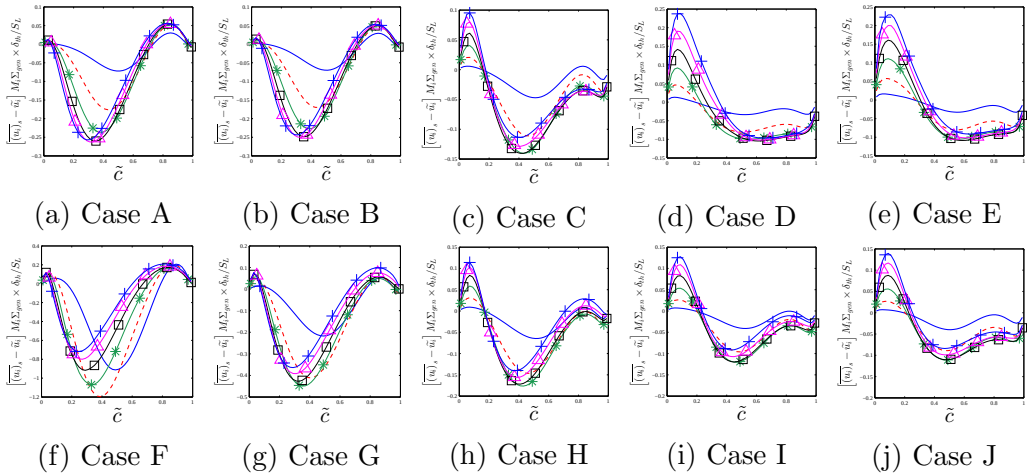

(a) Case A (b) Case B (c) Case C (d) Case D (e) Case E

(f) Case F (g) Case G (h) Case H (i) Case I (j) Case J

Figure 6.4: Variations of normalised $[\overline{(u_i)}_s - \tilde{u}_i]\Sigma_{gen}$ with $\tilde{c}$ at filter widths $\Delta = 0.4\delta_{th}$ (——), $\Delta = 0.8\delta_{th}$ (– – –), $\Delta = 1.2\delta_{th}$ (—*—), $\Delta = 1.6\delta_{th}$ (—□—), $\Delta = 2.0\delta_{th}$ (—△—) and $\Delta = 2.4\delta_{th}$ (—+—), for cases A-J (a-j).

where K is a constant which depends on the isosurface of c representing the flame surface [66]. Hawkes [66] indicated that the first term on the right hand side of Eq. 6.27 might be seen to represent a component of transport connected with subgrid turbulent velocity fluctuation u'_Δ and can be modelled by conventional gradient transport. The second term is associated with heat release as indicated by Veynante et al. [155]. On the other hand the slip velocity $\overline{(u_i)}_P - \overline{(u_i)}_R$ can be scaled with $(-\tau S_L \Xi M_i)$ [158]. The magnitudes of subgrid turbulent velocity fluctuation u'_Δ and Ξ increase with increasing Δ which determines the dependence of the magnitude of $[\overline{(u_i)}_s - \tilde{u}_i]M_i\Sigma_{gen}$ for the $Le = 0.34$, 0.6 and 0.8 flames. As $[\overline{(u_i)}_s - \tilde{u}_i]M_i\Sigma_{gen}$ is primarily driven by subgrid turbulent velocity fluctuation u'_Δ for the cases C-E and H-J, the magnitude of $[\overline{(u_i)}_s - \tilde{u}_i]M_i\Sigma_{gen}$ increases with increasing Δ due to strengthening of the effects of u'_Δ.

6.1.2.2 Behaviour of the Tangential Strain Rate Term

The variations of T_2 conditionally averaged on $\tilde{c}$ values are shown Fig. 6.6 for cases A-J. The peak value of conditionally averaged T_2 shifts from $\tilde{c} > 0.5$ to $\tilde{c} \approx 0.5$ with increasing Δ for $Le = 0.8$, 1.0 and 1.2 flames. However, in the $Le = 0.34$ and 0.6 flames the profile of T_2 is skewed towards $\tilde{c} < 0.5$ for $\Delta \gg \delta_{th}$filter widths. For

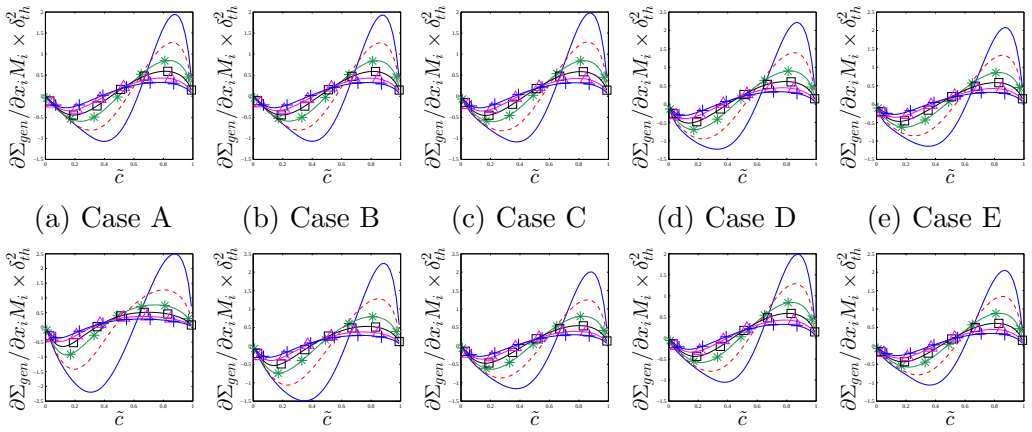

(a) Case A (b) Case B (c) Case C (d) Case D (e) Case E

(f) Case F (g) Case G (h) Case H (i) Case I (j) Case J

Figure 6.5: Variations of normalised $(\partial\Sigma_{gen}/\partial x_i)M_i$ with $\tilde{c}$ at filter widths $\Delta = 0.4\delta_{th}$ (——), $\Delta = 0.8\delta_{th}$ (– – –), $\Delta = 1.2\delta_{th}$ (—*—), $\Delta = 1.6\delta_{th}$ (—□—), $\Delta = 2.0\delta_{th}$ (—△—) and $\Delta = 2.4\delta_{th}$ (—|—), for cases A-J (a-j).

cases A-E the quantitative behaviour of T_2 throughout the flame brush remains the same, but the magnitude of T_2 can be seen to increase with increasing Re_t. In the flames with $Le \ll 1$ the non-dimensional temperature T and reaction progress variable c fields become significantly different from each other and this makes the distribution of $|\nabla c|$ and $\nabla.\vec{u}$ within these flames significantly different from those in the $Le \approx 1.0$ flames. This makes the distribution of T_2 in the $Le = 0.34$ flame different from the $Le = 0.8$, 1.0 and 1.2 flames. The magnitude of the term T_2 also decreases with increasing Δ for all cases because of averaging over a larger volume where the contributions arising from the close to the centre of the filter volume are weighted more heavily. Moreover, it can be seen Fig. 6.6 that the magnitude of T_2 for a given filter width decreases with increasing Le.

The term T_2 can further be split in the following manner:

$$T_2 = \underbrace{\left(\overline{\frac{\partial u_i}{\partial x_i}}\right)_s \Sigma_{gen}}_{T_D} \underbrace{-\overline{\left(N_i N_j \frac{\partial u_i}{\partial x_j}\right)_s \Sigma_{gen}}}_{(-T_N)} \tag{6.28}$$

where T_D and $(-T_N)$ are dilatation rate and normal strain contributions to the FSD transport. The variations of T_D and $(-T_N)$ are shown in Fig. 6.7 and Fig.

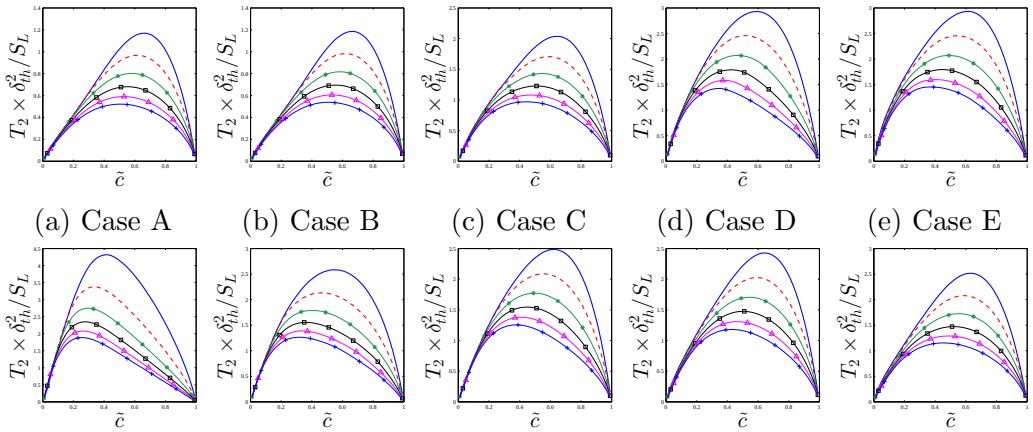

(a) Case A (b) Case B (c) Case C (d) Case D (e) Case E

(f) Case F (g) Case G (h) Case H (i) Case I (j) Case J

Figure 6.6: Variations of normalised T_2 with $\tilde{c}$ at filter widths $\Delta = 0.4\delta_{th}$ (——), $\Delta = 0.8\delta_{th}$ (– – –), $\Delta = 1.2\delta_{th}$ (—*—), $\Delta = 1.6\delta_{th}$ (—□—), $\Delta = 2.0\delta_{th}$ (—△—) and $\Delta = 2.4\delta_{th}$ (—+—), for cases A-J (a-j).

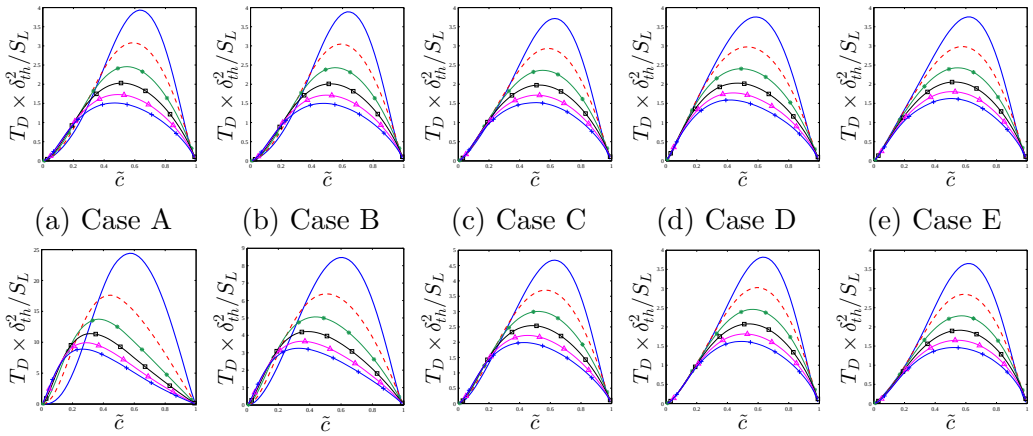

(a) Case A (b) Case B (c) Case C (d) Case D (e) Case E

(f) Case F (g) Case G (h) Case H (i) Case I (j) Case J

Figure 6.7: Variations of normalised T_D with $\tilde{c}$ at filter widths $\Delta = 0.4\delta_{th}$ (——), $\Delta = 0.8\delta_{th}$ (– – –), $\Delta = 1.2\delta_{th}$ (—*—), $\Delta = 1.6\delta_{th}$ (—□—), $\Delta = 2.0\delta_{th}$ (—△—) and $\Delta = 2.4\delta_{th}$ (—+—), for cases A-J (a-j).

6.8. The term T_D is positive throughout the flame brush because of predominantly positive dilatation rate $\nabla.\vec{u}$. As the effects of heat release is stronger in $Le \ll 1$ flames, dilatation rate take higher values which in turn gives rise to increasing magnitude of T_D with decreasing Le at a given Δ (see Fig. 6.7).

The normal strain rate term $(-T_N)$ assumes predominantly negative values

for the major portion of the flame brush for all the flames but positive values have also been observed towards the unburned and burned gas side of the flame brush for the $Le = 0.8$, 1.0 and 1.2 flames. It was shown by Chakraborty and Swaminathan [31], Chakraborty et al. [39], Swaminathan and Grout [143] that ∇c alignment with local principal strain rate depends on the relative strengths of turbulent straining a_{turb} and strain rate induced by chemical heat release a_{chem}. The quantity ∇c aligns with the most extensive principal strain rate if a_{chem} dominates over a_{turb}. By contrast, ∇c aligns with the most compressive principal strain rate if a_{turb} dominates over a_{chem}. Predominant alignment of ∇c with the most extensive (compressive) principal strain rate yields a negative (positive) contribution of $(-T_N)$. It was demonstrated by Chakraborty et al. [39] that the extent of alignment of ∇c most extensive (compressive) principal strain rate increases (decreases) with decreasing Le because of strong heat release effects in flames with small values of Le. Even in the $Le \approx 1.0$ flames a_{chem} in the reaction zone may become strong enough to overcome a_{turb} to yield a preferential alignment of ∇c with the most extensive principal strain rate, which gives rise to negative contributions of $(-T_N)$. The effects of heat release becomes weak towards both unburned and burned sides of the flame brush where ∇c aligns with the most compressive principal strain rate, which leads to positive values of $(-T_N)$ towards unburned and burned gas side of the flame brush. As the effects of heat release are stronger in and the extent of alignment of ∇c with the most extensive principal strain rate is greater in the $Le \ll 1$ flames, the term $(-T_N)$ assumes larger negative values for flames with small Lewis number flames. The magnitudes of T_D and $(-T_N)$ decrease with increasing Δ because of the convolution operation involved in LES operation as explained earlier. A comparison between T_D and $(-T_N)$ reveals that T_D overcomes $(-T_N)$ to yield a positive value of T_2 and high magnitude of T_D in small Le cases gives rise to high values of T_2 (see Fig. 6.6).

6.1.2.3 Behaviour of the FSD Curvature Term

The variations of T_3 with $\tilde{c}$ for different filter widths Δ are shown in Fig. 6.9. There is a significant difference between the statistical behaviour of T_3 in response

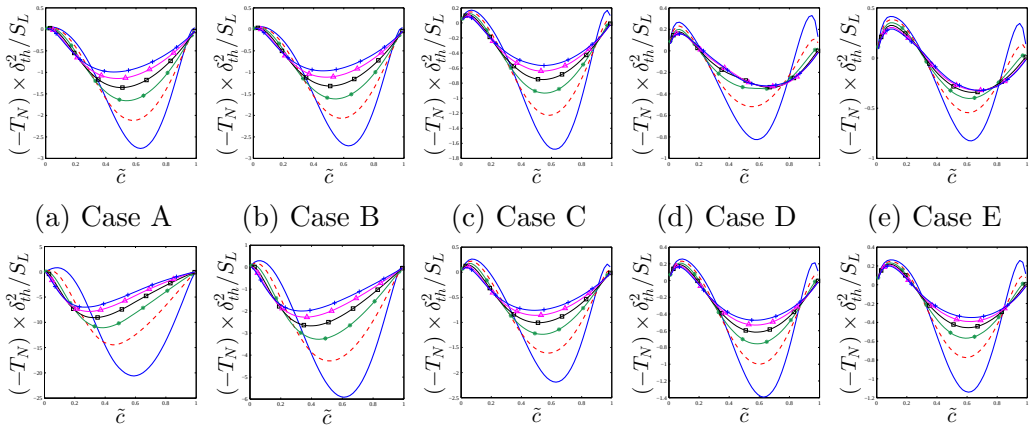

(a) Case A (b) Case B (c) Case C (d) Case D (e) Case E

(f) Case F (g) Case G (h) Case H (i) Case I (j) Case J

Figure 6.8: Variations of normalised $(-T_N)$ with $\tilde{c}$ at filter widths $\Delta = 0.4\delta_{th}$ (——), $\Delta = 0.8\delta_{th}$ (– – –), $\Delta = 1.2\delta_{th}$ (—*—), $\Delta = 1.6\delta_{th}$ (—□—), $\Delta = 2.0\delta_{th}$ (—△—) and $\Delta = 2.4\delta_{th}$ (—+—), for cases A-J (a-j).

to changes in Le, while increasing Re_t results in an increase in the magnitude of T_3 term. Moreover T_3 remains negative throughout the flame brush for the $Le \approx 1.0$ cases. However, for the $Le = 0.34$ flame the contribution of T_3 remains positive for very small filter width Δ (i.e. $\Delta = 4\Delta_m$) whereas this term remains positive (negative) towards the unburned (burned) gas side of the flame brush for large values of LES filter width Δ. Similar behaviour can be seen for the $Le = 0.6$ flame. However, in the $Le = 0.8$, 1.0 and 1.2 flames the contribution of T_3 remains negative throughout the flame brush.

In order to explain this behaviour it is useful to write T_3 in the following manner:

$$T_3 = \underbrace{2\overline{[(S_r + S_n)\kappa_m]}_s\Sigma_{gen}}_{T_{31}} \underbrace{-4\overline{(D\kappa_m^2)}_s\Sigma_{gen}}_{T_{32}} \tag{6.29}$$

The variations of T_{31} and T_{32} with $\tilde{c}$ for different filter widths are shown in Fig. 6.10 and Fig. 6.11. It can be seen from Eq. 6.29 that T_{32} remains deterministically negative throughout the flame brush for all filter widths. As the extent of flame wrinkling increases with decreasing Le, the magnitude of κ_m^2 remains greater for smaller Lewis number flames. This along with higher value of diffusivity D in the smaller Lewis number cases gives rise to larger magnitude of T_{32} at a given filter width Δ. Similarly when Re_t increases, the magnitude of κ_m^2 increases due

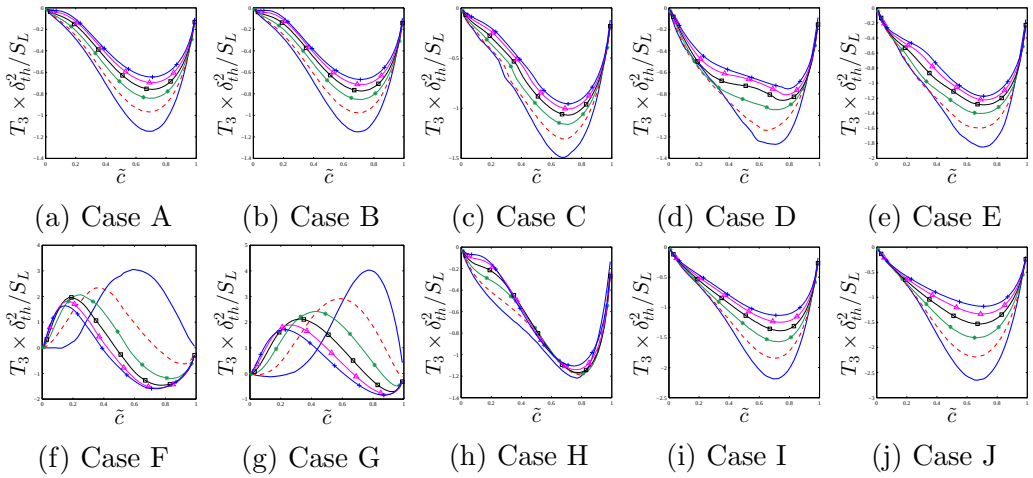

(a) Case A (b) Case B (c) Case C (d) Case D (e) Case E

(f) Case F (g) Case G (h) Case H (i) Case I (j) Case J

Figure 6.9: Variations of normalised T_3 with $\tilde{c}$ at filter widths $\Delta = 0.4\delta_{th}$ (——), $\Delta = 0.8\delta_{th}$ (– – –), $\Delta = 1.2\delta_{th}$ (—✳—), $\Delta = 1.6\delta_{th}$ (—□—), $\Delta = 2.0\delta_{th}$ (—△—) and $\Delta = 2.4\delta_{th}$ (—+—), for cases A-J (a-j).

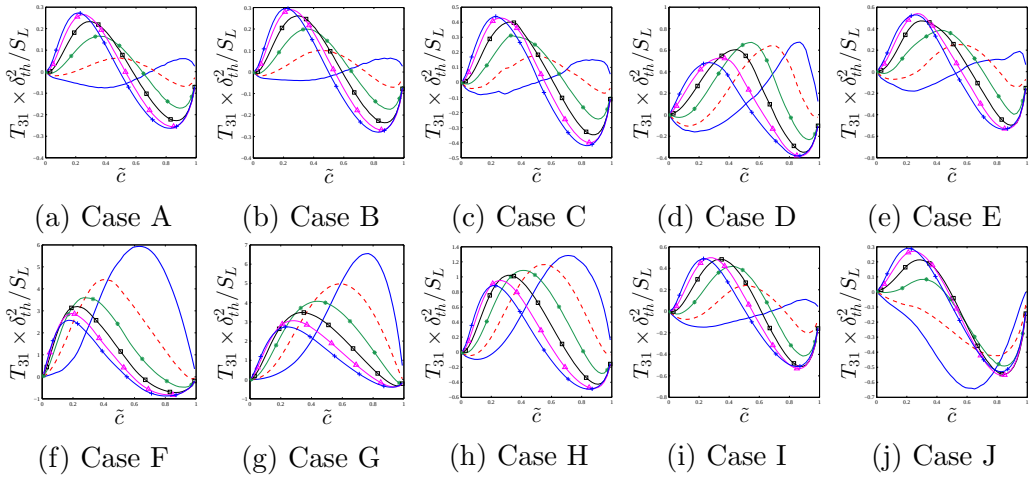

(a) Case A (b) Case B (c) Case C (d) Case D (e) Case E

(f) Case F (g) Case G (h) Case H (i) Case I (j) Case J

Figure 6.10: Variations of normalised T_{31} with $\tilde{c}$ at filter widths $\Delta = 0.4\delta_{th}$ (——), $\Delta = 0.8\delta_{th}$ (– – –), $\Delta = 1.2\delta_{th}$ (—✳—), $\Delta = 1.6\delta_{th}$ (—□—), $\Delta = 2.0\delta_{th}$ (—△—) and $\Delta = 2.4\delta_{th}$ (—+—), for cases A-J (a-j).

to greater extent of flame wrinkling, which results in greater magnitude of T_{32}.

For the $Le = 1.0$ and 1.2 flames the contribution of T_{31} remains weakly negative for small values of Δ but the magnitude of this contribution increases with increasing filter width Δ. By contrast, in the $Le = 0.34$, 0.6 and 0.8 flames T_{31} remains positive throughout the flame brush for small values of Δ but the

magnitude of the contribution of T_{31} decreases with increasing filter width Δ and this contribution remains positive (negative) towards the unburned (burned) gas side of the flame brush. As T_{31} remains greater than T_{32} for small Δ (i.e. $\Delta = 4\Delta_m$) for the $Le = 0.34$ and 0.6 flame, a positive contribution of T_3 is observed throughout the flame brush. At large filter widths (i.e. $\Delta \gg \delta_{th}$) the positive contribution of T_{31} dominates over negative T_{32} towards the unburned gas side to result in a positive contribution of T_3 towards the unburned gas side for the $Le = 0.34$ and 0.6 cases. However, the negative contribution of T_{32} dominates over the positive contribution of T_{31} towards the reactants in the $Le \approx 1.0$ flames, which leads to negative contribution of T_3 throughout the flame brush. The correlation coefficients for the $(S_r + S_n) - \kappa_m$ and $|\nabla c| - \kappa_m$ correlations for five different c isosurfaces are shown in Fig. 6.12, which show that both $(S_r + S_n)$ and $|\nabla c|$ remain positively (negatively) correlated with curvature for the $Le < 1$ ($Le > 1$) flames which give rise to predominantly positive contributions of T_{31} for the $Le = 0.34$ and 0.6 cases for small values of Δ and the extent of positive contribution increases with decreasing Le for the $Le < 1$ flames. As both $(S_r + S_n)$ and $|\nabla c|$ are weakly correlated with κ_m for $Le = 1$ flame and thus T_{31} remains positive (negative) towards the unburned (burned) gas side of the flame brush, as $\overline{(\kappa_m)}_s$ remains positive (negative) towards the unburned (burned) gas side. The extent of negative contribution of T_{31} is greater in the $Le = 1.2$ flame because of negative $(S_r + S_n) - \kappa_m$ and $|\nabla c| - \kappa_m$ correlations.

6.1.2.4 Behaviour of the FSD Propagation Term

The variations of T_4 conditionally averaged on $\tilde{c}$ values are shown in Fig. 6.13 for different LES filter widths. The term T_4 can be written as: $T_4 = \nabla.\overline{(S_d \nabla c)}$ and thus it acts as a diffusive term where S_d plays the role of diffusivity. The probability of finding positive S_d supersedes the probability of finding negative values, which can be substantiated in Fig. 6.14 where $\overline{(S_d)}_s$ for different filter widths are shown. It can be seen from Fig. 6.13 that $\overline{(S_d)}_s$ increases from unburned to burned gas side of the flame brush because of heat release and the value of $\overline{(S_d)}_s$ increases with decreasing Le because of enhanced rate of burning arising from thermo-diffusive instabilities [40]. Due of predominantly positive

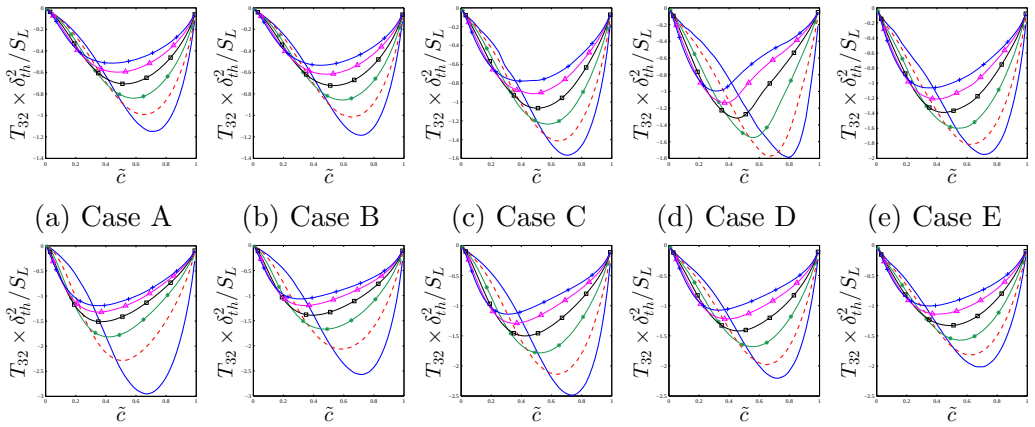

(a) Case A (b) Case B (c) Case C (d) Case D (e) Case E

(f) Case F (g) Case G (h) Case H (i) Case I (j) Case J

Figure 6.11: Variations of normalised T_{32} with $\tilde{c}$ at filter widths $\Delta = 0.4\delta_{th}$ (——), $\Delta = 0.8\delta_{th}$ (– – –), $\Delta = 1.2\delta_{th}$ (—*—), $\Delta = 1.6\delta_{th}$ (—□—), $\Delta = 2.0\delta_{th}$ (—△—) and $\Delta = 2.4\delta_{th}$ (—|—), for cases A-J (a-j).

values of S_d, the term T_4 is positive (negative) towards the unburned (burned) gas side similar to molecular diffusion term $\nabla.\overline{(\rho D \nabla c)}$. The higher magnitude of $\overline{(S_d)}_s$ in the $Le = 0.34$ flame gives rise to larger magnitude of T_4 in comparison to the $Le = 0.8$, 1.0 and 1.2 flames although the qualitative variation remains unaffected by the change in Le.

The resolved part of T_4 can be expressed in the following manner [22, 29, 35, 67, 68]:

$$\text{Resolved part of: } T_4 = -\frac{\partial}{\partial x_i}[\overline{(S_d)}_s \overline{(N_i)}_s \Sigma_{gen}] \tag{6.30}$$

The contribution of T_4 and $-\nabla[\overline{(S_d)}_s \overline{(N_i)}_s \Sigma_{gen}]$ are compared in Fig. 6.15, which shows that $-\nabla[\overline{(S_d)}_s \overline{(N_i)}_s \Sigma_{gen}]$ accurately captures T_4 for all filter widths for all cases. This is because S_d and N_i are statistically independent of each other [29, 35], in turn this enables one to write $\overline{(S_d N_i)}_s = \overline{(S_d)}_s \overline{(N_i)}_s$ which is consistent with earlier findings [22, 29, 35]. However the prediction of Eq. 6.30 is calculated based on $\overline{(S_d)}_s$ extracted from DNS and thus the accuracy of this modelling in actual LES implementation will depend significantly on the modelling of the surface averaged displacement speed $\overline{(S_d)}_s$. The modelling of the $\overline{(S_d)}_s$ is discussed in §6.2.

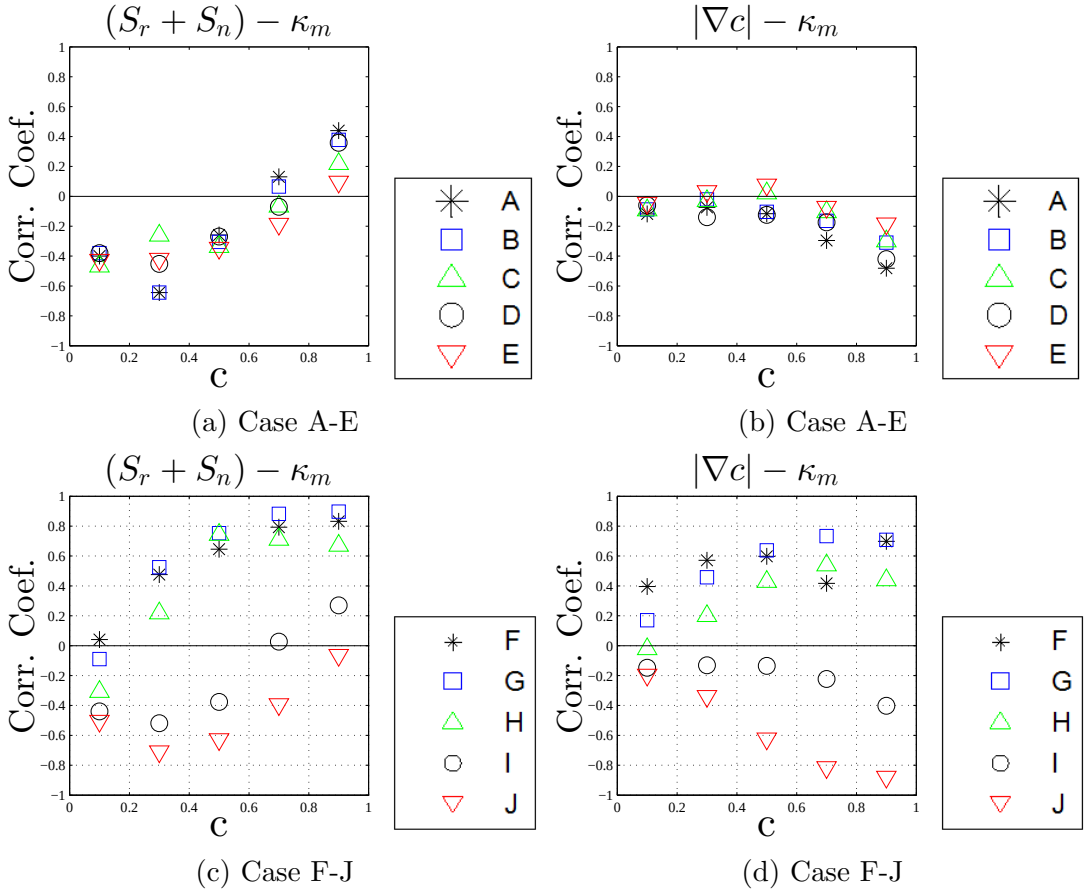

(a) Case A-E

(b) Case A-E

(c) Case F-J

(d) Case F-J

Figure 6.12: Correlation coefficients for $(S_r + S_n) - \kappa_m$ and $|\nabla c| - \kappa_m$ correlations across the flame brush.

6.1.3 Existing Models for the Subgrid Convection Term

The modelling of the subgrid FSD transport term T_1 depends on the modelling of the subgrid FSD flux:

$$[\overline{(u_i)}_s - \tilde{u}_i]\Sigma_{gen} \tag{6.31}$$

In order to model for the subgrid flux of FSD the subgrid flux of progress variable must be examined [36, 47, 149, 155]. In order for gradient transport to take place in the x_1 direction the following inequality must be met:

$$\frac{\partial \tilde{c}}{\partial x_i} \times \rho(\widetilde{u_i c} - \tilde{u}_i \tilde{c}) < 0 \tag{6.32}$$

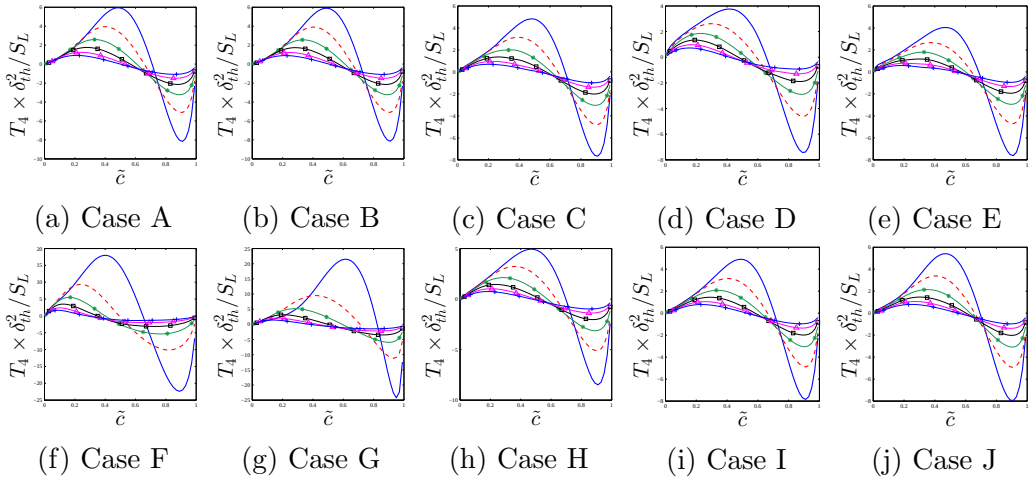

(a) Case A (b) Case B (c) Case C (d) Case D (e) Case E

(f) Case F (g) Case G (h) Case H (i) Case I (j) Case J

Figure 6.13: Variations of normalised T_4 with $\tilde{c}$ at filter widths $\Delta = 0.4\delta_{th}$ (——), $\Delta = 0.8\delta_{th}$ (– – –), $\Delta = 1.2\delta_{th}$ (—*—), $\Delta = 1.6\delta_{th}$ (—▫—), $\Delta = 2.0\delta_{th}$ (—△—) and $\Delta = 2.4\delta_{th}$ (—+—), for cases A-J (a-j).

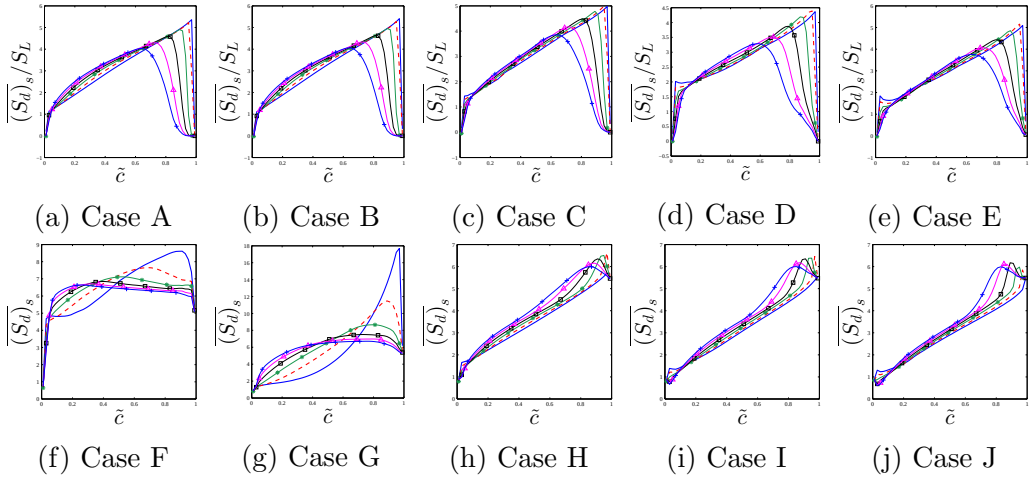

(a) Case A (b) Case B (c) Case C (d) Case D (e) Case E

(f) Case F (g) Case G (h) Case H (i) Case I (j) Case J

Figure 6.14: Variations of normalised $\overline{(S_d)}_s$ with $\tilde{c}$ at filter widths $\Delta = 0.4\delta_{th}$ (——), $\Delta = 0.8\delta_{th}$ (– – –), $\Delta = 1.2\delta_{th}$ (—*—), $\Delta = 1.6\delta_{th}$ (—▫—), $\Delta = 2.0\delta_{th}$ (—△—) and $\Delta = 2.4\delta_{th}$ (—+—), for cases A-J (a-j).

else counter gradient transport occurs. In the case of a gradient transport, the following closure can be used:

$$\bar{\rho}(\widetilde{u_i c} - \tilde{u}_i \tilde{c}) = -\bar{\rho}\frac{\nu_t}{Sc_{sg}}\frac{\partial \tilde{c}}{\partial x_i} \tag{6.33}$$

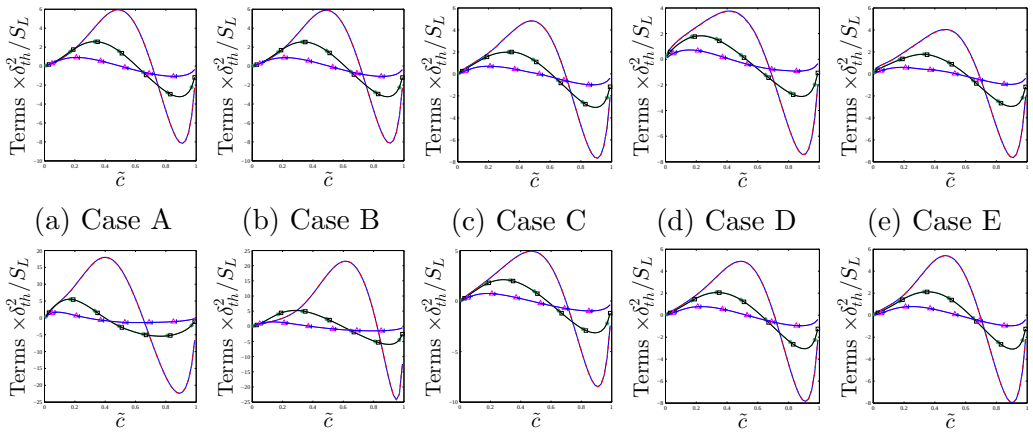

(a) Case A (b) Case B (c) Case C (d) Case D (e) Case E

(f) Case F (g) Case G (h) Case H (i) Case I (j) Case J

Figure 6.15: Variations of normalised T_4 term ($0.4\delta_{th}$: (——), $1.2\delta_{th}$: (—*—) and $2.4\delta_{th}$: (—△—)) and its model given by Eq. 6.30 ($0.4\delta_{th}$: (– – –), $1.2\delta_{th}$ (—□—), $2.4\delta_{th}$ (—|—)), for cases A-J (a-j).

where ν_t is the kinematic eddy viscosity and Sc_{sg} is the subgrid Schmidt number. Hawkes and Cant [67], Weller et al. [159] and Hawkes and Cant [68] have used gradient transport for their LES simulations. It was reported by Boger et al. [8] that counter-gradient transport can occur, based on DNS studies. Additionally, it was found by Tullis [149], Tullis and Cant [150] that counter gradient type transport occurs in the context of LES based on *a priori* DNS analysis.

If the assumption of a strong flamelet is used then the subgrid progress variable flux can be given by the following expression:

$$\widetilde{u_i c} - \tilde{u}_i \tilde{c} = \tilde{c}(1-\tilde{c})[\overline{(u_i)}_P - \overline{(u_i)}_R] \tag{6.34}$$

The expression in Eq. 6.34 accounts for counter gradient transport as in the case of heat release dominating over the turbulence, which would result in $[\overline{(u_i)}_P - \overline{(u_i)}_R] > 0$, resulting in counter gradient transport if $\partial\tilde{c}/\partial x_i > 0$ [155]. Conversely, if the turbulent velocity field decays across the flame such that $[\overline{(u_i)}_P - \overline{(u_i)}_R] < 0$ and $\partial\tilde{c}/\partial x_i > 0$, a gradient type transport occurs [155]. Veynante et al. [155] were then able to use these finding in order to propose the following model for

the unclosed scalar flux which takes the following form in the context of LES:

$$\widetilde{u_i c} - \tilde{u}_i \tilde{c} = -M_i(\tau S_L - 2\Gamma u')\tilde{c}(1-\tilde{c}) \tag{6.35}$$

where the term on the right hand side involving S_L originates from the fact that in the limiting case of planar laminar flame the slip velocity is given by [155]:

$$[\overline{(u_i)}_P - \overline{(u_i)}_R] = -\tau S_L M_i \tag{6.36}$$

The other term involving turbulent velocity fluctuation u' is to be modelled by the usual gradient assumption and the quantity Γ is an efficiency function [155]. Using the expression given in Eq. 6.35 Veynante et al. [155] proposed a parameter N_B which determines the nature of scalar transport:

$$N_B = \frac{\tau S_L}{2\Gamma u'} \tag{6.37}$$

Counter-gradient transport is realised for high values of N_B (i.e. $N_B \gg 1$) and gradient type transport is observed for $N_B \ll 1$. Based on a strong flamelet assumption flame surface velocity component $(u_i)_s$ and Favre filtered velocity component $\tilde{u}_i$ are given by [155]:

$$(u_i)_s = (u_i)_R + K[(u_i)_P - (u_i)_R] \tag{6.38}$$

$$\tilde{u}_i = \overline{(u_i)}_R + \tilde{c}[\overline{(u_i)}_P - \overline{(u_i)}_R] \tag{6.39}$$

Using Eq. 6.38 and 6.39 the subgrid transport is given by:

$$\overline{(u_i)}_s - \tilde{u}_i = -(K-\tilde{c})[\overline{(u_i)}_P - \overline{(u_i)}_R] = -(K-\tilde{c})M_i(\tau S_L - 2\Gamma u') \tag{6.40}$$

where K depends on the isosurface used to define the flame. Veynante et al. [155] used a value of 0.5 for K for the FSD flux modelling in the context of RANS, while Hawkes [66] used $K = c^*$ where the isosurface $c = c^*$ defines the flame surface. Based on Eq. 6.35, 6.36 and 6.40 it is clear that the subgrid transport of FSD is closely related to the subgrid flux of c. Eq. 6.40 may be written in the

following manner: using Eq. 6.38 and 6.39 the subgrid transport is given by:

$$\overline{u_i''}_s = \overline{(u_i)}_s - \tilde{u}_i = \underbrace{\overline{(u_i)}_{Rs} = \overline{(u_i)}_R + K[\{\overline{(u_i)}_{Ps} - \overline{(u_i)}_P\} - \{\overline{(u_i)}_{Rs} - \overline{(u_i)}_R\}]}_{T_f} + \underbrace{(K-\tilde{c})[\overline{(u_i)}_P - \overline{(u_i)}_R]}_{T_s} \tag{6.41}$$

Hawkes [66] noted that the term T_f is a component of transport that is connected with turbulent fluctuations in velocity and can be modelled by conventional gradient transport:

$$T_f = -\frac{1}{\Sigma_{gen}} \frac{\bar{\rho}\nu_t}{Sc_\Sigma} \frac{\partial}{\partial x_i} \left(\frac{\Sigma_{gen}}{\bar{\rho}} \right) \tag{6.42}$$

Veynante et al. [155] modelled the term T_s from Eq. 6.40 as:

$$T_s = -(K - \tilde{c})\tau S_L M_i \tag{6.43}$$

However the above approach does not account for the effect of subgrid wrinkling and the variation of velocity in the products. Any increase in filter size results in increased subgrid wrinkling, which consequently results in increased burning rate thus resulting in increased slip velocity. On the other hand with increased flame wrinkling the subgrid normals become more randomly oriented which tends to decrease the slip velocity [66]. Therefore Hawkes [66] modelled the slip velocity in the following manner:

$$\overline{(u_i)}_P - \overline{(u_i)}_R = -\tau S_L \overline{(N_i)}_s \tag{6.44}$$

Alternatively a model was proposed by Weller et al. [159] for the slip velocity as:

$$\overline{(u_i)}_P - \overline{(u_i)}_R = -\tau S_L \Xi M_i \tag{6.45}$$

The model by Weller et al. [159] for the slip velocity, given by Eq. 6.45, was examined by Tullis [149] who found that this model overestimates slip velocity as the model does not account for the flame normal acceleration. Tullis [149]

suggests the following model for the slip velocity:

$$\overline{(u_i)}_P - \overline{(u_i)}_R = -\tau S_L \Xi_{eff} M_i \tag{6.46}$$

where Ξ_{eff} is an effective wrinkling factor given by $\Xi_{eff} = \Xi - 0.6(\Xi - 1)^{1.64}$ The models for the slip velocity discussed so far do not account for the stretch effects on the local flame speed. Under a strong flamelet assumption the following relationship can be invoked [22]:

$$(u_i)_P - (u_i)_R = -\tau \frac{\rho S_d N_i}{\rho_0} \tag{6.47}$$

This expression reduces to $(u_i)_P - (u_i)_R = -\tau S_L N_i$ for a laminar flame, as $\rho S_d = \rho_0 S_L$. When the above expression is filtered it results in:

$$\overline{(u_i)}_P - \overline{(u_i)}_R = -\tau \frac{\overline{\rho S_d N_i}}{\rho_0} \tag{6.48}$$

Chakraborty [22] and Chakraborty and Cant [36] notes that the above expression maybe used to model $[\overline{(u_i)}_P - \overline{(u_i)}_R]\Sigma_{gen}$ is approximated as follows:

$$[\overline{(u_i)}_P - \overline{(u_i)}_R]\Sigma_{gen} \approx -\tau \frac{\overline{(\rho S_d)}_s}{\rho_0} \overline{(N_i)}_s \Sigma_{gen} \tag{6.49}$$

In order to evaluate the above approximation the variation of $\tau\overline{(\rho S_d)}_s\overline{(N_i)}_s M_i \Sigma_{gen}/\rho_0$ with $\tau\overline{(\rho S_d N_i)} M_i \Sigma_{gen}/\rho_0$ is presented in Figs. 6.16 and 6.17 where a filter widths $0.8\delta_{th}$ and $2.4\delta_{th}$ are presented for cases A, C, D and F, J, I respectively. It is evident from both the Figs. 6.16 and 6.17 that a good approximation is given from the model, although the scatter can be seen to increase with increasing filter width. Another quantity that is required to be modelled in Eq. 6.49 is the surface averaged density weighted displacement speed $\overline{(\rho S_d)}_s$, which is also required to be evaluated for the successful closure of $[\overline{(u_i)}_P - \overline{(u_i)}_R]\Sigma_{gen}$. In the Figs. 6.16 and 6.17, $\overline{(\rho S_d)}_s$ was evaluated using DNS extracted data. In LES the quantity $\overline{(\rho S_d)}_s$ can be taken as $\rho_0 S'_L$, where S'_L is a modified flame speed, which is defined

as [22]:

$$S'_L \frac{\overline{(\rho S_d)}_s}{\rho_0} = S_{LS} - 2\frac{\rho D}{\rho_0}\overline{(\kappa_m)}_s \tag{6.50}$$

where S_{LS} is defined by Chakraborty [22] as: $\overline{(\rho S_r + \rho S_n)}_s = \rho_0 S_{LS}$. By then substituting S'_L into Eq. 6.49 Chakraborty [22] proposed the following model:

$$[\overline{(u_i)}_P - \overline{(u_i)}_R]\Sigma_{gen} \approx -\tau S'_L \overline{(N_i)}_s \Sigma_{gen} \tag{6.51}$$

In the above expression the effects of strain rate and curvature are included through the use of the modified flame speed S'_L [22]. By then using Eq. 6.40 and replacing $[\overline{(u_i)}_P - \overline{(u_i)}_R]\Sigma_{gen}$ by Eq. 6.51 in the $[\overline{(u_i)}_s - \tilde{u}_i]\Sigma_{gen}$ results in:

$$\frac{\partial}{\partial x_i}\left[\overline{[(u_i)_s - \tilde{u}_i]\Sigma_{gen}}\right] = -\frac{\partial}{\partial x_i}\left[\frac{\bar{\rho}\nu_t}{Sc_\Sigma}\frac{\partial}{\partial x_i}\left(\frac{\Sigma_{gen}}{\bar{\rho}}\right)\right] - \frac{\partial}{\partial x_i}[(K-\tilde{c})\tau S'_L \overline{(N_i)_s}\Sigma_{gen}] \tag{6.52}$$

The second term acts as a propagation term with propagation speed $-(K-\tilde{c})S'_L$ in the FSD transport equation when the subgrid convection term is written on the right hand side of FSD transport equation as $-\nabla[\overline{(u_i)}_s - \tilde{u}_i]\Sigma_{gen}$.

6.2 Modelling Methodology for the Surface Averaged Displacement Speed

It has been discussed earlier that the $\overline{(S_d)}_s$ plays a key role in the closure of T_1, T_3 and T_4 terms. The surface filtered displacement speed $\overline{(S_d)}_s$ can be evaluated from the following expression [66]:

$$\overline{(S_d)}_s = \frac{\overline{(\rho S_d)}_s}{(\rho)_s} = \frac{\overline{(\rho S_d)}_s}{\rho_0}(1+\tau c^*) \tag{6.53}$$

In the above expression the assumptions of low Mach number, adiabatic and unity Lewis number, whereby allowing for the density on a c isosurface $(\rho)_s$ can be written as:

$$(\rho)_s = \frac{\rho_0}{1+\tau c^*} \tag{6.54}$$

where $c = c^*$ is the isosurface on which the surface averaging is performed. The final form of the modelled transport equation will be independent of the choice of c^* (see Chapter 9). Chakraborty [22] and Chakraborty and Cant [29, 36] indicate that the above expression is acceptable for cases with Lewis number close to unity. From Eq. 6.53 it is clear that the modelling of $\overline{(S_d)}_s$ is necessary. Chakraborty [22] states that $\overline{(\rho S_d)}_s$ can be written as, where the assumption of constant ρD was implied according to [62]:

$$\overline{(\rho S_d)}_s = \rho_0 S_{LS} - 2\overline{(\rho D \kappa_m)}_s \tag{6.55}$$

If the quantity S_{LS} is modelled using laminar flame library, the modelling of $(\rho S_d)_s$ depends on the modelling of surface averaged curvature $\overline{(\kappa_m)}_s$, which can be written in the following form for a homogeneous filter:

$$2\overline{(\kappa_m)}_s = \frac{\overline{\nabla.\vec{N}|\nabla c|}}{\Sigma_{gen}} = \frac{\partial\overline{(N_i)}_s}{\partial x_i} - \frac{1}{\Sigma_{gen}}\left[\overline{N_i\frac{\partial|\nabla c|}{\partial x_i}} - \overline{(N_i)}_s\frac{\partial\Sigma_{gen}}{\partial x_i}\right] \tag{6.56}$$

In the above equation the expression within the square brackets must be modelled. For a statistically planar flame the contribution of this term is close to zero for most locations. The contribution from this term is significant in regions where cusps and bulges are found [22].

Chakraborty [22] and Chakraborty and Cant [29, 36] suggest that $(\overline{N_i\partial\sigma/\partial x_i} - \overline{(N_i)}_s\partial\Sigma_{gen}/\partial x_i)$ can be modelled using scale similarity relationship:

$$\left[\overline{N_i\frac{\partial|\nabla c|}{\partial x_i}} - \overline{(N_i)}_s\frac{\partial\Sigma_{gen}}{\partial x_i}\right] = A\left[\overline{M_i\frac{\partial|\nabla\bar{c}|}{\partial x_i}} - \frac{\overline{M_i|\nabla\bar{c}|}}{\overline{|\nabla\bar{c}|}}\right] \tag{6.57}$$

where the modelling constant A is evaluated using a dynamic approach. The scale similarity expression on the test filter scale can be written as [29, 36, 49, 76]:

$$\widehat{\overline{N_i\frac{\partial|\nabla c|}{\partial x_i}}} - \widehat{\overline{(N_i)}}_s\frac{\partial\widehat{|\nabla c|}}{\partial x_i} = A\left[\widehat{\overline{M_i\frac{\partial|\nabla c|}{\partial x_i}}} - \frac{\widehat{\overline{M_i|\nabla\bar{c}|}}}{\widehat{\overline{|\nabla\bar{c}|}}}\frac{\partial\widehat{|\nabla\bar{c}|}}{\partial x_i}\right] \tag{6.58}$$

In the above expression A is a model parameter that is evaluated as:

$$A = \left\langle \widehat{\overline{N_i \frac{\partial |\nabla c|}{\partial x_i}}} - \widehat{\overline{(N_i)}_s} \frac{\partial \widehat{\overline{|\nabla c|}}}{\partial x_i} \right\rangle_e \Big/ \left\langle \frac{\widehat{\overline{M_i |\nabla \bar{c}|}}}{\overline{|\nabla c|}} - \frac{\widehat{\overline{M_i |\nabla \bar{c}|}}}{\widehat{\overline{|\nabla \bar{c}}}} \frac{\partial \widehat{\overline{|\nabla \bar{c}|}}}{\partial x_i} \right\rangle_e \tag{6.59}$$

where $\langle \dots \rangle_e$ indicates an ensemble averaging operation in the direction of mean flame propagation in order to avoid unphysical numerical oscillations typical of dynamic models [49].

The model prediction for $(\overline{N_i \partial |\nabla c| / \partial x_i} - \overline{(N_i)}_s \partial \Sigma_{gen} / \partial x_i)$ is compared with the same quantity obtained from DNS in Figs. 6.18 and Fig. 6.19, where it is clear that the model shown in Eq. 6.58 and 6.59 captures the behaviour adequately. Additionally the modelled expression for $\overline{(\rho S_d)}_s \Sigma_{gen}$ evaluated using Eq. 6.53 to 6.59 on different $\tilde{c}$ isosurfaces across the flame brush is compared to $\overline{(\rho S_d)}_s \Sigma_{gen}$ extracted from DNS data across the flame brush is also shown in Figs. 6.20 and 6.21, where it is clear that the model satisfactorily captures the behaviour of $\overline{(\rho S_d)}_s \Sigma_{gen}$ across the flame brush irrespective of Re_t and Le values.

6.2.1 Summary

The statistical behaviour of generalised FSD and the term of its transport equation were analysed in detail based on explicitly filtered DNS data. The peak Σ_{gen} conditional on $\tilde{c}$ was found to decrease and shift towards $\tilde{c} < 0.5$ with increasing filter width. This can be attributed to the convolution process characteristic of LES filtering. The Σ_{gen} was found to increase with increasing turbulent Reynolds number and with decreasing Lewis number, both of which can be attributed to the increased flame area generation at those conditions. The unclosed terms of the generalised FSD are the subgrid convection term, strain rate term, curvature term and the propagation term, were analysed for a range of different filter widths.

It has been found that the propagation term plays an important role for all filter widths in all cases, and it assumes predominantly positive (negative) values towards the unburned (burned) gas side of the flame brush. The magnitude of the propagation term was found to be affected by the Lewis number, whereas the turbulent Reynolds number has a marginal influence on its behaviour. The

behaviour of the propagation term was shown to be influenced by the behaviour of the surface filtered displacement speed $\overline{(S_d)}_s$, which was shown to increase across the flame brush due to heat release and this effect strengthens with decreasing Lewis number. An expression had been identified which captures the unclosed propagation term satisfactorily for a range of different filter widths, although the correct prediction of the $\overline{(S_d)}_s$ will greatly influence this closure in an actual LES simulation.

The strain rate term acts as a major source term throughout the flame brush for all cases and at all filter widths. The magnitude of the term was found to increase with increasing turbulent Reynolds number and decreasing Lewis number. The statistical behaviour of the term was examined by decomposing into the dilatation rate and normal strain rate contributions. The dilatation rate term remains a source term throughout the flame brush for all cases, and its magnitude was found to increase with decreasing Lewis number due to strengthening of heat release effects. However the normal strain rate term contribution remains predominantly negative although its magnitude remains smaller than the dilatation term, for all the cases and all filter widths. Thus as the dilatation rate overcomes the normal strain rate term to give rise to a predominantly positive strain rate term contribution for all cases and all filter widths. The statistical behaviour of the normal strain rate term is principally governed by the ∇c alignment with the local principal strain rates.

Curvature term of the Σ_{gen} transport equation assumes predominantly negative values for cases with approximately unity Lewis number (i.e. $Le \approx 1.0$). However for cases with Lewis number less than unity (i.e. $Le \ll 1.0$) the curvature assumes a positive (negative) value towards the reactant (product) side of the flame brush for $\Delta \gg \delta_{th}$. In order to understand this underlying behaviour the curvature term was decomposed into a component arising due to the reaction and normal diffusion components of displacement speed T_{31}, and the another component arising due to the tangential diffusion component of displacement speed T_{32}. The T_{32} term remains negative through the flame brush and its magnitude increases with decreasing Lewis number and increasing turbulent Reynolds number, which can be attributed to the increase in flame wrinkling under these conditions. The positive contribution of T_{31} term increases with decreasing Le.

The modelling of the curvature term was shown to be dependent on the accurate modelling of the surface filtered displacement speed.

The subgrid convection term was found to be weakest contributor to the Σ_{gen} transport. The behaviour of the subgrid convection is influenced by the subgrid flux of FSD and reaction progress variable. The subgrid flux of FSD is shown to be predominantly gradient type for the $Le \approx 1.0$ cases considered here. However, the extent of counter-gradient transport increases with decreasing Le and predominantly counter-gradient behaviour has been observed for the $Le \leq 0.6$ flames considered here. The modelling for the subgrid flux was discussed in detail and a possible model has been identified, however the proper evaluation of surface filtered displacement speed will affect the models predictions.

As the statistical behaviours of the subgrid convection, propagation and curvature terms are dependent on the proper evaluation of the surface filtered displacement speed, a dynamic model for evaluating $\overline{(S_d)}_s$ is considered. The predictions of this dynamic model for $\overline{(S_d)}_s$ yielded good agreement for all ranges of filter widths and flame conditions which were examined in this analysis. Based on the physical understanding obtained here, the modelling of strain rate and curvature terms of the FSD transport equation will be addressed in the next two chapters. The final form of the modelled transport equation of Σ_{gen} is provided in chapter 9.

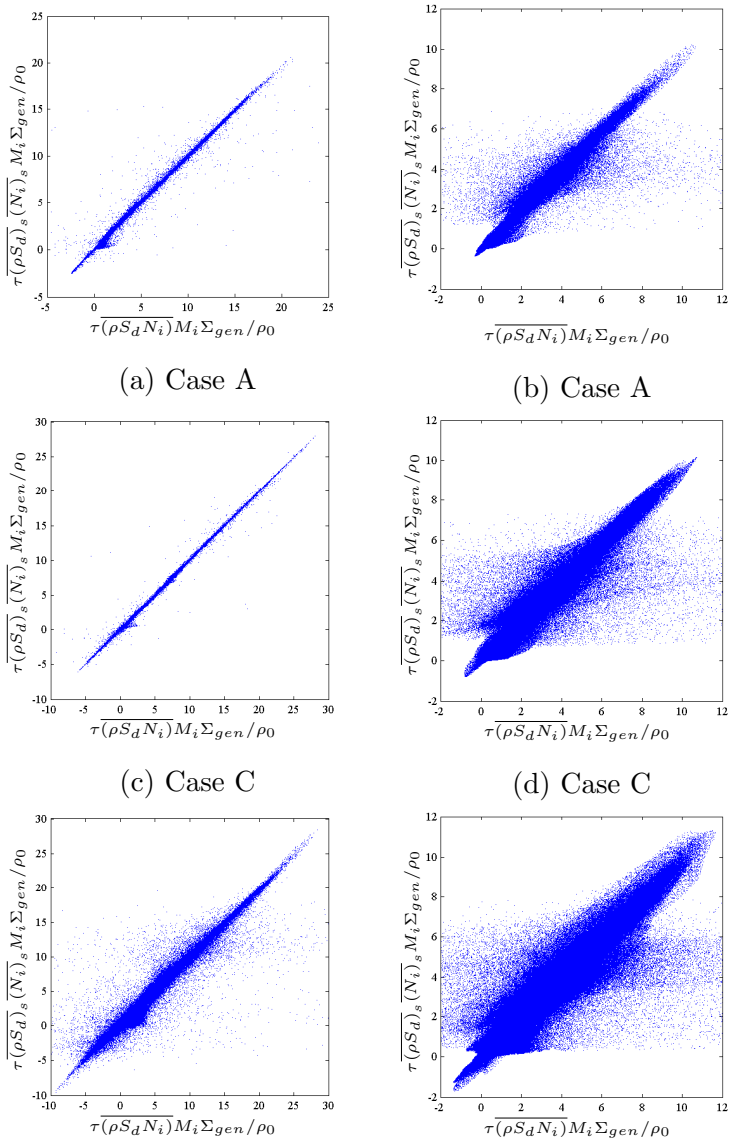

(a) Case A (b) Case A

(c) Case C (d) Case C

(e) Case E (f) Case E

Figure 6.16: Variation of $\tau\overline{(\rho S_d N_i)} M_i \Sigma_{gen}/\rho_0$ with $\tau\overline{(\rho S_d)}_s\overline{(N_i)}_s M_i \Sigma_{gen}/\rho_0$ at the filter widths $\Delta = 0.8\delta_{th}$ (top row) and $\Delta = 2.4\delta_{th}$ (bottom row) shown for cases A, C and E (cases B and D are qualitatively similar to cases A and E respectively and thus are not shown).

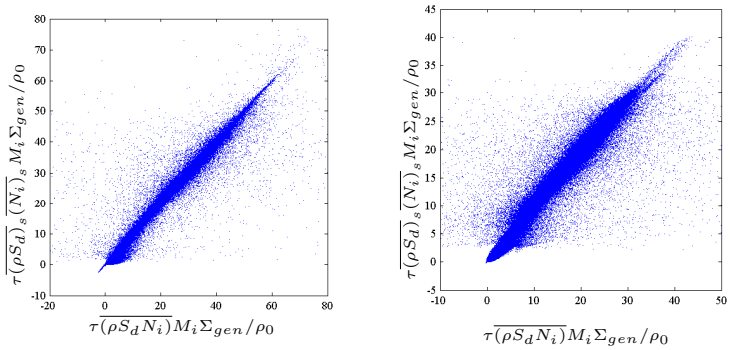

(a) Case F

(b) Case F

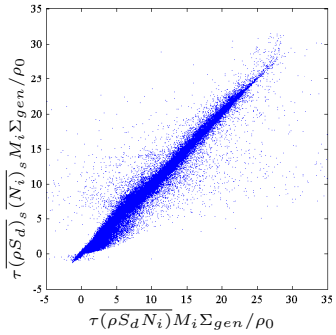

(c) Case G

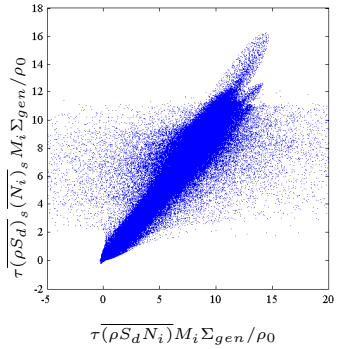

(d) Case G

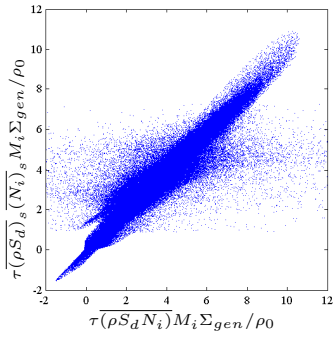

(e) Case J

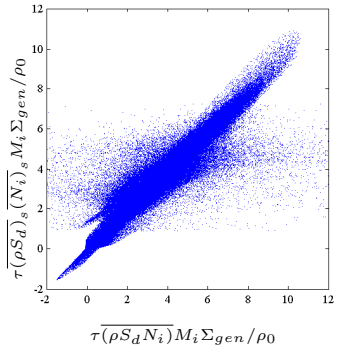

(f) Case J

Figure 6.17: Variation of $\tau\overline{(\rho S_d N_i)}M_i\Sigma_{gen}/\rho_0$ with $\tau\overline{(\rho S_d)}_s\overline{(N_i)}_s M_i\Sigma_{gen}/\rho_0$ at the filter widths $\Delta = 0.8\delta_{th}$ (top row) and $\Delta = 2.4\delta_{th}$ (bottom row) shown for cases F, G and J (cases H and I are qualitatively similar to case C and thus are not shown).

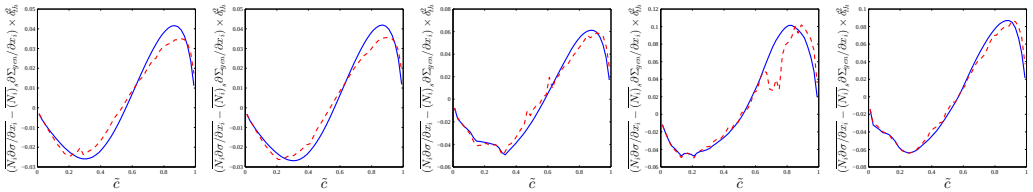

(a) Case A (b) Case B (c) Case C (d) Case D (e) Case E

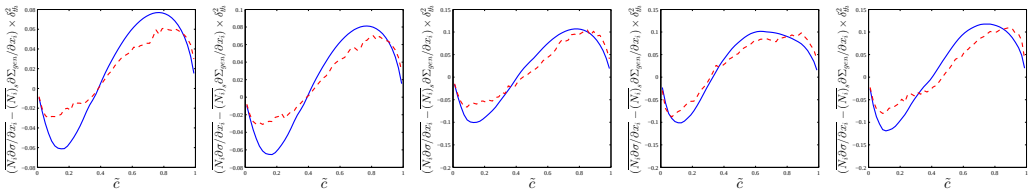

(f) Case A (g) Case B (h) Case C (i) Case D (j) Case E

Figure 6.18: The variation of $(\overline{N_i \partial|\nabla c|/\partial x_i} - \overline{(N_i)}_s \partial\Sigma_{gen}/\partial x_i) \times \delta_{th}^2$ from DNS (——) and the dynamic model shown in Eqs. 6.58 and 6.59 (– – –) for cases A-E at filter width $\Delta = 0.8\delta_{th}$ (left column) and $\Delta = 2.4\delta_{th}$ (right column).

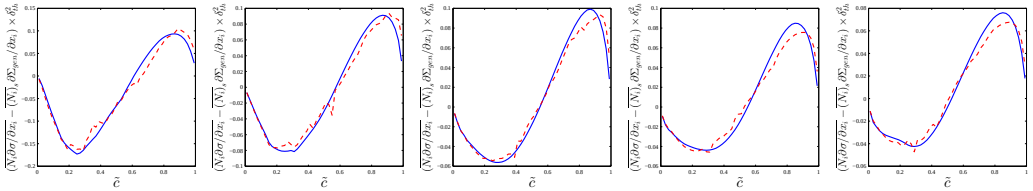

(a) Case F (b) Case G (c) Case H (d) Case I (e) Case J

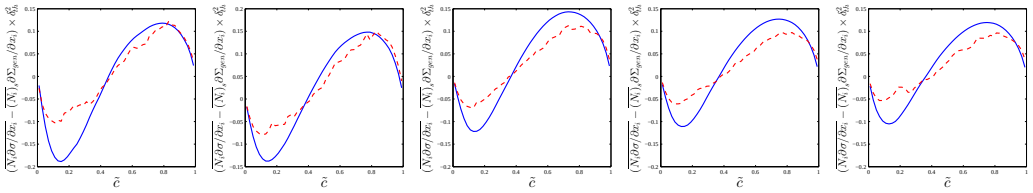

(f) Case F (g) Case G (h) Case H (i) Case I (j) Case J

Figure 6.19: The variation of $(\overline{N_i \partial\sigma/\partial x_i} - \overline{(N_i)}_s \partial\Sigma_{gen}/\partial x_i) \times \delta_{th}^2$ from DNS (——) and the dynamic model shown in Eqs. 6.58 and 6.59 (– – –) for cases F-J at filter width $\Delta = 0.8\delta_{th}$ (left column) and $\Delta = 2.4\delta_{th}$ (right column).

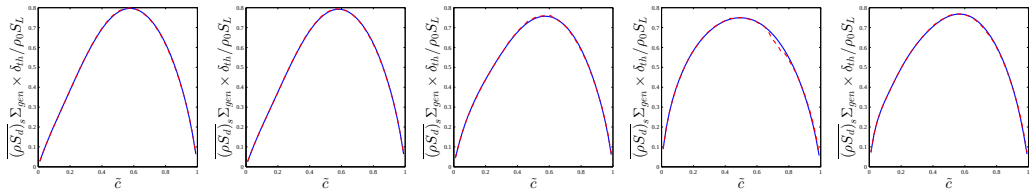

(a) Case A (b) Case B (c) Case C (d) Case D (e) Case E

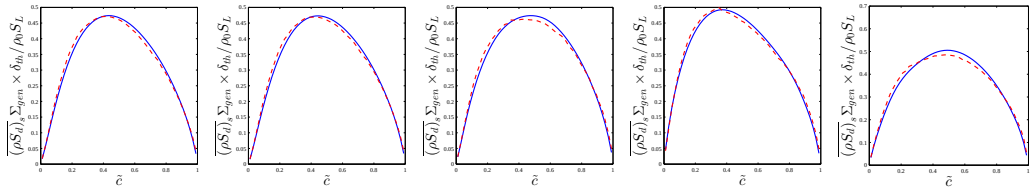

(f) Case A (g) Case B (h) Case C (i) Case D (j) Case E

Figure 6.20: The variation of $\overline{(\rho S_d)}_s \Sigma_{gen} \times \delta_{th}/\rho_0 S_L$ from DNS (——) and the dynamic model shown in Eqs. 6.53 - 6.58 (– – –) for cases A-E at filter width $\Delta = 0.8\delta_{th}$ (top row) and $\Delta = 2.4\delta_{th}$ (bottom row).

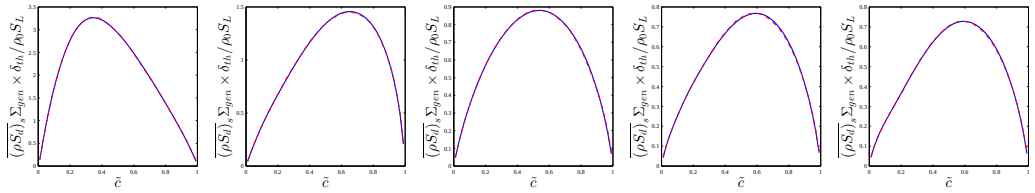

(a) Case F (b) Case G (c) Case H (d) Case I (e) Case J

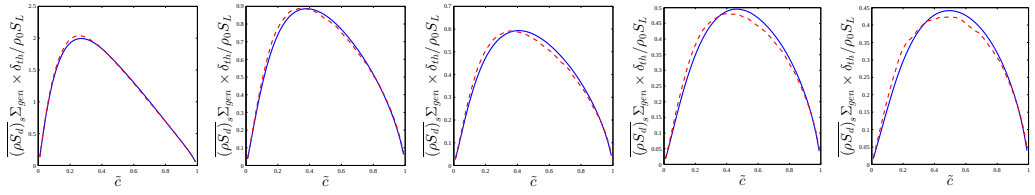

(f) Case F (g) Case G (h) Case H (i) Case I (j) Case J

Figure 6.21: The variation of $\overline{(\rho S_d)}_s \Sigma_{gen} \times \delta_{th}/\rho_0 S_L$ from DNS (——) and the dynamic model shown in Eqs. 6.53 - 6.58 (– – –) for cases F-J at filter width $\Delta = 0.8\delta_{th}$ (top row) and $\Delta = 2.4\delta_{th}$ (bottom row).

Chapter 7

Modelling Curvature Term of the FSD Transport Equation

In this chapter a brief summary of existing models for the curvature term of the FSD equation is presented and a new approach to modelling this term in the context of RANS and LES will be discussed. The models have been proposed in such a manner that they are valid for a wide range of values of turbulent Reynolds numbers and global Lewis numbers. The newly proposed models have been validated against the curvature terms extracted from the DNS database based on *a priori* analysis.

7.1 RANS Modelling of Curvature Term

A suitable approach to solving for the reaction rate closure in RANS simulation of turbulent premixed flames is to solve a transport equation for the generalised FSD Σ_{gen}. The exact formulation for the generalised FSD for RANS takes the following form:

$$\frac{\partial \Sigma_{gen}}{\partial t} + \frac{\partial (\underset{\sim}{u}_j \Sigma_{gen})}{\partial x_j} = - \frac{\partial \{ [\underline{(u_i)}_s - \underset{\sim}{u}_i] \Sigma_{gen} \}}{\partial x_i} + \underline{\left[(\delta_{ij} - N_i N_j) \frac{\partial u_i}{\partial x_j} \right]}_s \Sigma_{gen} - \frac{\partial \underline{(S_d N_i)}_s \Sigma_{gen}}{\partial x_j} + \underline{\left[S_d \left(\frac{\partial N_i}{\partial x_i} \right) \right]}_s \Sigma_{gen} \tag{7.1}$$

where the generalised FSD is defined in RANS context as $\Sigma_{gen} = \underline{|\nabla c|}$, $\underset{\sim}{u}_i = \underline{\rho u_i}/\underline{\rho}$ and $u_i'' = u_i - \underset{\sim}{u}_i$ are the Favre mean and fluctuating velocity components in the i^{th} direction, ρ is the fluid density, $\vec{N} = -\nabla c/|\nabla c|$ is the local flame normal vector and $\underline{(Q)}_s = \underline{Q|\nabla c|}/\Sigma_{gen}$ defines the surface averaging process in context of RANS for a general quantity Q, the under tilde (i.e. $\underset{\sim}{(\ldots)}$) defines a Favre averaged quantity. In Eq. 7.1 the terms on the right hand side are unclosed. The first term on the right hand side of Eq. 7.1 refers to the turbulent transport of Σ_{gen}, the second term on the right hand side of Eq. 7.1 accounts for the flame area generation due to tangential strain rate (i.e. $a_T = (\delta_{ij} - N_i N_j)\partial u_i/\partial x_j$) and the third term is due to the flame normal propagation and thus commonly referred to as the propagation term. The last term ($\underline{(S_d \nabla.\vec{N})}_s \Sigma_{gen}$) of Eq. 7.1 is referred to as the curvature term as it arises due to the flame curvature $\kappa_m = \nabla.\vec{N}/2$. Peters [107] indicated that the curvature κ_m dependence of S_d strengthens with increasing Karlovitz number $Ka = (u'/S_L)^{3/2}(l/\delta_{th})^{-1/2}$. As curvature dependence of S_d is influenced by Ka and Le, the statistical behaviours of $\underline{(S_d \nabla.\vec{N})}_s \Sigma_{gen}$ are also likely to be influenced by $Re_t = \rho_0 u' l/\mu_0 \sim Da^2 Ka^2$ where $Da = l S_L/u'\delta_{th}$ is the Damköhler number, and ρ_0 and μ_0 are the unburned gas density and viscosity, respectively. The effects of the turbulent Reynolds number Re_t and Lewis number Le on the statistical behaviour and modelling of the FSD curvature term in the context of RANS simulations are yet to be addressed in detail. Therefore the main aims and objectives of this section analysis are as follows:

1. To analyse and explain the effects of Re_t and Le on the statistical behaviours of $\underline{(S_d \nabla.\vec{N})}_s \Sigma_{gen}$ in turbulent premixed flames.

2. To carry out *a priori* DNS analysis to propose models for different components of the FSD curvature term $\underline{(S_d \nabla.\vec{N})}_s \Sigma_{gen}$, for turbulent premixed flames.

7.1.1 Existing Models for RANS Curvature Term

There are several models available for the curvature term of the generalised FSD transport equation, Cant et al. [21] proposed the following model for $\underline{(S_d\nabla.\vec{N})}_s\Sigma_{gen}$:

$$\underline{(S_d\nabla.\vec{N})}_s\Sigma_{gen} = (\delta_{ij} - n_{ij})\left(\frac{\partial\underline{(S_d)}_s\underline{(N_i)}_s}{\partial x_j}\right) - \frac{C_H S_L \Sigma_{gen}^2}{1-\underline{c}} \tag{7.2}$$

where $n_{ij} = \underline{(N_i)}_s\underline{(N_j)}_s + (\delta_{ij}/3)[1 - \underline{(N_k)}_s\underline{(N_i)}_s]$ and $C_H = \alpha_N(1 - (1/3)[1 - \exp(-10(1-\underline{c})\underline{\epsilon}/\Sigma_{gen}S_L\underline{\tilde{k}})])$ are the model parameters [21] and $\alpha_N = [1-\underline{(N_k)}_s\underline{(N_k)}_s]$ is a resolution factor. According to the Eq. 7.2 when the flow becomes fully resolved the right hand side will tend to $S_d\nabla.\vec{N}|\nabla c|$. Veynante et al. [153] proposed a model for $\underline{(S_d\nabla.\vec{N})}_s\Sigma_{gen}$ in the context of Coherent Flamelet Model (CFM) which takes the following manner:

$$\underline{(S_d\nabla.\vec{N})}_s\Sigma_{gen} = -\beta_{CFM}\overline{(S_d)}_s(\underline{c}-c_0)\frac{\Sigma_{gen}^2}{\underline{c}(1-\underline{c})} \tag{7.3}$$

where β_{CFM} and c_0 are the model parameters, and are taken as 0.4 and 0.5, respectively, in the analysis by Veynante et al. [153]. It should be noted that the right hand side of Eq. 7.3 does not tend to $S_d\nabla.\vec{N}|\nabla c|$ as the flow becomes fully resolved. The models shown in Eqs. 7.2 and 7.3 will be referred to as CPB and CFM respectively in the following sections where model comparisons are made.

7.1.2 Modelling the Effects of Turbulent Reynolds Number and Lewis Number

Modelling $\underline{(S_d\nabla.\vec{N})}_s\Sigma_{gen}$ will require a complete understanding of its behaviour, in order to achieve this Katragadda et al. [81] decompose the curvature term into the following components which arise due to the decomposition of the displacement speed (Eq. 2.103):

$$\underline{(S_d\nabla.\vec{N})}_s\Sigma_{gen} = A_1 + A_2 = 2\underbrace{[(S_r+S_n)\kappa_m]_s\Sigma_{gen}}_{A_1}\underbrace{-4(D\kappa_m^2)_s\Sigma_{gen}}_{A_2} \tag{7.4}$$

It becomes clear from Eq. 7.4 that the term A_2 will be deterministically negative, whereas the term A_1 depends on the curvature κ_m, which relies on $(S_r + S_n)$ and $|\nabla c|$. The terms A_1 and A_2 can be decomposed into the resolved and unresolved parts as follows [81]:

$$A_1 = \underline{[(S_r + S_n)(\partial N_i/\partial x_i)]}_s \Sigma_{gen} = \underbrace{(\rho_0 S_L/\underline{\rho})[\partial(\underline{N_i})_s/\partial x_i]\Sigma_{gen}}_{A_{1r}} + A_{1ur} \tag{7.5a}$$

$$A_2 = -\underline{[D(\partial N_i/\partial x_i)^2]}_s \Sigma_{gen} = \underbrace{-\underset{\sim}{D}[\partial(\underline{N_i})_s/\partial x_i]^2\Sigma_{gen}}_{A_{2r}} + A_{2ur} \tag{7.5b}$$

where the terms A_{1r} and A_{2r} are resolved parts of the terms A_1 and A_2 while the terms A_{1ur} and A_{2ur} are unresolved parts, respectively. The variations of the curvature term and its components (i.e. A_1, A_2, A_{1r}, A_{2r}, A_{1ur}, A_{2ur} and $(A_1 + A_2)$) with $\underset{\sim}{c}$ across the flame brush are shown in Fig. 7.1 for cases A-J. Figs. 7.1(a-j) show that A_{1r} and A_{2r} remain negligible in comparison to A_{1ur} and A_{2ur}, respectively, and the terms A_1 and A_2 remain almost equal to A_{1ur} and A_{2ur}, respectively. The contributions of A_2 and A_{2ur} remain deterministically negative for all cases and that the magnitude of A_2 and A_{2ur} are found to increase with increasing values of Re_t. The magnitude of $\underline{(\kappa_m^2)}_s$ increases with decreasing Le because of the increased extent of flame wrinkling which contributes to the increase of the magnitudes of A_2 and A_{2ur}. This can be substantiated from the variations of $\underline{(\kappa_m^2)}_s \times \delta_{th}^2$ and the wrinkling factor Ξ with $\underset{\sim}{c}$, as shown in Figs. 7.2(d) and 7.2(e), respectively. Figs. 7.1(a-e) show that the contribution of A_1 and A_{1ur} remain positive towards the unburned gas side of the flame brush before becoming negative towards the burned gas side for cases A-E. Further comparison of Fig. 7.1(a-e) reveals that the extent of positive (negative) contribution of A_1 and A_{1ur} remains similar for cases A-E with a transition occurring at $\underset{\sim}{c} \approx 0.4$, however the magnitude of A_1 and A_{1ur} are found to increase slightly with increasing values of Re_t. From Figs. 7.1(f-j) it is possible to deduce that for the $Le \ll 1$ flames the contribution of A_1 and A_{1ur} remain positive for the major portion of flame brush before becoming negative towards the burned gas side. Comparing Figs. 7.1(f-j) reveals that the extent of positive (negative) contributions of A_1 and A_{1ur} decreases (increases) with increasing Le.

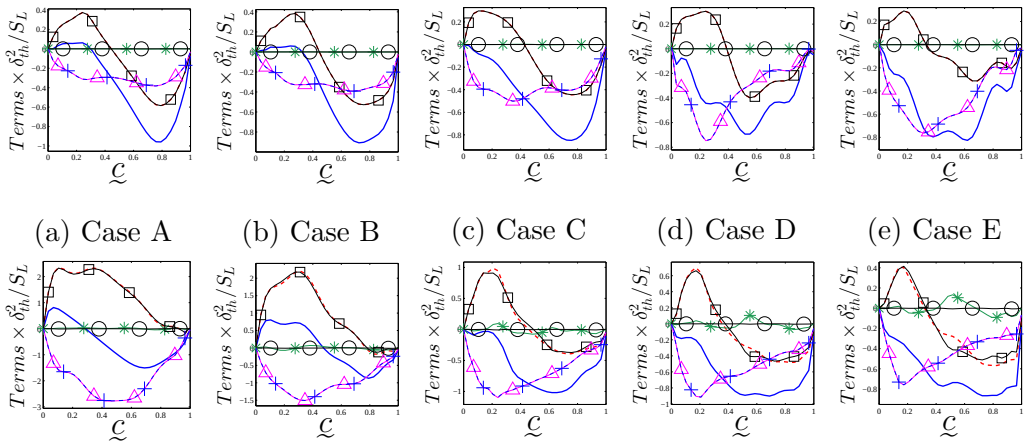

(a) Case A (b) Case B (c) Case C (d) Case D (e) Case E

(f) Case F (g) Case G (h) Case H (i) Case I (j) Case J

Figure 7.1: Variation of conditionally averaged A_1 (– – –), A_{1r} (—✳—), A_{1ur} (—□—), A_2 (—△—), A_{2r} (—○—), A_{2ur} (–+–) and $A_1 + A_2$ (——) with $\underset{\sim}{c}$ shown for cases A-J.

To explain the statistical behaviours of A_1 and A_{1ur} it is useful to examine the nature of the variation of $\overline{(\kappa_m)}_s \times \delta_{th}$ with $\tilde{c}$ and the correlations of $(S_r + S_n)$ and $|\nabla c|$ with κ_m. The variations of $\overline{(\kappa_m)}_s \times \delta_{th}$ are shown in Fig. 7.9 with $\tilde{c}$ are presented in Fig. 7.9 for cases A-E and Fig. 7.14 for cases F-J, which shows that $\underline{(\kappa_m)}_s$ remains positive (negative) towards the unburned (burned) gas side of the flame brush for all cases. The correlation coefficients for the $|\nabla c| - \kappa_m$ and $(S_r + S_n) - \kappa_m$ correlations for five different c isosurfaces across the flame brush are shown graphically in Figs. 6.12(a) and 6.12(b), respectively, for cases A-E. Similarly for cases F-J the correlation coefficients for $|\nabla c| - \kappa_m$ and $(S_r + S_n) - \kappa_m$ correlations for five different c isosurfaces are given by Figs. 6.12(c) and 6.12(d), respectively.

It is evident from Fig. 6.12(a) that $(S_r + S_n)$ and κ_m remain negatively correlated for the majority of the flame brush before showing positive correlation towards the burned gas side of the flame brush for all cases, however this correlation remains weak for cases A-E. Fig. 6.12(b) shows that $|\nabla c|$ and κ_m remain weakly correlated across the flame brush for cases A-E. As both $(S_r + S_n)$ and $|\nabla c|$ are relatively weakly correlated with κ_m in all cases, the curvature terms A_1 and A_{1ur} remain positive (negative) towards the unburned (burned) gas side of the

flame brush due to the positive (negative) values of $\overline{(\kappa_m)}_s$ towards the unburned (burned) gas side of the flame brush. It should be noted from Figs. 7.1(a-e) that the negative values of A_2 generally dominate over the positive values of A_1 in all cases, which leads to a negative contribution of $(A_1 + A_2)$ throughout the flame brush. However, for small values of Re_t (i.e. cases A and B), where the magnitudes of A_2 and A_{2ur} assumes small magnitudes due to the $\underline{(\kappa_m^2)}_s$ dependency discussed earlier, small positive values of $(A_1 + A_2)$ have been observed towards the unburned gas side of the flame brush. It is evident from Figs. 6.12(c) and 6.12(d) that both $(S_r + S_n)$ and $|\nabla c|$ remain positively (negatively) correlated with curvature for the $Le < 1$ ($Le > 1$) flames which give rise to predominantly positive contributions of A_1 and A_{1ur} for cases F and G, and the transition from positive to negative value for A_1 and A_{1ur} takes place towards the unburned gas side for case J. As both $(S_r + S_n)$ and $|\nabla c|$ are weakly correlated with κ_m in cases A-E, H and I the curvature term A_1 and A_{1ur} remain positive (negative) towards the unburned (burned) gas side of the flame brush due to the positive (negative) values of $\underline{(\kappa_m)}_s$ towards the unburned (burned) gas side. The predominant contribution of A_1 in cases F and G gives rise to predominantly positive values of $(A_1 + A_2)$ towards the unburned gas side of the flame brush and this contribution becomes negative towards the burned gas side of flame brush (see Figs. 7.1(f) and 7.1(g)). By contrast in cases C-E, H and I negative values of A_2 dominate over positive values of A_1 which leads to a negative contribution of $(A_1 + A_2)$ throughout the flame brush (see Fig. 7.1). The physical explanations for the differences in κ_m dependencies $(S_r + S_n)$ and $|\nabla c|$ in response to the changes in Re_t and Le have been discussed elsewhere [23, 26, 30, 32], and thus are not repeated here.

The modelling of A_{1ur} depends on the statistical behaviours of $\underline{(\partial N_i/\partial x_i)}_s - \partial\underline{(N_i)}_s/\partial x_i$ and $\underline{(S_r + S_n)}_s$ which are scaled here in the following manner [81]:

$$A_{1ur} \sim S_L \left[1 - \underline{(N_k)}_s \underline{(N_k)}_s\right] \Sigma_{gen}^2 \text{ and } (S_r + S_n) \sim S_L \tag{7.6}$$

According to Eq. 7.5a, the term A_{1ur} scales as $A_{1ur} \sim O(S_L[1 - \underline{(N_k)}_s \underline{(N_k)}_s]\Sigma_{gen}^2)$. As the term is unresolved, the expression $1 - \underline{(N_k)}_s \underline{(N_k)}_s$ is used to act as a resolution factor which tends to zero as the flow becomes resolved. Based on Eq.

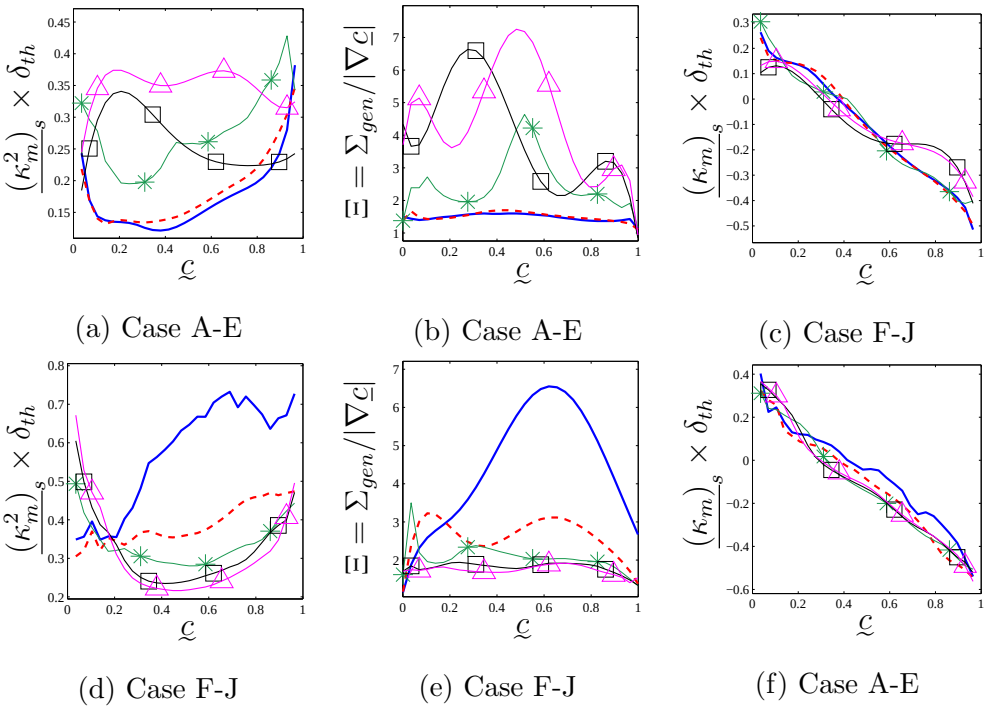

(a) Case A-E (b) Case A-E (c) Case F-J

(d) Case F-J (e) Case F-J (f) Case A-E

Figure 7.2: Variation of $\widetilde{(\kappa_m^2)}_s \times \delta_{th}$ (a, d), Ξ (b, e) and $\widetilde{(\kappa_m)}_s \times \delta_{th}$ (c, f) with $\underline{\tilde{c}}$ for cases A-E (top row: A (——), B (– – –), C (—✳—) D (—□—), E (—△—)) and for cases F-J (bottom row: F (——), G (– – –), H (—✳—) I (—□—), J (—△—))

7.6 following model is proposed for A_{1ur}:

$$A_{1ur} = -\beta_{A1UR} S_L \left[1 - \widetilde{(N_k)}_s \widetilde{(N_k)}_s\right] (\underline{\tilde{c}} - a^*) \Sigma_{gen}^2 f(\underline{\tilde{c}}, \underline{\tilde{c}}) \tag{7.7}$$

where β_{A1UR}, a^* and $f(\underline{\tilde{c}}, \underline{\tilde{c}})$ are model parameters. The model parameter a^* is responsible for the transition of A_{1ur} from positive to negative values. It has been discussed before that the sign of A_{1ur} depends on the local curvature κ_m dependencies of $(S_r + S_n)$ and $|\nabla c|$. However, these local curvature κ_m dependencies of $(S_r + S_n)$ and $|\nabla c|$ are influenced by the regime of combustion (characterized by the Karlovitz number) [23, 107], global Lewis number [26, 28] and turbulent Reynolds number [40] and therefore, a^* is expected to have Karlovitz number, Lewis number and turbulent Reynolds number dependencies. The function $f(\underline{\tilde{c}}, \underline{\tilde{c}})$ is used to capture the qualitative behaviour of A_{1ur} across the flame brush and β_{T1UR} accounts for the magnitude of the term A_{1ur}. The parameter

$[1 - \underline{(N_k)}_s \underline{(N_k)}_s]$ in Eq. 7.7 ensures that A_{1ur} vanishes when the flow is fully resolved. It can be seen from Fig. 7.3 that the model given by Eq. 7.7 captures A_{1ur} satisfactorily for all cases considered here when the following expressions of β_{T1UR}, a^* and $f(\underline{c}, \underset{\sim}{c})$ are used:

$$\beta_{A1UR} = (7.24Le^{-0.68})(1 + Ka_L)^{-0.25} \tag{7.8a}$$

$$a^* = \frac{1.27\exp(-0.77Le)}{\mathrm{erf}[(1 + Ka_L)^{1.1}/4.85]} \times \left[1.0 + \frac{f_2(Re_L) - 1.0}{\{1.0 + \exp(-5.0(Ka_L - 1.90))\}^{5.0}}\right] \tag{7.8b}$$

$$f_2(Re_L) = 0.49\frac{Re_L^{0.46} + 0.69}{0.46Re_L^{0.46} + 0.56} \tag{7.8c}$$

$$f(\underline{c}, \underset{\sim}{c}) = 1.0 - \frac{\exp(-9.0(1 - \underset{\sim}{c}))}{\underline{c}(1.0 - \underline{c})^m} \tag{7.8d}$$

$$m = 1.56\frac{\exp(-0.24Le)}{\mathrm{erf}((1.0 + Ka_L)/1.5)} \tag{7.8e}$$

where Ka_L is the local Karlovitz number defined in the context of RANS as:

$$Ka_L = \frac{(\underset{\sim}{\epsilon}\delta_{th})^{1/2}}{S_L^{3/2}} \tag{7.9}$$

and Re_L is the local RANS turbulent Reynolds number defined as:

$$Re_L = \rho_0(\underset{\sim}{k}^2/\underline{\epsilon})/\mu_0 \tag{7.10}$$

In Eqs. 7.8(1-e), the models were defined based on curves which are optimised using the current DNS database. As such, the parameterisation is expected to hold for the values that have been examined, however, it is unclear if the exact form will be valid for values either greater or smaller than what has been examined. In Eq. 7.8a a power-law is used to express the relationship of β_{A1UR} with Le; this was carried out by fitting to the DNS data and as such there are doubts to its applicability for $Le > 1.2$ or $Le < 0.34$. Similarly β_{A1UR} relationship with Ka_L was parameterised using a power-law by using the current DNS database

and a case in the corrugated flamelets regime (which can be found in [80] and its initial conditions in appendix B). Again as this function is based on a fitting to the current DNS dataset it remains unclear if the exact parameterisation will hold for values beyond the current range. Similarly, in Eq. 7.8b the effects of Le and Ka were included in the first term based on the current DNS database. The second term arises, to fit to the effects of Re_t which were only studied in the thin reaction zones regime, therefore a bridging function based on Ka_L is used, whereby for low Ka_L (corrugated flamelets regime) the right hand side term tends to unity. Eq. 7.8c is based on optimizing this parameter for the thin reaction zones regime where Re_t was varied in isolation, and this term appears in Eq. 7.8b. Finally as stated previously the transition location, along $\tilde{c}$, of A_{1UR} is determined by Ka and Le, which were fitted according to the current DNS database using Eqs. 7.8d and 7.8e. In order to examine the effectiveness of the parameters, *a posteriori* analysis must be used with comparisons being made against measured experimental data. A relationship between $\underset{\sim}{c}$ with $\underline{c}$ is required as the latter is not available in a RANS simulation, and based on the existing DNS database an expression is proposed in §8.1.2, Eq. 8.11 [80]. These model parameters shown in Eqs. 7.8 were optimised based on a least squares method. The predictions of Eq. 7.7 with the model parameters given by Eq. 7.8 are compared with A_{1ur} obtained from the DNS data in Fig. 7.3, which shows that Eq. 7.7 satisfactorily predicts A_{1ur} for all cases considered here. Equation 7.8b ensures an increase in a^* with increasing Re_L and Ka_L before assuming an asymptotic value for large values of Re_L and Ka_L. The local turbulent Reynolds number Re_L and Karlovitz number Ka_L parameterisation of a^* account for the influences of turbulent Reynolds and Karlovitz numbers on the curvature κ_m dependencies of $(S_r + S_n)$ and $|\nabla c|$, as demonstrated in Fig. 6.12. The quantity $\underline{[D(\partial N_i/\partial x_i)^2]}_s - \underset{\sim}{D}[\partial \underline{(N_i)}_a/\partial x_i]^2$ plays a key role in determining the statistical behaviour of A_{2ur} (see Eq. 7.5b). It has been shown in Fig. 7.2 that $\underline{(\kappa_m^2)_s}$ increases in magnitude with increasing Ξ, which is utilised here to scale $\underline{[D(\partial N_i/\partial x_i)^2]}_s - \underset{\sim}{D}[\partial \underline{(N_i)}_s/\partial x_i]^2$ in the following manner [81]:

$$\underline{[D(\partial N_i/\partial x_i)^2]}_s - \underset{\sim}{D}[\partial \underline{(N_i)}_s/\partial x_i]^2 \sim D_0\{[(\Sigma_{gen}/|\nabla \underline{c}|) - 1]^n S_L/\alpha_{T0}\}^2 \qquad (7.11)$$

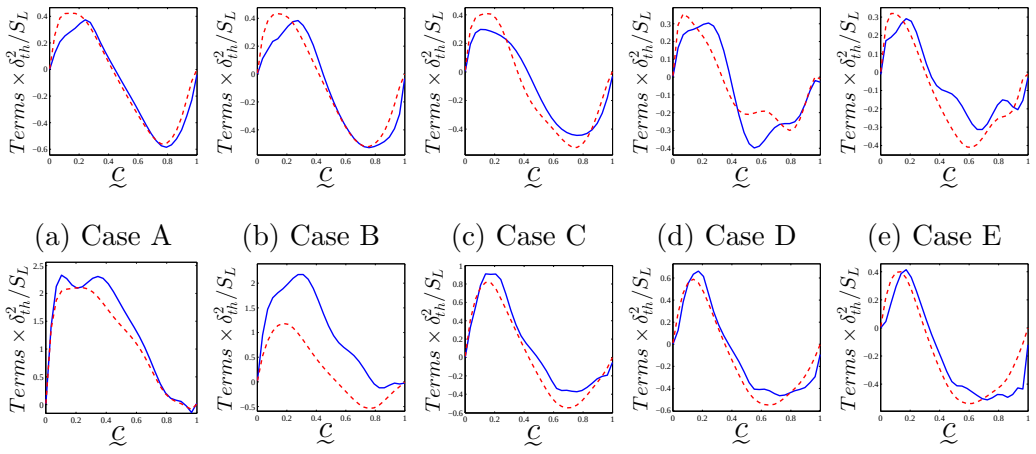

(a) Case A (b) Case B (c) Case C (d) Case D (e) Case E

(f) Case F (g) Case G (h) Case H (i) Case I (j) Case J

Figure 7.3: Variation of A_{1ur} with $\underset{\sim}{c}$ (——) along with the prediction of Eq. 7.7 (– – –) for cases A-J.

The above scaling is used to propose the following model for A_{2ur}:

$$A_{2ur} = -\beta_{A2UR}\left[\left(\frac{\Sigma_{gen}}{|\nabla \underset{\sim}{c}|} - 1.0\right)^n \frac{S_L}{\alpha_{T0}}\right]^2 D_0 \Sigma_{gen} \tag{7.12}$$

where β_{A2UR} and n are model parameters which are expected to increase with increasing turbulent Reynolds number because of large extent of wrinkling for high values of Re_t. It has been found that the model given by Eq. 7.12 captures A_{2ur} satisfactorily for all cases considered here when the following expression for β_{A2UR} is used:

$$\beta_{A2UR} = f(Le)\left\{1.0 + \frac{f_2(Re_L) - 1.0}{[1.0 - \exp(-5.0(Ka_L - 1.0))]^{5.0}}\right\} \tag{7.13a}$$

$$f(Le) = 0.91\frac{Le^{4.73} + 1.74}{1.52Le^{4.73} + 0.79} \tag{7.13b}$$

$$f_2(Re_L) = 0.22\frac{Re_L^{2.07} + 0.22}{0.22Re_L^{2.07} + 0.59} \tag{7.13c}$$

$$n = 0.43\exp(-1.4Le) \tag{7.13d}$$

The above parameterisation was carried out based on parametric optimisation using the present DNS dataset, as such it is unclear if it is expected to hold for a range of Re_t, Le and Ka_L values beyond the current tested range. In order to check the validity of these parameterisations they should be tested using *a posteriori* analysis based on experimental data. The model in Eq. 7.13a was found to vary with changing Le which leads to the parameterisation shown in Eq. 7.13b. Secondly the effects of Re_t were studied in the thin reaction zones regime and to capture these effects Eq. 7.13c is used. In order to capture the Re_t effects in the thin reaction zones regime only, a bridging function is used which tends to unity for small Ka_L (i.e. in the corrugated flamelet regime). Moreover this bridging function is identical to the one in Eq. 7.8b. Finally, the resolution factor $\Sigma_{gen}/|\nabla \underline{c}|$ is raised to a power n which was found be a function of Le. This is proposed as the probability of finding high values of κ_m^2 and $|\nabla c|$ increases with decreasing Le (which can be seen in the magnitudes of T_2 for cases F-J). Recently Hawkes et al. [71] proposed a model for A_2 which takes the following form:

$$A_2 = -D_{\text{eff}}\beta_H \left[1 - \underline{(N_k)}_s \underline{(N_k)}_s\right]^2 \frac{\Sigma_{gen}^3}{\underline{c}^2(1-\underline{c})^2} \tag{7.14a}$$

$$\beta_H = 2.24 Le^{-0.85} + \frac{0.5}{1+\exp(20-Re_L)} \tag{7.14b}$$

In Eq. 7.14a, β_H is a model parameter and D_{eff} is an effective diffusivity which is expected to approach to the mass diffusivity for low Da combustion [71]. The parameterisation of β_H shown in Eq. 7.14b was carried out based on the current DNS database. In the current analysis, D_{eff} is taken to be the unburned gas diffusivity D_0 for all cases. The model prediction based on Eq. 7.12 are added with T_{2r} to show the resulting prediction of A_2 in Fig. 7.4. Additionally the model predictions from Hawkes et al. [71] is shown in Fig. 7.4 with model parameter β_H given by Eq. 7.14b. It is evident from Fig. 7.4 that the predictions from Eq. 7.12 and Eq. 7.14a show comparable performance in predicting A_2. Although a slight skewing towards the fresh gas side is seen to occur for the model given in Eq. 7.12 for cases with low Re_t (i.e. cases A and B). This is due to a slight overprediction from the model parameterisation shown in Eq. 7.13.

The complete model for the curvature term $(A_1 + A_2)$ of FSD transport equa-

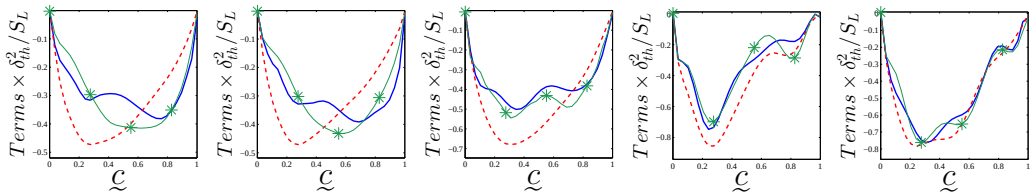

(a) Case A (b) Case B (c) Case C (d) Case D (e) Case E

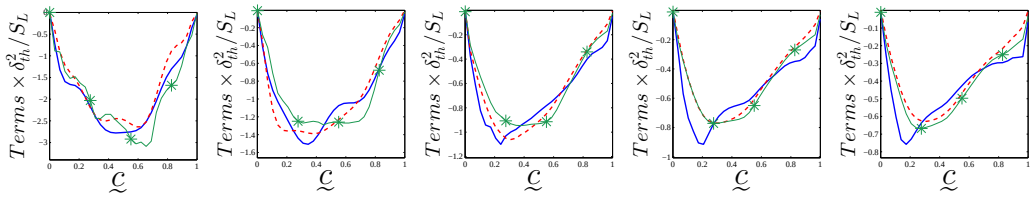

(f) Case F (g) Case G (h) Case H (i) Case I (j) Case J

Figure 7.4: Variation of A_{2ur} with $\underset{\sim}{c}$ (——) along with the prediction of Eq. 7.7 with A_{2ur} (i.e: T_2=Eq. 7.7+A_{2ur}) (– – –) and Hawkes et al. [16] model shown in Eq. 7.14a (—✳—), for cases A-J.

tion takes the following form when using the definitions shown in Eq. 7.5a and Eq. 7.5b, and using the models proposed in Eq. 7.7 and Eq. 7.12:

$$\begin{aligned}\underline{(S_d\nabla.\vec{N})}_s\Sigma_{gen} &= (\rho_0 S_L/\underline{\rho})[\partial\underline{(N_i)}_s/\partial x_i]\Sigma_{gen} - \underset{\sim}{D}[\partial\underline{(N_i)}_s/\partial x_i]^2\Sigma_{gen} \\ &- \beta_{A1UR}S_L\left[1-\underline{(N_k)}_s\underline{(N_k)}_s\right](\underline{c}-a^*)\Sigma_{gen}^2 f(\underline{c},\underset{\sim}{c}) \\ &- \beta_{A2UR}\left[\left(\frac{\Sigma_{gen}}{|\nabla\underline{c}|}-1.0\right)^n\frac{S_L}{\alpha_{T0}}\right]^2 D_0\Sigma_{gen}\end{aligned} \tag{7.15}$$

The predictions of Eqs. 7.2, 7.3 and 7.15 are compared with $\underline{(S_d\nabla.\vec{N})}_s\Sigma_{gen}$ obtained from the DNS data in Fig. 7.5 where the predictions of Eqs. 7.2 and 7.3 (with $\beta_{CFM}=0.4$ and $c_0=0.5$) are referred to as CPB and CFM, respectively. It is evident from Fig. 7.5 that the predictions of Eqs. 7.2 and 7.3 significantly underpredict the negative contribution of $\underline{(S_d\nabla.\vec{N})}_s\Sigma_{gen}$ for all flames considered in this analysis for the values β_{CFM} and c_0 originally proposed by Veynante et al. [153]. Furthermore, Eq. 7.2 predicts negative values of $\underline{(S_d\nabla.\vec{N})}_s\Sigma_{gen}$ throughout the flame brush in all cases, whereas $\underline{(S_d\nabla.\vec{N})}_s\Sigma_{gen}$ assumes positive values towards the unburned gas side of the flame brush for small values of Re_t (i.e. cases

A and B). It should be noted, however, that the models given by Eqs. 7.2 and 7.3 were proposed in the context of the corrugated flamelets regime and therefore the inadequacies of these models for the thin reaction zones regime flames are not unexpected. However, modifying β_{CFM} and c_0 values enable Eq. 7.3 to capture the general qualitative behaviour of $\underline{(S_d\nabla.\vec{N})}_s\Sigma_{gen}$ for all cases considered here. It has been found that Eq. 7.3 can capture the behaviour of $\underline{(S_d\nabla.\vec{N})}_s\Sigma_{gen}$ when β_{CFM} and c_0 are expressed as:

$$\beta_{CFM} = 0.9Le^{-0.7}[1 - \overline{(N_k)}_s\overline{(N_k)}_s]\text{erf}[1 + \exp\left(-(Re_L - 7.0)\right)] \tag{7.16}$$

$$c_0 = 0.6 - 0.5\text{erf}(5.1Le^{7.0})(4 - 3/(1 + \exp(7.0 - Re_L))) \tag{7.17}$$

The prediction of Eq. 7.3 with β_{CFM} given in Eq. 7.16 and c_0 given by Eq. 7.17 is referred to be CFM-MOD in Fig. 7.5. It can be seen from Fig. 7.5 that Eq. 7.15 satisfactorily captures both qualitative and quantitative behaviours of $\underline{(S_d\nabla.\vec{N})}_s\Sigma_{gen}$ for all flames considered in this analysis and the performance of Eq. 7.15 remains either comparable to or better than the CPB, CFM and CFM-MOD models. The model given by Eq. 7.15 works well for the flames in corrugated flamelets regime and with different values of τ which is demonstrated in appendix B.

7.1.3 Summary

Modelling of the curvature term of the FSD transport equation has been examined in the context of RANS based on *a priori* analysis of a DNS database of turbulent premixed flames with a wide range of Re_t and Le. The curvature term has been decomposed into components arising from the components of displacement speed S_d [107] and the statistical behaviours of the individual components have been analysed in detail. New models have been developed for individual components of the FSD curvature term in the context of RANS where the effects of Ka_L, Re_t and global Le have been accounted for explicitly. The model predictions were compared with respect to the curvature terms extracted from DNS data, which demonstrated that the performance of the newly proposed model is either better than or is comparable for the range of Lewis numbers and turbulent Reynolds

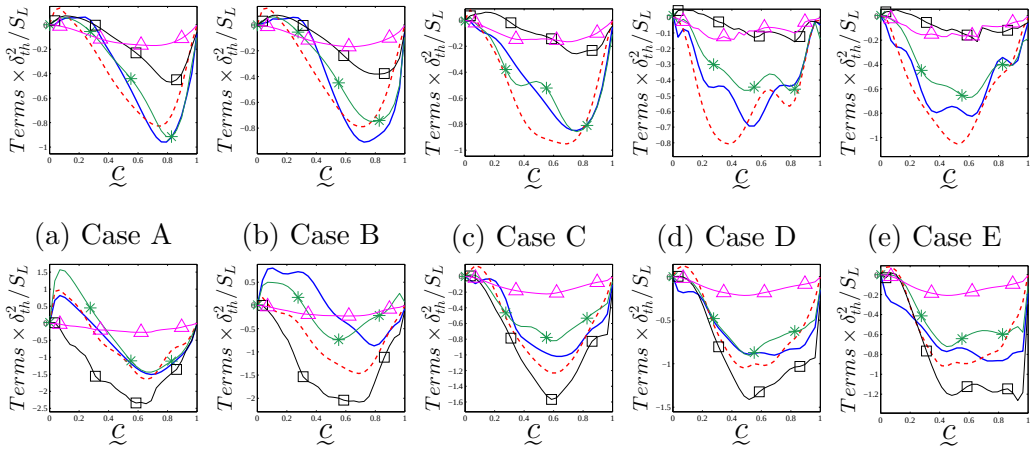

(a) Case A (b) Case B (c) Case C (d) Case D (e) Case E

(f) Case F (g) Case G (h) Case H (i) Case I (j) Case J

Figure 7.5: Variation of $A_1 + A_2$ (——) with $\underset{\sim}{c}$ along with the predictions of CPB (—△—), CFM (—□—), CFM-MOD (—✳—) and the combined model given in Eq. 7.15 (– – –), shown for cases A-J.

numbers. This approach forms a starting point for the modelling of the curvature term in context of LES.

7.2 LES Modelling of Curvature Terms

In this section the modelling of the curvature of the the generalised FSD term, in the context of LES will be discussed. The curvature term is given as:

$$\overline{\left[S_d\left(\frac{\partial N_i}{\partial x_i}\right)\right]}_s \Sigma_{gen} \tag{7.18}$$

The curvature term describes the production/destruction of Σ_{gen} due to flame curvature $\kappa_m = (\partial N_i/\partial x_i)/2$ [29, 35, 48, 66, 67, 68]. The statistical behaviour of $\overline{(S_d \nabla . \vec{N})}_s \Sigma_{gen}$ is significantly affected by curvature dependence on S_d [29, 35] as described in previous chapters. It was demonstrated in earlier studies by Chakraborty and Cant [29, 35] that the existing models for the subgrid curvature term C_{sg} often do not capture its correct qualitative and quantitative behaviours, particularly in the thin reaction zones regime flames. Additionally, *a priori* DNS analyses [29, 35] showed that existing models for the subgrid curvature term C_{sg}

do not adequately capture the qualitative behaviour of this term obtained from DNS data. It was also shown by Chakraborty and Cant [29, 35], that the model parameters for the existing subgrid curvature term C_{sg} are found to be strong functions of the LES filter width Δ [29, 35]. To date, most existing FSD based models have been proposed for unity Lewis number flames where the differential diffusion of heat and mass has been ignored. The effects of Le on the statistical behaviour of the FSD curvature term $\overline{(S_d\nabla.\vec{N})}_s\Sigma_{gen}$ are yet to be analysed in detail. With these facts in mind the following objectives were set:

1. To analyse the statistical behaviours of the subgrid FSD curvature term in the context of LES, for flames with different values of Lewis number.

2. To propose models for the subgrid FSD curvature terms and assess their performances in comparison to the corresponding quantities extracted from DNS data.

7.2.1 Existing LES the Curvature Term Models

The curvature term of the FSD $\overline{(S_d\nabla.\vec{N})}_s\Sigma_{gen}$ is often decomposed in the following manner [29, 35, 48, 66, 67, 68]:

$$\overline{\left[S_d\left(\frac{\partial N_i}{\partial x_i}\right)\right]}_s\Sigma_{gen} = C_{mean} + C_{sg} \tag{7.19}$$

where C_{mean} and C_{sg} are the resolved and subgrid components of the FSD curvature term respectively. The resolved curvature term C_{mean} can be expressed in three different manners [29, 35, 66] as shown described in Chapter 3:

$$C_{mean} = \overline{(S_d)}_s\frac{\partial\overline{(N_i)}_s}{\partial x_i}\Sigma_{gen} \tag{7.20a}$$

$$C_{mean} = \overline{(S_d)}_s\frac{\partial M_i}{\partial x_i}\Sigma_{gen} \tag{7.20b}$$

$$C_{mean} = (\delta_{ij} - \overline{(N_iN_j)}_s)\frac{\partial\overline{(S_d)}_s\overline{(N_i)}_s}{\partial x_j}\Sigma_{gen} \tag{7.20c}$$

Chakraborty and Cant [29, 35] demonstrate that the expression given by Eq. 7.20a provides the best option for the C_{mean}, as it resulted in the smallest magnitude of C_{sg}. In this work the expressions given by Eq. 7.20(a-c) were tested and Eq. 7.20a was found to perform the best (not shown here). This is advantageous from the perspective of efficient modelling of the FSD curvature term $\overline{(S_d\nabla.\vec{N})}_s\Sigma_{gen}$ as most of the modelling uncertainty is associated with C_{sg}. Moreover, Eq. 7.20a has also been used for the modelling of $\overline{(S_d\nabla.\vec{N})}_s\Sigma_{gen}$ in previous LES simulations [66, 67, 68, 73]. For the present analysis Eq. 7.20a will be considered for the resolved curvature term C_{mean}.

Decomposition of the displacement speed S_d, as described in Chapter 2 (see Eq. 2.103), was used in order to model the curvature term. The following expression for C_{sg} can be obtained using Eq. 2.103 and $C_{mean} = \overline{(S_d)}_s[\partial\overline{(N_i)}_s/\partial x_i]\Sigma_{gen}$ [82, 83]:

$$C_{sg} = C_{sg1} + C_{sg2} = \overline{\left(S_d\frac{\partial N_i}{\partial x_i}\right)}_s\Sigma_{gen} - \overline{(S_d)}_s\frac{\partial\overline{(N_i)}_s}{\partial x_i}\Sigma_{gen} \tag{7.21}$$

where

$$C_{sg1} = \overline{\left[(S_r+S_n)\frac{\partial N_i}{\partial x_i}\right]}_s\Sigma_{gen} - \overline{(S_r+S_n)}_s\frac{\partial\overline{(N_i)}_s}{\partial x_i}\Sigma_{gen} \tag{7.22a}$$

$$C_{sg2} = -\overline{\left[D\left(\frac{\partial N_i}{\partial x_i}\right)^2\right]}_s\Sigma_{gen} - \overline{\left[D\left(\frac{\partial N_i}{\partial x_i}\right)\right]}_s\frac{\partial\overline{(N_i)}_s}{\partial x_i}\Sigma_{gen} \tag{7.22b}$$

Eq. 7.22a indicates that curvature ($\kappa_m = \nabla.\vec{N}/2$) dependencies of (S_r+S_n) and $|\nabla c|$, significantly influence the statistical behaviour of C_{sg1}. Eq. 7.22b suggests that C_{sg2} is expected to assume negative values throughout the flame brush as:

$$\left|\overline{\left[D\left(\frac{\partial N_i}{\partial x_i}\right)^2\right]}_s\Sigma_{gen}\right| \gg \left|\overline{\left[D\left(\frac{\partial N_i}{\partial x_i}\right)\right]}_s\frac{\partial\overline{(N_i)}_s}{\partial x_i}\Sigma_{gen}\right| \tag{7.23}$$

Hawkes and Cant [67, 68] modified a version of the Coherent Flamelet Model (CFM) by Candel and Poinsot [18] as:

$$C_{sg} = -\frac{\alpha_N\beta_1 S_L\Sigma_{gen}^2}{(1-\bar{c})} \tag{7.24}$$

where $\alpha_N = 1 - \overline{(N_k)}_s \overline{(N_k)}_s$ is a resolution parameter which vanishes when the flow is fully resolved and β_1 is a model parameter. Hawkes [66] discussed a possibility of modifying a RANS model proposed by Cant et al. [21] for the purpose of LES as:

$$C_{sg} = -\frac{C_H S_L \Sigma_{gen}^2}{(1-\bar{c})} \tag{7.25}$$

where $C_H = \alpha_H \beta_2 (1 - (1/3)[1 - \exp(1-\bar{c})\sqrt{\tilde{k}}/\Sigma_{gen} S_L \Delta])$, $A = 10.0$, $u'_\Delta = \sqrt{(2\tilde{k}/3)}$ is the subgrid turbulent velocity fluctuation, $\tilde{k} = (\overline{\rho u_i u_i} - \bar{\rho}\tilde{u}_i\tilde{u}_i/2\bar{\rho})$ is the subgrid kinetic energy and β_2 is a model parameter. Another model of C_{sg} was proposed by Charlette et al. [48]:

$$C_{sg} = -\beta_3 S_L (\Sigma_{gen} - |\nabla \bar{c}|) \frac{\Sigma_{gen}}{\bar{c}(1-\bar{c})} \tag{7.26}$$

where β_3 is a model parameter. The models given by Eq. (7.24-7.25) (henceforth will be referred to as CSGCFM, CSGCPB and CSGCHAR respectively) ensure that C_{sg} vanishes when the flow is fully resolved (i.e. $\overline{(N_k)}_s \overline{(N_k)}_s = 1.0$ and $\Sigma_{gen} = |\nabla \bar{c}| = |\nabla c|$). *A-priori* DNS assessment of the CSGCFM, CSGCPB and CSGCHAR models and the modelling of C_{sg1} and C_{sg2} discussed in the following subsection in this chapter.

7.2.2 Behaviour of the Curvature Term

7.2.2.1 Turbulent Reynolds Number

The variations of the ensemble averaged values of $\overline{(S_d \nabla . \vec{N})}_s \Sigma_{gen}$ conditional on $\tilde{c}$-isosurfaces for all cases are shown in Fig. 7.6 for $\Delta = 8\Delta_m \approx 0.8\delta_{th}$ and $\Delta = 24\Delta_m \approx 2.4\delta_{th}$. The filter widths $\Delta = 8\Delta_m \approx 0.8\delta_{th}$ and $\Delta = 24\Delta_m \approx 2.4\delta_{th}$ correspond to two representative situations, where the flame is partially resolved and where the flame is fully unresolved, respectively. Fig. 7.6 shows that $\overline{(S_d \nabla . \vec{N})}_s \Sigma_{gen}$ assumes predominantly negative values throughout the flame brush. Although the resolved curvature term $C_{mean} = \overline{(S_d)}_s \partial \overline{(N_i)}_s / \partial x_i \Sigma_{gen}$ captures the qualitative behaviour of $\overline{(S_d \nabla . \vec{N})}_s \Sigma_{gen}$ throughout the flame brush, the magnitude of C_{mean} remains smaller than the magnitude of $\overline{(S_d \nabla . \vec{N})}_s \Sigma_{gen}$ for the major portion of the flame brush in all cases for all values of Δ (see Fig. 7.6).

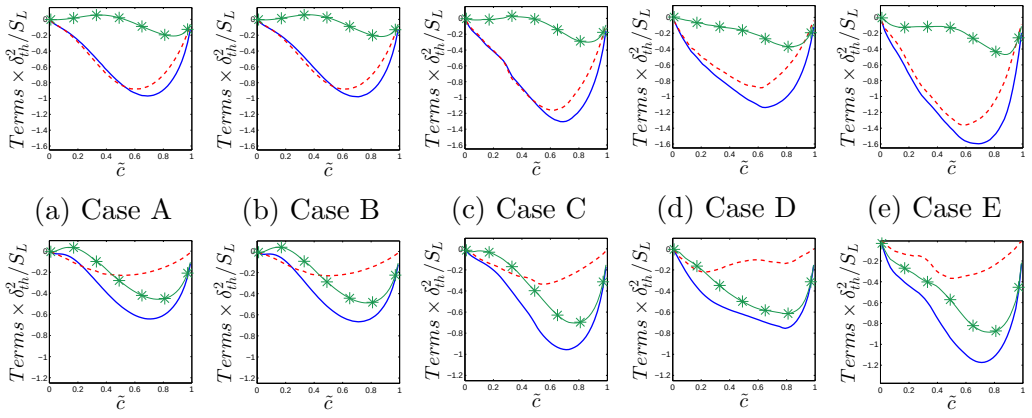

(a) Case A (b) Case B (c) Case C (d) Case D (e) Case E

(f) Case A (g) Case B (h) Case C (i) Case D (j) Case E

Figure 7.6: Variation of $\overline{(S_d\nabla.\vec{N})}_s\Sigma_{gen}$ (——), C_{mean} (– – –) and C_{sg} (—✱—) conditionally averaged in bins of $\tilde{c}$ across the flame brush for filter sizes $0.8\delta_{th}$ (top row) and $2.4\delta_{th}$ (bottom row) for cases A-E.

This leads to predominantly negative values of C_{sg}, although the ensemble averaged values of C_{sg} on $\tilde{c}$-isosurfaces exhibits positive values towards the unburned gas side of the flame brush for the flames with low and moderate values of turbulent Reynolds number (e.g. cases A-C). By contrast, the variation of ensemble averaged values of C_{sg} on $\tilde{c}$-isosurfaces exhibits only negative values throughout the flame brush for the flames with relatively higher values of turbulent Reynolds number (e.g. cases D and E). The models of C_{sg} given by Eqs. 7.24-7.26 only predicts negative values of C_{sg} and thus will not be capable of predicting the positive values of C_{sg} in cases A-C.

Comparing $\overline{(S_d\nabla.\vec{N})}_s\Sigma_{gen}$, C_{mean} and C_{sg} magnitudes for $\Delta = 8\Delta_m \approx 0.8\delta_{th}$ and $\Delta = 24\Delta_m \approx 2.4\delta_{th}$ reveals that the magnitudes of $\overline{(S_d\nabla.\vec{N})}_s\Sigma_{gen}$ and C_{mean} decrease with increasing Δ, whereas the magnitude of C_{sg} increases with increasing Δ. This observation is consistent with previous findings [29, 35]. The smearing of local information as a result of the weighted-averaging process involved in LES filtering leads to the decrease in the magnitudes of $\overline{(S_d\nabla.\vec{N})}_s\Sigma_{gen}$ and C_{mean} for increasing values of Δ. The flow becomes increasingly unresolved with increasing Δ and thus the flame curvature and its influence on the FSD evolution are increasingly felt at the subgrid scale, which is reflected in the high magnitudes of C_{sg} for large values of Δ.

7.2.2.2 Lewis Number

The variations of $\overline{(S_d\nabla.\vec{N})}_s\Sigma_{gen}$, C_{mean} and C_{sg} conditionally averaged in bins of $\tilde{c}$ isosurfaces for cases F-J are shown in Fig. 7.7 for filter widths $\Delta = 8\Delta_m \approx 0.8\delta_{th}$ and $\Delta = 24\Delta_m \approx 2.4\delta_{th}$. It is evident from Fig. 7.7 that Le significantly affects the statistical behaviours of the curvature terms. The filter widths $\Delta = 8\Delta_m \approx 0.8\delta_{th}$ and $\Delta = 24\Delta_m \approx 2.4\delta_{th}$ span a useful range of length scales (i.e. from Δ comparable to $0.8\delta_{th}$ where the flame is partially resolved, up to $2.4\delta_{th}$ where the flame becomes fully unresolved and Δ is comparable to the integral length scale). In the $Le \ll 1$ flames (e.g. cases F and G) the FSD curvature term $\overline{(S_d\nabla.\vec{N})}_s\Sigma_{gen}$ behaves as a source term for the major part of the flame brush before assuming negative values towards the burned gas side for $\Delta = 8\Delta_m \approx 0.8\delta_{th}$. For $\Delta = 24\Delta_m \approx 2.4\delta_{th}$, the FSD curvature term $\overline{(S_d\nabla.\vec{N})}_s\Sigma_{gen}$ acts as a source (sink) term towards the unburned (burned) gas side of the flame brush in the $Le \ll 1$ flames. In the case of $Le \approx 1$ flames (i.e. cases H-J) the curvature term $\overline{(S_d\nabla.\vec{N})}_s\Sigma_{gen}$ behaves as a sink type term throughout the flame brush for all filter widths. It can be seen from Fig. 7.7 that C_{mean} acts as a source (sink) term for cases F and G (H-J). The magnitude of C_{mean} (C_{sg}) decreases (increases) with increasing Δ in all cases, and for large filter widths $\overline{(S_d\nabla.\vec{N})}_s\Sigma_{gen}$ is principally made up of C_{sg}. The LES filtering is a convolution process, and the weighted averaging involved in this filtering leads to a decrease in the magnitude of C_{mean} with increasing filter width Δ. The flow becomes increasingly unresolved with increasing filter width Δ and this is reflected in the rise in C_{sg} magnitude with the increase in filter width Δ.

The resolved curvature term $C_{mean} = \overline{(S_d)}_s\partial\overline{(N_i)}_s/\partial x_i\Sigma_{gen}$ can be seen to capture the behaviour of the curvature term $\overline{(S_d\nabla.\vec{N})}_s\Sigma_{gen}$ satisfactorily at small filter widths (i.e. $\Delta \leq \delta_{th}$) for the flames with $Le \approx 1.0$. However, the magnitude of C_{mean} decreases with increasing Δ and it does not capture the behaviour of the FSD curvature term $\overline{(S_d\nabla.\vec{N})}_s\Sigma_{gen}$ for the $Le \ll 1.0$ flames. The subgrid curvature term, C_{sg} follows the behaviour of the FSD curvature term $\overline{(S_d\nabla.\vec{N})}_s\Sigma_{gen}$ for all filter widths. The subgrid curvature term C_{sg} almost entirely makes up the FSD curvature term $\overline{(S_d\nabla.\vec{N})}_s\Sigma_{gen}$ for $\Delta \gg \delta_{th}$ and this is especially true for the $Le \ll 1.0$ cases. It can further be observed from Fig. 7.7 that C_{sg} assumes

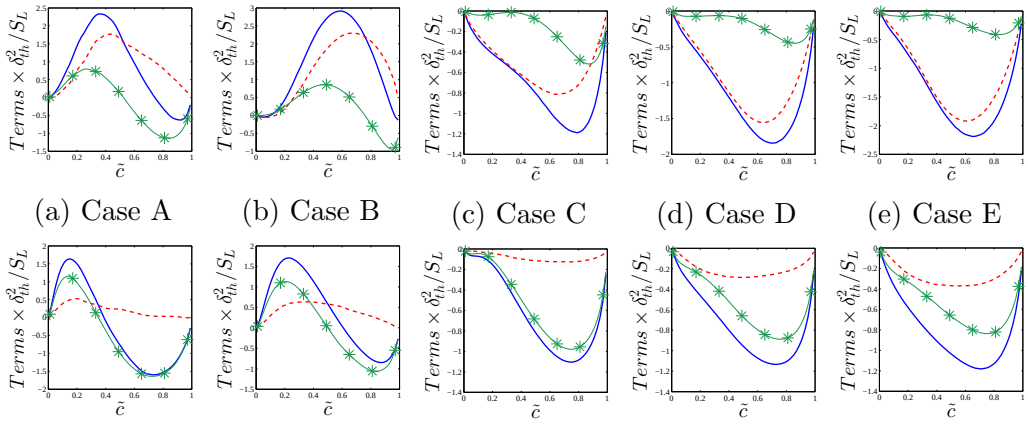

(a) Case A (b) Case B (c) Case C (d) Case D (e) Case E

(f) Case A (g) Case B (h) Case C (i) Case D (j) Case E

Figure 7.7: Variation of $\overline{(S_d\nabla.\vec{N})}_s\Sigma_{gen}$ (——), C_{mean} (– – –) and C_{sg} (—✱—) conditionally averaged in bins of $\tilde{c}$ across the flame brush for filter sizes $0.8\delta_{th}$ (top row) and $2.4\delta_{th}$ (bottow row) for cases F-J.

positive values towards the unburned gas side of the flame brush in the $Le \ll 1$ flames (e.g. cases F and G), whereas the existing models for C_{sg} allows for only negative values (see Eqs. 7.24-7.26). This suggests that new models for C_{sg} are warranted to account for the influences of non-unity Lewis number.

7.2.3 Modelling the effects of Turbulent Reynolds number

It is useful to examine the statistical behaviours of C_{sg1} and C_{sg2} in order to explain the differences in the behaviours of C_{sg} for flames with different Re_t. The variations of the ensemble averaged values of $\overline{[(S_r+S_n)\nabla.\vec{N}]}_s\Sigma_{gen}$, $(-\overline{(D(\nabla.\vec{N})^2)}_s\Sigma_{gen} = -4\overline{(D\kappa_m^2)}_s\Sigma_{gen})$, C_{sg1} and C_{sg2} conditional on $\tilde{c}$-isosurfaces are shown in Fig. 7.8 for cases A-E for $\Delta = 8\Delta_m \approx 0.8\delta_{th}$ and $\Delta = 24\Delta_m \approx 2.4\delta_{th}$ respectively. Fig. 7.8 demonstrates that both $\overline{[(S_r+S_n)\nabla.\vec{N}]}_s\Sigma_{gen}$ and C_{sg1} remain predominantly positive (negative) towards the unburned (burned) gas side of the flame brush for all values of Δ considered here. The contribution of $-4\overline{(D\kappa_m^2)}_s\Sigma_{gen}$ and C_{sg2} remain deterministically negative throughout the flame brush (see Fig. 7.8). It is evident from Fig. 7.8 that $-4\overline{(D\kappa_m^2)}_s\Sigma_{gen}$ remains a leading order contributor to $\overline{(S_d\nabla.\vec{N})}_s\Sigma_{gen}$ for all the flames at all values of Δ (see Fig. 7.8), which is consistent with the expected behaviour in the thin reaction zones regime

where $-4\overline{(D\kappa_m^2)}_s\Sigma_{gen}$ is expected to play an important role [107]. Fig. 7.8 further shows that C_{sg1} remains close to the magnitude of $\overline{[(S_r+S_n)\nabla.\vec{N}]}_s\Sigma_{gen}$ for all Δ for all cases considered here, indicating that $\overline{(S_r+S_n)}_s\partial\overline{(N_i)}_s/\partial\overline{(N_i)}_s/\partial x_i\Sigma_{gen}$ does not play a major role in capturing the behaviour of $\overline{[(S_r+S_n)\nabla.\vec{N}]}_s\Sigma_{gen}$. By contrast, there is a significant difference between $-4\overline{(D\kappa_m^2)}_s\Sigma_{gen}$ and C_{sg2} for all cases for small values of Δ, and the difference between these quantities decrease with increasing Δ. As most of the contribution of $-4\overline{(D\kappa_m^2)}_s\Sigma_{gen}$ remains unresolved for large values of Δ (i.e. $\Delta \gg \delta_{th}$), C_{sg2} remains the leading order contributor to $-4\overline{(D\kappa_m^2)}_s\Sigma_{gen}$, indicating that $-\overline{(D\partial N_i/\partial x_i)}_s\partial\overline{(N_i)}_s/\partial x_i\Sigma_{gen}$ plays a progressively less important role for increasing values of where the flame is fully unresolved. However, the contribution of $-\overline{(D\partial N_i/\partial x_i)}_s\partial\overline{(N_i)}_s/\partial x_i\Sigma_{gen}$ remains significant for small values of Δ when the flame is partially resolved. Fig. 7.8 further shows that the order of magnitudes of both C_{sg1} and C_{sg2} remain comparable for large values of Δ (i.e. $\Delta \gg \delta_{th}$) and thus accurate modelling of C_{sg1} and C_{sg2} are necessary for accurate modelling of C_{sg}. As the range of κ_m values obtained on a flame surface increases with increasing flame wrinkling at higher values of $u'/S_L \sim Re_t^{1/4}Ka^{1/2} \sim Re_t^{1/2}/Da^{1/2}$, the magnitude of $-4\overline{(D\kappa_m^2)}_s\Sigma_{gen}$ increases with increasing Re_t, which in turn leads to increasing magnitude of $-4\overline{(D\kappa_m^2)}_s\Sigma_{gen}$ and C_{sg2} with increasing Re_t for a given value of Da or Ka (see Fig. 7.8). The positive contribution of C_{sg1} overcomes the negative contribution of C_{sg2} towards the unburned gas side of the flame brush for the flames with small and moderate values of turbulent Reynolds number (i.e. cases A-C) and yields a net positive contribution of C_{sg} towards the reactant side of the flame brush (see Fig. 7.6).

The statistical behaviours of $\overline{[(S_r+S_n)\nabla.\vec{N}]}_s\Sigma_{gen}$ and C_{sg1} depends on the nature of the correlations between (S_r+S_n) and $\kappa_m = \nabla.\vec{N}/2$ and between $|\nabla c|$ and κ_m , and the variation of $\overline{(\kappa_m)}_s$ across the flame brush. The correlation coefficients for the $(S_r+S_n)-\kappa_m$ and $|\nabla c|-\kappa_m$ dependencies for five different c isosurfaces across the flame brush for all cases are shown in Fig. 6.12(a) and 6.12(b) respectively. For unity Lewis number flames $S_t = -2D\kappa_m$ is deterministically negatively correlated with κ_m with a correlation coefficient equal to -1.0. Fig. 6.12(a) suggests that $(S_r+S_n)-\kappa_m$ correlation is much weaker than the $S_t-\kappa_m$ correlation in all cases. Moreover, Fig. 6.12(b) demonstrates that $|\nabla c|$

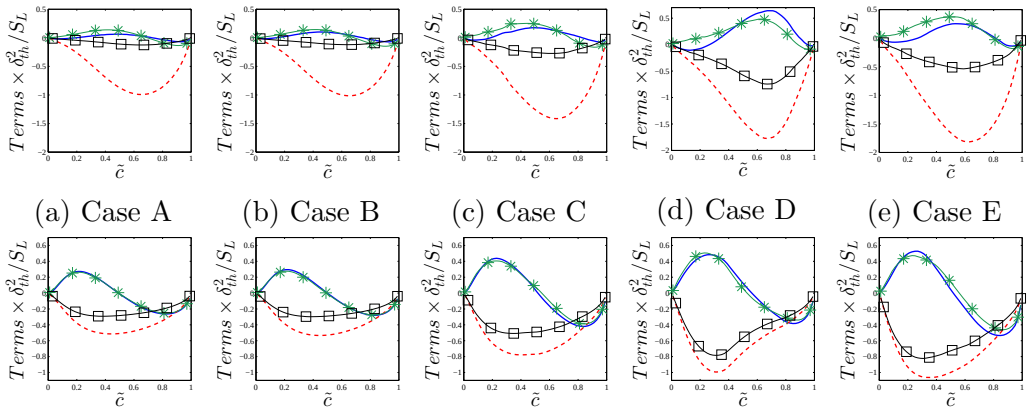

(a) Case A (b) Case B (c) Case C (d) Case D (e) Case E

(f) Case A (g) Case B (h) Case C (i) Case D (j) Case E

Figure 7.8: Variation of $\overline{((S_r+S_n)\nabla.\vec{N})}_s\Sigma_{gen}$ (——), $-4\overline{(D\kappa_m^2)}_s\Sigma_{gen}$ (– – –), C_{sg1} (—✳—), C_{sg2} (—□—) conditionally averaged in bins of $\tilde{c}$ across the flame brush for filter width $\Delta = 0.8\delta_{th}$ (top row) and $2.4\delta_{th}$ (bottom row) for cases F-J.

and κ_m remain weakly correlated throughout the flame brush for all cases. Figs. 6.12(a) and 6.12(b) demonstrate that the curvature dependencies of $(S_r + S_n)$ and $|\nabla c|$ remain qualitatively similar for all the flames [44]. The physical explanations of the observed curvature dependencies of $(S_r + S_n)$ and $|\nabla c|$ have been discussed elsewhere [44] and will not be repeated here.

The variation of the ensemble averaged values of $\overline{(\kappa_m)}_s$ conditional on $\tilde{c}$-isosurfaces for all cases are shown in Figs. 7.9a and 7.9b for $\Delta = 8\Delta_m \approx 0.8\delta_{th}$ and $\Delta = 24\Delta_m \approx 2.4\delta_{th}$, respectively, which demonstrates that $\overline{(\kappa_m)}_s$ predominantly assumes positive (negative) values towards the unburned (burned) gas side of the flame brush and the magnitude of $\overline{(\kappa_m)}_s$ increases with increasing Δ. The quantity $\overline{(\kappa_m)}_s$ approaches κ_m for small values of Δ (i.e. $\lim_{\Delta\rightarrow 0}\overline{(\kappa_m)}_s = \kappa_m|\nabla c|/|\nabla c| = \kappa_m$) and the mean value of $\kappa_m = \nabla.\vec{N}/2$ remains negligible for all the $|\nabla c|$-isosurfaces due to the statistical planar nature of the flames. However, subgrid level curvature increases with increasing Δ and thus the magnitude of $\overline{(\kappa_m)}_s$ increases with increasing values of Δ. Relatively weak curvature dependencies of $(S_r + S_n)$ and $|\nabla c|$ lead to positive (negative) values of $\overline{[(S_r+S_n)\nabla.\vec{N}]}_s\Sigma_{gen}$ and C_{sg1} towards the unburned (burned) gas side of the flame brush due to positive (negative) value of $\overline{(\kappa_m)}_s$. The contribution of resolved curvature term $\overline{(S_r+S_n)}_s\partial\overline{(N_i)}_s/\partial x_i\Sigma_{gen}$ remains negligible in comparison

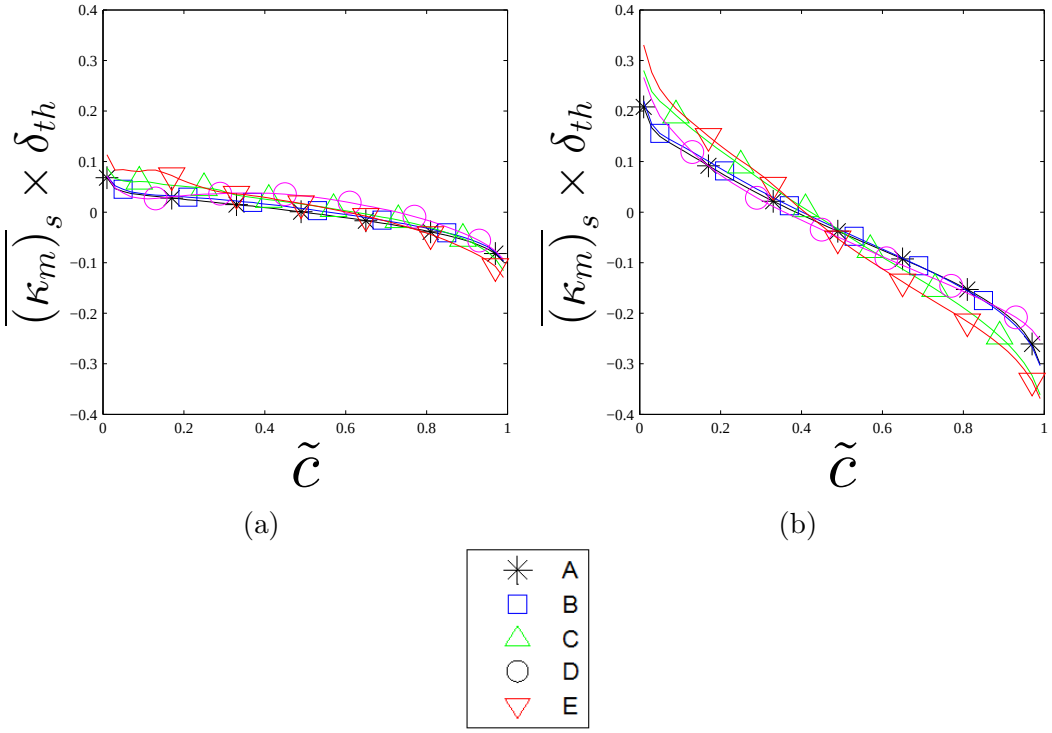

Figure 7.9: Variation of $\overline{(\kappa_m)}_s \times \delta_{th}$ with $\tilde{c}$ across the flame brush for filter widths $0.8\delta_{th}$ (a) and $2.4\delta_{th}$ (b).

to $\overline{[(S_r + S_n)\nabla.\vec{N}]}_s\Sigma_{gen}$, due to relatively small values of $\partial\overline{(N_i)}_s/\partial x_i$ in statistically planar flames. Thus the contributions of $\overline{[(S_r + S_n)\nabla.\vec{N}]}_s\Sigma_{gen}$ and C_{sg1} remain close to each other for all values of Δ (see Fig. 7.8).

The subgrid fluctuations of the surface-weighted contributions of $(S_r + S_n)$ and $\nabla.\vec{N}$ are taken to scale with S_L and $(\Sigma_{gen} - |\nabla\bar{c}|)$ respectively to propose the following model for C_{sg1} in this analysis:

$$C_{sg1} = -\beta_4 \frac{(\Sigma_{gen} - |\nabla\bar{c}|)(\bar{c} - c^{\circ})S_L\Sigma_{gen}}{\exp[-a_\Sigma(1-\bar{c})]\bar{c}(1-\bar{c})^m} \tag{7.27}$$

where β_4, c°, a_Σ and m are the model parameters. The function $(\bar{c}-c^{\circ})/\{\exp[-a_\Sigma(1-\bar{c})]\bar{c}(1-\bar{c})^m\}$ in Eq. 7.27 is used to capture the correct qualitative behaviour of C_{sg1} across the flame brush. In a compressible LES simulation $\tilde{c}$ is readily available and $\bar{c}$ needs to be extracted from $\tilde{c}$. The methodology of extracting $\bar{c}$ from $\tilde{c}$ in the context of LES was discussed elsewhere [29, 35] and will not

be discussed in detail in this chapter. The model parameter c° ensures that the transition from positive to negative value of C_{sg1} takes place at the correct location within the flame brush. The quantity $(\Sigma_{gen} - |\nabla \bar{c}|)$ vanishes when the flow is fully resolved and thus C_{sg1} becomes exactly equal to zero when the flow is fully resolved (i.e.$\Delta \rightarrow 0$) according to Eq. 7.27. It has been found that $m = 1.85$ enables Eq. 7.27 to capture the qualitative behaviour of C_{sg1} when the optimal values of c° and a_{Σ} are chosen. The optimum value of $c^{\circ}, (a_{\Sigma})$ tends to increase with decreasing (increasing) Δ. The κ_m dependencies of $(S_r + S_n)$ and $|\nabla c|$ are reflected mostly in the resolved scale but these effects weaken with increasing values of Δ [29, 35]. As the resolved and subgrid curvature terms are closely related [29, 35], the qualitative behaviour of C_{sg1} is also affected by the κ_m dependencies of $(S_r + S_n)$ and $|\nabla c|$, which leads to the variation of the optimum values of a_{Σ} and c°. The model parameter β_4 is found to decrease with decreasing values of Σ_{gen} for satisfactory quantitative prediction of C_{sg1}, which is accounted for by expressing β_4 as: $\beta_4 = 9.8\Sigma_{gen}\delta_{th}$. The prediction of Eq. 7.27 ensemble averaged on $\tilde{c}$-isosurfaces is compared with the ensemble averaged values of C_{sg1} in Fig. 7.10 for all cases for the optimum values of c° and a_{Σ}, for $\Delta = 0.8\delta_{th}$ and $\Delta = 2.4\delta_{th}$, when β_4 and m are taken to be $\beta_4 = 9.8\Sigma_{gen}\delta_{th}$ and $m = 1.85$. The optimum values of c° and a_{Σ} are estimated by calibrating the prediction of Eq. 7.27 with respect to the values of C_{sg1} obtained from DNS data and the variation of the global mean optimum values of c° and a_{Σ} with Δ/δ_{th} for all cases are shown in Fig. 7.11. The optimum values of c° and a_{Σ} are parameterised here as:

$$c^{\circ} = k_1 + \left[\frac{(k_2 - k_1)}{\{1.0 + \exp(-2.0(\Delta/\delta_{th} - 1.5))\}}\right] \tag{7.28a}$$

$$a_{\Sigma} = \frac{k_4}{1.0 + \exp(-5.0(\Delta/\delta_{th} - 1.0))} \tag{7.28b}$$

$$k_1 = 0.75 + \frac{0.15}{1.0 + \exp[-5.0(k_4 - 4.6)]} \tag{7.28c}$$

$$k_2 = 0.65 + \frac{0.05}{1.0 + \exp[-9.0(k_4 - 4.0)]} \tag{7.28d}$$

$$k_4 = 0.81 - \frac{0.67}{1.0 + \exp[-5.0(k_4 - 4.6)]} \tag{7.28e}$$

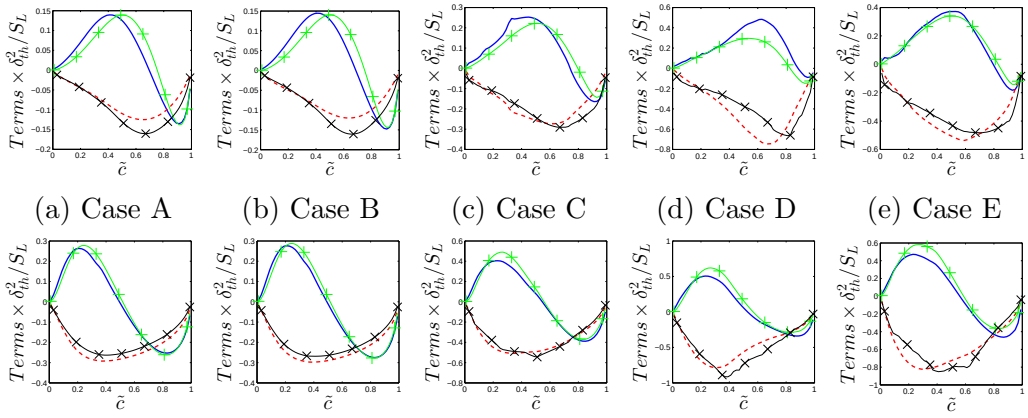

(a) Case A (b) Case B (c) Case C (d) Case D (e) Case E

(f) Case A (g) Case B (h) Case C (i) Case D (j) Case E

Figure 7.10: Variations of C_{sg1} (——) and C_{sg2} (– – –) conditionally averaged in bins of $\tilde{c}$ across the flame brush along with the predictions of Eqs. 7.27 (—+—) and 7.29 (—×—) for filter widths Δ, $0.8\delta_{th}$ (top row) and $2.4\delta_{th}$ (bottom row).

$$k_3 = \frac{Re_{\Delta}^{0.83} + 0.1}{(\Delta/\delta_{th})^{1.73} + 0.1} \tag{7.28f}$$

Fig. 7.10 shows that Eq. 7.27 satisfactorily predicts C_{sg1} when $\beta_4 = 9.8\Sigma_{gen}\delta_{th}$ and $m = 1.85$, and Eq. 7.28 is used for c° and a_{Σ}.

Here the contribution of $\overline{(D\kappa_m^2)}_s - \overline{D\partial N_i/\partial x_i}\partial\overline{(N_i)}_s/\partial x_i$ is scaled with $(\Xi - 1)^n S_L\Sigma_{gen}$ (i.e.) $\overline{(D\kappa_m^2)}_s - \overline{D\partial N_i/\partial x_i}\partial\overline{(N_i)}_s/\partial x_i \sim [(\Sigma_{gen}/|\nabla\bar{c}|) - 1]^n S_L\Sigma_{gen}$ where the subgrid fluctuations of D is taken to scale with S_L/Σ_{gen} (i.e.$D \sim S_L/\Sigma_{gen}$). The above relations are utilised here to propose a model for C_{sg2} in the following manner:

$$C_{sg2} = -\beta_5 \frac{(\Xi - 1)^n S_L \Sigma_{gen}^2}{\bar{c}(1 - \bar{c})} \tag{7.29}$$

where β_5 is a model parameter and $\bar{c}(1-\bar{c})$ is used to capture the correct qualitative behaviour of C_{sg2}. According to Eq. 7.29, C_{sg2} vanishes when the flow is fully resolved. It has been found that Eq. 7.29 satisfactorily captures the behaviour of C_{sg2} throughout the flame brush for $n = 1.0$ in all cases considered here when a suitable value of β_5 is used. The variation of the global mean optimum values of β_5 with Δ/δ_{th} for all cases are shown in Fig. 7.11. The optimum values of β_5

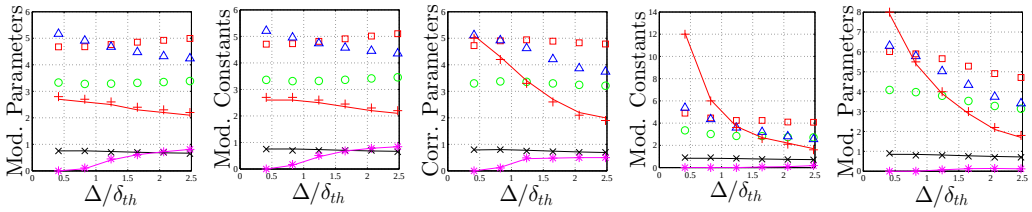

(a) Case A (b) Case B (c) Case C (d) Case D (e) Case E

Figure 7.11: Variation of model parameters β_1 (○), β_2 (□), β_3 (△), β_5 (+) and its model prediction given by Eq. 7.30 (–), a_Σ (∗) and its model given by Eq. 7.28b (–), c° (×) and its model given by Eq. 7.28a (–) with Δ for cases A-E.

has been parameterised here in the following manner:

$$\beta_5 = \frac{Re_\Delta}{Re_\Delta + 1.0} \times \left[r_1 + \frac{r_2 - r_1}{1.0 + \exp\{-5.0(Re_\Delta - r_3)\}} \right] \tag{7.30}$$

where

$$r_1 = 1.6\frac{r_4^{1.23} + 6.24}{7.17r_4^{1.23} + 0.26} \tag{7.31a}$$

$$r_2 = 1.35\frac{r_4^{3.53} + 6.10}{13.25r_4^{3.53} + 0.56} \tag{7.31b}$$

$$r_3 = 35\text{erf}[\exp 5.3(1.37r_4 - 1.0)] \tag{7.31c}$$

$$r_4 = \frac{\Delta}{\Delta + \delta_{th}} \tag{7.31d}$$

The predictions for the parameterisations of c°, a_Σ and β_5 are shown in Fig. 7.11. The predictions of Eq. 7.29 ensemble averaged on $\tilde{c}$ isosurfaces are compared with ensemble averaged values of C_{sg2} in Fig. 7.10 all for cases for $\Delta = 0.8\delta_{th}$ and $\Delta = 2.4\delta_{th}$, which show that Eq. 7.29 satisfactorily predicts the statistical behaviour of C_{sg2} when $n = 1.0$ and Eq. 7.31 is used for β_5.

Eqs. 7.27 and 7.29 can be combined to propose a model for C_{sg} in the following manner:

$$C_{sg} = -\beta_4 \frac{(\Sigma_{gen} - |\nabla\bar{c}|)(\bar{c} - c^\circ)S_L\Sigma_{gen}}{\exp[-a_\Sigma(1-\bar{c})]\bar{c}(1-\bar{c})^m} - \beta_5 \frac{(\Xi - 1)^n S_L \Sigma_{gen}^2}{\bar{c}(1-\bar{c})} \tag{7.32}$$

The above model will henceforth be referred to CSGNEW model in this thesis. Eq. 7.32 allows for a positive contribution of C_{sg} through the contribution of $-\beta_4(\Sigma_{gen} - |\nabla\bar{c}|)(\bar{c} - c^{\circ})S_L\Sigma_{gen}/\{\exp[-a_\Sigma(1-\bar{c})]\bar{c}(1-\bar{c})^m\}$, which is absent in the CSGCAND, CSGCANT and CSGCHAR models. The predictions of the CSGCAND, CSGCANT, CSGCHAR and CSGNEW models for $\Delta = 0.8\delta_{th}$ and $\Delta = 2.4\delta_{th}$ are compared with C_{sg} obtained from DNS in Fig. 7.11 for optimum values of β_1, β_2 and β_3 where the optimum values are estimated by calibrating the models based on the ensemble-averaged value of C_{sg} obtained from DNS data. The variations of the optimum values of β_1, β_2 and β_3 with Δ for cases A-E are also shown in Figs. 7.11(a-e) respectively, which demonstrate that the model constants β_1, β_2 and β_3 remain greater than unity for all cases. This is found to be consistent with the realisability analysis by Hawkes and Cant [69]. Fig. 7.11(a-e) demonstrate that the optimum values of β_1, β_2 and β_3 change with respect to Δ, which is also consistent with earlier findings Chakraborty and Cant [29]. Moreover, optimum values of β_1, β_2 and β_3 for a given value of Δ vary between cases considered here (see 7.11(a-e)). The optimum values of β_1, β_2 and β_3 can also be parameterised in the same manner in which β_5 is parameterised in Eq. 7.31. However, this is not presented here as the models given by Eqs. 7.24-7.26 fail to capture the positive contribution of C_{sg} for cases A-C. Moreover, the CSGCAND, CSGCANT and CSGCHAR models do not capture the correct qualitative behaviour of C_{sg} even when the optimum values of β_2 and β_3 are used. It is evident from Fig. 7.12 that the CSGCAND, CSGCANT and CSGCHAR models predict the general qualitative behaviour of C_{sg} for the major portion for the flame brush all values of Δ. However, CSGCHAR tends to overpredict the negative values of C_{sg} towards the unburned gas side and this behaviour becomes more prominent with increasing filter size. Fig. 7.12 shows that for $\Delta = 2.4\delta_{th}$, the CSGCHAR model predicts the maximum magnitude of C_{sg} near the middle of the flame whereas the actual maximum magnitude of C_{sg} is attained slightly towards the burned gas side. The CSGCAND and CSGCANT models predict the correct magnitude of C_{sg} for optimum values of β_1 and β_2, but they do not satisfactorily capture the qualitative behaviour of C_{sg}, and underpredict (overpredict) its magnitude towards the burned gas side (middle) of the flame brush. Fig. 7.12 demonstrates that the CSGNEW model captures the qualitative

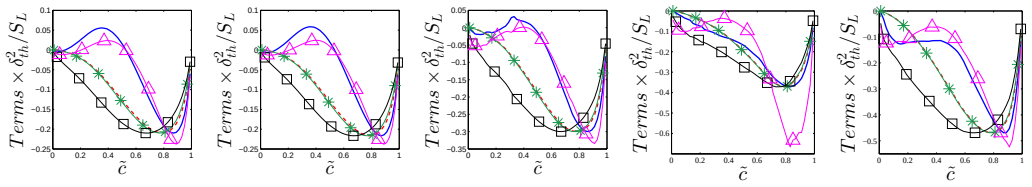

(a) Case A (b) Case B (c) Case C (d) Case D (e) Case E

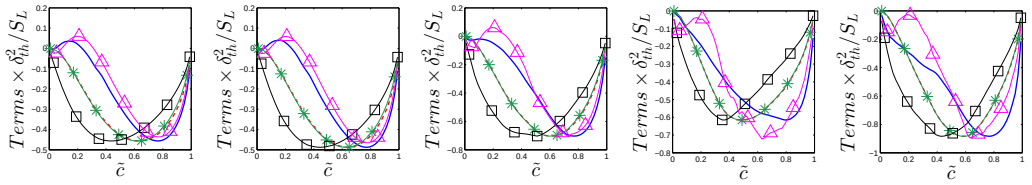

(f) Case A (g) Case B (h) Case C (i) Case D (j) Case E

Figure 7.12: Variations of C_{sg} (——) conditionally averaged in bins of $\tilde{c}$ across the flame brush along with the predictions of CSGCAND (—✱—), CSGCANT (– – –), CSGCHAR (—▫—), CSGNEW (—△—) for filter widths $\Delta = 0.8\delta_{th}$ (top row) and $2.4\delta_{th}$ (bottom row).

behaviour of C_{sg} in a better manner than the CSGCAND and CSGCANT models, and the quantitative agreement between C_{sg} and the CSGNEW model remains better than the CSGCAND, CSGCANT and CSGCHAR models for the major part of the flame brush for all cases, when optimum values of β_4, β_5, a_Σ and c° are used.

7.2.4 Modelling the effects of Lewis number

Similar analysis to the previous section was carried out for cases F-J, to show that the modelling approach used earlier (i.e. the decomposition of C_{sg} into C_{sg1} and C_{sg2}) is a viable strategy. In order to accomplish this task, the variations of $\overline{[(S_r + S_n)\nabla.\vec{N}]}_s\Sigma_{gen}$, $(\overline{-(D(\nabla.\vec{N})^2)}_s\Sigma_{gen} = -4\overline{(D\kappa_m^2)}_s\Sigma_{gen})$, C_{sg1} and C_{sg2} conditional on $\tilde{c}$-isosurfaces are shown for cases F-J in Fig. 7.13 for filter widths $\Delta = 0.8\delta_{th}$ and $\Delta = 2.4\delta_{th}$. It is evident from Fig. 7.13 that C_{sg2} remains negative throughout the flame brush for all cases and follows the qualitative behaviour of $-4\overline{(D\kappa_m^2)}_s\Sigma_{gen}$. A comparison between $\overline{((S_r + S_n)\nabla.\vec{N})}_s\Sigma_{gen}$ and $-4\overline{(D\kappa_m^2)}_s\Sigma_{gen}$ reveals that $-4\overline{(D\kappa_m^2)}_s\Sigma_{gen}$ remains the major contributor to $\overline{(S_d\nabla.\vec{N})}_s\Sigma_{gen}$ for all the flames at all values of Le, which is consistent with the expected behaviour

in the thin reaction zones regime [107]. The contribution of $\overline{((S_r+S_n)\nabla.\vec{N})}_s\Sigma_{gen}$ remains significant for the $Le<1$ cases (i.e. cases F, G and H) but its contribution remains weak in comparison to the magnitude of $-4\overline{(D\kappa_m^2)}_s\Sigma_{gen}$ in the $Le=1.0$ and $Le=1.2$ flames (i.e. cases I and J). Fig. 7.13 demonstrates that C_{sg1} remains close to $\overline{((S_r+S_n)\nabla.\vec{N})}_s\Sigma_{gen}$ for all Δ for the $Le=1.0$ flame (i.e. case I), indicating that $\overline{((S_r+S_n)\nabla.\vec{N})}_s\Sigma_{gen}$ does not play a major role in capturing the behaviour of $\overline{((S_r+S_n)\nabla.\vec{N})}_s\Sigma_{gen}$. However, there is a significant difference in magnitudes of $\overline{((S_r+S_n)\nabla.\vec{N})}_s\Sigma_{gen}$ and C_{sg1} for small values of Δ (i.e. $\Delta<\delta_{th}$) in the non-unity Lewis number flames (i.e. cases F-H and J) flames, which indicates that $\overline{(S_r+S_n)}_s\partial\overline{(N_i)}_s/\partial x_i\Sigma_{gen}$ plays a key role for small values of filter width in these flames. For large values of filter width (i.e. $\Delta\gg\delta_{th}$) C_{sg1} remains the major contributor to $\overline{((S_r+S_n)\nabla.\vec{N})}_s\Sigma_{gen}$ for all cases considered here, indicating that $\overline{(S_r+S_n)}_s\partial\overline{(N_i)}_s/\partial x_i\Sigma_{gen}$ plays progressively less important role for increasing values of Δ.

Fig. 7.13 shows that there is a significant difference between $-4\overline{(D\kappa_m^2)}_s\Sigma_{gen}$ and C_{sg2} for all the cases for small Δ, and the difference between these quantities decrease with increasing Δ. As most of the contribution of $-4\overline{(D\kappa_m^2)}_s\Sigma_{gen}$ remain unresolved for large values of Δ (i.e. $\Delta>\delta_{th}$), the subgrid curvature term C_{sg2} remains the major contributor to $-4\overline{(D\kappa_m^2)}_s\Sigma_{gen}$, indicating that $(-\overline{(D\partial N_i/\partial x_i)}_s\partial\overline{(N_i)}_s/\partial x_i\Sigma_{gen})$ plays progressively less important role for increasing values of Δ where the flame is fully unresolved. However, the contribution of $(-\overline{(D\partial N_i/\partial x_i)}_s\partial\overline{(N_i)}_s/\partial x_i\Sigma_{gen})$ remains significant for small values of Δ, where the flame is partially resolved. Fig. 7.13 further shows that the order of magnitudes of both C_{sg1} and C_{sg2} remain comparable and thus accurate modelling of C_{sg1} and C_{sg2} is necessary for precise predictions of C_{sg}. As the range of κ_m values obtained on a flame surface increases with increasing flame wrinkling, the magnitude of $-4\overline{(D\kappa_m^2)}_s$ increases with decreasing Le, which in turn leads to increasing magnitude of $-4\overline{(D\kappa_m^2)}_s$ and C_{sg2} (see Fig. 7.13). The positive contribution of C_{sg1} overcomes the negative contribution of C_{sg2} towards the unburned gas side of the flame brush for the $Le=0.34$ and $Le=0.6$ flames (i.e. cases F and G), and yields a net positive contribution of C_{sg} towards the reactant side of the flame brush (see Fig. 7.7).

The statistical behaviours of $\overline{((S_r+S_n)\nabla.\vec{N})}_s\Sigma_{gen}$ and C_{sg1} depends on the

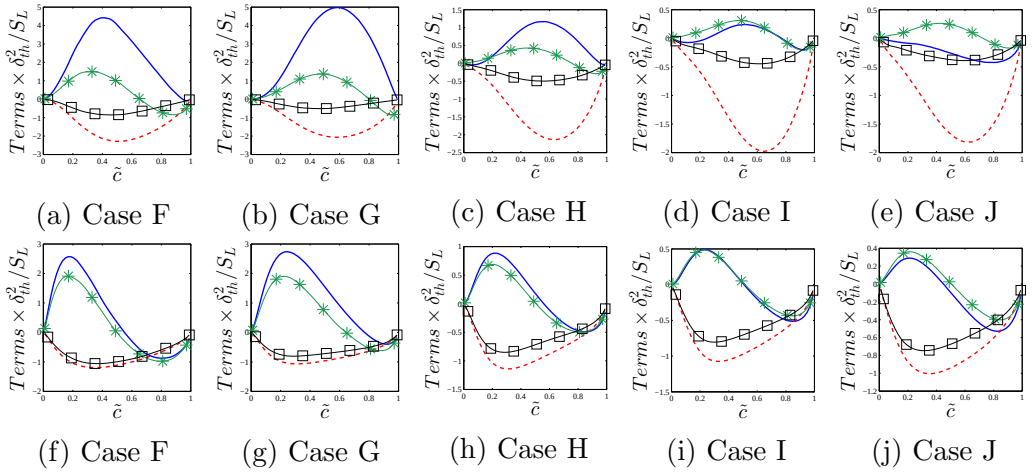

(a) Case F (b) Case G (c) Case H (d) Case I (e) Case J

(f) Case F (g) Case G (h) Case H (i) Case I (j) Case J

Figure 7.13: Variation of $\overline{((S_r+S_n)\nabla.\vec{N})}_s\Sigma_{gen}$ (——), $-4\overline{(D\kappa_m^2)}_s\Sigma_{gen}$ (– – –), C_{sg1} (—✳—), C_{sg2} (—□—) conditionally averaged in bins of $\tilde{c}$ across the flame brush for filter width $\Delta = 0.8\delta_{th}$ (top row) and $2.4\delta_{th}$ (bottom row) for cases F-J.

nature of the curvature $\kappa_m = \nabla.\vec{N}/2$ dependencies of $(S_r + S_n)$ and $|\nabla c|$, and the variation of $\overline{(\kappa_m)}_s$ across the flame brush. The correlation coefficients for $(S_r + S_n) - \kappa_m$ and $|\nabla c| - \kappa_m$ for five different c isosurfaces across the flame brush for all the cases are shown in Figs. 6.12(c) and 6.12(d) respectively. For all cases $S_t = -2D\kappa_m$ remains negatively correlated with κ_m with a correlation coefficient close to (-1.0). However, Figs. 6.12(c) and 6.12(d) demonstrate that Le significantly affects the curvature κ_m dependencies of $(S_r + S_n)$ and $|\nabla c|$. It can be seen that (S_r+S_n) and $|\nabla c|$ remain positively (negatively) correlated with κ_m for the $Le < 1.0$ ($Le > 1.0$) flames, whereas both $(S_r + S_n)$ and $|\nabla c|$ show weak curvature dependencies in the unity Lewis number flames. The positive correlations between (S_r+S_n) and κ_m, and between $|\nabla c|$ and κ_m strengthen with decreasing Le for the $Le < 1$ flames.

The variations of $\overline{(\kappa_m)}_s$ conditionally averaged in bins of $\tilde{c}$ isosurfaces for cases F-J are shown in Figs. 7.14a and d for filter widths $\Delta = 8\Delta_m \approx 0.8\delta_{th}$ and $\Delta = 24\Delta_m \approx 2.4\delta_{th}$ respectively. It is evident from Figs. 7.14a and d that $\overline{(\kappa_m)}_s$ assumes positive (negative) values towards the unburned (burned) gas side of the flame brush. For small values of Δ the surface-weighted filtered value of curvature $\overline{(\kappa_m)}_s$ approaches κ_m (i.e. $\lim_{\Delta\to 0}\overline{(\kappa_m)}_s = \kappa_m|\nabla c|/|\nabla c| = \kappa_m$) and thus the ensemble averaged value of $\overline{(\kappa_m)}_s$ remains small for small values of filter

width as the ensemble averaged value of κ_m remains negligible for statistically planar flames. The difference between the ensemble averaged values of $\overline{(\kappa_m)}_s$ and κ_m increase with increasing filter width Δ, as flame wrinkling increasingly takes place at the subgrid level. For the $Le = 1.0$ flame (i.e. case J) the combination of positive (negative) value of $\overline{(\kappa_m)}_s$ and weak $(S_r + S_n) - \kappa_m$ and $|\nabla c| - \kappa_m$ correlations gives rise to positive (negative) values of the ensemble averaged values of $\overline{((S_r + S_n)\nabla.\vec{N})}_s\Sigma_{gen}$ and C_{sg1} towards the unburned (burned) gas side of the flame brush for all values of Δ. The predominant positive $(S_r + S_n) - \kappa_m$ and $|\nabla c| - \kappa_m$ correlations give rise to positive values of the ensemble averaged values of $\overline{((S_r + S_n)\nabla.\vec{N})}_s\Sigma_{gen}$ and C_{sg1} throughout the flame brush for small values of Δ in the $Le = 0.34$, 0.6 and 0.8 flames. By contrast, negative $(S_r + S_n) - \kappa_m$ and $|\nabla c| - \kappa_m$ correlations (see Fig. 6.12(c)) give rise to negative values of the ensemble averaged values of $\overline{((S_r + S_n)\nabla.\vec{N})}_s\Sigma_{gen}$ and C_{sg1} throughout the flame brush for small values of Δ in the $Le = 1.2$ flame. These local dependencies are progressively smeared with increasing Δ because of the convolution operation associated with LES filtering process and this leads to positive (negative) values of $\overline{((S_r + S_n)\nabla.\vec{N})}_s\Sigma_{gen}$ and C_{sg1} towards the unburned (burned) gas side of the flame brush for all cases considered here, including the non-unity Lewis number flames where the curvature dependencies of $(S_r + S_n)$ and $|\nabla c|$ are particularly strong.

The dependencies of $\overline{(S_r + S_n)}_s$ and Σ_{gen} on $0.5 \times \partial\overline{(N_i)}_s/\partial x_i\Sigma_{gen}$ are likely to capture some of κ_m dependencies of $(S_r + S_n)$ and $|\nabla c|$ at small values of filter widths Δ (i.e. $\Delta < \delta_{th}$) where the flame is partially resolved. This effect is particularly prevalent in the non-unity Lewis number flames where both $(S_r + S_n)$ and $|\nabla c|$ are strongly correlated with curvature κ_m even though the flames are statistically planar in nature. As a result of this, the contribution of $\overline{(S_r + S_n)}_s\partial\overline{(N_i)}_s/\partial x_i\Sigma_{gen}$ remains close to that of $\overline{((S_r + S_n)\nabla.\vec{N})}_s\Sigma_{gen}$ for small filter widths (i.e. $\Delta < \delta_{th}$), which is reflected in the small contribution of C_{sg1} (see $\Delta = 0.8\delta_{th}$ variations in Figs. 7.13a-c and e). The correlation between the filtered quantities (e.g. dependencies of $\overline{(S_r + S_n)}_s$ and Σ_{gen} on $0.5 \times \partial\overline{(N_i)}_s/\partial x_i\Sigma_{gen}$) weaken with increasing filter width Δ due to smearing of local information. Moreover, physical processes take place increasingly at the subgrid level for $\Delta \gg \delta_{th}$, and thus $\overline{(S_r + S_n)}_s\partial\overline{(N_i)}_s/\partial x_i\Sigma_{gen}$ does not capture

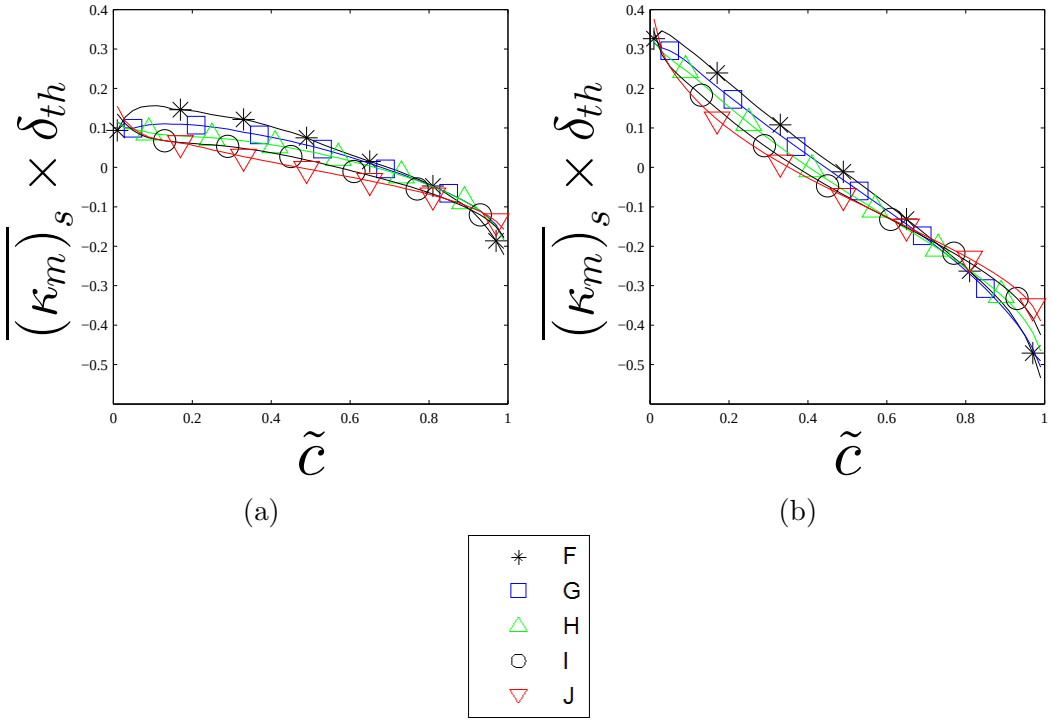

Figure 7.14: Variation of $\overline{(\kappa_m)}_s \times \delta_{th}$ with $\tilde{c}$ across the flame brush for filter widths $0.8\delta_{th}$ (a) and $2.4\delta_{th}$ (b).

the behaviour of $\overline{((S_r + S_n)\nabla.\vec{N})}_s\Sigma_{gen}$ for large filter widths (i.e. $\Delta > \delta_{th}$) in all cases considered here, including the non-unity Lewis number flames where the curvature dependencies of $(S_r + S_n)$ and $|\nabla c|$ are particularly strong. This leads to $C_{sg1} \approx \overline{((S_r + S_n)\nabla.\vec{N})}_s\Sigma_{gen}$ for $\Delta \gg \delta_{th}$ in all cases considered here (see $\Delta = 2.4\delta_{th}$ variations in Figs. 7.13f-j). It can be seen from Fig. 7.13 that the positive contribution of C_{sg1} overcomes the negative contribution of C_{sg2} towards the unburned gas side of the flame brush in the $Le = 0.34$ and $Le = 0.6$ flames, which lead to positive value of $C_{sg} = C_{sg1} + C_{sg2}$ towards the unburned gas side for all values of Δ in these cases (see Fig. 7.7). By contrast, negative values of C_{sg2} overcome the positive contributions of C_{sg1} towards the unburned gas side of the flame brush in the $Le = 0.8$, 1.0 and 1.2 flames, which lead to negative values of $C_{sg} = C_{sg1} + C_{sg2}$ throughout the flame brush in these cases (see Fig. 7.7).

The subgrid fluctuations of the surface-weighted contributions of $(S_r + S_n)$

and $\nabla.\vec{N}$ are scaled here using S_L and $(\Sigma_{gen} - |\nabla\bar{c}|)$ respectively to propose the following model for C_{sg1} as previously described in Eq. 7.27:

$$C_{sg1} = -\beta_4 \frac{(\Sigma_{gen} - |\nabla\bar{c}|)(\bar{c} - c^{\circ})S_L\Sigma_{gen}}{\exp[-a_{\Sigma}(1-\bar{c})]\bar{c}(1-\bar{c})^m} \tag{7.33}$$

where β_4, c°, a_{Σ} and m are the model parameters. The optimum values of c°, (a_{Σ}) tend to increase with decreasing (increasing) Δ for cases F-J. The κ_m dependencies of $(S_r + S_n)$ and $|\nabla c|$ are influenced by Le (see Figsures 6.12(c) and 6.12(b)), and these local dependencies appear in the resolved scale but their strength diminishes with increasing Δ due to filtering operation. As the resolved and subgrid curvature terms are closely related [29, 35], the qualitative behaviour of C_{sg1} is also affected by the curvature dependencies of displacement speed components and scalar gradient in the resolved scale, which leads to the variation of the optimum values of a_{Σ}, β_4 and c° with Le and Δ. The model parameter β_4 needs to be deceased for decreasing values of Σ_{gen} for satisfactory prediction of Eq. 7.33. The prediction of Eq. 7.33 ensemble averaged on $\tilde{c}$-isosurfaces is compared with the ensemble averaged values of C_{sg1} in Fig. 7.15 for all the cases considered here for the optimum values of β_4, c° and a_{Σ} for $\Delta = 0.8\delta_{th}$ and $\Delta = 2.4\delta_{th}$ when m is taken to equal 1.85. The optimum values of β_4, c° and a_{Σ} were estimated by calibrating the prediction of Eq. 7.33 with respect to the ensemble-averaged values of C_{sg1} obtained from DNS data and the variation of the global mean optimum values of $\beta_4/\beta_{4(Le=1.0)}$, c° and a_{Σ} with Δ/δ_{th} for all the cases are shown in Fig. 7.16. The optimum values of β_4, c° and a_{Σ} are parameterised here as:

$$\frac{\beta_4}{\beta_{4(Le=1.0)}} = \left[l_1 + \frac{(l_2 - l_1)}{1.0 + \exp[-10.0(Le-1)]^{1/2}} \right] \tag{7.34}$$

where

$$l_1 = 1.6\frac{[\Delta^{2.79} + 1.2(\Delta + \delta_{th})^{2.79}]}{1.33(\Delta + \delta_{th})^{2.79}} \tag{7.35a}$$

$$l_2 = 1.34\frac{[\Delta^{0.67} + 0.53(\Delta + \delta_{th})^{0.67}]}{[3.1\Delta^{0.67} + 0.1(\Delta + \delta_{th})^{0.67}]} \tag{7.35b}$$

$$c^{\circ} = k_1 + \frac{k_2 - k_1}{1.0 + \exp(-2.0(\Delta/\delta_{th} - 1.5))} \tag{7.35c}$$

$$a_{\Sigma} = \frac{k_4}{1.0 + \exp(-5.0(\Delta/\delta_{th}) - 1.0))} \tag{7.35d}$$

where

$$k_1 = 0.75 + \frac{0.15}{1.0 + \exp(-5.0(k_3 - 4.6))} \tag{7.36a}$$

$$k_2 = 0.65 + \frac{0.05}{1.0\exp(-9.0(k_3 - 4.0))} \tag{7.36b}$$

$$k_4 = 0.81 = \frac{0.67}{1.0 + \exp(-5.0(k_3 - 4.6))} \tag{7.36c}$$

$$k_3 = \frac{(Re_{\Delta}^{0.83} + 0.1)}{[(\Delta/\delta_{th}^{1.73}) + 0.1]} \tag{7.36d}$$

$$Re_{\Delta} = 4\rho_0 \frac{\sqrt{(2\tilde{k}/3)}}{\mu_0} \tag{7.36e}$$

Fig. 7.15 shows that Eq. 7.33 satisfactorily predicts C_{sg1} when $m = 1.85$, and the optimum values of β_4/Σ_{gen}, c° and a_{Σ} are used. According to the parameterisation given by Eq. 7.35 β_4 increases with decreasing Le, as the effects of chemical reaction strengthens with decreasing Lewis number. Moreover, β_4/Σ_{gen}, c° and a_{Σ} approach to asymptotic values for large values of Δ and turbulent Reynolds number based on LES filter width Re_{Δ}. As stated in the previous section $\overline{(D\kappa_m^2)}_s - \overline{(D\partial N_i/\partial x_i)}_s \partial\overline{(N_i)}_s/\partial x_i$ is scaled with $(\Xi - 1)^n S_L \Sigma_{gen}$ (i.e. $\overline{(D\kappa_m^2)}_s - \overline{(D\partial N_i/\partial x_i)}_s \partial\overline{(N_i)}_s/\partial x_i \sim (\Xi - 1)^n S_L \Sigma_{gen}$) where the subgrid fluctuations of D is taken to scale with S_L/Σ_{gen} (i.e. $sg(D) \sim S_L/\Sigma_{gen}$). The above relations are utilised here to propose a model for C_{sg2} in the following manner as previously shown in Eq. 7.29:

$$C_{sg2} = -\beta_5 \frac{S_L(\Xi - 1)^n \Sigma_{gen}^2}{\bar{c}(1 - \bar{c})} \tag{7.37}$$

where β_5 is a model parameter and $\bar{c}(1-\bar{c})$ is used to capture the correct qualitative behaviour of C_{sg2}. Subsequently, the predictions of these parameterisations

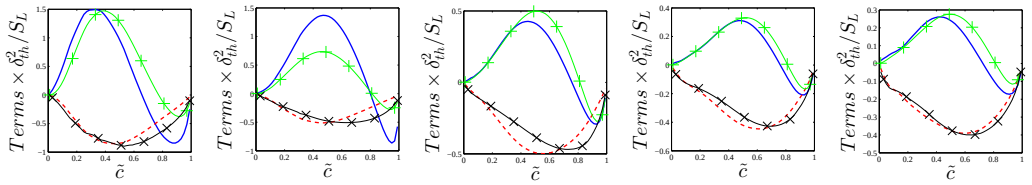

(a) Case A (b) Case B (c) Case C (d) Case D (e) Case E

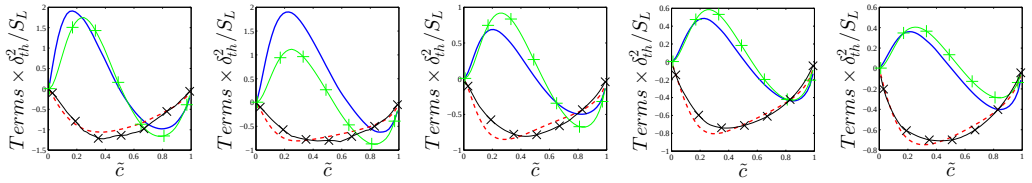

(f) Case A (g) Case B (h) Case C (i) Case D (j) Case E

Figure 7.15: Variations of C_{sg1} (——) and C_{sg2} (– – –) conditionally averaged in bins of $\tilde{c}$ across the flame brush along with the predictions of Eqs. 7.27 (—|—) and 7.29 (—×—) for filter widths Δ, $0.8\delta_{th}$ (top row) and $2.4\delta_{th}$ (bottom row).

for c° and a_{Σ} (Eq. 7.35), β_4 (Eq. 7.34) and β_5 (Eq. 7.38) are shown in Fig. 7.16. It has been found that Eq. 7.37 satisfactorily captures the behaviour of throughout the flame brush for $n = 1.0$ in all cases when a suitable value of β_5 is used. The variation of the global mean optimum values of β_5 with Δ/δ_{th} for all the cases consider here are shown in Fig. 7.16 respectively. The optimum values of β_5 has been parameterised here in the following manner:

$$\beta_5/\beta_{5(Le=1.0)} = m(Le)\left(\frac{Re_{\Delta}}{Re_{\Delta}+1.0}\right)\left\{r_1 + \frac{r_2 - r_1}{1.0 + \exp(-5.0(Re_{\Delta} - r_3))}\right\} \quad (7.38)$$

where

$$r_1 = 1.6\frac{r_4^{1.23} + 6.24}{7.17r_4^{1.23} + 0.26} \quad (7.39a)$$

$$r_2 = 1.88\frac{r_4^{2.27} + 5.92}{8.47r_4^{2.27} + 0.47} \quad (7.39b)$$

$$r_3 = 35.0\mathrm{erf}[\exp(5.3(r_4 - 1.0))] \quad (7.39c)$$

$$r_4 = \frac{\Delta}{\Delta + \delta_{th}} \quad (7.39d)$$

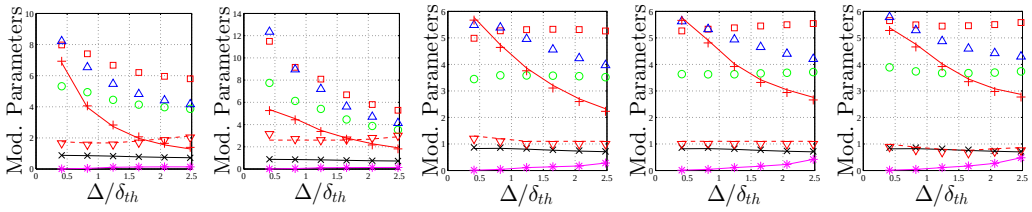

(a) Case F (b) Case G (c) Case H (d) Case I (e) Case J

Figure 7.16: Variation of model parameters β_1 (○), β_2 (□), β_3 (△), β_4/Σ_{gen} (▽) and its model given in Eq. 7.34 (--), β_5 (+) and its model give in Eq. 7.38 (–), a_Σ (∗) and its model given in Eq. 7.28b (–), c° (×) and its model given in Eq. 7.28a (–) with Δ for cases A-E.

$$m(Le) = \left(r_5 + \frac{1.0 - r_5}{1.0 + \exp[-10.0(Le - 1.0)]^{1/4}}\right) \tag{7.39e}$$

$$r_5 = 0.46\frac{r_4^{5.22} + 4.53}{8.0r_4^{5.22} + 2.96} \tag{7.39f}$$

The predictions of Eq. 7.37 ensemble averaged on $\tilde{c}$-isosurfaces are compared with ensemble averaged values of C_{sg2} in Fig. 7.15 for all cases at $\Delta = 0.8\delta_{th}$ and $\Delta = 2.4\delta_{th}$, which show that Eq. 7.37 satisfactorily predicts the statistical behaviour of C_{sg2} when $n = 1.0$ and optimum value of β_5 was used. According to Eq. 7.38 β_5 approaches to asymptotic values for large values of Δ and turbulent Reynolds number based on LES filter width Re_Δ. Equations 7.33 and 7.37 can be combined to propose a model for C_{sg} in the following manner:

$$C_{sg} = -\beta_4\frac{(\Sigma_{gen} - |\nabla\bar{c}|)(\bar{c} - c^\circ)S_L\Sigma_{gen}}{\exp[-a_\Sigma(1-\bar{c})]\bar{c}(1-\bar{c})^m} - \beta_5\frac{S_L(\Xi-1)^n\Sigma_{gen}^2}{\bar{c}(1-\bar{c})} \tag{7.40}$$

Eq. 7.40 allows for a positive contribution of C_{sg}, which is absent in the CSGCAND, CSGCANT and CSGCHAR models. The predictions of the CSGCAND, CSGCANT, CSGCHAR and CSGNEW models for $\Delta = 0.8\delta_{th}$ and $\Delta = 2.4\delta_{th}$ are compared with C_{sg} obtained from DNS in Fig. 7.17 for the optimum values of β_1, β_2, β_3, β_3 and β_5. The optimum values of β_1, β_2 and β_3 are estimated by calibrating the models based on the ensemble-averaged value of C_{sg} obtained from DNS data. The variations of the optimum values of β_1, β_2 and β_3 with Δ for cases F, G and H are also shown in Figs. 7.16 respectively. It is evident from Fig.

7.16 which demonstrates that β_1, β_2, β_3 and β_5 remain greater than unity for all cases. This is found to be consistent with the realisability analysis by Hawkes and Cant [68]. Fig. 7.16 further demonstrates that the optimum values of β_1, β_2 and β_3 change appreciably with increasing Δ, which is consistent with earlier findings [29, 35]. Moreover, optimum values of β_1, β_2 and β_3 for a given Δ vary between cases considered here (see Fig. 7.16). It is worth noting that parameterisation of the optimum values of β_1, β_2 and β_3 also yields complex relations as given earlier. However, such parameterisation is not attempted here because the CSGCAND, CSGCANT and CSGCHAR models do not capture the qualitative behaviour of C_{sg} for the $Le = 0.34$ and $Le = 0.6$ flames.

It can further be seen from Fig. 7.17 that the CSGCHAR model tends to overpredict the negative values of C_{sg} towards the unburned gas side and this behaviour becomes more prominent with increasing filter size. It is clear from Fig. 7.17 that for $\Delta = 2.4\delta_{th}$ the CSGCHAR model predicts the maximum magnitude of C_{sg} near the middle of the flame whereas the actual maximum magnitude of C_{sg} is attained slightly towards the burned gas side. The CSGCAND and CSGCANT models give comparable performance for optimum values of β_1 and β_2. However, the CSGCAND and CSGCANT models do not satisfactorily capture the qualitative behaviour of C_{sg}, and underpredict (overpredict) the magnitude of C_{sg} towards the burned gas side (middle) of the flame brush. Fig. 7.17 demonstrates that the CSGNEW model captures the qualitative behaviour of C_{sg} in a better manner than the CSGCAND and CSGCANT models and the quantitative agreement between and the CSGNEW models remain better than the CSGCAND, CSGCANT and CSGCHAR models in all cases for all values of Δ when optimum values of β_4, β_5, a_Σ and c° are used.

7.2.5 Summary

Modelling for the curvature term $\overline{(S_d \nabla . \vec{N})}_s \Sigma_{gen}$ of the generalised FSD transport equation was carried out using a simplified chemistry based DNS database of freely propagating statistically planar turbulent premixed flames with wide variation of Lewis number and turbulent Reynolds numbers. The sub grid curvature term was decomposed into components arising due to the combined reaction and

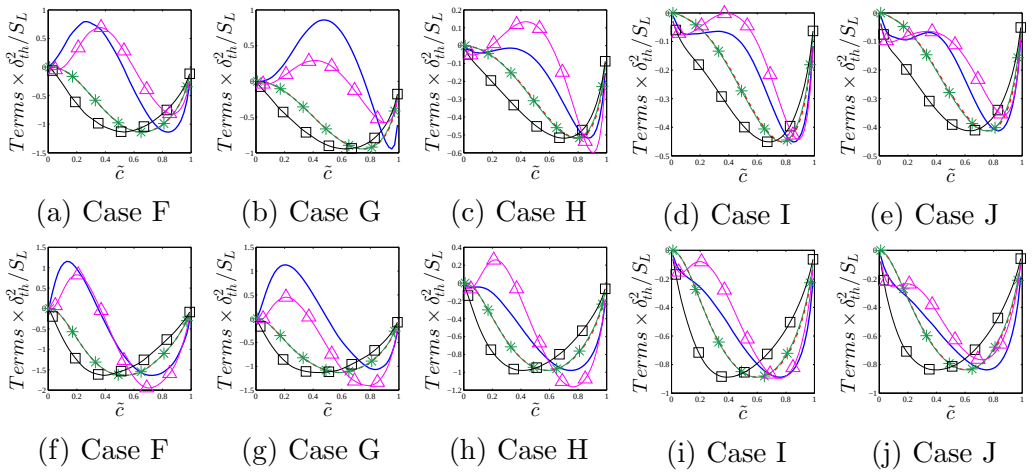

(a) Case F (b) Case G (c) Case H (d) Case I (e) Case J

(f) Case F (g) Case G (h) Case H (i) Case I (j) Case J

Figure 7.17: Variations of C_{sg} (——) conditionally averaged in bins of $\tilde{c}$ across the flame brush along with the predictions of CSGCAND (—✳—), CSGCANT (– – –), CSGCHAR (—□—), CSGNEW (—△—) for filter widths $\Delta = 0.8\delta_{th}$ (top row) and $2.4\delta_{th}$ (bottom row).

normal diffusion and tangential diffusion components of displacement speed. The unclosed FSD curvature terms were extracted from the DNS database for a wide range of filter widths and detailed physical explanations were provided for the effects of Lewis number and Reynolds number on the individual components of sub grid curvature term. This allowed models to be proposed for the components of sub grid curvature terms. When these models were combined it allowed for accurate prediction of positive values of sub grid curvature term. Existing models were found to be insufficient at predicting the sub grid curvature term especially for cases with the Lewis number to significantly smaller than unity. The model proposed in this study for the sub grid curvature was shown to be sufficiently capable of predicting C_{sg} accurately for a range of different filter widths, Lewis numbers and turbulent Reynolds numbers.

Chapter 8

Modelling the Strain Rate Term of FSD Transport Equation

8.1 RANS Modelling of Strain Rate Term

The tangential strain rate term of the Σ_{gen} transport equation (see Eq. 7.1) in the context of RANS is given as follow:

$$\underline{(a_T)}_s \Sigma_{gen} = \underline{\left[(\delta_{ij} - N_i N_j)\frac{\partial u_i}{\partial x_j}\right]}_s \Sigma_{gen} \tag{8.1}$$

The term $\underline{(a_T)}_s \Sigma_{gen}$ can be split in the following manner:

$$\underline{(a_T)}_s \Sigma_{gen} = \underbrace{[\delta_{ij} - \underline{(N_i N_j)}_s]\frac{\partial u_i}{\partial x_j}}_{S_R} \Sigma_{gen} + \underbrace{\underline{\left([\delta_{ij} - N_i N_j]\frac{\partial u_i''}{\partial x_j}\right)}_s \Sigma_{gen}}_{S_{UR}} \tag{8.2}$$

where $a_T = (\delta_{ij} - N_i N_j)\partial u_i/\partial x_j$ is the tangential strain rate acting on the flame surface and $\vec{N} = -\nabla c/|\nabla c|$ is the flame normal vector. Cant et al. [21] and Candel et al. [19] proposed models for both the resolved and the unresolved parts of the tangential strain rate contribution of the Σ_{gen} transport (i.e. S_R and S_{UR} respectively) in the context of RANS simulation. Duclos et al. [54] and Prasad and Gore [126] assessed the performances of the models for S_{UR} based on RANS simulations. Veynante et al. [152] and Veynante et al. [153] assessed the

performance of models for S_R based on experimental data. The aforementioned studies [19, 21, 54, 126, 152, 153] were carried out in the corrugated flamelets regime, where the flame thickness remains smaller than the Kolmogorov length scale. Recently, Katragadda et al. [80] carried out *a priori* analysis for existing S_R and S_{UR} models in both the corrugated flamelets and thin reaction zones regime, while accounting for a variation of Lewis number and heat release parameter. It was shown by Katragadda et al. [80] that both the dilatation rate $\partial u_i/\partial x_i$ and the relative alignment of ∇c with the fluid-dynamics strain rate $e_{ij} = 0.5(\partial u_i/\partial x_j + \partial u_j/\partial x_j)$ significantly affects the behaviour of the strain rate term $\underline{(a_T)}_s \Sigma_{gen}$. Global Lewis number Le is known to have significant influences on the both the dilatation rate and scalar-gradient alignment statistics in the turbulent premixed flames [39]. Additionally it was shown in recent studies [31, 39, 143] that the Damköhler number significantly affects the relative strength of dilatation rate in comparison to turbulent straining and alignment characteristics of ∇c with local principal strain rates. As the turbulent Reynolds number scales as $Re_t \sim Ka^2Da^2$ it is expected that the modelling of the strain rate term will also show some Re_t dependence.

8.1.1 Existing RANS Models of Strain Rate Term

The strain rate term $\underline{(a_T)}_s \Sigma_{gen}$ is often modelled by splitting it into the resolved S_R and unresolved S_{UR} components as shown earlier in Eq. 8.2. For the purpose of evaluating S_R the quantity $\underline{(N_i N_j)}_s$ requires modelling. Cant et al. [21] modelled S_R as:

$$S_R = (1.0 - n_{ij}) \frac{\partial \tilde{u}_i}{\partial x_j} \Sigma_{gen} \tag{8.3}$$

where n_{ij} takes the following form in context of RANS:

$$n_{ij} = \underline{(N_i N_j)}_s = \underline{(N_i)}_s \underline{(N_j)}_s + \frac{\delta_{ij}}{3} \left[1 - \underline{(N_k)}_s \underline{(N_k)}_s \right] \tag{8.4}$$

Veynante et al. [153] modelled $\underline{(N_i N_j)}_s$ as:

$$\underline{(N_i N_i)}_s = \frac{\sum_{k \neq i} \widetilde{(u_k'' u_k'')}}{4\underline{\widetilde{k}}} \text{ and } \underline{(N_i N_{j \neq i})}_s = \frac{\widetilde{u_i u_j}}{2k} \tag{8.5}$$

where $\underset{\sim}{k} = \underbrace{u_i'' u_i''}/2$ is the turbulent kinetic energy. Cant et al. [21] modelled for the unresolved strain rate S_{UR} in the following manner:

$$S_{UR} = 0.28\sqrt{\frac{\rho_0 \underset{\sim}{\epsilon}}{\mu_0}} \tag{8.6}$$

where ρ_0 and μ_0 are the unburned gas density and viscosity respectively, and $\underset{\sim}{\epsilon}$ is the dissipation rate of $\underset{\sim}{k}$. In the context of Coherent-Flamelet Modelling (CFM) [54] S_{UR} is modelled as:

$$S_{UR} = \alpha_0 \Gamma_k \frac{\underset{\sim}{\epsilon}}{\underset{\sim}{k}} \tag{8.7}$$

where α_0 is a model constant of the order of unity (i.e. $\alpha_0 = 2.0$) and Γ_k is the efficiency function proposed by Meneveau and Poinsot [102] which is a function of $l_t.S_L/\alpha_{T0}$ and $\sqrt{(2\underset{\sim}{k}/3)}/S_L$, with α_{T0} and l_t being the thermal diffusivity in the unburned gas and local integral length scale, respectively.

The strain rate term can additionally be decomposed as follows:

$$\underline{(a_T)}_s \Sigma_{gen} = S_R + S_{UR} = \underbrace{\underline{(\partial u_j/\partial x_j)}_s \Sigma_{gen}}_{T_D} - \underbrace{\underline{(N_i N_j \partial u_i/\partial x_j)}_s \Sigma_{gen}}_{T_N} \tag{8.8}$$

The terms T_D and $(-T_N)$ represent contributions of dilatation rate and flame normal strain rate on the Σ_{gen} transport. The dilatation term T_D can be split into the resolved and unresolved contributions as follows:

$$T_D = \underbrace{\left[\frac{\partial \underset{\sim}{u}_i}{\partial x_i}|\nabla \underline{c}|\right]}_{T_{D1}} + \underbrace{\underline{\left[\frac{\partial u_i}{\partial x_i}|\nabla c|\right]} - \left[\frac{\partial \underset{\sim}{u}_i}{\partial x_i}|\nabla \underline{c}|\right]}_{T_{D2}} \tag{8.9}$$

From the above expression it is clear that the resolved dilatation term T_{D1} can be closed if a suitable relationship between $\underline{c}$ and $\underset{\sim}{c}$ can be found. The contribution of the normal strain rate term $(-T_N)$ can be split as:

$$-T_N = \underbrace{-\underline{(N_i N_j)}_s \frac{\partial \underset{\sim}{u}_i}{\partial x_j} \Sigma_{gen}}_{T_{N1}} \underbrace{- \underline{\left(N_i N_j \frac{\partial u_i''}{\partial x_j}\right)}_s \Sigma_{gen}}_{T_{N2}} \tag{8.10}$$

The quantity $(-T_{N1})$ can be closed by using the models for $\underline{(N_i N_j)}_s$. This can be carried out as shown in Eq. 8.4 and Eq. 8.5. The modelling of the terms $(-T_{N2})$ and T_{D2} will be discussed based on *a priori* analysis using the current database in the following sections.

8.1.2 Modelling the Effects of Turbulent Reynolds Number and Lewis Number

The variations of $\underline{(a_T)}_s \Sigma_{gen}$, S_R, S_{UR}, T_D and $(-T_N)$ with $\underset{\sim}{c}$ for all the cases are shown in Figs. 8.1 a-j, which show that $\underline{(a_T)}_s \Sigma_{gen}$, S_R, S_{UR} and T_D assume positive values throughout the flame brush and the contribution of S_{UR} supersedes that of the S_R in all the cases, in accordance with earlier findings [19, 21, 29, 35, 54, 68, 126, 152, 153]. However, it can be seen from Figs. 8.1 f-j that the contribution of T_D decreases with increasing Le as the effects of $\nabla.\vec{u}$ weakens with increasing Le, while T_D is found to increase with decreasing Re_t from examining Figs. 8.1 a-e. As $\nabla.\vec{u}$ remains principally positive within the flame brush and Σ_{gen} is a positive quantity, the term T_D remains positive throughout the flame brush. However, the term $(-T_N)$ exhibits marked differences from one case to other. The term $(-T_N)$ remains negative for cases A, B, D, E, F, G and H, whereas in cases C, I and J the term is positive towards the reactants and negative towards the products. The behaviour of $T_N = \underline{(N_i N_j \partial u_i/\partial x_j |\nabla c|)} = \underline{(N_i N_j \partial u_i/\partial x_j)}_s \Sigma_{gen}$ is determined by the alignment of ∇c with local principal strain rates. For passive scalars, the scalar-gradient is known to align with the most compressive principal strain rate $e_{\gamma\gamma}$ [3, 5, 136] but recent studies [31, 34, 39, 143] have shown that ∇c may locally align with the most extensive principal strain rate $e_{\alpha\alpha}$, where the strain rate induced by chemical heat release overcomes the effects of turbulent straining.

The strain rate induced by heat release can be scaled as $a_{chem} \sim \tau S_L/\delta_{th}$ for the $Le = 1.0$ flames, whereas turbulent straining can be scaled as $a_{turb} \sim u'/l$, which gives rise to: $a_{chem}/a_{turb} \sim \tau l S_l/u'\delta_{th} \sim \tau.Da$ [31]. Alternatively the turbulent straining a_{turb} can be scaled as: $a_{turb} \sim u'/\lambda$ following Tennekes and Lumley [145] where λ is the Taylor micro-scale, which leads to: $a_{chem}/a_{turb} \sim \tau Da/Re_t^{1/2}$. The scaling $a_{chem}/a_{turb} \sim \tau l S_l/u'\delta_{th} \sim \tau.Da$ ($a_{chem}/a_{turb} \sim \tau Da/Re_t^{1/2}$) indicates

that ∇c may predominantly align with $e_{\alpha\alpha}$ to yield a positive (negative) contribution of $T_N(-T_N)$ for large Da flames. By contrast, in cases C, I and J, Da remains small (i.e. $Da < 1$), so the effects of a_{turb} overwhelm the effects of a_{chem}, giving rise to predominant alignment of ∇c with $e_{\gamma\gamma}$ for the major portion of the flame brush, except in the heat releasing zone where the effects of a_{chem} overcome the effects of a_{turb}. This is reflected in the predominantly negative (positive) value of $T_N(-T_N)$ towards the unburned gas side, and a positive (negative) value of $T_N(-T_N)$ towards the burned gas side in cases C, I and J. Chakraborty et al. [39] demonstrated that the strength of a_{chem} increases with decreasing Le and this effect is particularly strong for the $Le \ll 1$ flames due high values of heat release rate. As a result, under non-unity Lewis number conditions, the ratio a_{chem}/a_{turb} scales as $a_{chem}/a_{turb} \sim \tau f(Le).Da$ ($a_{chem}/a_{turb} \sim f(Le)Da/Re_t^{1/2}$), where $f(Le)$ is a function of Lewis number, which increases with decreasing Le [39]. This suggests that a_{chem} may become significantly strong for small values of Le, for a given value of Da. Strong a_{chem} in the Le =0.34, 0.6 and 0.8 flames overcomes the effects of a_{turb} and induces preferential alignment of ∇c with $e_{\alpha\alpha}$. This gives rise to positive (negative) values of $T_N(-T_N)$ for the major portion of the flame brush. As the strength of a_{chem} decreases with increasing Le, the extent of negative contribution of $(-T_N)$ progressively decreases with increasing Le, as evident from Figs. 8.1 h-j. Figs. 8.1 a-j show that the magnitude of $(-T_N)$ remains smaller than the magnitude of T_D for all the cases, which yields a positive contribution of $\underline{(a_T)}_s \Sigma_{gen}$ throughout the flame brush even when the contribution of $(-T_N)$ remains negative. In all the cases the a_{turb} remains of the same order of magnitude as that of a_{chem} (i.e. $a_{chem}/a_{turb} \sim f(Le)\tau Da \sim O(1)$ or $\sim f(Le)Da/Re_t^{1/2} \sim O(1)$) and thus the effect of a_{turb} is partially nullified by the effects induced by a_{chem}, which gives rise to a smaller magnitude of the normal strain rate contribution $(-T_N)$ than the magnitude of the dilatation rate term T_D.

In the study by Katragadda et al. [80] the modelling for the strain rate term of the generalised flame surface density was carried out based on the separate modelling of the strain rate components T_D and $(-T_N)$ In Eq. 8.9 the decomposition of the dilation term T_D was carried out, which gives rise to $T_{D1} = \partial \underline{u}_i/\partial x_i|\nabla c|$ and $T_{D2} = \underline{(\partial u_i/\partial x_i|\nabla c|)} - \partial \underline{u}_i/\partial x_i|\nabla c|$. As mentioned earlier the resolved dilatation

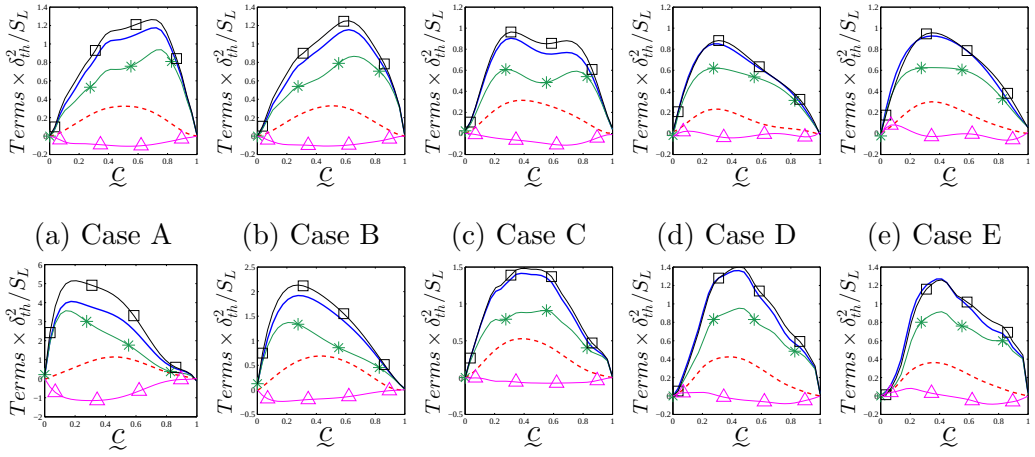

(a) Case A (b) Case B (c) Case C (d) Case D (e) Case E

(f) Case F (g) Case G (h) Case H (i) Case I (j) Case J

Figure 8.1: Variations of mean values of $\underline{(a_T)}_s \Sigma_{gen}$ (——), S_R (– – –), S_{UR} (—✳—), T_D (—□—) and $(-T_N)$ (—△—) conditional on $\underset{\sim}{c}$ for all cases.

strain rate term T_{D1} can be closed if a suitable relationship can be established between $\underset{\sim}{c}$ and $\underline{c}$.

According to Bray-Moss-Libby (BML) analysis [13], this can be carried out using the expression $\underline{c} = (1+\tau)\underset{\sim}{c}/(1+\tau\underset{\sim}{c}) + O(\gamma)$ where $O(\gamma)$ accounts for the contribution of the reacting mixture. The contribution of $O(\gamma)$ remains negligible for high Da flames but it might be non-negligible for low Da combustion. It was shown by Katragadda et al. [80] based on *a priori* analysis that the BML expression fails to predict for cases belonging to the thin reaction zones regime, where as it predicts accurately for the corrugated flamelets regime. Additionally the following model was proposed for a relationship between $\underset{\sim}{c}$ and $\underline{c}$ [80]:

$$\underline{c} = \frac{(1+\tau.g^a.Le^{-b})\underset{\sim}{c}}{(1+\tau.g^a.Le^{-b}.\underset{\sim}{c})} \tag{8.11}$$

where $g = \underset{\sim}{c''^2}/\underset{\sim}{c}(1-\underset{\sim}{c})$ is the segregation factor, and a and b are model parameters. The contribution of Le^{-b} accounts for strengthening of heat release effects for decreasing values of Le. Although the relation between $\underline{c}$ and $\underset{\sim}{c}$ according to Eq. 8.11 is empirical, one obtains the BML relation when $Le = 1.0$ and $g = 1.0$. The variation of the BML approximation and the model given in Eq. 8.11 is shown in

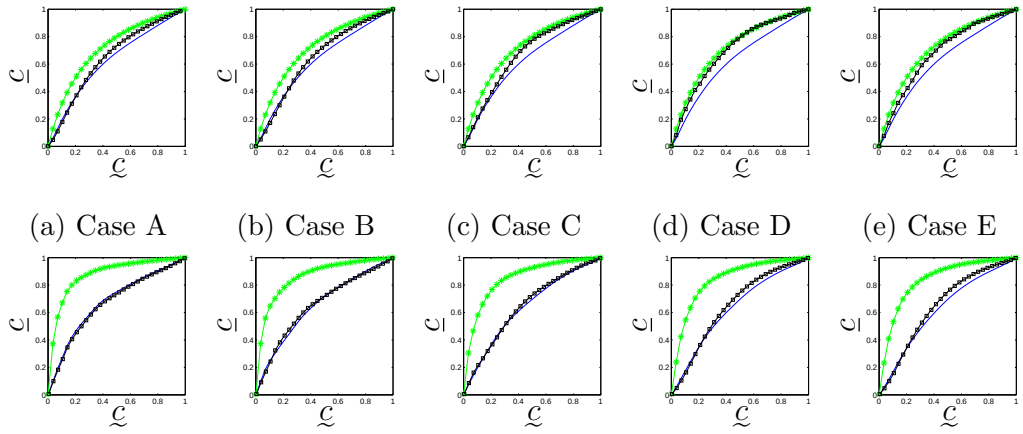

(a) Case A (b) Case B (c) Case C (d) Case D (e) Case E

(f) Case F (g) Case G (h) Case H (i) Case I (j) Case J

Figure 8.2: Variation of $\underline{c}$ with $\underset{\sim}{c}$ from DNS (——) compared with the predictions based on the BML relation (—✳—) and model given by Eq. 8.11 (—▫—).

Fig. 8.2. Based on Fig. 8.2 it has been found that Eq. 8.11 captures $\underline{c}$ variations with $\underset{\sim}{c}$ for all the flames with the model parameters set as $a = 1.5$ and $b = 0.26$. A relationship between $\underset{\sim}{c}$ and $\underline{c}$ was proposed by Kolla et al. [91], which is applicable for $Le = 1.0$, and takes the following form:

$$\underline{c} = \frac{(1 + g\underset{\sim}{c})\underset{\sim}{c} + \tau\underset{\sim}{c}^2(1 - g)}{(1 + \tau\underset{\sim}{c})} \tag{8.12}$$

The unresolved part of T_{D2} can be modelled as:

$$T_{D2} = 2\frac{B_{T2}}{(1 + Ka_L)^n}\frac{\tau S_L(\Sigma_{gen} - |\nabla\underline{c}|)}{\delta_{th}(1 - \underset{\sim}{c})^{m_1} Le^{m_2}} \tag{8.13}$$

where the model parameters $B_{T2} = 1.8$, $n = 0.35$, $m_1 = 1.8Le - 1.5$ and $m_2 = 1.845$. In Eq. 8.13 the velocity $\underset{\sim}{u}_i$ is scaled with S_L and as the term is an unresolved quantity a resolution factor $(\Sigma_{gen} - |\nabla\underline{c}|)$ is introduced. The heat release parameter accounts for the effects of changing heat release, which arises as a result of a DNS case with heat release of 3.0 instead of 4.0 for unity Le [80]. The term $(1+Ka_L)^n$ arises as a result of using a DNS case in corrugated flamelets regime [80]. Additionally $(1 - \underset{\sim}{c})^{m_1}$ is used to capture the transition point of T_{D2}

which was found to be a function of Le.

In Eq. 8.13 the dilatation rate is scaled as: $\nabla.\vec{u} \sim \tau.S_L/\delta_{th}Le^{m_2}$ as the strength of dilatation rate increases with decreasing Le, and $(1-\underset{\sim}{c})^{m_1}$ is used to adequately capture the variation of T_{D2} with $\underset{\sim}{c}$ obtained from DNS where the exponent m_1 is likely to be a function of Le, as the variation of T_{D2} with $\underset{\sim}{c}$ is skewed with a peak towards the unburned gas side for $Le = 0.34$ and 0.6 flames, whereas the peak value of T_{D2} is attained close to the middle of the flame brush (i.e. $\underset{\sim}{c} \approx 0.4$) for the flames with Le close to unity. According to Eq.8.13, the contribution of T_{D2} vanishes when the flame is fully resolved and the net contribution of $(T_{D1}+T_{D2})$ becomes identical to $(\partial u_i/\partial x_i)|\nabla c|$. The contribution of T_{D2} is similar to the dilatation rate contribution $T_{DN} = 2\underline{(\nabla.\vec{u})\rho\nabla c''.\nabla c''}$ in the $\underset{\sim}{\epsilon_c} = \underline{\rho D\nabla c''.\nabla c''}/\underline{\rho}$ transport equation [34]. The term T_{DN} is modelled as:

$$T_{DN} = 2\underline{(\nabla.\vec{u})\rho D\nabla c''\nabla c''} = \tau.A_\epsilon\underline{\rho}\underset{\sim}{\epsilon_c}S_L/\delta_{th} \tag{8.14}$$

In Eq. 8.14 A_ϵ is taken to be $A_\epsilon = B_\epsilon/(1+Ka_L)^{1/2}$ with B_ϵ being a constant of the order of unity, and $Ka_L = (\underset{\sim}{\epsilon}\delta_{th})^{1/2}/S_L^{3/2}$ the local Karlovitz number. The Ka_L dependence of A_ϵ ensures that the strength of the dilatation contribution to the $\underset{\sim}{\epsilon_c}$ transport diminishes with increasing Ka_L when combustion situation tends towards the broken reaction zones regime [107]. Following the same procedure, the model in Eq. 8.13 uses the dependence of $1/(1+Ka_L)^n$.

The predictions for the model given in Eq. 8.13 can be seen in Fig. 8.3 with T_{D2} for cases A-J. The model performs satisfactorily over the wide range of Lewis number and turbulent Reynolds numbers.

The contribution of $(-T_N)$ was shown to be decomposed into its constituents as shown in Eq. 8.10. The variation of $(-T_{N1})$ and $(-T_{N2})$ are shown in Fig. 8.4 with $\underset{\sim}{c}$ for cases A-J. The predictions for $(-T_{N1})$ according to the $\underline{(N_iN_j)}_s$ models proposed by Cant et al. [21] and Veynante et al. [153] are also shown in Fig. 8.4 for cases A-J. The predictions of $(-T_{N1})$ according to Cant et al. [21] and Veynante et al. [153] models (denoted as TN1CPB and TN1V models respectively) are shown in 8.4, which shows that the performance of both the models are comparable, and both satisfactorily predict $(-T_{N1})$ for all the flames considered here. However, the prediction of the TN1V model is closer to the

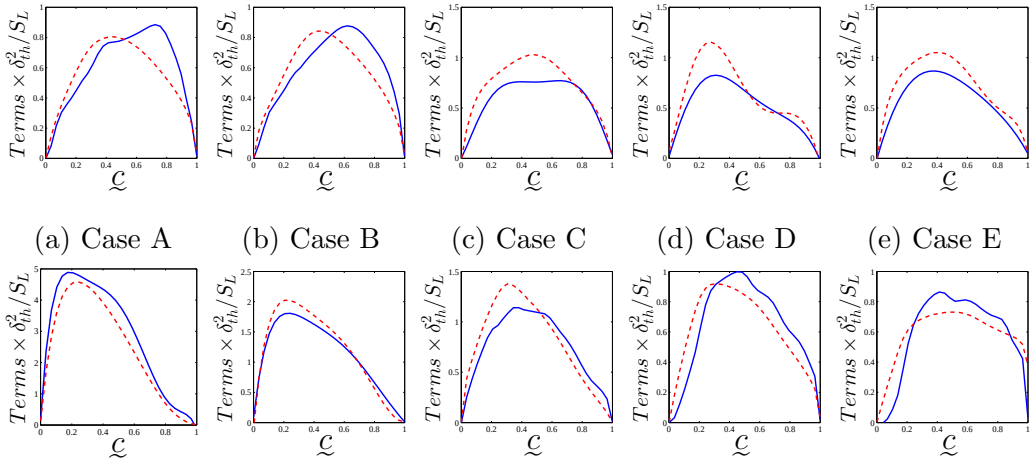

(a) Case A (b) Case B (c) Case C (d) Case D (e) Case E

(f) Case F (g) Case G (h) Case H (i) Case I (j) Case J

Figure 8.3: Variations of T_{D2} (——), Eq. 8.13 (– – –) conditional on $\underset{\sim}{c}$ for all cases.

DNS data than the TN1CPB model. The model given by Eq. 8.4 overpredicts the unresolved part of $\underline{(N_iN_j)}_s$ (i.e. $\underline{(N_iN_j)}_s - \underline{(N_i)}_s\underline{(N_j)}_s = \delta_{ij}(1 - \underline{(N_k)}_s\underline{(N_k)}_s)$) due to the assumption of isotropy of the unresolved flame normal fluctuations. However, experimental data [152, 153] suggested that the assumption of isotropy does not hold, and this result has been verified here by the overprediction of $(-T_{N1})$ by the TN1CPB model. However, $\underline{(N_iN_j)}_s$ reverts to N_iN_j when the flame is fully resolved according to the TN1CPB model, but this realisability condition is not satisfied by the model given by Eq. 8.5.

It has been discussed earlier that the behaviour of $(-T_{N2})$ is governed by the alignment of ∇c with local principal fluid-dynamic strain rates. The effects of ∇c alignment with $e_{\gamma\gamma}$ due to turbulent straining a_{turb} on the term $(-T_{N2})$ can be scaled as: $C_1\underset{\sim}{\epsilon}/\underset{\sim}{k}\Sigma_{gen}$, where C_1 is a model parameter. On the other hand, the effects of the ∇c alignment with $e_{\alpha\alpha}$ due to the strain rate induced by chemical heat release a_{chem} on the term $(-T_{N2})$ can be scaled as: $-C_2 f(Le)\tau S_L\Sigma_{gen}/\delta_{th}$, where $f(Le)$ is a function of Le which increases with decreasing Le and the model parameter C_2 should decrease with Ka_L because the effects of a_{chem} are likely to weaken progressively with increasing Ka_L [34]. Combining the above scalings,

the following model for $(-T_{N2})$ can be proposed:

$$(-T_N) = \frac{\widetilde{\epsilon}}{\widetilde{k}}(C_1 - \tau C_2 Da_L)\Sigma_{gen} \tag{8.15}$$

where $Da_L = \widetilde{k}S_L/\widetilde{\epsilon}\delta_{th}$ is the local Damköhler number and C_1 is given as:

$$C_1 = 0.4 + 0.1\text{erf}[(Re_L + 1)/12] \tag{8.16}$$

while the following two parameterisations are proposed for the model parameter C_2 in Eq. 8.15:

$$C_2 = \frac{0.47[1 - \underline{(N_k)}_s\underline{(N_k)}_s]\widetilde{c}^{0.3Le^2}}{(1 + Ka_L)^b} f(Le) \tag{8.17a}$$

$$C_2 = \left(0.7 - 0.55\text{erf}\left[\frac{Re_L + 1}{30}\right]\right) \frac{0.47[1 - \underline{(N_k)}_s\underline{(N_k)}_s]\widetilde{c}^{0.3Le^2}}{(1 + Ka_L)^{0.35}} f(Le) \tag{8.17b}$$

where b in Eq. 8.17a is given as:

$$b = 0.12 + 0.7\text{erf}\left[\frac{LeRe_L + 1}{60}\right]^{0.8} \tag{8.18}$$

and $f(Le)$ from Eq. 8.15 is defined as follows:

$$f(Le) = [\exp(-Le^{-0.945}) - 1] \tag{8.19}$$

In Fig. 8.4 the predictions based on Eq. 8.15 using C_2 from Eq. 8.17a and Eq. 8.17b are compared with $(-T_{N2})$ from DNS, where the new parameterisations perform adequately for the range of turbulent Reynolds numbers and Lewis numbers.

Using $T_{N1} = -n_{ij}\partial\widetilde{u}_i/\partial x_j\Sigma_{gen}$ (see Eq. 8.4) and the models given by Eqs.

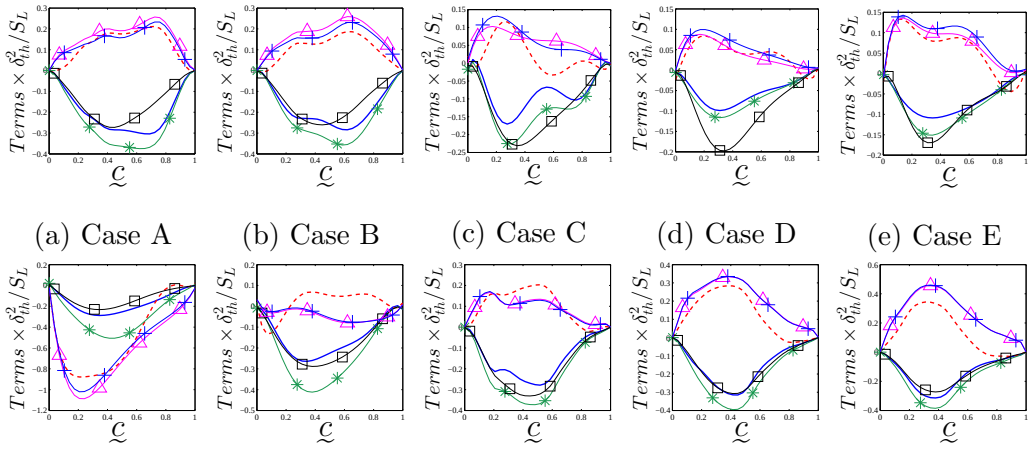

(a) Case A (b) Case B (c) Case C (d) Case D (e) Case E

(f) Case F (g) Case G (h) Case H (i) Case I (j) Case J

Figure 8.4: Variations of $(-T_N1)$ (——) and $(-T_N2)$ (– – –) with $\underset{\sim}{c}$ across the flame brush for cases A-J along with the predictions of TN1CPB given by Eq. 8.4 (—✳—), TN1V given by Eq. 8.5 (—▫—) and the newly proposed models for $-T_{N2}$ given by Eq. 8.15 using C_2 given by Eq. 8.17a (—△—) and C_2 given by Eq. 8.17b (—+—).

8.13 and 8.15 yields the following expression:

$$\underline{(a_T)}_s\Sigma_{gen} = 2\frac{B_{T2}}{(1+Ka_L)^n}\frac{\tau S_L(\Sigma_{gen}-|\nabla\underline{c}|)}{\delta_{th}(1-\underset{\sim}{c})^{m_1}Le^{m_2}} + \frac{\underset{\sim}{\epsilon}}{\underset{\sim}{k}}(C_1-\tau C_2 Da_L)\Sigma_{gen} + \frac{\partial \underset{\sim}{u_i}}{\partial x_j}(\delta_{ij}|\nabla\underline{c}|-n_{ij}\Sigma_{gen}) \tag{8.20}$$

It should be noted that the second term in the right hand side of Eq. 8.20 involves $1-\underline{(N_k)}_s\underline{(N_k)}_s$, which ensures that this term vanishes when the flow becomes laminar (i.e. $\underline{(N_k)}_s\underline{(N_k)}_s = 1.0$). Moreover, the first term in the right hand side of Eq. 8.20 also becomes zero for laminar conditions and therefore, $(a_T)_s\Sigma_{gen}$ becomes equal to $(\delta_{ij}-N_iN_j)\partial u_i/\partial x_j|\nabla c|$ as expected. The prediction of $\underline{(a_T)}_s\Sigma_{gen}$ according to Eq. 8.20 based on the parameterisation shown in Eqs. 8.17a and 8.17b in Figs. 8.5 a-j for cases A-J along with the predictions of the models proposed by Cant et al. [21] (i.e. CPB model) and CFM methodology [54, 152, 153], where S_R and S_{UR} are modelled by Eqs. 8.4 and 8.6 in the context of the CPB model and by Eqs. 8.5 and 8.7 in the context of the CFM

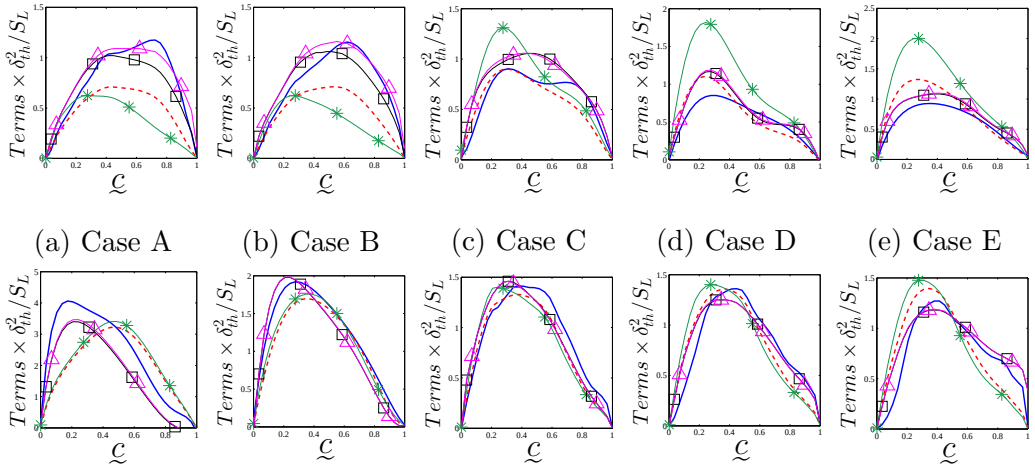

(a) Case A (b) Case B (c) Case C (d) Case D (e) Case E

(f) Case F (g) Case G (h) Case H (i) Case I (j) Case J

Figure 8.5: Variations of $\underline{(a_T)}_s \Sigma_{gen}$ (——) with $\underset{\sim}{c}$ across the flame brush for cases A-J along with the predictions of CPB (– – –), CFM (—✳—) and the newly proposed models given by Eq. 8.20 using C_2 given by Eq. 8.17a (—□—) and C_2 given by Eq. 8.17b (—△—).

model, respectively. The CFM model is found to show a peak at $\underset{\sim}{c} \approx 0.3$ which is qualitatively similar to cases C-E, H-J, while in cases A and B the peak $\underline{(a_T)}_s \Sigma_{gen}$ occurs towards the products (i.e. $\underset{\sim}{c} \approx 0.6$) and in cases F and G the peak $\underline{(a_T)}_s \Sigma_{gen}$ occurs towards the reactants (i.e. $\underset{\sim}{c} \approx 0.2$). Although the CFM model performs adequately for cases F-J, its found that in cases A, B, D and E it fails to capture as well as the other models. From Fig. 8.5 the model CPB can be seen predict correct qualitative for most of the cases whereas in cases A and B it fails to capture correct magnitude of $\underline{(a_T)}_s \Sigma_{gen}$. The new model performs well for all the cases and the difference between the two parameterisations for C_2 can be seen to make very little difference. The newly proposed model given by Eq. 8.20 with c_2 given by Eqs. 8.17(a and b) also captures the behaviours of $\underline{(a_T)}_s \Sigma_{gen}$ satisfactorily for the flames representing the corrugated flamelets regime and different values of τ, which is demonstrated in appendix B.

8.1.3 Summary

The modelling of the tangential strain rate term of the generalised FSD transport equation, in context of RANS, has been addressed with *a priori* analysis using a DNS database of varying Lewis number and turbulent Reynolds numbers. It was found that the dilatation rate contribution to the generalised FSD transport equation strengthens with decreasing Lewis number. The contribution of the normal strain rate contribution was found to increase with decreasing Lewis number and with turbulent Reynolds number. Additionally the behaviour of the normal strain rate term was seen to be predominantly negative for cases where a_{chem} dominates over a_{turb} (e.g. cases with $Le \gg 1.0$ and cases F and G), while in the remaining cases it was found to be positive towards the reactants side of the flame brush and negative towards the burnt gas side. This analysis gave way to the modelling of the unresolved normal strain rate and dilatation rate contributions, explicitly. The performance of the new model was compared with the predictions of (CPB and CFM models), using *a priori* DNS analysis, and the performances of the new model has been found to be either better than or comparable to the existing models.

8.2 LES Modelling of Strain Rate Term

The tangential strain rate term of LES generalised FSD Σ_{gen} (see Eq. 6.1) transport equation is given as follows:

$$\overline{(a_T)}_s\Sigma_{gen} = \overline{\left[(\delta_{ij} - N_iN_j)\frac{\partial u_i}{\partial x_j}\right]}_s \Sigma_{gen} \tag{8.21}$$

In the following sections an introduction to the existing modelling strategy for the strain rate term $\overline{(a_T)}_s\Sigma_{gen}$ is presented and a detailed discussion is carried out on the behaviour of the strain rate term, in context of LES. Based on this analysis a new model is presented for the subgrid strain rate term, which is then utilised to compare the performances of existing models for $\overline{(a_T)}_s\Sigma_{gen}$. This is followed by a summary of the model performances.

8.2.1 Existing LES Models of Strain Rate Term

For the purpose of modelling $\overline{(a_T)}_s\Sigma_{gen}$ is often decomposed in the following manner [22, 35, 66, 67, 68]:

$$\overline{(a_T)}_s\Sigma_{gen} = S_m + S_{hr} + S_{sg} \tag{8.22}$$

where S_m, S_{hr} and S_{sg} are contribution arising from the resolved velocity gradient, heat release and subgrid processes. The term S_m can be defined in the following manner [22, 28, 35, 66, 67, 68, 131]:

$$S_m = \left[\delta_{ij} - \overline{(N_iN_j)}_s\right]\frac{\partial\tilde{u}_i}{\partial x_j}\Sigma_{gen} \tag{8.23}$$

It can be seen from Eq. 8.23 that $\overline{(N_iN_j)}_s$ needs to be modelled in order to evaluate S_m. Hawkes [66] and Hawkes and Cant [67, 68] argued that S_{hr} can be taken to be the resolved part of the following expression:

$$S_{hr} = \text{Res}\left[\overline{\left((\delta_{ij} - N_iN_j)\frac{\partial[(u_i)_s - \tilde{u}_i]}{\partial x_j}\right)_s}\Sigma_{gen}\right] \tag{8.24}$$

where Res$\{Q\}$ denotes the resolved part of a general quantity Q. Under flamelet assumption the ith component of flame surface-filtered velocity component $\overline{(u_i)}_s$ and Favre filtered velocity component $\tilde{u}_i$ are given as [66]:

$$\overline{(u_i)}_s = \overline{(u_i)}_R + K\left[\overline{(u_i)}_P - \overline{(u_i)}_R\right] \tag{8.25a}$$

$$\tilde{u}_i = \overline{(u_i)}_R\tilde{c}\left[\overline{(u_i)}_P - \overline{(u_i)}_R\right] \tag{8.25b}$$

where K is a parameter which relies on a choice of the c isosurface, which represents the flame surface [22, 66, 67, 68]. Using Eqs. 8.25(a and b) it is possible to write:

$$\overline{(u_i)}_s - \tilde{u}_i = (K - \tilde{c})\left[\overline{(u_i)}_P - \overline{(u_i)}_R\right] \tag{8.26}$$

where the $\left[\overline{(u_i)}_P - \overline{(u_i)}_R\right]$ can be modelled as [22, 36, 66] (previously shown in Eq. 6.49):

$$[\overline{(u_i)}_P - \overline{(u_i)}_R] \approx -\tau \frac{\overline{(\rho S_d)}_s}{\rho_0} \overline{(N_i)}_s \tag{8.27}$$

If the above expression is substituted into Eq. 8.26 yields:

$$\overline{(u_i)}_s - \tilde{u}_i = (K - \tilde{c}) \frac{\overline{(\rho S_d)}_s}{\rho_0} \overline{(N_i)}_s \tag{8.28}$$

Comparing the above equation with Eq. 8.24 yields the following expression for S_{hr}, which was proposed by Hawkes [66] and Hawkes and Cant [68]:

$$S_{hr} = -\tau (K - \tilde{c}) \frac{\overline{(\rho S_d)}_s}{\rho_0} \frac{\partial \overline{(N_i)}_s}{\partial x_i} \Sigma_{gen} \tag{8.29}$$

In Eq. 8.29 K is taken to be equal to the local value of c, following previous analysis in [22, 35]. Rearranging Eq. 8.22 results in the following expression for the subgrid strain rate term S_{sg}:

$$S_{sg} = \overline{(a_T)}_s - (S_m)_M - S_{hr} \tag{8.30}$$

where $(S_m)_M$ is a modelled expression for the mean strain rate given as:

$$(S_m)_M = \left((\delta_{ij} - n_{ij}) \frac{\partial \tilde{u}_i}{\partial x_j} \right) \Sigma_{gen} \tag{8.31}$$

where, as stated before, n_{ij} refers to the modelled expression of $\overline{(N_i N_j)}_s$ which is carried out by extending the RANS model proposed by Cant et al. [21] in the following manner:

$$n_{ij} = \overline{(N_i)}_s \overline{(N_j)}_s + \frac{\delta_{ij}}{3} [1 - \overline{(N_k)}_s \overline{(N_k)}_s] \tag{8.32}$$

Based on Eq. 8.30 it can be argued that the modelling of S_{sg} relies on the models used for S_m and S_{hr}. The modelling for the subgrid strain rate term S_{sg}

is typically modelled in the following manner [22, 35, 66, 67, 68]:

$$S_{sg} = \Phi\Gamma \left(\frac{u'_\Delta}{\Delta}\right) \Sigma_{gen} \tag{8.33}$$

where u'_Δ is the subgrid turbulent velocity fluctuation, Δ is the LES filter width, Φ is a model parameter and Γ is an efficiency function which is a function of $\sqrt{(\tilde{k})}/S_L$ and $\Delta S_L/\alpha_{T0}$ [2, 22, 35, 48, 66, 67, 68]. The efficiency function proposed by Charlette et al. [48] (given by: Γ_{CHAR})and Angelberger et al. [2] (given by: Γ_{ANG}) were used by Hawkes [66] and Hawkes and Cant [67, 68] in order to model for the subgrid strain rate term S_{sg}. Charlette et al. [48] proposed the following expression for the efficiency function Γ_{CHAR}:

$$\begin{aligned}\log_{10}(\Gamma_{CHAR}) = &- \frac{\exp(-(s+0.4))}{s+0.4} \\ &+ [1-\exp(-(s+0.4))]\left(\sigma_1\left(\frac{u'_\Delta}{S_L}\right)s - 0.11\right)\end{aligned} \tag{8.34}$$

where

$$S = \log_{10}\frac{\Delta S_L}{\alpha_{T0}} \tag{8.35a}$$

$$\sigma_1\left(\frac{u'_\Delta}{S_L}\right) = \frac{2}{3}\left\{1-\exp\left[-\left(\frac{u'_\Delta}{S_L}\right)\right]\right\} \tag{8.35b}$$

The efficiency function Γ_{ANG} by Angelberger et al. [2] is given as:

$$\Gamma_{ANG} = 0.75\exp\left(\frac{1.2}{(u'/S_L)^{0.3}}\right)\left(\frac{\Delta S_L}{\alpha_{T0}}\right)^{2/3} \tag{8.36}$$

In the following sections the performance of Eqs. 8.35 and 8.36 will be compared based on the S_{sg} extracted from explicitly filtered DNS data.

8.2.2 Behaviour of the Strain Rate Term

8.2.2.1 Effects of Turbulent Reynolds Number

The variations of the mean values of $\overline{(a_T)}_s\Sigma_{gen}$, S_m, S_{hr} and S_{sg} conditional on $\tilde{c}$ values for $\Delta = 0.8\delta_{th}$ and $\Delta = 2.4\delta_{th}$ for cases A-E are shown in Fig. 8.6. The filter sizes $\Delta = 0.8\delta_{th}$ and $\Delta = 2.4\delta_{th}$ are representative of the situations where the flame is partially resolved and fully unresolved, however in the actual analysis the filter widths $0.4\delta_{th}$, $0.8\delta_{th}$, $1.2\delta_{th}$, $1.6\delta_{th}$, $2.0\delta_{th}$ and $2.4\delta_{th}$ were used. It is evident from Fig. 8.6 that the contributions of $\overline{(a_T)}_s\Sigma_{gen}$ and S_m remain positive throughout the flame brush for all cases considered here. The maximum magnitude of $\overline{(a_T)}_s\Sigma_{gen}$ decreases with increasing Δ as the weighted averaging process associated with LES filtering acts to decrease the peak magnitude of $\overline{(a_T)}_s\Sigma_{gen}$ with increasing Δ. It can further be seen from Fig. 8.6 that the relative contribution of S_m (S_{sg}) to $\overline{(a_T)}_s\Sigma_{gen}$ decreases (increases) with increasing Δ as the physical process occur increasingly at the subgrid scale with an increase in filter width. The mean value of the strain rate term due to heat release S_{hr} conditional on $\tilde{c}$ remains predominantly negative throughout the flame brush for the range of filter widths considered in this analysis. The contribution of S_{hr} can be compared to the resolved part of the FSD curvature term given by:

$$C_{mean} = \mathrm{Res}\left\{\overline{\left((\delta_{ij} - N_iN_j)\frac{\partial(u_{iP} - u_{iR})|_s}{\partial x_j}\right)_s}\Sigma_{gen}\right\} \tag{8.37}$$

It was shown in several previous analyses [22, 28, 35, 66, 67, 68, 82, 84] that C_{mean} remains predominantly negative throughout the flame brush for unity Lewis number flames (see §7.2.2.1 and 7.2.2.2). The term S_{hr} behaves like C_{mean} with a different propagation velocity (i.e. $-\tau(\kappa - \tilde{c}) \times \overline{(\rho S_d)}_s/\rho_0$ instead of $\overline{(S_d)}_s$ so the behaviour of S_{hr} remains qualitatively similar to that of C_{mean}. The contribution of S_{sg} remains positive throughout the flame brush for all cases considered here. For these cases the peak magnitude location for S_{sg} remains skewed slightly towards the burned gas side of the flame brush for small values of Δ (i.e. $\Delta < \delta_{th}$) but the peak value location shifts towards the middle of the flame brush (i.e. $\tilde{c} \approx 0.5$) with increasing filter width Δ.

The decomposition of the tangential strain rate term $\underline{(a_T)}_s\Sigma_{gen}$ as shown in

Eq. 8.8, for RANS, can be applied to LES formulation in the following manner:

$$\overline{(a_T)}_s\Sigma_{gen} = \underbrace{\overline{\nabla.\vec{u}|\nabla c|}}_{T_D} - \underbrace{\overline{(N_iN_j\partial u_i/\partial x_j)|\nabla c|}}_{T_N} \tag{8.38}$$

where T_D and $(-T_N)$ are the dilatation and normal strain rate contributions to $\overline{(a_T)}_s\Sigma_{gen}$. The variations of the mean values of T_D and $(-T_N)$ conditional on $\tilde{c}$ values for $\Delta = 0.8\delta_{th}$ and $\Delta = 2.4\delta_{th}$ for cases A-E are also shown in Fig. 8.7. It is evident that T_D remains positive throughout the flame brush for all filter widths. As dilatation rate $\nabla.\vec{u}$ remains predominantly positive throughout the flame brush, the contribution of T_D remains positive for all cases throughout the flame brush. The contribution of $(-T_N)$ remains positive (negative) towards the unburned (burned) gas side of the flame brush for all filter widths. In order to explain this behaviour it is worth expressing $(-T_N)$ in the following manner:

$$(-T_N) = -\overline{(e_{\alpha\alpha}\cos^2\alpha + e_{\beta\beta}\cos^2\beta + e_{\gamma\gamma}\cos^2\gamma)|\nabla c|} \tag{8.39}$$

where $e_{\alpha\alpha}$, $e_{\beta\beta}$ and $e_{\gamma\gamma}$ are the most extensive, intermediate and the most compressive principal strain rates, and their angles with ∇c are given by α, β and γ respectively. The ∇c aligns with $e_{\alpha\alpha}$ with the effects of strain rate induced by chemical reaction a_{chem} overcome the effects of turbulent straining a_{turb} and *vice versa* [31, 39]. The strain rate induced by chemical heat release is expected to scale as $a_{chem} \sim \tau f(Ka)S_L/\delta_{th}$ where $f(Ka)$ is expected to decrease with increasing Karlovitz number Ka, as the combustion starts to show attributes of the broken reaction zones regime where the effects of heat release are expected to be weak. Following Meneveau and Poinsot [102] the turbulent strain rate a_{turb} can be scaled as: $a_{turb} \sim u'/l$, which leads to the following scaling $a_{chem}/a_{turb} \sim \tau f(Ka)Da \sim f(Re_t^{1/2}/Da)Da$. Alternatively the turbulent straining a_{turb} can be scaled as: $a_{turb} \sim u'/\lambda$ following Tennekes and Lumley [145] where λ is the Taylor microscale, which leads to: $a_{chem}/a_{turb} \sim \tau f(Re_t^{1/2}/Da)Da/Re_t^{1/2} \sim \tau f(Ka)/Ka$. The above scaling arguments suggest that the strength of a_{chem} with respect to a_{turb} increases with increasing Damköhler number Da for a given value of turbulent Reynolds number.

Analysis by Chakraborty and Swaminathan [31], Chakraborty et al. [39] demon-

strated that ∇c indeed predominantly aligns with $e_{\alpha\alpha}$ for $Da \gg 1$ flames whereas ∇c aligns with $e_{\gamma\gamma}$ in $Da < 1$ flames with comparable value of Re_t. Both the scaling $a_{chem}/a_{turb} \sim \tau f(Ka)Da$ and $a_{chem}/a_{turb} \sim \tau f(Re_t^{1/2}/Da)Da/Re_t^{1/2} \sim \tau f(Ka)/Ka$ suggest that an increase in $Ka \sim Re_t^{1/2}/Da$ for a given value of Da (e.g. cases A, C and E) results in weakening the effects of a_{chem} in comparison to a_{turb} . This in turn leads to an increasing tendency of ∇c alignment with $e_{\gamma\gamma}$ with increasing Ka when Da is held constant as in cases A, C and E. In cases A and C, ∇c predominantly aligns with $e_{\alpha\alpha}$ however the extent of this alignment decreases from A to C. This predominant alignment of ∇c with $e_{\alpha\alpha}$ for cases A and C leads to negative contribution of $(-T_N)$. In case E, ∇c predominantly aligns with $e_{\gamma\gamma}$ in the unburned gas region but the effects of a_{chem} overcome the effects of a_{turb} in the regions of intense heat release and ∇c starts to align with $e_{\alpha\alpha}$ in the reaction zone in case E. Thus $(-T_N)$ assume positive (negative) values towards the unburned (burned) gas sides of the flame brush in case E. The scaling $a_{chem}/a_{turb} \sim f(Ka)Da/Re_t^{1/2}$ indicates that the strength of a_{chem} weakens in comparison to a_{turb} with decreasing value of $\tau Da/Re_t^{1/2}$. The quantity $\tau Da/Re_t^{1/2}$ assumes values equal to 0.96, 0.55 and 0.49 for cases B, C and D respectively when the statistics were extracted. This gives rise to greater extent of ∇c alignment with $e_{\gamma\gamma}$ in case D (case C) than in case C (case B). This leads to predominantly negative contribution of $(-T_N)$ in cases B and C, whereas $(-T_N)$ assumes positive (negative) values towards the unburned (burned) gas sides of the flame brush in case D as the effects of a_{chem} overcome the effects of a_{turb} in the regions of intense heat release and starts to align with $e_{\alpha\alpha}$ in the reaction zone. As both $\tau Da/Re_t^{1/2}$ and τDa remain of the order of unity, the effects of a_{chem} is almost nullified by a_{tub} and as a result the magnitudes of $(-T_N)$ remains negligible in comparison to that of T_D for all cases considered here. Thus the predominant positive contribution of T_D leads to positive contributions of $\overline{(a_T)}_s\Sigma_{gen}$, S_m, and S_{sg}. The magnitudes of T_D and $(-T_N)$ decrease with increasing Δ due to weighted-averaging process involved in LES filtering.

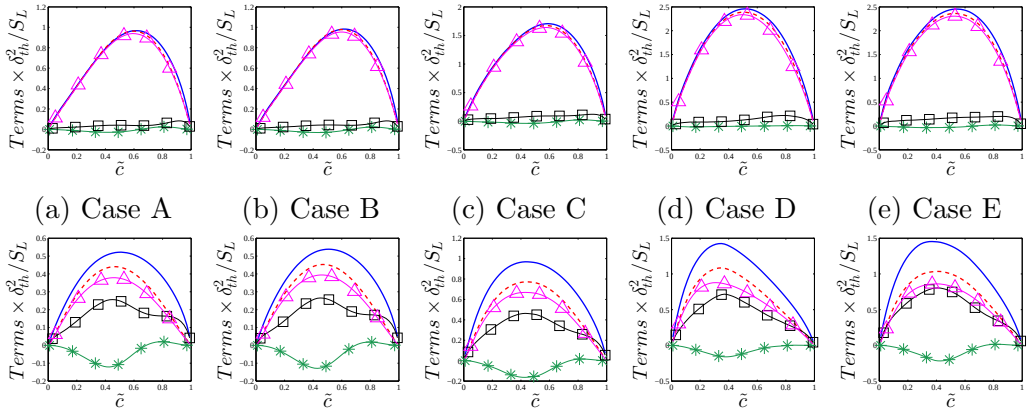

(a) Case A (b) Case B (c) Case C (d) Case D (e) Case E

(f) Case A (g) Case B (h) Case C (i) Case D (j) Case E

Figure 8.6: Variation of mean values of $\overline{(a_T)}_s\Sigma_{gen}$ (——), S_m (– – –), $(S_m)_M$ (—△—), S_{hr} (—✱—) and S_{sg} (—□—) conditional on $\tilde{c}$ for filter widths Δ of $0.8\delta_{th}$ (top row) and $2.4\delta_{th}$ (bottom row).

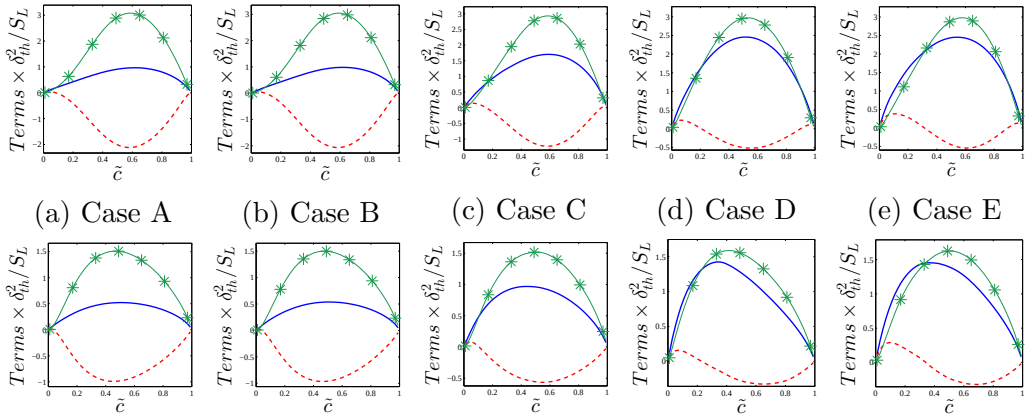

(a) Case A (b) Case B (c) Case C (d) Case D (e) Case E

(f) Case A (g) Case B (h) Case C (i) Case D (j) Case E

Figure 8.7: Variation of mean values of $\overline{(a_T)}_s\Sigma_{gen}$ (——), T_D (—✱—), $(-T_N)$ (– – –) across the flame brush for filter widths Δ of $0.8\delta_{th}$ (top row) and $2.4\delta_{th}$ (bottom row).

8.2.2.2 Effects of Lewis Number

The variations of the mean values of $\overline{(a_T)}_s\Sigma_{gen}$, S_m, S_{hr} and S_{sg} conditional on $\tilde{c}$ values for $\Delta = 0.8\delta_{th}$ and $\Delta = 2.4\delta_{th}$ for cases F-J in Fig. 8.8. It is evident from Fig. 8.8 that the contributions of $\overline{(a_T)}_s\Sigma_{gen}$ and S_m remain positive throughout the flame brush for all cases considered here. The maximum magnitude of

$\overline{(a_T)}_s\Sigma_{gen}$ decreases with increasing Δ as the weighted averaging process associated with LES filtering takes place over a larger volume, which acts to decrease the peak magnitude of $\overline{(a_T)}_s\Sigma_{gen}$ with increasing Δ. It can further be seen from Fig. 8.8 that the relative contribution of S_m (S_{sg}) to $\overline{(a_T)}_s\Sigma_{gen}$ increases with increasing Δ as the physical process occur increasingly at the subgrid scale with the increase in filter width. It can be seen from Fig. 8.8 that the contribution of S_{hr} remains negative in the middle of the flame brush, although small positive values can be discerned on both unburned and burned gas sides. It is evident from Fig. 8.8 that the magnitude of S_{hr} increases with decreasing Le due to high magnitudes of $\overline{(\rho S_d)_s}$ for small values of Le as demonstrated by Chakraborty and Cant [40], in the context of RANS. The contribution of S_{sg} remains positive throughout the flame brush for the $Le \approx 1.0$ (i.e. $Le = 0.8, 1.0$ and 1.2) cases considered here but S_{sg} assumes small negative values towards the burned gas side of the flame brush for the $Le = 0.34$ flame. Moreover, the peak magnitude of S_{sg} in the $Le \approx 1.0$ (i.e. $Le = 0.8, 1.0$ and 1.2) cases is obtained near the middle of the flame brush. For these cases the peak magnitude location remains skewed slightly towards the burned gas side of the flame brush for small values of Δ (i.e. $\Delta < \delta_{th}$) but the peak location shifts towards the middle of the flame brush (i.e. $\tilde{c} \approx 0.5$) with increasing filter size Δ. By contrast, the peak magnitude of S_{sg} for the $Le = 0.34$ case takes place towards the middle of the flame brush for small filter widths (i.e. $\Delta < \delta_{th}$) but for $\Delta > \delta_{th}$ the location of the peak shifts towards the unburned gas side of the flame brush (i.e. $\tilde{c} < 0.5$).

The variations of mean T_D and $(-T_N)$ conditional on $\tilde{c}$ values for $\Delta = 0.8\delta_{th}$ and $\Delta = 2.4\delta_{th}$ for cases F-J are shown in Fig. 8.9. Based on the Fig. 8.9 it is evident that T_D remains positive throughout the flame for all filter widths and all Lewis numbers. As mentioned for the cases A-E, the dilatation rate $\nabla.\vec{u}$ remains predominantly positive throughout the flame brush, the contribution of T_D thus remains positive for all cases examined. The contribution of $(-T_N)$ remains negative for cases where the $Le \ll 1.0$ (i.e. cases F and G) and when the $Le \approx 1.0$ it behaves as described for cases A-E, where a positive (negative) prediction occurs towards the reactants (products) side of the flame brush. As in the cases A-E this can be explained using the expression for $(-T_N)$ in Eq. 8.39, Chakraborty et al. [39] demonstrated that the extent of ∇c alignment with $e_{\alpha\alpha}$

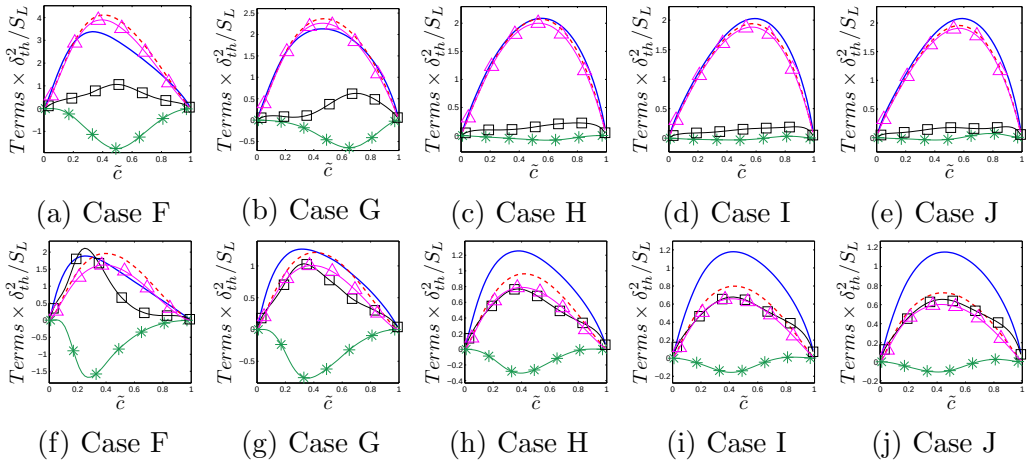

(a) Case F (b) Case G (c) Case H (d) Case I (e) Case J

(f) Case F (g) Case G (h) Case H (i) Case I (j) Case J

Figure 8.8: Variation of mean values of $\overline{(a_T)}_s\Sigma_{gen}$ (——), S_m (– – –), $(S_m)_M$ (—△—), S_{hr} (—✱—) and S_{sg} (—▫—) conditional on $\tilde{c}$ for filter widths Δ of $0.8\delta_{th}$ (top row) and $2.4\delta_{th}$ (bottom row).

$(e_{\gamma\gamma})$ increases (decreases) with decreasing Le due to strengthening of strain rate induced by heat release in comparison to turbulent straining. This tendency is prevalent in the reaction zone due to strong heat release rate, which leads to high probability of $\sin^2\alpha \approx 0$ in the reaction zone, which occurs close to the burned gas side of the flame brush. Thus the preferential alignment of ∇c with $e_{\alpha\alpha}$, acts to reduce the positive magnitude of S_{sg} towards the burned gas side for $Le \ll 1.0$ flames (e.g. $Le = 0.34$ case considered here).

The variations of the mean values of S_m and $(S_m)_M$ conditional on $\tilde{c}$ values for $\Delta = 0.8\delta_{th}$ and $\Delta = 2.4\delta_{th}$ for $Le = 0.34$, 0.8, 1.0 and 1.2 flames are also shown in Fig. 8.8 where $\overline{(N_iN_j)}_s$ is modelled as: $n_{ij} = \overline{(N_i)}_s\overline{(N_j)}_s + (\delta_{ij}/3)[1 - \overline{(N_k)}_s\overline{(N_k)}_s]$ [21, 68]. It is evident from Fig. 8.8 that $(S_m)_M$ underpredicts S_m for all filter widths for all cases and the level of this underprediction increases with increasing Δ. It is worth noting that the inaccuracies involved in the modelling of $\overline{(N_iN_j)}_s$ also contributes to the magnitude and modelling of S_{sg}.

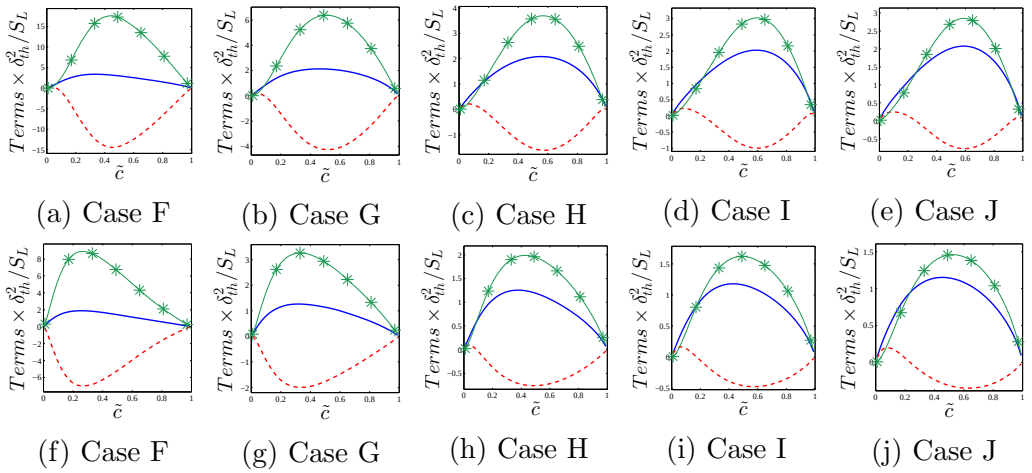

(a) Case F (b) Case G (c) Case H (d) Case I (e) Case J

(f) Case F (g) Case G (h) Case H (i) Case I (j) Case J

Figure 8.9: Variation of mean values of $\overline{(a_T)}_s\Sigma_{gen}$ (——), T_D (—*—), $(-T_N)$ (– – –) across the flame brush for filter widths Δ of $0.8\delta_{th}$ (top row) and $2.4\delta_{th}$ (bottom row).

8.2.3 LES Model for the subgrid Strain Rate Term

8.2.3.1 Mean Strain Rate Modelling

The variations of the mean values of S_m and $(S_m)_M$ conditional on $\tilde{c}$ values for $\Delta = 0.8\delta_{th}$ and $\Delta = 2.4\delta_{th}$, for cases A-E are also shown in Fig. 8.6 and for cases F-G in Fig. 8.8 where $\overline{(N_iN_j)}_s$ is modelled using Eq. 8.32 [21, 66]. It is evident from Figs. 8.6 and 8.8 that $(S_m)_M$ underpredicts S_m for all filter widths for all cases and the level of this underprediction increases with increasing Δ. It was demonstrated by Chakraborty and Cant [27] that Eq. 8.32 does not accurately capture $\overline{(N_iN_j)}_s - \overline{(N_i)}_s\overline{(N_j)}_s$ and this inaccuracy in the evaluation of $\overline{(N_iN_j)}_s$ contributes to the underprediction of S_m. It is also worth noting that the inaccuracies involved in the modelling of $\overline{(N_iN_j)}_s$ also contributes to the magnitude of S_{sg} indirectly.

8.2.3.2 Parameterisation Based on the effects of Turbulent Reynolds Number

The variations of the mean values of S_{sg} conditional on $\tilde{c}$ values for $\Delta = 0.8\delta_{th}$ and $\Delta = 2.4\delta_{th}$ for cases A-E are shown in Fig. 8.10 along with the prediction of the model given by Eq. 8.33. Hawkes [66] and Hawkes and Cant [67, 68]

proposed $\Phi = 1.0$ for their model but Fig. 8.10 suggests that Eq. 8.33 with $\Phi = 1.0$ significantly underpredicts the magnitude of S_{sg} for all filter widths for both Charlette et al. [48] and Angelberger et al. [2] efficiency functions (see Eqs. 8.35 and 8.36). However, an optimum choice of the model parameter Φ gives rise to satisfactory quantitative and qualitative predictions of S_{sg} in all cases considered here. The variations of the optimum values of Φ with Δ for all cases are shown in Fig. 8.11 which demonstrates that Φ shows appreciable filter size dependence in all cases. It is also evident from Fig. 8.11 that the optimum value of Φ changes from one case to another. Moreover, Φ for the efficiency function given by Eqs. 8.34 shows non-monotonic variation with Δ for all cases, whereas Φ for the efficiency function given by Eq. 8.36 increases with increasing Δ for all cases considered here. It can further be seen from Fig. 8.10 that Eq. 8.33 does not adequately capture the qualitative behaviour of S_{sg} obtained from DNS data for small filter widths (i.e. $\Delta \ll \delta_{th}$) for both the efficiency functions given by Eqs. 8.35 and 8.36 (see results for $\Delta \approx 0.8\delta_{th}$ in Fig. 8.10). However, the contribution of S_{sg} to $\overline{(a_T)}_s\Sigma_{gen}$ remains small for $\Delta \ll \delta_{th}$ so the implications of this inaccuracy is unlikely to be serious for small filter widths. Here a new model for S_{sg}, which is based on the RANS modelling shown earlier in Eq. 8.20, has been proposed as:

$$S_{sg} = \beta_{ssg}\tilde{c}^a\Gamma\left(\frac{u'_\Delta}{\Delta}\right)\Sigma_{gen} - \beta_{hr}\left(\frac{\tau S_L}{\delta_{th}}\right)\frac{[1-\overline{(N_k)}_s\overline{(N_k)}_s]}{(1+Ka_\Delta)^b}\Sigma_{gen} \tag{8.40}$$

where β_{ssg} and β_{hr} are the model parameters, Γ is taken to be:

$$\Gamma = 0.75\exp\left[-1.2\left(\frac{u'_\Delta}{S_L}\right)^{-0.3}\right]\left(\frac{\Delta S_L}{\alpha_{T0}}\right)^{2/3} \tag{8.41}$$

which is according to Angelberger et al. [2] and $Ka_\Delta = 6.66(u'_\Delta/S_L)^{3/2}\,(\Delta S_L/\alpha_{T0})^{-1/2}$ can be taken to be the subgrid scale Karlovitz number. In Eq. 8.40 the first term on the right hand side is similar to Eq. 8.33, and $\tilde{c}^a$ is introduced to capture the correct qualitative behaviour across the flame brush. The second term on the right hand side of Eq. 8.40 arises due to the local alignment of ∇c with the most extensive principal strain rate $e_{\alpha\alpha}$, which tends to destroy flame surface area [31,

39] following a previously proposed RANS model [80] (see §8.1.2). The prediction of Eq. 8.40 for $a = 0.3$ and $b = 0.35$ and optimum values of β_{ssg} and β_{hr} are shown in Fig. 8.10. The optimum values of β_{ssg} and β_{hr} are shown in Fig. 8.11, which shows that these model parameters also remain functions of Δ and the values change from one case to the other. The model parameters β_{ssg} and β_{hr} are expressed here as:

$$\beta_{ssg} = \frac{3.25}{1 + \{\exp[-(\Delta/\delta_{th} - 1.37)]\}^2} \tag{8.42a}$$

$$\beta_{hr} = 0.3\left\{2.0 - \frac{1.0}{1 + \{\exp[-15.0(P_2 - 3.3)]\}^2}\right\} \tag{8.42b}$$

$$P_2 = \frac{Re_{t\Delta}^{0.83} + 0.1}{(\Delta/\delta_{th})^{1.73} + 0.1} \tag{8.42c}$$

The quantity $Re_{t\Delta} = 4.0(\rho_0 u'_\Delta \Delta/\mu_0)$ can be taken as the local subgrid turbulent Reynolds number. It is evident from Fig. 8.11 that Eqs. 8.42 a-c capture the variations of β_{ssg} and β_{hr} with Δ for all cases considered here, although a slight underprediction is seen for the prediction of β_{hr} for the cases A and B. The model parameter β_{ssg} increases with increasing Δ which is qualitatively similar to the variation of Φ with Δ for the efficiency function given by Eq. 8.36. It is evident from Fig. 8.10 that the prediction of the model given by Eq. 8.40 remains either comparable or better than Eq. 8.33 for all cases for the parameterisation given by Eqs. 8.42 a-c. It is important to note that the variation of Φ for the efficiency function given by Eq. 8.36 can also be parameterised in a manner similar to Eqs. 8.42 a-c. Moreover, the model given by Eq. 8.40 accounts for local alignment of ∇c with the most extensive principal strain rate $e_{\alpha\alpha}$ under the action of heat release, which tends to destroy flame surface area but this physics is absent in the model given by Eq. 8.33.

8.2.3.3 Parameterisation Based on the effects of Lewis Number

The variations of the mean values of S_{sg} conditional on $\tilde{c}$ values for $\Delta = 0.8\delta_{th}$ and $\Delta = 2.4\delta_{th}$ for Le =0.34, 0.6, 0.8, 1.0 and 1.2 (cases F-J) flames are shown in Fig. 8.12 along with the prediction of the model given by Eq. 8.33. Hawkes

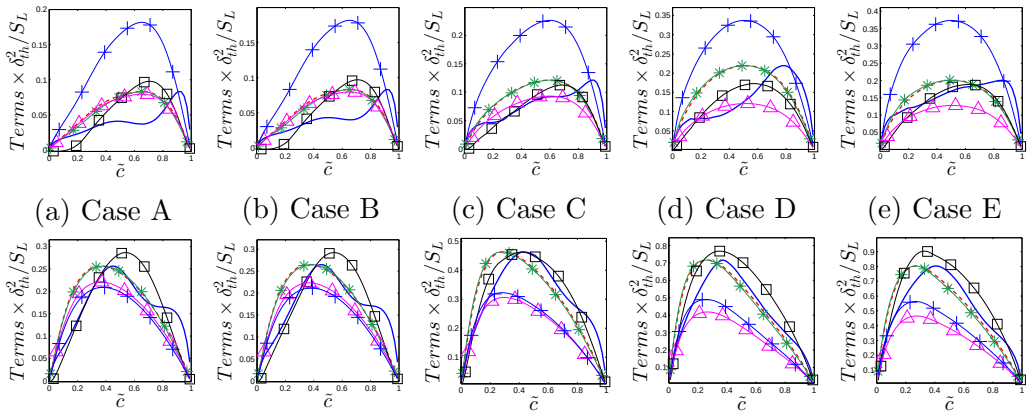

(a) Case A (b) Case B (c) Case C (d) Case D (e) Case E

(f) Case A (g) Case B (h) Case C (i) Case D (j) Case E

Figure 8.10: Variation of mean values of S_{sg} (——) conditional on $\tilde{c}$ across the flame brush along with the predictions of Eq. 8.33 with Γ according to Eq. 8.34 with $\Phi = 1.0$ (—△—), and optimum value of Φ (– – –), Eq. 8.33 with Γ according to Eq. 8.36 with $\Phi = 1.0$ (—+—) and with optimum value of Φ (—✳—) and the newly proposed model given by Eq. 8.40 (—▫—) for filter widths Δ of $0.8\delta_{th}$ (top row) and $2.4\delta_{th}$ (bottom row).

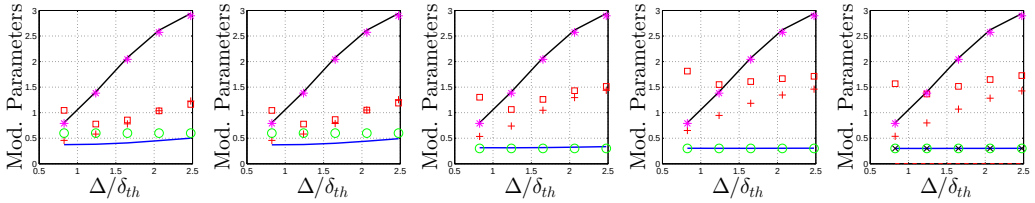

(a) Case A (b) Case B (c) Case C (d) Case D (e) Case E

Figure 8.11: Variation of optimum values of β_{ssg} (✳), Eq. 8.42a (——), β_{hr} (○), Eq. 8.42b (——), optimum values of Φ for Γ from Eq. 8.34 (□) and the optimum values of Φ for Γ from Eq. 8.36 (+) with Δ/δ_{th} for cases F-J

and Cant [68] proposed $\Phi = 1.0$ for their model but Fig. 8.12 suggests that Eq. 8.33 significantly underpredicts the magnitude of S_{sg} for all filter widths in all cases considered here for both Charlette et al. [48] and Angelberger et al. [2] efficiency functions. However, an optimum choice of the model parameter Φ gives rise to satisfactory quantitative and qualitative predictions of S_{sg} in the $Le \approx 1.0$ (i.e. Le =0.8, 1.0 and 1.2) cases considered here. However, Eq. 8.33 for the optimum value of Φ, fails to capture the qualitative behaviour of S_{sg} in the $Le = 0.34$ case and significantly overpredicts the magnitude of S_{sg} towards the

burned gas side of the flame brush. Moreover, the optimum value of Φ for both efficiency functions vary significantly with Δ and Le, which is demonstrated in Fig. 4. The optimum value of Φ has been found to increase with decreasing Le. The optimum value of Φ for the efficiency function proposed by Charlette et al. [48] does not exhibit any monotonic trend, whereas Φ for Angelberger et al. [2] efficiency function increases with increasing Δ. The model proposed in Eq. 8.40 is used to predict the S_{sg}. However, the parameterisation given by Eq. 8.42 a-c have been modified to account for, where the effects of Le are added to the prior parameterisation:

$$a = \frac{0.3}{1 + [\exp(-5.9(Le - 0.58))]^{5.9}} \tag{8.43a}$$

$$\beta_{ssg} = \frac{3.2 + 6.21\exp(-4.74Le^{2.31})}{1 + [\exp(-(\Delta/\delta_{th} - 1.37))]^2} \tag{8.43b}$$

$$\begin{aligned}\beta_{hr} =& [0.3 + 7.2\exp(-13.7Le^3.47)] \\ & \left\{2.0 - \frac{1.0}{1 + [\exp(-15.0(P_2 - 3.3))]^2}\right\}\end{aligned} \tag{8.43c}$$

$$P_2 = \frac{Re_{\Delta}^{0.83} + 0.1}{(\Delta/\delta_{th})^{1.73} + 0.1} \tag{8.43d}$$

The prediction of Eq. 8.40 for $b = 0.35$ and optimum values of a β_{ssg}, β_{hr} are shown in Fig. 8.12 .The optimum values of a, β_{ssg} and β_{hr} are shown in Fig. 8.13 along with the predictions for them based on the parameterisation shown in Eq. 8.43. Again the efficiency function Γ in the newly proposed model (Eq. 8.40) uses the proposed function by Angelberger et al. [2]. Based on the parameterisation shown in Eq. 8.43 a remains about 0.30 (i.e. $a \approx 0.3$) for the $Le \approx 1.0$ cases (i.e. $Le = 0.8$, 1.0 and 1.2: cases H, I and J). It is evident from examining Fig. 8.12 that the new model in Eq. 8.40 using the parameterisation proposed in Eq. 8.43 satisfactorily captures both qualitative and quantitative behaviours of S_{sg} for cases F-J for the range of filter widths examined ($0.4\delta_{th}$, $0.8\delta_{th}$, $1.2\delta_{th}$, $1.6\delta_{th}$, $2.0\delta_{th}$ and $2.4\delta_{th}$).

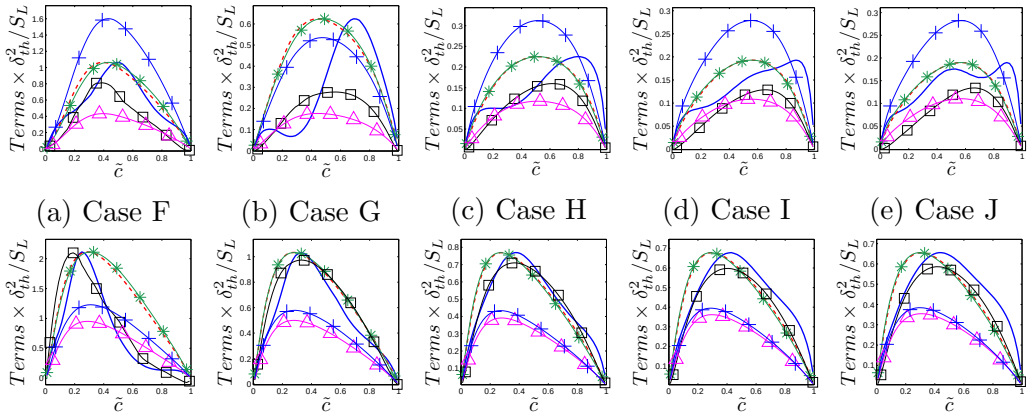

(a) Case F (b) Case G (c) Case H (d) Case I (e) Case J

(f) Case F (g) Case G (h) Case H (i) Case I (j) Case J

Figure 8.12: Variation of mean values of S_{sg} (——) conditional on $\tilde{c}$ across the flame brush along with the predictions of Eq. 8.33 with Γ according to Eq. 8.34 with $\Phi = 1.0$ (—△—), and optimum value of Φ (– – –), Eq. 8.33 with Γ according to Eq. 8.36 with $\Phi = 1.0$ (—+—) and with optimum value of Φ (—✳—) and the newly proposed model given by Eq. 8.40 using the parameterisation given in Eq. 8.43 (—▫—) for filter widths Δ of $0.8\delta_{th}$ (top row) and $2.4\delta_{th}$ (bottom row).

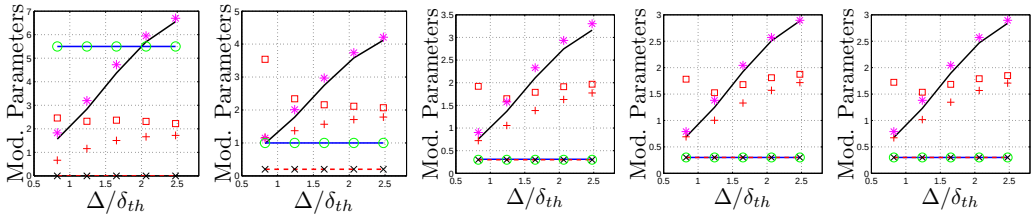

(a) Case A (b) Case B (c) Case C (d) Case D (e) Case E

Figure 8.13: Variation of optimum values of β_{ssg} (✳), Eq. 8.42a (——), β_{hr} (○), Eq. 8.42b (——), optimum values of Φ for Γ from Eq. 8.34 (□) and the optimum values of Φ for Γ from Eq. 8.36 (+) with Δ/δ_{th} for cases A-E

8.2.4 Summary

The strain rate term of the generalised FSD transport equation was decomposed into the contribution of mean strain rate, heat release and subgrid strain rate. These contributions were extracted from filtered DNS data at various filter widths. It was shown that for all the cases, and at all filter widths, the net contribution of the strain rate term remains positive. The magnitudes of the resolved strain rate term and the term arising due to heat release decreases with increasing

filter width. By contrast the magnitude of the subgrid strain rate was found to increase with increasing filter width. The performance of the existing models for the subgrid strain rate forms and mean strain rate were compared with a newly proposed model using the current DNS database. It was found that the existing models fail to capture the correct quantitative variation of the strain rate term without modification of the model parameters. The newly proposed model was found to capture the trends shown by the subgrid strain rate term for a range of different filter widths, Lewis numbers and turbulent Reynolds numbers.

Chapter 9

Conclusions and Future Work

9.1 Modelled Generalised FSD Transport Equation for LES

In earlier chapters the modelling of the individual terms of the generalised FSD transport equation were discussed. In this chapter the complete modelled transport equation of the Σ_{gen} is presented. In order to accomplish this, the following models were used:

- Subgrid convection term T_1 is modelled using expression given in Eq. 6.52.
- Strain rate term T_2 is modelled using the newly proposed expressions in Eqs. 8.31 ($(S_m)_M$), Eq. 8.29 (S_{hr}) and 8.43 (S_{sg}).
- Curvature term is modelled using the newly proposed expression shown in Eqs. 7.20a (C_{mean}) and 7.40 (C_{sg}).
- Propagation term is modelled using Eq. 6.30.

The modelled transport equation then take the following form:

$$\begin{aligned}\frac{\partial \Sigma_{gen}}{\partial t}+\frac{\partial(\tilde{u}_j\Sigma_{gen})}{\partial x_j} =& \underbrace{-\frac{\partial}{\partial x_i}\left[\frac{\mu_t}{Sc_\Sigma}\frac{\partial}{\partial x_i}\left(\frac{\Sigma_{gen}}{\bar{\rho}}\right)\right]-\frac{\partial}{\partial x_i}[(K-\tilde{c})\tau S_L'\overline{(N_i)_s}\Sigma_{gen}]}_{T_1}\\ &+(S_m)_M\underbrace{-\tau(K-\tilde{c})S_L'\frac{\partial\overline{(N_i)}_s}{\partial x_i}\Sigma_{gen}}_{S_{hr}}+S_{sg}\\ &+\underbrace{S_L'(1+\tau c^*)\frac{\partial\overline{(N_i)}_s}{\partial x_i}}_{C_{mean}}+C_{sg1}+C_{sg2}\\ &\underbrace{-\frac{\partial}{\partial x_i}[S_L'(1+\tau c^*)\overline{(N_i)}_s\Sigma_{gen}]}_{T_4}\end{aligned} \tag{9.1}$$

where μ_t is the eddy viscosity, Sc_Σ is turbulent Schmidt number for FSD. Based on the analysis of Hawkes and Cant [68] the Sc_Σ must satisfy $Sc_\Sigma = Sc_t \geq 1.0$. In Eqs. 7.20a and 6.30 $\overline{(S_d)}_s$ is expressed as $\rho_0 S_L'/\rho_s = S_L'(1+\tau c^*)$ where ρ_s is density conditional on c^* isosurface. The surface filtered density weighted displacement speed $\overline{(\rho S_d)}_s$ is evaluated based on the dynamic model presented in Eq. 6.58. The surface average flame normal is given by $\overline{(N_i)}_s = -(1/\Sigma_{gen})(\partial\bar{c}/\partial x_i)$, where $\bar{c}$ to $\tilde{c}$ must be evaluated based on relationship by Chakraborty and Cant [35, 47]:

$$\tilde{c} = \frac{(1+\tau)\tilde{c}}{(1+\tau\tilde{c})}\left[1-\exp\left(\frac{-\Theta\Delta}{\delta_z}\right)\right]+\tilde{c}\exp\left(\frac{-\Theta\Delta}{\delta_z}\right) \tag{9.2}$$

where $\Theta = 1/5$. The modified flame speed S_L' in Eq. 9.1 can be evaluated in the following manner [22] (previously shown in Eq. 6.50):

$$S_L'\frac{\overline{(\rho S_d)}_s}{\rho_0} = S_{LS} - 2\frac{\rho D}{\rho_0}\overline{(\kappa_m)}_s \tag{9.3}$$

where $\overline{(\kappa_m)}_s$ is given as:

$$\overline{(\kappa_m)}_s = \frac{\overline{(\nabla.\vec{N}|\nabla c|)}}{2\Sigma_{gen}} = \frac{1}{2}\frac{\partial\overline{(N_i)}_s}{\partial x_i} - \frac{1}{\Sigma_{gen}}\left[\overline{(N_i\frac{\partial|\nabla c|}{\partial x_i})} - \overline{(N_i)}_s\frac{\partial\Sigma_{gen}}{\partial x_i}\right] \tag{9.4}$$

The term $(S_m)_M$ in Eq. 8.31 is used to model the S_m using Eq. 8.23 and is repeated here:

$$(S_m)_M = [\delta_{ij} - n_{ij}]\frac{\partial\tilde{u}_i}{\partial x_j}\Sigma_{gen} \tag{9.5}$$

The term n_{ij} in Eq. 9.5 is modelled expression of $\overline{(N_iN_j)}_s$ which can be expressed as [21]:

$$n_{ij} = \overline{(N_i)}_s\overline{(N_j)}_s + \frac{\delta_{ij}}{3}\left[1 - \overline{(N_k)}_s\overline{(N_k)}_s\right] \tag{9.6}$$

The subgrid strain rate term S_{sg} in Eq. 9.1 is given as (see Eq. 8.40):

$$S_{sg} = \beta_{ssg}\tilde{c}^a\Gamma\left(\frac{u'_\Delta}{\Delta}\right)\Sigma_{gen} - \beta_{hr}\left(\frac{\tau S_L}{\delta_{th}}\right)\frac{[1 - \overline{(N_k)}_s\overline{(N_k)}_s]}{(1 + Ka_\Delta)^b}\Sigma_{gen} \tag{9.7}$$

where the model parameters β_{ssg} and β_{hr} are given by Eqs. 8.42a and 8.42b respectively, and the efficiency function Γ is based on the findings of Angelberger et al. [2]. The terms C_{sg1} and C_{sg2} are given as:

$$\begin{aligned} C_{sg1} &= -\beta_4\frac{(\Sigma_{gen} - |\nabla\bar{c}|)(\bar{c} - c^\circ)S_L\Sigma_{gen}}{\exp[-a_\Sigma(1-\bar{c})]\bar{c}(1-\bar{c})^m} \\ C_{sg2} &= -\beta_5\frac{S_L(\Xi - 1)^n\Sigma_{gen}^2}{\bar{c}(1-\bar{c})} \end{aligned} \tag{9.8}$$

where $m = 1.85$ and β_4, β_5, c° and a_Σ are the model parameters given by Eqs. 7.34, 7.38 and 7.35, respectively.

The modelled generalised FSD transport given by Eq. 9.1 is dependent on the choice of K and the c isosurface value of c^*. Thus the modelld transport equation given in Eq. 9.1 is not a true field equation due to its dependence on c^*,

while $\Sigma_{gen} = \overline{|\nabla c|}$ is a field quantity. Based on the derivations of Hawkes [66] and Chakraborty [22] the dependency of a given c^* can be avoided if K is equated with c^* (i.e. $K = c^*$). Once $K = c^*$ is applied to Eq. 9.1 the following modelled transport equation can be derived for the generalised FSD:

$$\frac{\partial \Sigma_{gen}}{\partial t} + \frac{\partial (\tilde{u}_j \Sigma_{gen})}{\partial x_j} = \underbrace{-\frac{\partial}{\partial x_i}\left[\frac{\mu_t}{Sc_\Sigma}\frac{\partial}{\partial x_i}\left(\frac{\Sigma_{gen}}{\bar{\rho}}\right)\right]}_{T_1}$$

$$\underbrace{+(\delta_{ij} - N_{ij})\frac{\partial \tilde{u}_i}{\partial x_j}\Sigma_{gen} + \beta_{ssg}\tilde{c}^a \Gamma\left(\frac{u'_\Delta}{\Delta}\right)\Sigma_{gen} - \beta_{hr}\left(\frac{\tau S_L}{\delta_{th}}\right)\frac{[1 - \overline{(N_k)}_s\overline{(N_k)}_s]}{(1 + Ka_\Delta)^b}\Sigma_{gen}}_{T_2}$$

$$\underbrace{+ S'_L(1 + \tau\tilde{c})\frac{\partial \overline{(N_i)}_s}{\partial x_i} - \beta_4\frac{(\Sigma_{gen} - |\nabla \bar{c}|)(\bar{c} - c^\circ)S_L\Sigma_{gen}}{\exp[-a_\Sigma(1 - \bar{c})]\bar{c}(1 - \bar{c})^m} - \beta_5\frac{S_L(\Xi - 1)^n\Sigma^2_{gen}}{\bar{c}(1 - \bar{c})}}_{T_3}$$

$$\underbrace{-\frac{\partial}{\partial x_i}[S'_L(1 + \tau\tilde{c})\overline{(N_i)}_s\Sigma_{gen}]}_{T_4} \tag{9.9}$$

The final form of the modelled transport equation for the generalised FSD given in Eq. 9.9 is a field equation which is independent of the choice of c^* isosurface.

9.2 Summary

The main objectives of this thesis were to examine the flamelet modelling approach and the closure of the mean/filtered reaction rate for premixed combustion, in context of LES and RANS. The closure for the mean reaction rate term using FSD is a popular approach, in context of RANS. However FSD modelling for LES is gaining increased industrial attention, as high performance computing becomes more affordable. In order to develop new models and test existing models for FSD based reaction rate closure, a three-dimensional compressible DNS database was used. In this database, a freely propagating turbulent premixed

flame with a single-step Arrhenius type chemistry was allowed to evolve in decaying homogeneous isotropic turbulence. The boundary conditions for all cases were taken to be partially nonreflecting in the direction of mean flow and the rest of the boundaries were taken to be periodic. The DNS database was setup in such a manner that a single parameter can be modified independently of the other parameters, which allowed for its effects on the flame to be studied in isolation.

The parameters of interest were chosen to be the turbulent Reynolds number and the Lewis number. In the DNS database the initial turbulent Reynolds number was controlled by changing the values for the Karlovitz number and Damköhler numbers independently of each other. All the cases of the DNS database correspond to the thin reaction zones regime, however it remains unclear if a flame with a Lewis number significantly small/greater than unity can be represented using a regime diagram such as the one proposed by Peters [107]. The extracted data was postprocessed either by Reynolds averaging or LES filtering, as appropriate. LES filtering of the DNS data was carried out with a Gaussian filter in physical space for a range of filter widths.

An increase in turbulent Reynolds results in increased flame wrinkling, which is due to increased flame area generation and thus gives rise to increased burning rates. Additionally as the turbulent Reynolds number increased for a given Damköhler number the preheat zone became increasingly distorted, which was as a result of increasing Karlovitz number. The Lewis number was varied from 0.34 to 1.2. A decrease in Lewis number gives rise to increased burning rate, heat release and flame area generation. This tendency is prevalent for $Le \ll 1.0$ flames due to thermo-diffusive instabilities.

Modelling for the generalised FSD can be carried out either by using an algebraic model or through a modelled transport equation. The algebraic modelling of the generalised FSD was examined in context of LES. Models for the wrinkling factor can be used to predict the generalised FSD Σ_{gen}, whereas many models currently exist for the generalised FSD itself. Existing models using a power-law based approach were analysed. Additionally the behaviours of the inner cutoff scale and the fractal dimension were examined using filtered DNS data. It was found that the Lewis number and turbulent Reynolds number both influence the fractal dimension, while the inner cut off scale was found to scale with the thermal

flame thickness. A power-law based model was proposed for the generalised FSD, with fractal dimension parameterised based on Lewis number and local Karlovitz and turbulent Reynolds numbers. The newly proposed model for Σ_{gen} was designed in such a manner that when the filter width was smaller than thermal flame thickness it would predict Σ_{gen} based on the resolved FSD $|\nabla\tilde{c}|$, and when the filter width is greater than the flame thickness it would predict based on a power-law model, with the newly parametrised fractal dimension and the inner cut off scaled assumed to equal the thermal flame thickness. The statistical predictions from the new model were compared with the existing power law models, and the prediction of the new model has been found to be either better than or comparable to the existing models for a range of different values of filter widths, turbulent Reynolds numbers and Lewis numbers. The correlations coefficient between the model predictions for generalised FSD and the actual generalised FSD obtained from DNS were found to decrease from unity as the filter width was increased. This trend was seen to be common for all models, although some models showed greater depreciation with filter width.

While algebraic model predictions were found to reach performances of $\pm 15\%$ this approach can have shortfalls, i.e. when the curvature and strain rate contributions to stretch rate are out of balance. In such conditions solving a modelled transport equation for the generalised FSD can be seen to be advantageous. The transport equation of the generalised FSD has four unclosed terms which are the subgrid convection term, tangential strain rate term, curvature term and the propagation term. In order to develop for the unclosed terms, their statistical behaviours have been examined for a range of filter widths. The behaviour of the subgrid convection term was found to be significantly affected by the Lewis number, as predominantly gradient type behaviour was observed for the $Le \approx 1.0$ cases, whereas $Le \leq 0.6$ cases show counter-gradient transport. To understand this behaviour the flux of generalised FSD was analysed. Additionally an existing model for subgrid flux closure was analysed, and it was found to work satisfactorily for the whole range of filter widths and for all DNS cases considered here. However the model performance depends on the accurate prediction of surface-filtered displacement speed in an actual LES simulation.

The propagation term of the generalised FSD transport equation was shown

to play an important role in the FSD transport for all filter widths tested and all DNS cases. The propagation term assumes predominantly positive values towards the reactants and negative values towards the products. The magnitude of the propagation term increases with decreasing Lewis number. This was shown to be as a result of the increased magnitude of surface filtered displacement speed at small values of Lewis number. Moreover, an expression for the propagation has been identified which was shown to work extremely well, but the accurate prediction of this model depends on the accurate modelling of surface filtered displacement speed.

As the modelling of the surface filtered displacement speed plays such an important role in the closure based on generalised FSD, an existing model for $\overline{(S_d)}_s$ was assessed, which was found to perform adequately for all the cases at all the filter widths. This ensures the accurate predictions for the propagation, subgrid convection and curvature terms.

The curvature term of the generalised FSD transport equation was found to be predominantly negative for flames with $Le \approx 1.0$ but the terms assumes positive (negative) values towards the reactants (products) side of the flame brush for $Le \ll 1$. In order to explain this behaviour, the curvature term was decomposed into contributions arising due to the reaction and normal diffusion component of displacement speed, and the curvature term component arising due to tangential diffusion component of displacement speed. The curvature component due to tangential diffusion component of displacement speed was shown to be negative throughout the flame brush for both LES and RANS. The component of curvature term arising from the reaction and normal diffusion components of displacement speed was found to be significantly affected by the global Lewis number, which was shown to explain the different behaviour of the curvature term in response to Lewis number. The modelling for the curvature term was firstly carried out in context of RANS in order to examine if it was suitable. Models were proposed for the unresolved components of the curvature term following the decomposition based on the displacement speed. The newly proposed model was parameterised in terms of local Karlovitz number, local Reynolds number and global Lewis number. This parameterisation was shown to predict the curvature term accurately for all the flame conditions in the current DNS database, in context of RANS.

With this in mind the same strategy was applied for LES, where models were proposed for the subgrid curvature term components arising from different components of displacement speed. Again a parameterisation was proposed for new model which incorporated the effects of subgrid turbulent Reynolds number and Lewis number. The predictions based on this parameterisation were found to accurately predict the curvature term for a range of filter widths for all cases considered here.

The strain rate term of the generalised FSD transport equation was found to be predominantly positive throughout the flame brush for all cases at all filter widths, although its magnitude increases with decreasing Lewis number. To investigate this behaviour the strain rate term was decomposed into two components, namely the dilatation rate and the normal strain rate term. It was found that the dilatation rate term was predominantly positive for all cases and its magnitude increases with decreasing Lewis number, which was shown to be due to increased heat release. The normal strain rate term however was found to be negative for the entire flame brush for all filter widths for the cases considered here, this behaviour was explained based on the scalar gradient alignment with local principal strain rates. The magnitude of the normal strain rate contribution was found to be smaller than the magnitude of the dilatation rate, which was shown to result in the predominantly positive behavior of the tangential strain rate term of the generalised FSD transport equation.

In order to investigate a LES modelling approach for the strain rate term of the generalised FSD transport equation, it was firstly modelled in context of RANS. Similar behaviour was observed in RANS for the dilation and normal strain rate contributions to the generalised FSD transport equation, i.e. strengthening of the dilatation rate term with decreasing Lewis number and positive contribution of the tangential strain rate term. The dilatation rate term and normal strain rate terms were decomposed into the resolved and the unresolved contributions, and models were proposed for the unresolved contributions. The resolved contributions in RANS were found to be relatively small in comparison to the unresolved components. The newly proposed models for the unresolved dilatation rate and normal strain rate terms have been utilised to predict the tangential strain rate term with greater or comparable accuracy in comparison to the existing models,

in context of RANS.

The modelling for the strain rate term of the generalised FSD transport equation in context of LES involves decomposition into components arising from resolved strain rate, strain rate due to heat release and the subgrid strain rate, in order to make the final form of the modelled transport equation independent of the choice of c [66]. The model for the resolved strain rate term was found to underpredict the DNS value in all cases considered here. This resulted in the increased modelling that had to be carried on the subgrid strain rate term. Modelling was performed for the strain rate terms due to heat release and subgrid strain rate, where the parameterisation for subgrid strain rate took into consideration the effects of subgrid turbulent Reynolds number, subgrid Karlovitz number and global Lewis number. The predictions for the subgrid strain rate term according to the newly proposed model was found to be of better accuracy than the existing models. Finally a modelled transport equation is proposed for the generalised FSD in context of LES, which is expected to be suitable for a range of different values of Lewis number and turbulent Reynolds number, and spanning different combustion regimes.

9.3 Future Work

In the current work many important modelling issues in the context of the generalised FSD based closure of turbulent premixed combustion have been addressed. However many questions still remain unanswered or unaddressed in the current work, some of these are described below:

9.3.1 Detailed Chemistry

In the current investigation a single step Arrhenius mechanism was used to represent the reaction rate. Although this is a good approximation, it is not physically true. In recent times computational power has grown rapidly allowing for simulations with many chemical species, reaction mechanisms and three dimensional turbulence. It is currently unclear how such an investigation will differ from

the current analysis. Additionally a parametric study such as the current DNS database will be difficult based on detailed chemistry based simulations, as each species will have its own Lewis number and modification of Lewis number will result in modification of other parameters such as the Zel'dovich number. However a detailed chemistry based DNS offers an opportunity to test the proposed models in a setup where a range of local Lewis numbers can be obtained. In essence the current models with global Lewis number can be substituted with a local Lewis number, but the accuracy of such approach is yet to assessed. One of the likely advantages of using detailed chemistry DNS data would perhaps be in the additional improved modelling of the surface filtered displacement speed, where the stretch affects on the reaction and normal diffusion components can be addressed with greater accuracy.

9.3.2 Turbulent Reynolds Number

In the current DNS database modest values of turbulent Reynolds numbers were used, while turbulent Reynolds numbers for real burners are extremely expensive to achieve using DNS. *A priori* analysis based on modest values of Re_t still provide valuable insight and confirm the asymptotic trends which were subsequently utilised to propose improved models. One way to circumnavigate this issue is to carry out experimental assessment of the proposed models for higher value of turbulent Reynolds number. Although experimental measurement of $|\nabla c|$ remains a major problem but significant advances have been made recently in this regard [140, 141].

9.3.3 *A posteriori* Analysis

The models proposed in this work were shown to perform either better than or comparably to the existing models, but the true test depends on the implementation of these models in LES/RANS. In actual LES some of the input parameters to the combustion models (e.g. u'_Δ) must be modelled, and the accuracy of the turbulence models affects the performance of the combustion models. In LES of industrial flows the turbulence models such as the Smagorinsky-Lilly model

[138] are commonly used, however it is unclear if such models are suitable for combustion where heat release plays a major role. As such it is hard to pinpoint the source of errors in such analysis. Once these issues are suitably addressed, a direct *a posteriori* validation for the proposed models can be carried out by comparing LES simulation predictions in a configuration for which experimental measurements are readily available.

9.3.4 Effects of Geometry and Non-planar Flames

In the current study a canonical geometry was used, which is not representative of realistic engineering configurations. Moreover heat loss at the near wall regions plays an important role in flame quenching, overall heat release and mean flame propagation rate. Additionally flames in practical combustors may have considerable mean curvature which might affect $|\nabla c|$ statistics [40]. The effects of geometry, heat loss and presence of walls on the FSD based closure are rarely addressed in the existing literature and should be investigated.

9.3.5 Stratified Combustion, Equivalence Ratio and Fuel Blending

A modification of equivalence ratio and blending of fuel gives rise to changes in Zel'dovich number and global Lewis number, which cannot be addressed quantitatively based on simple chemistry based DNS simulation. However, FSD based modelling for turbulent stratified flames in the context of RANS is in infancy [99], and modelling of FSD for LES of turbulent stratified combustion is yet to be addressed in detail. The above issues warrant for advanced three-dimensional DNS simulation with detailed chemistry, which should form the basis of future investigations.

Appendix A

Numerical Implementation

A.1 Numerical schemes

First and second order spatial derivatives for the internal grid points are carried out using a tenth order central differencing scheme, in the code SENGA which can be expressed in the following manner:

$$f'_i = \sum_{j=1}^{j=n^\circ/2} \frac{a_j}{2jh}(f_{i+j} - f_{i-j}) \tag{A.1a}$$

$$f''_i = \sum_{j=1}^{j=n^\circ/2} \frac{a_j}{j^2h^2}(f_{i+j} - 2f_i + f_{i-j}) \tag{A.1b}$$

where the values of the constants a_j are determined by expanding the Taylor series and equating coefficient for the successive orders of grid spacing h. In Eq. A.1, n° is the order of approximating [77]. Five grid points are required on either side of the differential grid point for the tenth order scheme. The order of accuracy for spatial differentiation decreases towards the non-periodic boundaries. The order of accuracy gradually decreases to an one sided second order finite difference scheme.

The time marching, in the code SENGA, is handled by a low storage third order Runge-Kutta scheme [161]. Each time step is explicitly broken into three sub steps for this scheme. Each grid location requires two storage locations, one for the time derivative and another for the dependent variable at the boundary nodes.

A.2 Initialisation

The DNS database used in this thesis represents flame turbulence interaction under decaying turbulence. For this type of setup, where there is no turbulence generation, it is useful to prescribe an initial condition that resembles a good approximation to a turbulent flow solution of the Navier-Stokes equations. This method was chosen to minimise the time required for the simulation to reach a developed turbulent solution.

A pseudo spectral method proposed by Rogallo [133] is used to generate a homogeneous isotropic incompressible turbulent velocity field. The domain for this numerical solution is periodic in all directions. Solution to this velocity field is generated in Fourier space and it is inverse Fourier transformed into real space for implementing into the actual simulation. To generate the turbulence field SENGA begins by generating a velocity field in Fourier space $\hat{u}$, which satisfies the continuity of an incompressible flow. The mass conservation equation for an incompressible flow takes the following form in physical space:

$$\nabla.\vec{u} = 0 \tag{A.2}$$

The Fourier transform of Eq. A.2 yields:

$$\vec{\kappa}.\hat{u} = 0 \tag{A.3}$$

where $\hat{u}$ is the velocity field in Fourier space and $\vec{\kappa}$ is the linear wave number

vector. It is evident from Eq. A.3 that $\vec{\kappa}$ and $\hat{u}$ are orthogonal to each other, and thus $\hat{u}$ can be expressed as follows:

$$\hat{u} = \alpha(\kappa)\vec{e}_1 + \beta(\kappa)\vec{e}_2 \tag{A.4}$$

where the unit basis vectors are given by $\vec{e}_1$, $\vec{e}_2$ and $\vec{e}_3$, and $\vec{e}_3$ is assumed to be aligned with $\vec{\kappa}$. The unit vectors $\vec{e}_1$ and $\vec{e}_2$ are chosen randomly so that they are normal to each other. The coefficients $\alpha(\kappa)$ and $\beta(\kappa)$, in Eq. A.4 are generated with random phase, and their magnitude are set in such a manner that each Fourier mode conforms to the average turbulent kinetic energy described by the energy spectrum $E(\kappa)$. For the present analysis $E(\kappa)$ is assumed to follow the Batchelor and Townsend spectrum [6] which represent the final period of decay of the grid turbulence. The Batchelor and Townsend spectrum [6] is give:

$$E(\kappa) = C_0 \left(\frac{\kappa}{\kappa_0}\right)^4 \exp\left[-\left(\frac{\kappa}{\kappa_0}\right)^2\right] \tag{A.5}$$

The coefficients $\alpha(\kappa)$ and $\beta(\kappa)$, in Eq. A.4 are given by:

$$\alpha(\kappa) = \left(\frac{E(\kappa)}{4\pi\kappa^2}\right)^{1/2} e^{i\theta_1} cos\phi \tag{A.6a}$$

$$\beta(\kappa) = \left(\frac{E(\kappa)}{4\pi\kappa^2}\right)^{1/2} e^{i\theta_2} sin\phi \tag{A.6b}$$

where θ_1, θ_2, ϕ are uniformly distributed random angles. If $\vec{e}_1$ is to lie on the $x-y$ plane then:

$$\vec{e}_1 = \left(\frac{\kappa_2}{M}, \frac{\kappa_1}{M}, 0\right) \tag{A.7a}$$

$$\vec{e}_2 = \left(\frac{\kappa_1\kappa_3}{\kappa M}, \frac{\kappa_2\kappa_3}{\kappa M}, \frac{\kappa_1^2 + \kappa_2^2}{\kappa M}\right) \tag{A.7b}$$

$$\vec{e}_3 = \left(\frac{\kappa_1}{\kappa}, \frac{\kappa_2}{\kappa}, \frac{\kappa_3}{\kappa}\right) \tag{A.7c}$$

where $M = \sqrt{\kappa_1^2 + \kappa_2^2}$ and the Fourier space velocity vectors are given as:

$$\vec{u}_1(\kappa) = \frac{\alpha\kappa\kappa_1 + \beta\kappa_1\kappa_3}{\kappa\sqrt{\kappa_1^2 + \kappa_2^2}} \tag{A.8a}$$

$$\vec{u}_2(\kappa) = \frac{-\alpha\kappa\kappa_1 + \beta\kappa_2\kappa_3}{\kappa\sqrt{\kappa_1^2 + \kappa_2^2}} \tag{A.8b}$$

$$\vec{u}_3(\kappa) = -\frac{\beta(\kappa_1^2 + \kappa_2^2)}{\kappa} \tag{A.8c}$$

Generating the velocity field in Fourier space is only done for half the computational domain. By using the expression $\hat{u}(\kappa) = \hat{u}^*(-\kappa)$ it is possible to justify only calculating velocities for only half the domain, where the superscript * refers to the complex conjugate values. When the velocity field is inverse Fourier transformed the velocities are real due to the above method. The x_3 direction represents a special case; the upper half of the wave number domain is filled with computational data from Eq. A.4. Inverse Fourier transform is carried on the $\kappa_1 - \kappa_2$ planes, first to produce a partial inverse Fourier transform using the following formula:

$$\hat{u}_i^{1,2}(x_1, x_2, x_3) = \iint \hat{u}_i(\kappa_1, \kappa_2, \kappa_3) e^{-i2\pi(\kappa_1 x_1 + \kappa_2 x_2)} d\kappa_1 d\kappa_2 \tag{A.9}$$

By using the symmetry condition it is possible to set the Fourier coefficient required in x_3 direction. Finally an inverse Fourier transform in the x_3 direction completes the initialisation process for the turbulent velocity field.

$$u_i(x_1, x_2, x_3) = \iint \hat{u}_i^{(1,2)}(x_1, x_2, \kappa_3) e^{-i2\pi\kappa_3 x_3} d\kappa_3 \tag{A.10}$$

All Fourier transforms operations in SENGA are carried out using the FFT (Fast Fourier Transform) algorithm.

In order to simulate a statistically planar turbulent premixed flame, a steady one dimensional unstrained laminar flame solution is superimposed on to the tur-

bulent flow field. The flame solution is generated using a 1D version of SENGA. The reaction progress variable, temperature and velocity field for the laminar flame simulation are then initialised using an asymptotic steady laminar flame solution given by [119].

$$c(x) = T(x) = \left(1 - \frac{1}{\beta}\right) \exp\left(\frac{x - x_c}{\delta_z}\right) \qquad \text{when } (x - x_c) < 0 \quad \text{(A.11a)}$$

$$c(x) = T(x) = \left(1 - \frac{1}{\beta}\right) \exp\left(\frac{(1-\beta)(x - x_c)}{\delta_z}\right) \qquad \text{when } (x - x_c) > 0 \quad \text{(A.11b)}$$

$$u(x) = u_1 + \frac{S_L \alpha T(x)}{1 - \alpha} \qquad \text{(A.11c)}$$

where T is the nondimensional temperature, $u_1 \approx S_L$ is the mean velocity of the reactant and δ_z is the Zeldovich flame thickness defined as:

$$\delta_z = \frac{\lambda}{\rho C_p S_L} \qquad \text{(A.12)}$$

The coefficients β and α in Eq. A.11 are the Zel'dovich number and heat release parameter, respectively. x_c corresponds to the location where $T = 1 - (1/\beta)$.

A.3 Boundary conditions

Boundary conditions impact greatly on the results of CFD simulations. In the current database the boundaries in the normal direction of mean flame propagation are taken to be periodic rather than walls. This was done in order to produce a DNS database for analysing the effects of various parameters, in the absence of the wall induced effects. The boundary treatment in the mean flame propagation is much more demanding. This is due to the compressibility of the flow, where wave reflections on the boundaries can also lead to artificial effects. In gas turbine engines, if the right conditions arise, these acoustic waves are capable of interacting with the flame and cause combustion instabilities. In a

similar manner artificial interaction can arise in the DNS if propagating waves are not handled properly. When a reflective outflow boundary is implemented in DNS, the acoustic waves become trapped and lead to artificial flame acoustic interactions. It was discussed by Poinsot and Lele [113] that when an inflow and outflow boundary conditions are chosen, the discretisation at the boundaries can lead to unphysical numerical waves which lead to artificial coupling between inlet and outlet boundaries. The Navier Stokes characteristic boundary conditions (NSCBC) formulation was used in SENGA to provide accurate boundary condition description. A detailed discussion on NSCBC can be found in Poinsot and Lele [113], a short description is provided here.

Poinsot and Lele [113] state that the boundary conditions for compressible DNS are of two categories, they are either physical or numerical boundary conditions. Known physical behaviour of one of more dependent variables can be imposed on the boundaries through physical boundary conditions. An example of such a physical boundary condition is the velocity boundary conditions on a nonslip wall. From the example it is evident that these conditions are independent of numerical methods which might need to be employed for the purpose of solving the governing equations. On the other hand the numerical boundary conditions come into play when the number of physical boundary conditions is smaller than the number of primitive variables. Thus numerical boundary conditions are required due to the discretisation of the problem. In the Euler characteristic boundary conditions (ECBC), some variable can be accounted for on the boundaries through extrapolation from within the domain and other conditions can inferred to from partial set of characteristic relations. However, in the NSCBC method, which is an extension of the ECBC for viscous flow, avoids using extrapolation since the problem can become over constrained through boundary conditions and is unable to handle acoustic wave reflections.

The ECBCs and additional viscous boundary conditions form the NSCBC. The viscous boundary conditions are needed to account for viscous dissipation, thermal diffusion and species diffusion [113]. The physical boundary conditions arise from the well-posedness of the Euler equations. The numerical boundary

conditions arise from a Local One-Dimensional Inviscid (LODI) approximation [119] for a wave crossing the boundary in either direction. The amplitude variations of the outgoing waves are only dependent on the internal solution of the domain only, and these are estimated using the internal solution according to the LODI scheme [119]. It is not possible to estimate any incoming waves using the internal solution and therefore, the incoming wave amplitudes are estimated by the specification of physical boundary conditions whenever necessary. These amplitude variations are then used in association with a reduced set of conservation equations to determine any variables that are not specified by the physical boundary conditions.

The LODI scheme is based on characteristic analysis of a system of locally one dimensional conservative system of equations:

$$\frac{\partial \tilde{\phi}_i}{\partial t} + \frac{\partial F_i}{\partial c} + C'_i = 0, \text{ where } i = 1 \text{ to } n \tag{A.13}$$

where ϕ_i is the conservative variable vector, F_i is a representative flux vector and C'_i is a non-homogeneous term without derivatives. Eq. A.13 can be recast in terms of the dependent variable ϕ_i as:

$$\frac{\partial \phi_i}{\partial t} + A_{ij}\frac{\partial \phi_j}{\partial x} + C_i = 0 \tag{A.14}$$

Eqs. A.13 and A.14 are related in the following manner:

$$\frac{\partial \tilde{\phi}_i}{\partial t} = P_{ij}\frac{\partial \phi_j}{\partial t} \quad \frac{\partial F_i}{\partial x} = Q_{ij}\frac{\partial \phi_j}{\partial x} \tag{A.15a}$$

$$P_{ij} = \frac{\partial \tilde{\phi}_i}{\partial \phi_j} \qquad Q_{ij} = \frac{\partial F_i}{\partial \phi_j} \tag{A.15b}$$

In Eq. A.14, $A_{ij} = P_{ij}^{-1}Q_{kj}$ and $C_i = P_i k^{-1} C'_k$ where A_{ij}, P_{ij} and Q_{ij} are components of the $n \times n$ matrices. The matrix A_{ij} has n linearly independent

eigenvectors in order to allow for the following relationship:

$$S_{ik}A_{kp}S_{pj} = \Lambda_{ij} \tag{A.16}$$

where S_{ij} is the eigenvector matrix and Λ_{ij} is the diagonal matrix, which is given by $\Lambda_{ij=i} = \lambda_i$ where λ_i indicates the eigenvalues. By using this eigenvector matrix S_{ij}, Eq. A.13 can be expressed as:

$$S_{ij}\frac{\partial \phi_j}{\partial t} + \Lambda_{ik}S_{kj}\frac{\partial \phi_j}{\partial x} + S_{ij}C_j = 0 \tag{A.17}$$

A new vector $\vec{\psi}$ can be defined by using same methodology as deriving Eq. A.17:

$$d\psi_i = S_{ij}d\phi_j + S_{ij}C_j dt \tag{A.18}$$

It is then possible to transform Eq. A.17 using Eq. A.18 as follows:

$$\frac{\partial \psi_i}{\partial t} + \Lambda_{ik}\frac{\partial \psi_k}{\partial x} = 0 \text{ or } \frac{\partial \psi_i}{\partial t} + \lambda_i\frac{\partial \psi_i}{\partial x} = 0 \tag{A.19}$$

Eq. A.19 defines a set of wave equations which have a characteristic velocity of λ_i and the second term on the left hand side of Eq. A.17 is known as the wave amplitude variation L_i which can be expressed as:

$$L_i = \Lambda_{ik}S_{kj}\frac{\partial \psi_j}{\partial x} \tag{A.20}$$

The well-posedness of the problem is ensured by implementing the numerical boundary conditions, which are derived from the LODI scheme. These numerical boundary conditions are crucial for evaluating derivatives normal to the boundary. The derivatives are replaced by L_is in the NSCBC formulation. Thompson [146] states that the L_is can be expressed in terms of different characteristic physical waves crossing the boundary in inviscid flow situations. Each L_i can be found out using characteristic analysis of three dimensional extension of Eqs. A.13–

A.20 which are described in detail in [146]. Taking x_1 to be the normal direction to boundary, various L_i can be defined as:

$$L_1 = \lambda_1 \left(\frac{\partial P}{\partial x_1} - \rho a_c \frac{\partial u_1}{\partial x_1} \right) \tag{A.21a}$$

$$L_2 = \lambda_2 \left(a_c^2 \frac{\partial \rho}{\partial x_1} - \frac{\partial P}{\partial x_1} \right) \tag{A.21b}$$

$$L_3 = \lambda_3 \frac{\partial u_2}{\partial x_1} \tag{A.21c}$$

$$L_4 = \lambda_4 \frac{\partial u_3}{\partial x_1} \tag{A.21d}$$

$$L_5 = \lambda_5 \left(\frac{\partial P}{\partial x_1} + \rho a_c \frac{\partial u_1}{\partial x_1} \right) \tag{A.21e}$$

where λ_i represents the characteristic wave velocities of corresponding L_i and a_c is the sonic speed. The characteristic velocities λ_i are defined as follows:

$$\lambda_1 = u_1 - a_c \tag{A.22a}$$

$$\lambda_2 = \lambda_3 = \lambda_4 = u_1 \tag{A.22b}$$

$$\lambda_5 = u_1 + a_c \tag{A.22c}$$

The schematic diagram of wave amplitudes crossing the boundaries in the x_1 direction is shown in Fig. A.1. The wave amplitude variation L_1 is a wave travelling towards the negative x_1 direction and L_5 is associated with a wave travelling in the positive x_1 direction. The wave amplitude L_2 corresponds to an entropy wave and L_3 and L_4 correspond to the advection in the x_2 and x_3 directions, respectively. The NSCBC is a general methodology that can be used for various boundary conditions. Poinsot and Lele [113] highlight a few of these boundary conditions such as an iso-thermal no slip wall, an adiabatic slip wall, an adiabatic no slip wall, a subsonic inflow, a subsonic non-reflecting inflow and a subsonic reflecting outflow. Many of the listed boundary condition's speci-

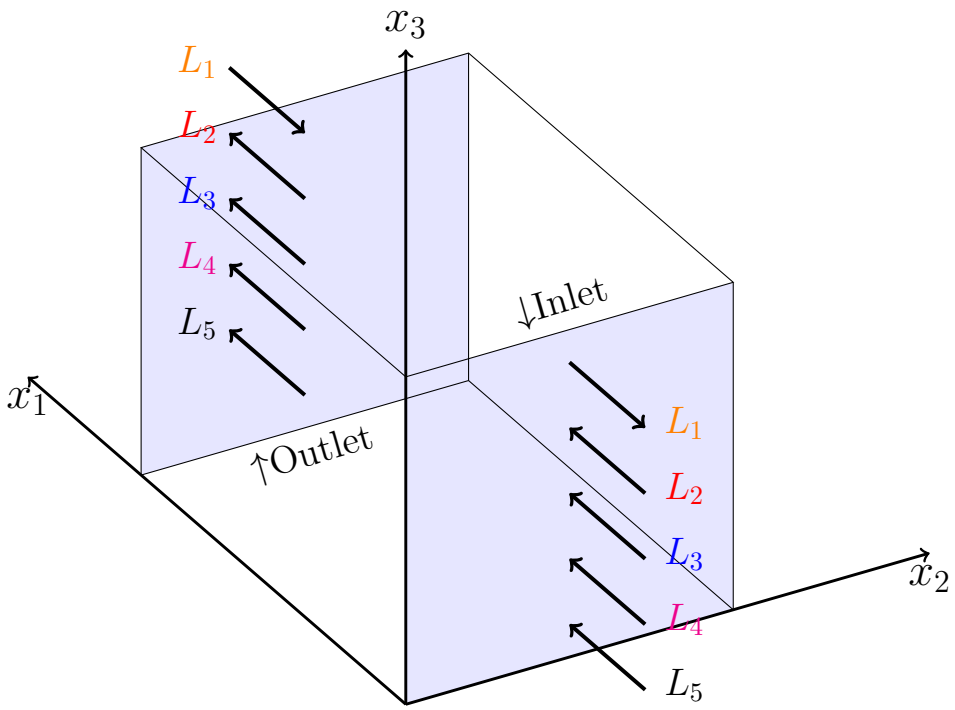

Figure A.1: The wave amplitude variations L_i travelling into and out of the domain at the inflow and outflow boundaries.

fications can be found in Poinsot and Veynante [119]. In the current analysis the DNS, the boundaries in the mean flame propagation are defined as partially non-reflecting in nature. Poinsot and Lele [113] description on NSCBC for partially non-reflecting boundaries was used. As stated earlier boundaries normal to the mean flame propagation are considered to be periodic and thus they do not require additional boundary conditions. The wave amplitudes L_i, as defined in Eqs. A.21 a-e, give the necessary requirements of boundary conditions for Euler equations but additional conditions i.e. viscous conditions are needed for Navier-Stokes equations to ensure well-posedness. Poinsot and Lele [113] and Poinsot and Veynante [119] proposed the required number of boundary conditions for both Euler and Navier-Stokes equations which are summarised in Table A.1. Although boundary condition specification is an established field in CFD research it is still developing where improvements are sought for, especially in combustion simulations [128, 129, 130, 142].

Boundary type	Euler(non-reacting)	Navier-Stokes(non-reacting)	Navier-Stokes(reacting)
Supersonic inflow	5	5	$5 + N_s$
Subsonic inflow	4	5	$5 + N_s$
Supersonic outflow	0	4	$4 + N_s$
Subsonic outflow	1	4	$4 + N_s$

Table A.1: The number of boundary conditions required for well-posedness (for three-dimensional flow) where N_s is the number of reacting species.

A.3.1 Partially Non-reflecting Boundary Conditions

The partially non-reflecting boundary conditions are implemented by using the specification proposed by Poinsot and Lele [113]. If a velocity component normal to the boundary is directed inwards then this component is dealt with by a subsonic reflecting inflow boundary condition and this condition is implemented as suggested by Poinsot and Lele [113]. When acoustic waves are allowed to travel and interact with boundaries where a constant inflow with specified inlet velocity is specified is defined, it leads to complete reflection of the outgoing acoustic wave. This is noted by Poinsot and Lele [113] that it might not be inadequate for a compressible simulation. Poinsot and Lele [113] suggest that a more desirable method would involve a boundary condition that is capable of maintaining a recommended temperature (i.e. T^R and a recommended velocity u^R (i.e. u^R, v^R and w^R), acting as a partially non-reflecting boundary. It is possible to achieve this by using the following wave amplitude variations at the inlet:

$$L_2 = \sigma_2(T - T^R) \tag{A.23a}$$

$$L_3 = \sigma_3(v - v^R) \tag{A.23b}$$

$$L_4 = \sigma_4(w - w^R) \tag{A.23c}$$

$$L_5 = \sigma_4(u - u^R) \tag{A.23d}$$

where σ_2, σ_3, σ_4 and σ_5 are relaxation parameters and they are chosen based on the impedance of the inlet section. When the relaxation parameters are close to zero the boundary behaves similar to a perfectly reflecting boundary, i.e. the acoustic waves are not reflected but that recommended values begin to drift. If large values are chosen for the relaxation parameter acoustic waves are reflected and the recommended values do not drift. For intermediate values of relaxation parameter, the mean values of the inlet velocity and temperature vary about the predefined recommended velocity and temperature values but still allow acoustic waves to propagate through the inlet boundary with little reflection occurring. Poinsot and Lele [113] further suggest that the relaxation parameters must be adapted for each configuration. In order to account for the well-posedness problem the derivative in the x_1-direction is set to zero (i.e. $\partial\tau_{11}/\partial x_1 = 0$) [55, 113, 119]. The required physical boundary conditions are presented in tabulated format in Table A.2 [113].

The velocity components normal to the boundary that are exiting domain

	Navier-Stokes with N_s species			
	ECBC (inviscid) conditions	Viscous Conditions	Reaction Conditions	Total number of conditions
Partially non-reflecting inflow	No reflecting wave 4+N	$\frac{\partial \tau_{11}}{\partial x_1} = 0$	None (0)	$5 + N$
Partially non-reflecting outflow	Pressure at ∞ imposed (1)	$\frac{\partial \tau_{12}}{\partial x_1} = 0$ $\frac{\partial \tau_{12}}{\partial x_1} = 0$ $\frac{\partial q_1}{\partial x_1} = 0$ (3)	$\frac{\partial M_{k1}}{\partial x_1} = 0$ $k = 1, \ldots, N$	$4 + N$

Table A.2: The boundary conditions for three-dimensional reacting flows for partially non-reflecting inlet and outlet boundaries following NSCBC technique [113]. The total number of species is N_s and the boundaries are perpendicular to the x_1-direction.

are dealt with using subsonic partially non-reflecting outflow and are specified

according to Poinsot and Lele [113]. This ensures that acoustic waves are able to exit the domain. It was demonstrated by Poinsot and Lele [113] that a completely reflecting outflow boundary lead drifting of mean pressure field. Artificial acoustic wave reflections takes place when a reflecting outflow boundary condition is used. In order to control the drift and to avoid artificial reflection from the boundary partially non-reflecting boundaries are chosen for all the DNS simulations considered here.

The outflow boundary has four characteristic waves associated with wave amplitude variations these are L_2, L_3, L_4 and L_5 which leave the domain. This is advantageous since they can be calculated using one sided difference schemes which are highly stable. The wave amplitude L_1 on the other hand enters the domain and thus this must be defined. If the wave amplitude L_1 is set to 0 it leads to an outflow boundary which is fully non-reflecting. This is not desired since it leads to pressure drift, as there is no means of estimating the pressure at the outlet. Therefore a boundary condition is needed which describes the mean static pressure at infinity. Poinsot and Lele [113] note that a simple way of achieving this is to describe the wave amplitude L_1 using the pressure difference $P - P_\infty$. The wave amplitude L_1 can be described such a manner that if the outlet pressure is not close to P_∞ then reflected waves from the outlet will bring the pressure closer to P_∞ [113]. The wave amplitude L_1 takes the following form:

$$L_1 = K(P - P\infty) \tag{A.24}$$

The parameter K, if set to 0 results in an outflow boundary which is completely non-reflecting. The following definition was suggested by Rudy and Strikwerda [134] for the coefficient K.

$$K = \sigma_r(1 - Ma^2)\frac{a_c}{L_d} \tag{A.25}$$

where σ_r is a constant, Ma is the maximum Mach number in the domain, a_c is the local speed of sound and L is the domain size. The constant σ_r can lead to

possible mean pressure drift if it is close to 0 ($\sigma_r \approx 0$) and when $\sigma_r = 0$ then the boundary becomes fully non-reflecting. If a large value is chosen for σ_r it leads to strong reflections from the boundary. The value of $\sigma = 0.25$ has been used for this DNS database. As stated earlier the wave amplitude definitions do not fulfill the well-posedness additional specifications are needed. Simply defining L_1 is in fact sufficient if the problem was inviscid, but for viscous flow we have to specify τ_{12}, τ_{13}, heat flux (i.e. $q_1 = -\lambda \partial \hat{T}/\partial x_1$) and scalar flux (i.e. $M_{k1} = -\rho D_k \partial Y_k/\partial x_1$). Following the specification of Poinsot and Lele [113] these parameters were set in the following manner: in the x_1 direction:

$$\frac{\partial \tau_{12}}{\partial x_1} = 0 \tag{A.26a}$$

$$\frac{\partial \tau_{13}}{\partial x_1} = 0 \tag{A.26b}$$

$$\frac{\partial q_1}{\partial x_1} = 0 \tag{A.26c}$$

$$\frac{\partial M_{k1}}{\partial x_1} = 0 \tag{A.26d}$$

The above boundary conditions are also given in Table A.2 [119].

Appendix B

CF Regime and Varying Heat Release

The newly proposed model for the curvature term of the FSD transport equation in the context of RANS is given by Eq. 7.15, where the effects of local Karlovitz number Ka_L are included. This was done based on a DNS which represents the corrugated flamelets regime combustion, where initial turbulence and combustion parameters take the values: $u'/S_L = 1.41$, $l/\delta_{th} = 9.64$, $Re_t = 56.7$, $Da = 6.84$, $Ka = 0.54$, $\tau = 2.3$ and $Le = 1$ (referred to as case K). Additionally the effects of heat release parameter were also analysed using a DNS case with the following initial parameters: $u'/S_L = 7.5$, $l/\delta_{th} = 2.45$, $Re_t = 47.0$, $Da = 0.32$, $Ka = 13.17$, $\tau = 3.0$ and $Le = 1$ (referred to as case L). Cases L and I are similar, where only the heat release is modified 4.5 (in case J) to 3.0 (in case L). The prediction for the model given by Eq. 7.15 for the RANS curvature term of the generalised FSD transport equation is presented for cases K and L in Fig. B.1, which demonstrates that the model given by Eq. 7.15 predicts the curvature term satisfactorily in both cases K and L.

The model given by Eq. 8.20 was also parametrised using cases K and L, so that the effects of local Kalrlovitz number Ka_L are addressed. In Fig. B.2 the predictions of Eq.8.20 are shown, and it is evident from Fig. B.2 that newly

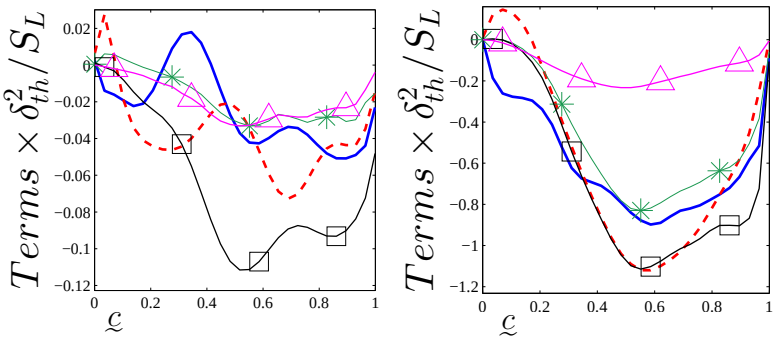

(a) Case K (b) Case L

Figure B.1: Variation of $A_1 + A_2$ (——) with $\underset{\sim}{c}$ along with the predictions of CPB (—△—), CFM (—▫—), CFM-MOD (—✳—) and the combined model given in Eq. 7.15 (– – –), shown for cases A-J.

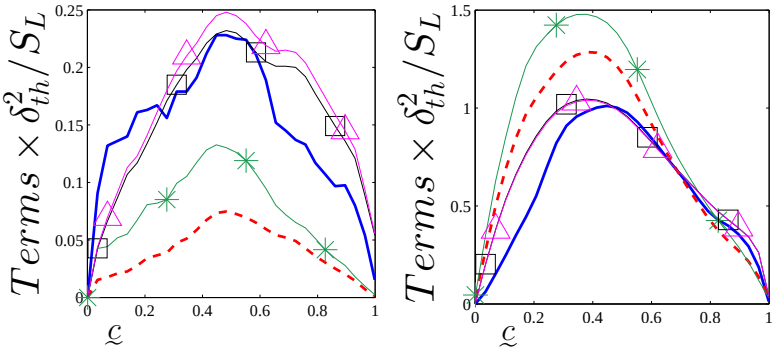

(a) Case K (b) Case L

Figure B.2: Variations of $\underline{(a_T)}_s \Sigma_{gen}$ (——) with $\underset{\sim}{c}$ across the flame brush for cases A-J along with the predictions of CPB (– – –), CFM (—✳—) and the newly proposed models given by Eq. 8.20 using C_2 given by Eq. 8.17a (—▫—) and C_2 given by Eq. 8.17b (—△—).

proposed model (8.20) provides satisfactory predictions for cases K and L.

References

[1] R. G. Abdel-Gayed, D. Bradley, M. N. Hamid, and M. Lawes, "Lewis number effects on turbulent burning velocity", *Symposium (International) on Combustion*, vol. 20, no. 1, pp. 505–512, 1985.

[2] C. Angelberger, D. Veynante, F. Egolfopoulos, and T. Poinsot, "Large Eddy Simulation of combustion instabilities in turbulent premixed flames", *Proceedings of the Summer Program*, Center for Turbulence Research, Stanford, 1998, pp. 66–82.

[3] W. T. Ashurst, A. R. Kerstein, R. M. Kerr, and C. H. Gibson, "Alignment of vorticity and scalar gradient with strain rate in simulated Navier–Stokes turbulence", *Physics of Fluids*, vol. 30, no. 8, pp. 2343–2353, 1987.

[4] W. T. Ashurst, N. Peters, and M. D. Smooke, "Numerical Simulation of Turbulent Flame Structure with Non-unity Lewis Number", *Combustion Science and Technology*, vol. 53, no. 4-6, pp. 339–375, 1987.

[5] G. K. Batchelor, "The effect of homogeneous turbulence on material lines and surfaces", *Proceedings of the Royal Society of London. Series A. Mathematical and Physical Sciences*, vol. 213, no. 1114, pp. 349–366, 1952.

[6] G. K. Batchelor and A. A. Townsend, "Decay of Turbulence in the Final Period", *Proceedings of the Royal Society of London. Series A. Mathematical and Physical Sciences*, vol. 194, no. 1039, pp. 527–543, 1948.

[7] R. W. Bilger, "Conditional moment closure for turbulent reacting flow", *Physics of Fluids A: Fluid Dynamics*, vol. 5, no. 2, pp. 436–444, 1993.

[8] M. Boger, D. Veynante, H. Boughanem, and A. Trouvé, "Direct numerical simulation analysis of flame surface density concept for large eddy simulation of turbulent premixed combustion", *Symposium (International) on Combustion*, vol. 27, no. 1, pp. 917–925, 1998.

[9] P. Boudier, S. Henriot, T. Poinsot, and T. Baritaud, "A model for turbulent flame ignition and propagation in spark ignition engines", *Symposium (International) on Combustion*, vol. 24, no. 1, pp. 503–510, 1992.

[10] K. N. C. Bray, "Turbulent flows with premixed reactants", *Turbulent flows with premixed reactants*, ed. by P. A. Libby and F. A. Williams, vol. 44, Topics in Applied Physics, Springer Berlin Heidelberg, 1980, pp. 115–183, ISBN: 978-3-540-10192-5.

[11] K. N. C. Bray, "Turbulent flows with premixed reactants", *Turbulent Reacting Flows*, ed. by P. Libby and F. Williams, vol. 44, Topics in Applied Physics, Springer Berlin/Heidelberg, 1980, pp. 115–183.

[12] K. N. C. Bray, "Studies of the turbulent burning velocity", *Proceedings of the Royal Society of London. Series A: Mathematical and Physical Sciences*, vol. 431, no. 1882, pp. 315–335, 1990.

[13] K. N. C. Bray, P. A. Libby, and J. B. Moss, "Unified modeling approach for premixed turbulent combustion - Part I: General formulation", *Combustion and Flame*, vol. 61, no. 1, pp. 87–102, 1985.

[14] K. N. C. Bray and N. Peters, "Laminar flamelets in turbulent flames", *Turbulent reacting flows*, ed. by P. A. Libby and F. A. Williams, London: Academic Press Limited, 1994, pp. 1–61.

[15] K. N. C. Bray and N. Peters, "Laminar flamelets in turbulent flames", *Turbulent reacting flows*, pp. 63–113, 1994.

[16] K. N. C. Bray and N. Swaminathan, "Scalar dissipation and flame surface density in premixed turbulent combustion", *Comptes Rendus Mecanique*, vol. 334, no. 8-9, Observation, analysis and modelling in complex fluid media, Special issue for the 60th birthday of Professor Roland Borghi, pp. 466–473, 2006.

[17] G. Bruneaux, T. Poinsot, and J. H. Ferziger, "Premixed flame wall interaction in a turbulent channel flow: budget for the flame surface density evolution equation and modelling", *Journal of Fluid Mechanics*, vol. 349, pp. 191–219, 1997.

[18] S. M. Candel and T. J. Poinsot, "Flame Stretch and the Balance Equation for the Flame Area", *Combustion Science and Technology*, vol. 70, no. 1-3, pp. 1–15, 1990.

[19] S. M. Candel, D. Veynante, F. Lacas, E. Maistret, N. Darabiha, and T. Poinsot, "Coherent flamelet model: applications and recent extensions", *Recent Advances in Combustion Modelling*, vol. 6, pp. 19–64, 1990.

[20] R. S. Cant and K. N. C. Bray, "Strained laminar flamelet calculations of premixed turbulent combustion in a closed vessel", *Symposium (International) on Combustion*, vol. 22, no. 1, pp. 791–799, 1989.

[21] R. S. Cant, S. B. Pope, and K. N. C. Bray, "Modelling of flamelet surface-to-volume ratio in turbulent premixed combustion", *Symposium (International) on Combustion*, vol. 23, no. 1, pp. 809–815, 1991.

[22] N. Chakraborty, "Fundamental Study of Turbulent Premixed Combustion using Direct Numerical Simulation (DNS)", PhD thesis, Cambridge, United Kingdom: University of Cambridge, 2004.

[23] N. Chakraborty, "Comparison of displacement speed statistics of turbulent premixed flames in the regimes representing combustion in corrugated flamelets and thin reaction zones", *Physics of Fluids*, vol. 19, no. 10, p. 105109, 2007.

[24] N. Chakraborty and R. S. Cant, *Tangential strain rate and curvature effects on the displacement speed of an unsteady turbulent premixed flame in a quasi-stationary configuration*, European Combustion Meeting,Orléans, France, Oct. 2003.

[25] N. Chakraborty and R. S. Cant, "Unsteady effects of strain rate and curvature on turbulent premixed flames in an inflow-outflow configuration", *Combustion and Flame*, vol. 137, no. 1, pp. 129–147, 2004.

[26] N. Chakraborty and R. S. Cant, "Influence of Lewis number on curvature effects in turbulent premixed flame propagation in the thin reaction zones regime", *Physics of Fluids*, vol. 17, no. 10, p. 105105, 2005.

[27] N. Chakraborty and R. S. Cant, "Statistical Behavior and Modeling of the Flame Normal Vector in Turbulent Premixed Flames", *Numerical Heat Transfer, Part A: Applications*, vol. 50, no. 7, pp. 623–643, 2006.

[28] N. Chakraborty and R. S. Cant, "Influence of Lewis number on strain rate effects in turbulent premixed flame propagation", *International Journal of Heat and Mass Transfer*, vol. 49, no. 13-14, pp. 2158–2172, 2006.

[29] N. Chakraborty and R. S. Cant, "A priori analysis of the curvature and propagation terms of the flame surface density transport equation for large eddy simulation", *Physics of Fluids*, vol. 19, no. 10, p. 105101, 2007.

[30] N. Chakraborty, M. Klein, and R. S. Cant, "Stretch rate effects on displacement speed in turbulent premixed flame kernels in the thin reaction zones regime", *Proceedings of the Combustion Institute*, vol. 31, no. 1, pp. 1385–1392, 2007.

[31] N. Chakraborty and N. Swaminathan, "Influence of the Damköhler number on turbulence-scalar interaction in premixed flames. I. Physical insight", *Physics of Fluids*, vol. 19, no. 4, p. 045103, 2007.

[32] N. Chakraborty and M. Klein, "Influence of Lewis number on the surface density function transport in the thin reaction zone regime for turbulent premixed flames", *Physics of Fluids*, vol. 20, no. 6, p. 065102, 2008.

[33] N. Chakraborty and M. Klein, "A priori direct numerical simulation assessment of algebraic flame surface density models for turbulent premixed flames in the context of large eddy simulation", *Physics of Fluids*, vol. 20, no. 8, p. 085108, 2008.

[34] N. Chakraborty, J. W. Rogerson, and N. Swaminathan, "A priori assessment of closures for scalar dissipation rate transport in turbulent premixed flames using direct numerical simulation", *Physics of Fluids*, vol. 20, no. 4, p. 045106, 2008.

[35] N. Chakraborty and R. S. Cant, "Direct Numerical Simulation analysis of the Flame Surface Density transport equation in the context of Large Eddy Simulation", *Proceedings of the Combustion Institute*, vol. 32, no. 1, pp. 1445–1453, 2009.

[36] N. Chakraborty and R. S. Cant, "Effects of Lewis number on scalar transport in turbulent premixed flames", *Physics of Fluids*, vol. 21, no. 3, p. 035110, 2009.

[37] N. Chakraborty and R. S. Cant, "Physical Insight and Modelling for Lewis Number Effects on Turbulent Heat and Mass Transport in Turbulent Premixed Flames", *Numerical Heat Transfer, Part A: Applications*, vol. 55, no. 8, pp. 762–779, 2009.

[38] N. Chakraborty and R. S. Cant, "Effects of Lewis number on turbulent scalar transport and its modelling in turbulent premixed flames", *Combustion and Flame*, vol. 156, no. 7, pp. 1427–1444, 2009.

[39] N. Chakraborty, M. Klein, and N. Swaminathan, "Effects of Lewis number on the reactive scalar gradient alignment with local strain rate in turbulent premixed flames", *Proceedings of the Combustion Institute*, vol. 32, no. 1, pp. 1409–1417, 2009.

[40] N. Chakraborty and R. S. Cant, "Effects of Lewis number on flame surface density transport in turbulent premixed combustion", *Combustion and Flame*, vol. 158, no. 9, pp. 1768–1787, 2011.

[41] N. Chakraborty, G. Hartung, M. Katragadda, and C. F. Kaminski, "Comparison of 2D and 3D density-weighted displacement speed statistics and implications for laser based measurements of flame displacement speed using direct numerical simulation data", *Combustion and Flame*, vol. 158, no. 7, pp. 1372–1390, 2011.

[42] N. Chakraborty, M. Katragadda, and R. S. Cant, "Statistics and Modelling of Turbulent Kinetic Energy Transport in Different Regimes of Premixed Combustion", *Flow, Turbulence and Combustion*, vol. 87, pp. 205–235, 2 2011.

[43] N. Chakraborty, M. Katragadda, and R. S. Cant, "Effects of Lewis number on turbulent kinetic energy transport in premixed flames", *Physics of Fluids*, vol. 23, no. 7, p. 075109, 2011.

[44] N. Chakraborty, M. Klein, and R. S. Cant, "Effects of Turbulent Reynolds Number on the Displacement Speed Statistics in the Thin Reaction Zones Regime of Turbulent Premixed Combustion", *Journal of Combustion*, vol. 2011, Article ID 473679, p. 19, 2011.

[45] N. Chakraborty and N. Swaminathan, "Effects of Lewis Number on Scalar Variance Transport in Premixed Flames", *Flow, Turbulence and Combustion*, vol. 87, no. 2, pp. 261–292, 2011.

[46] N. Chakraborty, M. Hudson, and R. S. Cant, "Statistical behaviour of dissipation rate of turbulent kinetic energy in turbulent premixed flames",

Proceedings of the Seventh International Symposium on Turbulence, Heat and Mass Transfer, University of Palermo, Palermo, Sicily, Italy: Begell House, Inc., 2012, pp. 717–720.

[47] N. Chakraborty and R. S. Cant, "Turbulent Reynolds number dependence of flame surface density transport in the context of Reynolds averaged Navier-Stokes simulations", *Proceedings of the Combustion Institute*, vol. 34, no. 1, pp. 1347–1356, 2013.

[48] F. Charlette, A. Trouvé, M. Boger, and D. Veynante, "A flame surface density model for Large Eddy Simulations of turbulent premixed flames", *The Combustion Institute Joint Meeting of the British, German and French Sections*, 1999.

[49] F. Charlette, C. Meneveau, and D. Veynante, "A power-law flame wrinkling model for LES of premixed turbulent combustion Part I: non-dynamic formulation and initial tests", *Combustion and Flame*, vol. 131, no. 1-2, pp. 159–180, 2002.

[50] F. Charlette, C. Meneveau, and D. Veynante, "A power-law flame wrinkling model for LES of premixed turbulent combustion Part II: dynamic formulation", *Combustion and Flame*, vol. 131, no. 1-2, pp. 181–197, 2002.

[51] W. K. Cheng and J. A. Diringer, *Numerical modelling of SI engine combustion with a flame sheet model*, Society of Automotive Engineers, 1991.

[52] C. R. Choi and K. Y. Huh, "Development of a Coherent Flamelet Model for a Spark-Ignited Turbulent Premixed Flame in a Closed Vessel", *Combustion and Flame*, vol. 114, no. 3-4, pp. 336–348, 1998.

[53] O. Colin, F. Ducros, D. Veynante, and T. Poinsot, "A thickened flame model for large eddy simulations of turbulent premixed combustion", *Physics of Fluids*, vol. 12, no. 7, pp. 1843–1863, 2000.

[54] J. M. Duclos, D. Veynante, and T. Poinsot, "A comparison of flamelet models for premixed turbulent combustion", *Combustion and Flame*, vol. 95, no. 1-2, pp. 101–117, 1993.

[55] P. Dutt, "Stable boundary conditions and difference schemes for Navier-Stokes equations", *SIAM journal on numerical analysis*, pp. 245–267, 1988.

[56] T. Echekki and J. H. Chen, "Unsteady strain rate and curvature effects in turbulent premixed methane-air flames", *Combustion and Flame*, vol. 106, no. 1, pp. 184–202, 1996.

[57] T. Echekki and J. H. Chen, "Analysis of the contribution of curvature to premixed flame propagation", *Combustion and Flame*, vol. 118, no. 1-2, pp. 308–311, 1999.

[58] C. Fureby, "A fractal flame-wrinkling large eddy simulation model for premixed turbulent combustion", *Proceedings of the Combustion Institute*, vol. 30, no. 1, pp. 593–601, 2005.

[59] M. Germano, U. Piomelli, P. Moin, and W. H. Cabot, "A dynamic subgrid-scale eddy viscosity model", *Physics of Fluids A: Fluid Dynamics*, vol. 3, no. 7, pp. 1760–1765, 1991.

[60] M. Germano, A. Maffio, S. Sello, and G. Mariotti, "On the Extension of the Dynamic Modelling Procedure to Turbulent Reacting Flows", *Direct and Large-Eddy Simulation II*, ed. by J.-P. Chollet, P. Voke, and L. Kleiser,

vol. 5, ERCOFTAC Series, Springer Netherlands, 1997, pp. 291–300, ISBN: 978-0-7923-4687-6.

[61] F. C. Gouldin, K. N. C. Bray, and J. Y. Chen, "Chemical closure model for fractal flamelets", *Combustion and Flame*, vol. 77, pp. 241–259, 1989.

[62] I. R. Gran, T. Echekki, and J. H. Chen, "Negative flame speed in an unsteady 2-D premixed flame: A computational study", *Symposium (International) on Combustion*, vol. 26, no. 1, pp. 323–329, 1996.

[63] Ö. L. Gülder, "Turbulent premixed combustion modelling using fractal geometry", *Symposium (International) on Combustion*, vol. 23, no. 1, pp. 835–842, 1991.

[64] Ö. L. Gülder and G. J. Smallwood, "Inner cutoff scale of flame surface wrinkling in turbulent premixed flames", *Combustion and Flame*, vol. 103, no. 1-2, pp. 107–114, 1995.

[65] I. Han and K. Y. Huh, "Roles of displacement speed on evolution of flame surface density for different turbulent intensities and Lewis numbers in turbulent premixed combustion", *Combustion and Flame*, vol. 152, no. 1-2, pp. 194–205, 2008.

[66] E. R. Hawkes, "Large Eddy Simulation of Premixed Turbulent Combustion", PhD thesis, Cambridge, United Kingdom: University of Cambridge, 2000.

[67] E. R. Hawkes and R. S. Cant, "A flame surface density approach to large-eddy simulation of premixed turbulent combustion", *Proceedings of the Combustion Institute*, vol. 28, no. 1, pp. 51–58, 2000.

[68] E. R. Hawkes and R. S. Cant, "Implications of a flame surface density approach to large eddy simulation of premixed turbulent combustion", *Combustion and Flame*, vol. 126, no. 3, pp. 1617–1629, 2001.

[69] E. R. Hawkes and R. S. Cant, "Physical and numerical realizability requirements for flame surface density approaches", *Combustion Theory and Modelling*, vol. 5, no. 4, pp. 699–720, 2001.

[70] E. R. Hawkes and J. H. Chen, "Evaluation of models for flame stretch due to curvature in the thin reaction zones regime", *Proceedings of the Combustion Institute*, vol. 30, no. 1, pp. 647–655, 2005.

[71] E. R. Hawkes, R. Sankaran, O. Colin, and J. H. Chen, "An Analysis of the Flame Surface Density Transport Equation Using Direct Numerical Simulation of a Methane-Air Jet", *Proceedings of Australian Combustion Symposium*, The University of Queensland, Brisbane, 2009.

[72] D. C. Haworth and T. J. Poinsot, "Numerical simulations of Lewis number effects in turbulent premixed flames", *Journal of Fluid Mechanics*, vol. 244, pp. 405–436, 1992.

[73] F. E. Hernández-Pérez, F. T. C. Yuen, C. P. T. Groth, and Ö. L. Gülder, "LES of a laboratory-scale turbulent premixed Bunsen flame using FSD, PCM-FPI and thickened flame models", *Proceedings of the Combustion Institute*, vol. 33, no. 1, pp. 1365–1371, 2011.

[74] H. G. Im, T. S. Lund, and J. H. Ferziger, "Large eddy simulation of turbulent front propagation with dynamic subgrid models", *Physics of Fluids*, vol. 9, no. 12, pp. 3826–3833, 1997.

[75] H. G. Im and J. H. Chen, "Preferential diffusion effects on the burning rate of interacting turbulent premixed hydrogen-air flames", *Combustion and Flame*, vol. 131, no. 3, pp. 246–258, 2002.

[76] F. A. Jaberi and S. James, "A dynamic similarity model for large eddy simulation of turbulent combustion", *Physics of Fluids*, vol. 10, no. 7, pp. 1775–1777, 1998.

[77] K. W. Jenkins and R. S. Cant, "DNS of turbulent flame kernels", *Proceedings Second AFOSR Conference on DNS and LES*, Rutgers University, Kluwer Academic Publishers, 1999, pp. 192–202.

[78] K. W. Jenkins and R. S. Cant, "Curvature effects on flame kernels in a turbulent environment", *Proceedings of the Combustion Institute*, vol. 29, no. 2, pp. 2023–2029, 2002.

[79] W. P. Jones and B. E. Launder, "The prediction of laminarization with a two-equation model of turbulence", *International Journal of Heat and Mass Transfer*, vol. 15, no. 2, pp. 301–314, 1972.

[80] M. Katragadda, S. P. Malkeson, and N. Chakraborty, "Modelling of the tangential strain rate term of the Flame Surface Density transport equation in the context of Reynolds Averaged Navier-Stokes simulation", *Proceedings of the Combustion Institute*, vol. 33, no. 1, pp. 1429–1437, 2011.

[81] M. Katragadda, S. P. Malkeson, and N. Chakraborty, "Modelling of curvature term of the Flame Surface Density transport equation in the context of Reynolds Averaged Navier Stokes simulations", *7th Mediterranean Combustion Symposium*, Sept. 2011.

[82] M. Katragadda and N. Chakraborty, "Modelling of the Curvature Term of the Flame Surface Density Transport Equation for Large Eddy Simulations", *Journal of Combustion*, vol. 2012, Article ID 915482, p. 12, 2012.

[83] M. Katragadda and N. Chakraborty, "A Priori Direct Numerical Simulation Modelling of the Curvature Term of the Flame Surface Density Transport Equation for Nonunity Lewis Number Flames in the Context of Large Eddy Simulations", *International Journal of Chemical Engineering*, vol. 2012, Article ID 103727, p. 12, 2012.

[84] M. Katragadda, N. Chakraborty, and R. S. Cant, "A Priori Assessment of Algebraic Flame Surface Density Models in the Context of Large Eddy Simulation for Nonunity Lewis Number Flames in the Thin Reaction Zones Regime", *Journal of Combustion*, vol. 2012, Article ID 794671, p. 17, 2012.

[85] M. Katragadda, N. Chakraborty, and R. S. Cant, "Effects of Turbulent Reynolds Number on the Performance of Algebraic Flame Surface Density Models for Large Eddy Simulation in the Thin Reaction Zones Regime: A Direct Numerical Simulation Analysis", *Journal of Combustion*, vol. 2012, Article ID 353257, p. 13, 2012.

[86] A. R. Kerstein, "Fractal Dimension of Turbulent Premixed Flames", *Combustion Science and Technology*, vol. 60, no. 4-6, pp. 441–445, 1988.

[87] W. W. Kim and S. Menon, "A new dynamic one-equation subgrid-scale model for large eddy simulations", *AIAA, Aerospace Sciences Meeting and Exhibit, 33 rd, Reno, NV*, 1995.

[88] W. Kim, S. Menon, and H. C. Mongia, "Large-Eddy Simulation of a Gas Turbine Combustor Flow", *Combustion Science and Technology*, vol. 143, no. 1-6, pp. 25–62, 1999.

[89] R. Knikker, D. Veynante, and C. Meneveau, "A dynamic flame surface density model for large eddy simulation of turbulent premixed combustion", *Physics of Fluids*, vol. 16, no. 11, pp. L91–L94, 2004.

[90] H. Kolla, J. W. Rogerson, N. Chakraborty, and N. Swaminathan, "Scalar Dissipation Rate Modeling and its Validation", *Combustion Science and Technology*, vol. 181, no. 3, pp. 518–535, 2009.

[91] H. Kolla, J. W. Rogerson, and N. Swaminathan, "Validation of a Turbulent Flame Speed Model across Combustion Regimes", *Combustion Science and Technology*, vol. 182, no. 3, pp. 284–308, 2010.

[92] W. Kollmann and J. H. Chen, "Pocket formation and the flame surface density equation", *Symposium (International) on Combustion*, vol. 27, no. 1, pp. 927–934, 1998.

[93] B. E. Launder and D. B. Spalding, "The numerical computation of turbulent flows", *Computer Methods in Applied Mechanics and Engineering*, vol. 3, no. 2, pp. 269–289, 1974.

[94] E. Lee, C. R. Choi, and K. Y. Huh, "Application of the Coherent Flamelet Model to Counterflow Turbulent Premixed Combustion and Extinction", *Combustion Science and Technology*, vol. 138, no. 1-6, pp. 1–25, 1998.

[95] P. A. Libby, A. Liñán, and F. A. Williams, "Strained Premixed Laminar Flames with Nonunity Lewis Numbers", *Combustion Science and Technology*, vol. 34, no. 1-6, pp. 257–293, 1983.

[96] D. K. Lilly, "A proposed modification of the Germano subgrid-scale closure method", *Physics of Fluids A: Fluid Dynamics*, vol. 4, no. 3, pp. 633–635, 1992.

[97] D. S. Louch and K. N. C. Bray, "Vorticity and scalar transport in premixed turbulent combustion", *Symposium (International) on Combustion*, vol. 27, no. 1, pp. 801–810, 1998.

[98] E. Maistret, N. Darabiha, T. Poinsot, D. Veynante, F. Lacas, S. M. Candel, and E. Esposito, "Recent developments in the coherent flamelet description of turbulent combustion", *Numerical Combustion*, ed. by A. Dervieux and B. Larrouturou, vol. 351, Lecture Notes in Physics, Springer Berlin / Heidelberg, 1989, pp. 98–117, ISBN: 978-3-540-51968-3.

[99] S. P. Malkeson and N. Chakraborty, "Statistical Analysis and a-priori Modelling of Flame Surface Density Transport in Turbulent Stratified Flames: A Direct Numerical Simulation Study", *Flow, Turbulence and Combustion*, vol. 90, no. 1, pp. 143–187, 2013.

[100] T. Mantel and R. Borghi, "A new model of premixed wrinkled flame propagation based on a scalar dissipation equation", *Combustion and Flame*, vol. 96, no. 4, pp. 443–457, 1994.

[101] F. E. Marble and J. E. Broadwell, "The coherent flame model of non-premixed turbulent combustion", *Project Squid TRW-9-PU, Project Squid Headquarters, Chaffee Hall, Purdue University* 1977.

[102] C. Meneveau and T. Poinsot, "Stretching and quenching of flamelets in premixed turbulent combustion", *Combustion and Flame*, vol. 86, no. 4, pp. 311–332, 1991.

[103] S. Menon and W. Jou, "Large-Eddy Simulations of Combustion Instability in an Axisymmetric Ramjet Combustor", *Combustion Science and Technology*, vol. 75, no. 1-3, pp. 53–72, 1991.

[104] K. Naitoh, K. Itoh, and Y. Takagi, "Large eddy Simulation of premixed flame in engine based on the multi-level formation and the renormalisation group theory", *SAE Paper 920590*, 1992.

[105] K. Naitoh, Y. Takagi, and K. Kuwahara, "Cycle-resolved computation of compressible turbulence and premixed flame in an engine", *Computers & Fluids*, vol. 22, no. 4-5, pp. 623–648, 1993.

[106] G. L. North and D. A. Santavicca, "The Fractal Nature of Premixed Turbulent Flames", *Combustion Science and Technology*, vol. 72, no. 4-6, pp. 215–232, 1990.

[107] N. Peters, *Turbulent Combustion*, Cambridge University Press, 2000.

[108] N. Peters, P. Terhoeven, J. H. Chen, and T. Echekki, "Statistics of flame displacement speeds from computations of 2-D unsteady methane-air flames", *Symposium (International) on Combustion*, vol. 27, no. 1, pp. 833–839, 1998.

[109] S. Pfadler, J. Kerl, F. Beyrau, A. Leipertz, A. Sadiki, J. Scheuerlein, and F. Dinkelacker, "Direct evaluation of the subgrid scale scalar flux in turbulent

premixed flames with conditioned dual-plane stereo PIV", *Proceedings of the Combustion Institute*, vol. 32, no. 2, pp. 1723–1730, 2009.

[110] J. Piana, F. Ducros, and D. Veynante, "Large eddy simulations of turbulent premixed flames based on the G-equation and a flame front wrinkling description", *11^th Symposium on Turbulent Shear Flows*, Grenoble, France, 1997, pp. 21–13.

[111] H. Pitsch and L. D. de Lageneste, "Large-eddy simulation of premixed turbulent combustion using a level-set approach", *Proceedings of the Combustion Institute*, vol. 29, no. 2, pp. 2001–2008, 2002.

[112] A. Pocheau, "Scale invariance in turbulent front propagation", *Phys. Rev. E*, vol. 49, pp. 1109–1122, 2 Feb. 1994.

[113] T. J. Poinsot and S. K. Lele, "Boundary conditions for direct simulations of compressible viscous flows", *Journal of Computational Physics*, vol. 101, no. 1, pp. 104–129, 1992.

[114] T. J. Poinsot, D. C. Haworth, and G. Bruneaux, "Direct simulation and modeling of flame-wall interaction for premixed turbulent combustion", *Combustion and Flame*, vol. 95, no. 1-2, pp. 118–132, 1993.

[115] T. Poinsot, D. Veynante, and S. M. Candel, "Diagrams of premixed turbulent combustion based on direct simulation", *Symposium (International) on Combustion*, vol. 23, no. 1, pp. 613–619, 1991.

[116] T. Poinsot, D. Veynante, and S. M. Candel, "Quenching processes and premixed turbulent combustion diagrams", *Journal of Fluid Mechanics*, vol. 228, pp. 561–606, 1991.

[117] T. Poinsot, T. Echekki, and M. G. Mungal, "A Study of the Laminar Flame Tip and Implications for Premixed Turbulent Combustion", *Combustion Science and Technology*, vol. 81, no. 1-3, pp. 45–73, 1992.

[118] T. Poinsot, S. M. Candel, and A. Trouvé, "Applications of direct numerical simulation to premixed turbulent combustion", *Progress in Energy and Combustion Science*, vol. 21, no. 6, pp. 531–576, 1995.

[119] T. Poinsot and D. Veynante, *Theoretical and Numerical Combustion*, Philadelphia, USA: R.T. Edwards Inc., 2005.

[120] S. B. Pope, "PDF methods for turbulent reactive flows", *Progress in Energy and Combustion Science*, vol. 11, no. 2, pp. 119–192, 1985.

[121] S. B. Pope, "The evolution of surfaces in turbulence", *International Journal of Engineering Science*, vol. 26, no. 5, pp. 445–469, 1988.

[122] S. B. Pope, "Computations of turbulent combustion: Progress and challenges", *Symposium (International) on Combustion*, vol. 23, no. 1, pp. 591–612, 1991.

[123] S. B. Pope, *Turbulent Flows*, Cambridge: Cambridge University press, 2000.

[124] S. B. Pope and W. K. Cheng, "The stochastic flamelet model of turbulent premixed combustion", *Symposium (International) on Combustion*, vol. 22, no. 1, pp. 781–789, 1989.

[125] S. B. Pope, P. K. Yeung, and S. S. Girimaji, "The curvature of material surfaces in isotropic turbulence", *Physics of Fluids A: Fluid Dynamics*, vol. 1, no. 12, pp. 2010–2018, 1989.

[126] R. O. S. Prasad and J. P. Gore, "An evaluation of flame surface density models for turbulent premixed jet flames", *Combustion and Flame*, vol. 116, no. 1-2, pp. 1–14, 1999.

[127] R. O. S. Prasad, R. N. Paul, Y. R. Sivathanu, and J. P. Gore, "An evaluation of combined flame surface density and mixture fraction models for nonisenthalpic premixed turbulent flames", *Combustion and Flame*, vol. 117, no. 3, pp. 514–528, 1999.

[128] R. Prosser, "Improved boundary conditions for the direct numerical simulation of turbulent subsonic flows. I. Inviscid flows", *Journal of Computational Physics*, vol. 207, no. 2, pp. 736–768, 2005.

[129] R. Prosser, "Towards improved boundary conditions for the DNS and LES of turbulent subsonic flows", *Journal of Computational Physics*, vol. 222, no. 2, pp. 469–474, 2007.

[130] R. Prosser, "Improved Boundary Conditions for the DNS of Reacting Subsonic Flows", English, *Flow, Turbulence and Combustion*, vol. 87, no. 2-3, pp. 351–376, 2011.

[131] H. Reddy and J. Abraham, "Two-dimensional direct numerical simulation evaluation of the flame-surface density model for flames developing from an ignition kernel in lean methane/air mixtures under engine conditions", *Physics of Fluids*, vol. 24, no. 10, p. 105108, 2012.

[132] B. Renou, A. Boukhalfa, D. Puechberty, and M. Trinité, "Effects of stretch on the local structure of preely propagating premixed low-turbulent flames with various lewis numbers", *Symposium (International) on Combustion*, vol. 27, no. 1, pp. 841–847, 1998.

[133] R. S. Rogallo, *Numerical experiments in homogeneous turbulence*, vol. 81315, NASA Ames Research Center, California: National Aeronautics and Space Administration, 1981.

[134] D. H. Rudy and J. C. Strikwerda, "A nonreflecting outflow boundary condition for subsonic navier-stokes calculations", *Journal of Computational Physics*, vol. 36, no. 1, pp. 55–70, 1980.

[135] C. J. Rutland and A. Trouvé, "Direct simulations of premixed turbulent flames with nonunity Lewis numbers", *Combustion and Flame*, vol. 94, no. 1-2, pp. 41–57, 1993.

[136] C. J. Rutland and R. S. Cant, "Turbulent transport in premixed flames", *Proceedings of the Summer Program*, Center for Turbulence Research, Stanford University/NASA-Ams, 1994, p. 75.

[137] G. I. Sivashinsky, "Instabilities, Pattern Formation, and Turbulence in Flames", *Annual Review of Fluid Mechanics*, vol. 15, no. 1, pp. 179–199, 1983.

[138] J. Smagorinsky, "General circulation experiments with the primitive equations", *Monthly weather review*, vol. 91, no. 3, pp. 99–164, 1963.

[139] V. Smiljanovski, V. Moser, and R. Klein, "A capturing - tracking hybrid scheme for deflagration discontinuities", *Combustion Theory and Modelling*, vol. 1, no. 2, pp. 183–215, 1997.

[140] A. M. Steinberg and J. F. Driscoll, "Stretch-rate relationships for turbulent premixed combustion LES subgrid models measured using temporally

resolved diagnostics", *Combustion and Flame*, vol. 157, no. 7, pp. 1422–1435, 2010.

[141] A. M. Steinberg, J. F. Driscoll, and N. Swaminathan, "Statistics and dynamics of turbulence-flame alignment in premixed combustion", *Combustion and Flame*, vol. 159, no. 8, pp. 2576–2588, 2012.

[142] J. C. Sutherland and C. A. Kennedy, "Improved boundary conditions for viscous, reacting, compressible flows", *Journal of Computational Physics*, vol. 191, no. 2, pp. 502–524, 2003.

[143] N. Swaminathan and R. W. Grout, "Interaction of turbulence and scalar fields in premixed flames", *Physics of Fluids*, vol. 18, no. 4, p. 045102, 2006.

[144] G. Tabor and H. G. Weller, "Large Eddy Simulation of Premixed Turbulent Combustion Using Ξ Flame Surface Wrinkling Model", *Flow, Turbulence and Combustion*, vol. 72, pp. 1–27, 1 2004.

[145] H. Tennekes and J. L. Lumley, *A first course in turbulence*, MIT press, 1972.

[146] K. W. Thompson, "Time dependent boundary conditions for hyperbolic systems", *Journal of Computational Physics*, vol. 68, no. 1, pp. 1–24, 1987.

[147] A. Trouvé, "The production of premixed flame surface area in turbulent shear flow", *Combustion and Flame*, vol. 99, no. 3-4, pp. 687–696, 1994.

[148] A. Trouvé and T. Poinsot, "The evolution equation for the flame surface density in turbulent premixed combustion", *Journal of Fluid Mechanics*, vol. 278, pp. 1–32, 1994.

[149] S. Tullis, "Large Eddy Simulation of scalar flux in turbulent premixed flames", PhD thesis, Cambridge, United Kingdom: University of Cambridge, 2003.

[150] S. Tullis and R. S. Cant, "Scalar transport modeling in large eddy simulation of turbulent premixed flames", *Proceedings of the Combustion Institute*, vol. 29, no. 2, pp. 2097–2104, 2002.

[151] L. Vervisch, E. Bidaux, K. N. C. Bray, and W. Kollmann, "Surface density function in premixed turbulent combustion modeling, similarities between probability density function and flame surface approaches", *Physics of Fluids*, vol. 7, no. 10, pp. 2496–2503, 1995.

[152] D. Veynante, J. M. Duclos, and J. Piana, "Experimental analysis of flamelet models for premixed turbulent combustion", *Symposium (International) on Combustion*, vol. 25, no. 1, pp. 1249–1256, 1994.

[153] D. Veynante, J. Piana, J. M. Duclos, and C. Martel, "Experimental analysis of flame surface density models for premixed turbulent combustion", *Symposium (International) on Combustion*, vol. 26, no. 1, pp. 413–420, 1996.

[154] D. Veynante and T. Poinsot, "Large eddy simulation of combustion instabilities in turbulent premixed burners", *Annual Research Briefs*, Stanford, U.S.A., 1997, pp. 253–274.

[155] D. Veynante, A. Trouvé, K. N. C. Bray, and T. Mantel, "Gradient and counter-gradient scalar transport in turbulent premixed flames", *Journal of Fluid Mechanics*, vol. 332, no. 1, pp. 263–293, 1997.

[156] D. Veynante and L. Vervisch, "Turbulent combustion modeling", *Progress in Energy and Combustion Science*, vol. 28, no. 3, pp. 193–266, 2002.

[157] H. G. Weller, "The development of a new flame area combustion model using conditional averaging", *Thermo-fluids section report TF 9307*, London, U.K., 1993.

[158] H. G. Weller, C. J. Marooney, and A. D. Gosman, "A new spectral method for calculation of the time-varying area of a laminar flame in homogeneous turbulence", *Symposium (International) on Combustion*, vol. 23, no. 1, pp. 629–636, 1991.

[159] H. G. Weller, G. Tabor, A. D. Gosman, and C. Fureby, "Application of a flame-wrinkling les combustion model to a turbulent mixing layer", *Symposium (International) on Combustion*, vol. 27, no. 1, pp. 899–907, 1998.

[160] F. A. Williams, "Turbulent Combustion", *The Mathematics of Combustion*, ed. by J. Buckmaster, Philadelphia: SIAM, 1985, chap. 3, pp. 97–131.

[161] A. A. Wray, "Minimal storage time advancement schemes for spectral methods", NASA Ames Research Center, California, Report No. MS 202 A-1, 1990.

[162] A. S. Wu and K. N. C. Bray, "A coherent flame model of premixed turbulent combustion in a counterflow geometry", *Combustion and Flame*, vol. 109, no. 1-2, pp. 43–64, 1997.

[163] V. Yakhot, "Propagation Velocity of Premixed Turbulent Flames", *Combustion Science and Technology*, vol. 60, no. 1-3, pp. 191–214, 1988.

[164] P. K. Yeung, S. S. Girimaji, and S. B. Pope, "Straining and scalar dissipation on material surfaces in turbulence: Implications for flamelets", *Combustion and Flame*, vol. 79, no. 3-4, pp. 340–365, 1990.

[165] J. Yuan, Y. Ju, and C. K. Law, "Coupled hydrodynamic and diffusional-thermal instabilities in flame propagation at subunity Lewis numbers", *Physics of Fluids*, vol. 17, no. 7, p. 074106, 2005.

[166] V. L. Zimont and A. N. Lipatnikov, "A numerical model of premixed turbulent combustion of gases", *Chem. Phys. Reports*, vol. 14, no. 7, pp. 993–1025, 1995.